GEOLOGY AND GEOCHEMISTRY OF PALEOPROTEROZOIC GWALIOR GROUP SEDIMENTS, BUNDELKHAND CRATON, CENTRAL INDIA: IMPLICATIONS FOR PROVENANCE, DEPOSITIONAL ENVIRONMENT, TECTONIC SETTING AND EVOLUTIONARY TREND OF UPPER CONTINENTAL CRUST

ABSTRACT

THESIS SUBMITTED FOR THE AWARD OF THE DEGREE OF

Doctor of Philosophy

IN

GEOLOGY

By

NURUL ABSAR

DEPARTMENT OF GEOLOGY
ALIGARH MUSLIM UNIVERSITY
ALIGARH – (INDIA)
2005

ABSTRACT

Continuous sedimentary rock records ranging in age from Mesoarchean to Mesoproterozoic are preserved in Gwalior sector of Bundelkhand Block which are unmetamorphosed and flat lying, thus provide an unparallel opportunity to study the geological processes of early earth's history. Paleoproterozoic depositional history of the area is represented by sedimentary rocks of Gwalior Group. The Gwalior Group is comprised of a basal clastic sequence of sandstone-shale association referred to as Par Formation and upper Chemogenic sequences referred to as Morar Formation, which is constituted of Banded Iron Formation (BIF) with minor limestones, ferruginous shales and ash beds. The whole sequence is traversed by 1791 Ma diabase dykes and sills. The Gwalior Group is unconformably overlained by sandstone-shale sequence of Mesoproterozoic Kaimur Group of Vindhyan Supergroup. The basement of Proterozoic sequences is predominantly consisting of Late Archean (~2.5 Ga) high K-granites with some very well preserved Mesoarchean xenolithic sedimentary enclaves of quartzite-phyllite association. This thesis is concerned with sedimentological, geochemical and isotopic investigations of sedimentary rocks of Gwalior Group and is aimed to constrain the composition and weathering conditions of upper continental crust, depositional environment and age of sedimentation, composition of sea water and relative continental to mantle flux to the Precambrian oceans. In addition, geochemistry of underlying Mesoarchean quartzites and overlying Mesoproterozoic Kaimur Group sandstones are also being carried out in attempt to deduce compositional evolution of upper continental crust during the Mesoarchean to Mesoproterozoic period.

Sedimentological analysis of Gwalior Group indicatesthat deposition of sediments took place in a stable cratonic shelf and was influenced by tidal, wave and storm activities. A range of facies of shorezone-shelf associations is recognized, viz. back barrier lagoonal system, shoreface- foreshore system, inner shelf and outer shelf systems. Tidal influence is evidenced by very well preserved tidal rhythmites/bundles in back barrier lagoonal zone and herringbone type bidirectional structures in the shoreface-foreshore system. Influence of wave activity is preserved as various wave produced structures in shoreface facies sediments. Storm related beds are preserved as Bouma sequences in the inner and outer shelf systems. Paleocurrent analysis revealed that sediments were transported to shelf from southern provenances possibly via river

systems, where reworking of sediments took place because of complex basinal hydrodynamic processes. The data suggest that sedimentation was laid down under a transgressive system tract in an accommodation dominated shelf. Presence of rare basal fluvial facies suggests that the basin probably started life as an alluvial basin and gradual opening up of the basin resulted in the landward encroachment of the sea. With rapid sea level rise, clastic sedimentation ceased and chemical environment prevailed, leading to the deposition of thick piles of BIF that overlapped all the earlier formed clastic facies.

The extreme quartz enrichment in sandstones of Gwalior Group signifies low upliftment and high insitu weathering of basement terrains. The geochemical data of Gwalior group clastic sediments also supports this view. These sediments are characterized by strong depletion of mobile constituents like Ca, Sr and Na, high Plagioclase Index of Alteration (PIA) values and strong positive correlation between Al_2O_3 and TiO_2, indicating severe weathering of upper crust and is in conformity with the world wide moist warm climates during the Paleoproterozoic. Positive correlation between $FeO^{(T)}$ and TiO_2 suggests iron retention in the Paleoweathering profiles and is attributed to oxygenated atmosphere. The sediments suffered post depositional potash metasomatism as indicated by comparatively low Chemical Index of Alteration (CIA) in A-CN-K systematics. K-enrichment from near zero to as high as 38% is inferred, with most of the shale samples show ~ 30% extraneous K2O additions. Depleted transition element (Ni, Cr, Co, Sc) contents, elevated LILE (K, Rb, Ba, Th, LREE) contents, fractionated REE patterns, strong negative Eu anomalies and high K_2O/Na_2O, Rb/Sr ratios (~10) in these sediments point toward K rich intracrustal granitic source component. The conspicuous depletion of Y over other LILEs in the Archean upper crust (AUC) normalised spidergram and steeper REE patterns (La/Yb_N ~ 12.57) compared to basement granites suggest a HREE depleted TTG source component. Minor contribution from tholeiitic mafic rock is evidenced by Th/Sc-Sc, La/Sc-Sc/Th, Co/Th-La/Sc systematics and positive correlation of transition elements with $FeO^{(T)}$ and TiO_2. Mixing calculations on the REE data suggest that upper continental crust of Bundelkhand craton was constituted of 40% granite, 40% TTG and 20% mafic rocks and thus convey the importance of LILE enriched subduction related granites in the upper crust during the Paleoproterozoic period.

On the contrary, the Mesoarchean basement quartzites are characterized by depleted LILE contents, very low K_2O/Na_2O and Rb/Sr ratios (~1), conspicuous HREE and Y depletion; and display steep REE patterns (La/Yb_N ~ 26.58) that are sub-parallel to

the basement TTG. These all features are consistent with the TTG composition of upper continental crust during the Mesoarchean. The trace element and REE systematics do not indicate any mafic component. However, presence of large negative Eu anomalies in these rocks suggests a possible HREE and K depleted Archean granite source.

The Kaimur Group sandstones are typically enriched in LILE, HFSE contents and severally depleted in transition metals. On the basis of A-CN-K systematics, relatively mild K-metasomatism and lesser weathering of source terrain is visualized, compared to Gwalior Group clastics. These samples display less fractionated REE patterns ($La/Yb_N \sim 8.29$) and are parallel to basement high-K granites (~2.5 Ga). These all features are compatible with their derivation from a sole granitic component.

These results have important implications on the crustal evolution of Bundelkhand craton during the Mesoarchean and Mesoproterozoic periods. The upper continental crust evolved from TTG composition at Mesoarchean to granitic composition at Mesoproterozoic period, with an intermediate composition during the Paleoproterozoic period. This phenomenon signifies the process of erosion. The erosion of upper TTG cover exposed the deep level granite batholiths that equally provided detritus to the Gwalior basin and signatures of which are attested in geochemistry of Gwalior clastics. The TTG cover was probably completely eroded during the Paleoproterozoic, thus no record of TTG is available in the Mesoproterozoic Kaimur sediments. The changes across the Archean-Proterozoic Boundary (APB) are governed by 'TTG effect' and 'subduction effect'. The REE patterns of sediments were flattened with time as the Archean sediments display steep REE pattern ($La/Yb_N \sim 26.58$) while the Paleoproterozoic Gwalior Group sediment display moderate fractionation (La/Yb_N ~12.57) and Mesoproterozoic Kaimur Group sediments show still lower fractionation ($La/Yb_N \sim 8.29$) of REE. This emphasizes the importance of 'TTG effect' over 'komatiite effect'. The excessive enrichment of LILEs and higher K_2O/Na_2O and Rb/Sr ratios in Proterozoic sediments compared to Archean sediments is governed by 'subduction effect'.

The Geochemical data of cherty Banded Iron Formation (BIF) of Gwalior Group suggest that these are near pure marine chemical precipitates and are characterized by modern seawater like components, such as negative Ce anomaly, positive La, Gd, Y anomaly and HREE enrichment over MREE and LREE in shale normalized REE+Y spidergram. The weak negative Ce anomalies in these BIFs suggest the beginning of global oxidative processes. The HREE enrichment, together with La spiking suggest

carbonate complexation of REEs and signify a possible alkaline pH of seawater. The REE patterns of some samples are identical to modern seawater while rest of the samples resemble with the patterns of coeval clastic rocks, indicating continental derivation of REEs as dissolved and as particulate load. The Nd isotope systematics of BIFs indicate very old crustal source of Nd and is consistent with results of clastic rocks. The εNd(T) of BIF varies from –6.29 to –13.67 and can be explained by the mixing of basement components such as 2.5 Ga old granites [εNd(T) ~ -8.75] and 3.3 Ga old Gneisses [εNd(T) ~ -13]. Pb and Sr isotope systematics of Gwalior Group BIFs and limestones also attest continental signature. However, three epsilon unit higher upper limit of εNd(T) [=-6.29] compared to basement granites [εNd(T)=-8.75], weak positive Eu anomalies and $(Eu/Sm)_{SN}$ ratio greater than one in these BIFs indicate a depleted mantle input to the sea water. The Nd isotope data of interbedded limestone also indicate dominant mantle inputs to the seawater and are characterized by positive to small negative εNd(T) values (-2.37 to +1.37) and younger Sm-Nd model ages (2090Ma-2562Ma) compared to the basement complex. Mass balance considerations also require a hydrothermal source of iron in BIF, as Fe poor felsic rocks can not yield enough Fe for precipitation of huge piles of BIFs. It is suggested that the surface water was oxic and was buffered with continent, while the anoxic bottom water received hydrothermal inputs and was buffered with mantle. Mixing of Fe rich anoxic bottom water and oxic surface water through the chemocline gave rise to the precipitation of BIFs. Since the REE content of continent derived surface water was many times greater than hydrothermal solutions, the REE patterns and Nd isotope systematics of BIFs prevalently show continent like signatures and juvenile mantle like signatures are masked.

The Pb-Pb systematics of Gwalior Group limestones yield an isochron age of 1914 ± 170 Ma and the overlying BIFs yield an age of 1850 Ma. Since these lithounits represent the upper sequence of Gwalior Group, an older age of the basal clastic sequence is obvious. Thus, the age of Gwalior Group seems to be bracketed between 2000 Ma and 1850 Ma. The BIFs of Gwalior Group represent the last phase of BIF metallogeny at the end of the Paleoproterozoic and are coeval to Gunflint Formation BIF of Canada. The data reveal that Gwalior Group is equivalent to the upper part of the Aravalli Supergroup of Rajasthan, which is bracketed between the age of 2200 and 1900Ma.

GEOLOGY AND GEOCHEMISTRY OF PALEOPROTEROZOIC GWALIOR GROUP SEDIMENTS, BUNDELKHAND CRATON, CENTRAL INDIA: IMPLICATIONS FOR PROVENANCE, DEPOSITIONAL ENVIRONMENT, TECTONIC SETTING AND EVOLUTIONARY TREND OF UPPER CONTINENTAL CRUST

THESIS

SUBMITTED FOR THE AWARD OF THE DEGREE OF

Doctor of Philosophy

IN

GEOLOGY

NURUL ABSAR

DEPARTMENT OF GEOLOGY
ALIGARH MUSLIM UNIVERSITY
ALIGARH (INDIA)
2005

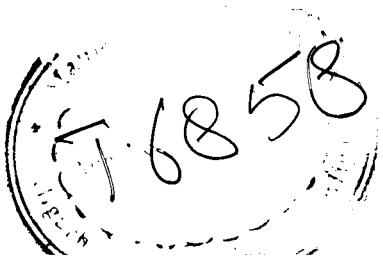
T 6858


T6858

DEDICATED
TO MY PARENTS

CERTIFICATE

This is to certify that the thesis entitled **"Geology and geochemistry of Paleoproterozoic Gwalior Group sediments, Bundelkhand craton, Central India: Implications for provenance, depositional environment, tectonic setting and evolutionary trend of upper continental crust"** is the record of bonafide research work carried out by Mr. Nurul Absar under our joint supervision. This work is an original contribution to the existing knowledge of the subject and has not been submitted any where for any other degree.

We allow Mr. Nurul Absar to submit the thesis for the award of the degree of **Doctor of Philosophy** in **Geology** of the Aligarh Muslim University, Aligarh, India.

Dr. (Mrs.) Minati Roy
(Co-supervisor)
Scientific Officer-F
Atomic Minerals Directorate for
Exploration and Research,
Department of Atomic Energy,
West Block-VII, R.K.Puram,
New Delhi-110066, India

Dr. Mahshar Raza
(Supervisor)
Professor of Geology
Department of Geology,
Aligarh Muslim University
Aligarh, U.P-202002,
India

ACKNOWLEDGEMENTS

I am highly indebted to Prof. Mahshar Raza and Dr.(Mrs.) Minati Roy for their supervision and guidance in carrying out this research work.

I express my sincere gratitude to Director, Atomic Minerals Directorate for Exploration and Research (AMD), Department of Atomic energy for granting permission and providing laboratory facilities to carry out this work.

I am highly obliged to Dr. S.M.Naqvi, F.N.A., for his kind guidance, help and encouragement.

Thanks are due to Mr. P.S.Parihar, Regional Director, AMD-New Delhi for his help and encouragement and extending logistics support for carrying out this work.

Helps and encouragement received from chairman, Department of Geology, A.M.U, Aligarh is gratefully acknowledged.

Innumerous discussions with Mr./s A.K.Roy, O.P.Somani, Vivek Bist, Sanjay Kumar, D.Bhattacharya, S.Srinivasan and P.K.Kothari of AMD-New Delhi during the field study helped me in understanding the geology of the area. Dr./s B.K.Pandey, Veena Krishna, U.K.Pandey, Mr./s S.Nayak, D.V.L.N Sastry, Mrs. N.Rupa and K.Asha of Geochronology Laboratory, AMD-Hyderabad, helped in generation of isotopic data. Mr. G.B.Rout and Y.Srinivas of INAA Laboratory, AMD-Hyderabad kindly analysed some of the samples for rare earth and trace elements. Dr. K.Shivkumar, Mr. K. Vijay Raj and P.K.Jain of XRF Laboratory, AMD-Nagpur, helped in obtaining the major and trace element data. I thank all these scientists for their help.

I am highly obliged to Dr.V.Balaram for allowing me to carry out geochemical analyses at ICP-MS Laboratory, National Geophysical Research Institute, Hyderabad. Dr. T. Gnaneswara Rao assisted in acquisition of rare earth and trace element data on ICP-MS and Mr. B.Dasaram assisted in sample preparation for ICP-MS analyses.

I have been greatly benefited by discussions with Dr. R.M.K. Khan for developing insights on the genesis of Precambrian BIFs. Discussions with Dr./s S.S.H.Jaffri, S.N.Charan, S.Dassharma, B.Sreenivas immensely helped me in understanding the Precambrian geological processes.

Thanks are due to Mr./s R.S.Redhu, L.N.Singh and N.K.Gautam for assistance in mapping and cartographic works.

This work would not nave been possible without the support and helps rendered by my friends Dr./s Shayak Ali, D.Srinivasa Sarma and M.Ramohan.

Professors. K.C. Condie, R.L.Cullers, P.G. Eriksson and Dr. M.E.A Mondal kindly provided reprints of some of their publications.

I thank all my family members for their patience and help.

Nurul Absar

NURUL ABSAR

CONTENTS

LIST OF TABLES

LIST OF PLATES

LIST OF FIGURES

INTRODUCTION

The Earth has several unique features among terrestrial planets; including the nature of it's crust, presence of oxygen bearing atmosphere and ocean system. Available data of the other planets indicate that none of the terrestrial planet seems to have continental crust. The geochemistry of the continental crust is the major problem in understanding the evolutionary history of the earth as a whole. What processes were involved in the formation of early crust? what was it's composition? and how it was evolved? are the basic questions of widespread interest and debate. Almost all the shield areas of the world have been extensively studied to address these questions and to understand the origin and evolution of earth's crust in space and time. These studies suggest considerable diversity in geological processes involved in evolution of the crust during different periods of earth's history. Two major factors are generally thought to be responsible for the formation of earth's continental crust, i.e. (i) the earth has significant amount of water and (ii) possibly it is the only planet on which plate tectonic processes have been operative (Condie, 1997). The evolution of Earth's crust-mantle-atmosphere-ocean system is now believed to be the result of interrelated processes which principally occurred because of secular cooling of the Earth since it's accretion at about 4.65 Ga ago. It is widely accepted that Archean heat flow was two to three times greater than that exists today and it has decreased exponentially since the early Archean (Condie, 1997, Eriksson et al., 2001). Smaller plates and faster recycling of oceanic crust is suggested for enhanced Archean heat loss (Windley, 1995). Although some forms of plate tectonics were operative during the Archean, it was fundamentally different from modern type plate tectonics. It has also been suggested that the Archean greenstones were generated as oceanic plateaus that were subsequently accreted to the continental nuclei (Abott, 1996; Condie, 1997; Polat et al., 1998; Puchtel et al., 1998). Therefore the first formed continental nuclei were probably submarine plateux produced from mafic and komatitic melts extracted from mantle plume. High temperature tail of mantle plume generated komatitic magma while the cooler head produced basaltic magma (Campbell and Griffiths, 1992). Underplating of spent plume material beneath the submarine plateux caused significant thickening of the lithosphere. First felsic magma comprising Tonalite – Trondhjemite - Granodiorite (TTG) associations was produced because of partial

melting of thickened mafic continental roots or mafic descending slabs. Since the Archean oceanic plate was warm and young, favourable conditions for melting reached only during slab dehydration due to steeper subduction geotherms. As a result, melting took place in the stability field of garnet and amphibole and both of these phases were left in residue, thus explaining the heavy REE and Y depletion of Archean TTG (Condie, 1997). Transition from plume generated greenstone tectonics to modern plate tectonic processes have taken place at the Archean-Proterozoic Boundary (APB), during which the influence on crust formation by large scale catastrophic mantle overturn events gave away to the plate tectonic processes similar to those of Phanerozoic and modern periods (Condie, 1997; Nelson, 1998). Near the end of the Archean, progressive cooling resulted in declining the thermal regime both in the upper and lower mantle. As a consequence, production of high-Mg komatiite magma ceased and submarine plateux became less frequent at the expense of island arcs. The cool post Archean subducting slab no longer melts, instead melting shifted to the metasomatised mantle wedge. The fluids released from descending slabs facilitated the melting of the mantle wedge, leading to the production of calc-alkaline basaltic magma that later underwent fractional crystallization to produce calc-alkaline felsic magma with distinct subduction geochemical component [Large Ion Lithophile Element (LILE) enrichment over Nb and Ta] but no HREE, Y depletion. Changes in thermal regime and style of plate tectonics consequently resulted in significant changes in igneous activity as outlined above and also in sedimentation, metamorphism, atmosphere, ocean and climate across the APB. The summary of these changes is listed in table 1. Many of these evolutionary events can be traced using the signatures left behind by them in the rock records accessible on the surface.

As a constraint on the evolution of crust-mantle system, it is important to know the temporal evolution of composition of continental crust. In spite of the ever-increasing database, it is still a matter of discussion and debate. Multidisciplinary approaches involving sedimentology, geochemistry and isotopic age data are required in this regard. Precise paleo-environmental reconstruction through sedimentological facies analysis can facilitate reconstruction of plate tectonic setting of the basin on the basis of modern analogues. In recent years the geochemistry of clastic sediment has been widely used as a tool to elucidate the composition of source area and upper continental crust. Indeed, the much of the present understanding about the composition and evolution of continental crust comes chiefly from geochemical and

Table1: Summary of changes across the APB

	Parameters	Archean	Proterozoic	Changes in the geologic record
1	Thermal Regime	High heat flow	Low heat flow	Nature of igneous, sedimentary and metamorphic rocks
2	Tectonics	Permobile tectonics, lack of distinction of stable and mobile regimes; whole-mantle convection	Plate tectonics, development of stable environments; Partial mantle convection	Nature of igneous and sedimentary processes
3	Igneous activity	Oceanic komatiitic basalt, high-Mg komatiites are frequent, felsic rocks are mainly TTG	Tholeiitic basalts, high-Mg komatiites infrequent, felsic rocks are mainly calc-alkaline granitoids	High Cr-Ni contents at similar Mg number in basalts in Archean; HREE enrichment, negative Eu anomaly in the Proterozoic granitoids.
4	Sedimentation	Greenstone belt association common, rare cratonic association	Cratonic association dominant	Decrease in Cr, Ni in Proterozoic sediments. Negative Eu anomaly and REE fractionation in the Proterozoic
5	Metamorphism	Low pressure	Intermediate to high pressure	Blueschists absent in Archean
6	Atmosphere	Reducing	Oxidizing	Appearance of red beds, laterites, iron-retaining paleosols, phosphorite in the Proterozoic, negative Ce anomaly in Proterozoic BIF.
7	Oceans	Mantle buffered sea water composition	Continent buffered sea water composition	High negative εNd in Proterozoic Chemical sediments, increase in $^{87}Sr/^{86}Sr$ in marine carbonates
8	Climates	Warm, rare local glaciation	Multiple global glaciations	Carbon cycle related global climatic fluctuations in the Proterozoic.

isotopic data gathered on sedimentary rocks (for e.g. Taylor and McLennan, 1985, 1995; Wronkiewicz and Condie, 1987, 1990; Naqvi et al., 1988, 2002; Condie, 1993,1997; Lahtinen, R., 2000; Condie et al., 2001; Bhat and Ghosh, 2001; Saha et al., 2004). Advantage of this approach lies in the fact that sediments preserve the 'memory' of the composition of contemporary upper continental crust, much of which is eroded from geological records. So this approach provides a window to look through the past tectonic processes and compositional evolution of continental crust. In this regard the most important are the relatively insoluble elements in natural water (such as REE, Th, Sc, Cr), which are transferred in bulk to the sediments, thus have the best potential for estimating crustal composition. Temporal evolution of upper continental crust can be deduced by comparing sedimentary rocks of different ages but of similar tectonic association. Trace elements and isotope systematics of marine precipitates provide a strong proxy to the ambient sea water composition thereby allow to study some of the aspects of chemical evolution of Precambrian ocean and atmosphere (e.g. Veizer et al., 1982, 1989, 1990; Jacobsen and Pimentel-Klose, 1988a, b; Derry and Jacobsen, 1990; Alibert and McCulloch, 1993; Bau and Moller, 1993; Bau et al., 1997). Because oceanic trace elements and isotope inventories reflect a balance between mantle-derived vs. continental derived input, the temporal evolution of seawater chemistry proxies offers important clues to past surface processes (Bolhar et al., 2004).

Although enough Precambrian rock record is available in Indian shield, very few studies have been carried out so far to characterize the evolutionary changes and crust building processes across the APB (Srinivasan and Naqvi, 1990; Bose, 1994; Bhushan, 1998; Sreenivas et al., 1999). Indian shield is a collage of several Precambrian blocks (Fig.1.1). The Tamil Nadu-Kerala block, Dharwar block, Bastar block and Singhbhum block, which were considered as separate entities during Archean, are believed to have been welded together to form the single South Indian Craton (SIC). Controversy however exists about the timing of their amalgamation (Radhakrishna, 1983; Radhakrishna and Naqvi, 1986; Radhakrishna and Ramkrishnan, 1988). The Bundelkhand block and Aravalli Block together constitute the North Indian Craton (NIC). The SIC and NIC were amalgamated along linear orogenic belt (Biswas, 1987), referred to as Central Indian Tectonic Zone (CITZ) or Son-Narmada Lineament (SNL). The SIC is characterized in well-developed and extensively studied Archean sequences but lacks unequivocal Paleoproterozoic rock

records. The NIC is characterized by the presence of Archean continental crust referred to as Bundelkhand Granite-Gneiss Complex (BGGC) in Bundelkhand block and Banded Gneissic Complex (BGC) in Aravalli block which served as basement for numerous younger Proterozoic sedimentary cover sequences. Continuous sedimentary record ranging in age from Mesoarchean to well into Neoproterozoic period is preserved in Bundelkhand-Aravalli block. In Aravalli block cover sequences are tightly folded and metamorphosed due to involvement in Delhi-Aravalli orogenic movements. However, the Proterozoic cover sequences of Bundelkhand block are flat lying and unmetamorphosed, as they have not affected by Proterozoic orogenic movements and hence are best-suited rock sequences to study the temporal evolution of upper continental crust.

In this regard the most important part of Bundelkhand block is the Gwalior sector where sedimentary rock records ranging in age from Mesoarchean to Mesoproterozoic is available within a small geographic area. The rocks show excellent preservation with subhorizontal dips and are completely unmetamorphosed as the area lies away from both the Aravalli-Delhi Fold Belt (ADFB) and Satpura Orogenic Belt. Moreover, the Archean Basements (Sarkar et al., 1984, 1986; Sarkar and Miller, 1996; Mondal et al., 1997,1998, 2002) as well as Proterozoic cover rocks (Rasmussen et al., 2002; Ray et al., 2002, 2003; Sarangi et al., 2004) are geochronologically well constrained and geological details of the area is available in the literature. Thus provide an excellent opportunity to study the geochemical evolution of upper crust by using the geochemistry of sedimentary rocks.

In Gwalior area, the basement complex is predominantly composed of 2.5 Ga high K-granite (Mondal et al., 2002) that contains well-preserved Archean metasedimentary enclaves of quartzite-phyllite association. Other than enclaves the Archean metasedimentary rocks also occur as separate outcrops having aerial extent upto 0.2 Sq.Km. Sedimentary rocks of Gwalior Group represent the Paleoproterozoic depositional history of the area and comprised of a basal clastic sequence (Par Formation) and a upper chemogenic sequence (Morar Formation), predominantly consisting of Banded Iron Formation (BIF). The Paleoproterozoic Gwalior Group is unconformably overlain by sandstone-shale sequence of Mesoproterozoic Kaimur Group of Vindhyan Supergroup.

Present study involves in sedimentological and geochemical examination, particularly of Gwalior Group sediments and also of older Archean metasediments (enclaves) and younger Vindhyan sediments with the following aims:

(i) Paleo-environmental reconstruction of Gwalior Group sediments by means of sedimentary facies analysis in order to infer the plate tectonic setting.

(ii) A classical whole rock geochemical investigation particularly of Gwalior Group sediments and also the underlying Archean metasediments and younger Mesoproterozoic Kaimur Group sediments by generating high quality geochemical data

(iii) To constrain the upper crustal composition and paleoweathering condition of Bundelkhand Craton during Paleoproterozoic by studying the geochemistry of clastic rocks of Gwalior Group.

(iv) To establish the temporal evolution of upper continental crust during Mesoarchean and Mesoproterozoic period and to infer differences in crust building processes at the Archean-Proterozoic Boundary (APB) by comparing geochemistry of Paleoproterozoic Gwalior Group clastics with those of basement Archean sediments and Mesoproterozoic Kaimur Group sediments.

(v) To infer the composition, paleo-redox condition of sea water; to establish relative continental flux and mantle flux to the sea water and chemical evolution of Precambrian sea water by studying trace element, REE, Nd, Sr, Pb isotope systematics of chemical sediments of Gwalior Group.

(vi) To generate isotope data on chemical sediments of Gwalior Group and utilize these data to date the age of sedimentation of Gwalior Group.

Present work is the first attempt to undertake a detailed geochemical study of sedimentary rock of Bundelkhand block. Although, informations on geology and stratigraphic positions of different rock formations are available in literature nothing is known about their geochemistry. Similarly, the basement rocks and overlying Vindhyan Group rocks are geochronologically well constrained but the Gwalior Group of rocks, particularly sediments have never been studied for the isotopic composition and thus no radiometric age data is available.

Organisation of the thesis:

The work is presented in eight chapters.

Chapter 1 deals with the general geological setting of Bundelkhand craton and stratigraphy of Gwalior Group sediments.

Chapter 2 provides detailed account of sedimentary facies analysis of Gwalior Group sediments. Different depositional systems are discussed and a depositional model is envisaged.

Chapter 3 contains the procedures of sampling, sample preparation and analytical techniques used for geochemical analysis of sedimentary rocks of different ages.

Chapter 4 describes the geochemical characteristics of clastic sediments of Gwalior Group. The composition and paleoweathering conditions of the provenance are discussed and inference regarding tectonic setting is drawn.

Chapter 5 deals with the geochemistry of underlying basement clastic metasediments (Archean) and overlying Kaimur Group clastic sediments (Mesoproterozoic) and compares them with the geochemistry of Paleoproterozoic Gwalior Group. The data is discussed in terms of geochemical changes across the APB and temporal evolution of upper crust during Mesoarchean and Mesoproterozoic.

Chapter 6 deals with geochemistry and Nd isotope systematics of BIFs of Morar Formation, Gwalior Group. The inferences regarding the source of iron and depositional environment of BIFs are drawn. The relative crustal and continental flux to the seawater and compositional evolution of seawater is discussed.

Chapter 7 describes the Pb, Sr, Nd isotope systematics of limestone and BIFs of Morar Formation, Gwalior Group. The age of sedimentation is established and isotopic signals are discussed in terms of provenance and relative continental to mantle flux to the seawater.

The summary and conclusion drawn from this work has been described in **Chapter 8**.

CHAPTER-I

General geological setting of Bundelkhand cratonic block and stratigraphy of Gwalior Group

1.1 General Geology of Bundelkhand Craton:

The Indian shield consists of two distinct crustal blocks (Fig.1.1) of composit nature occurring to the north and south of east-west trending Son Narmada Lineament (SNL) or Central Indian Tectonic zone (CITZ). These two crustal segments are distinctly different, not only in geological features but also in geophysical characteristics (Qureshi and Iqbaluddin, 1992; Verma and Banerjee, 1992) suggesting that they are apparently evolved independently (Mondal et al., 2002). The northern part referred herein as North Indian Craton (NIC) and is consisting of two Archean crustal blocks referred to as Bundelkhand Block (BB) and Aravalli Block (AB) occurring to the east and west of north-east trending Great Boundary Fault (GBF) respectively (Fig.1.1). Both of these blocks are characterized by the presence of Archean basement complexes i.e. Bundelkhand Granite-Gneiss Complex (BGGC) of BB and Banded Gneissic Complex (BGC) of AB which served as the basement for younger Proterozoic cover sequences ranging in age from Paleoproterozoic to Neoproterozoic. Bundelkhand Granite-Gneiss Complex (BGGC), covering an area of 26000 sq.km is situated in Central India. Recent high precision Pb-Pb Zircon ages of Bundelkhand massif (Mondal et al., 1997, 1998, 2002) confirm that both the BGGC and BGC share common geochemical characteristics and have similar temporal history, suggesting that these two prominent blocks of NIC evolved as single entity until at least 2.5 Ga ago. The Bundelkhand Block is overlain by cover sequences of Paleoproterozoic Gwalior basin in the northwest and those of Bijawar and Sonrai basin in the southeast and south (inset of Fig.1.2); which in-turn covered by Mesoproterozoic Vindhyan Supergroup. In the north BGGC appears to be extended well into the cover of recent sediments of Indo-Gangetic alluvium.

1.2 Geology of basement complex:

The dominant litho-unit of Bundelkhand block is a series of granitoid intrusions, which constitute about 80-90% of its exposed area. These granitoids were emplaced into granite-greenstone basement; consisting ultarmafics, amphibolites, fuchsite quartzites, banded iron formations (BIF), schists, calc-silicates and Tonalite-

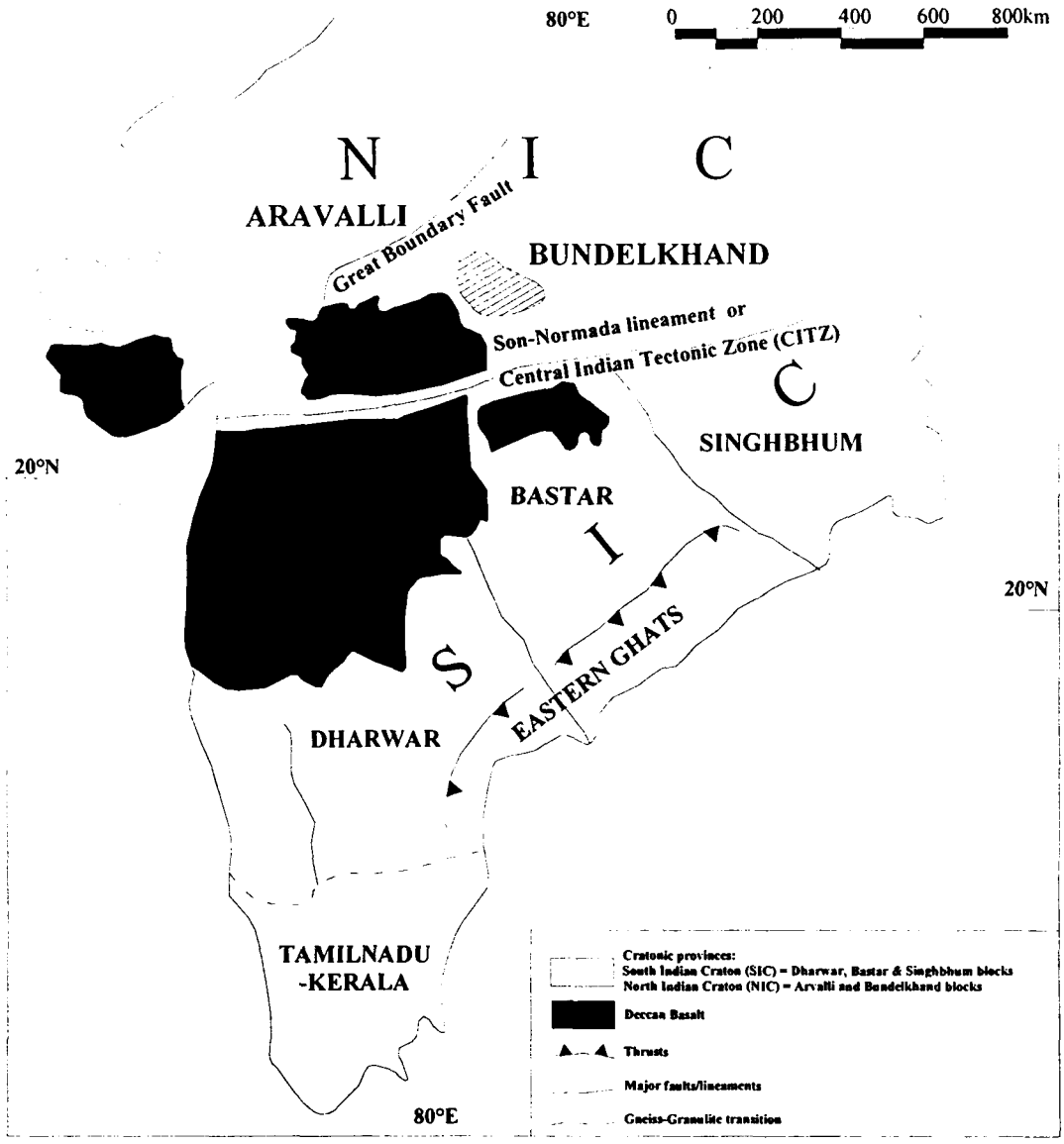

Fig.1.1: Sketch map of Indian shield showing various crustal blocks. The different crustal blocks of South Indian Craton (SIC) are separated by rifts. The Bundelkhand and Aravalli blocks of North Indian Craton (NIC) are separated by Great Boundary Fault (GBF). The location of Bundelkhand massif is shown as hatched area.

Trondhjemite-Granodiorite (TTG) and other metasediments which represent the rest of the outcrop of the area (Basu, 1986, Mondal & Zainuddin, 1995,1996, 1997, Mondal et al., 2002). These basement components of Archean age occur only as enclaves and sometime as separate outcrops. The basement rocks are intensely deformed, whereas the granitoids are generally undeformed, supporting the pre-granitoid origin of the gneisses and other metasedimentary enclaves (Basu, 1986). Three different phases of granitoids are identified in the massif viz. hornblende-, biotite- and leuco-granites, which were emplaced in chronological order (Mondal et al., 1997, 1998, 2002). It appears that a number of plutons have coalesced to give rise to major batholiths. In the Bundelkhand massif, large-scale granitic magmatism was followed by emplacement of a variety of minor intrusions. Amongst these the pegmatite veins, emplaced during different stages are wide spread. Porphyry rocks of varying composition and texture and acid volcanic rocks (rhyolites, dykes of rhyolitic breccia, with angular enclaves of porphyries) are also found. All the above lithologies are traversed by NE trending quartz reefs and NW trending mafic dyke swarms that represent the last magmatic activity in the massif (Basu, 1986, Mondal & Zainuddin, 1996, Mondal et al., 2002).

In Gwalior basin and surrounding area that is the subject of the present study, the basement rocks predominantly composed of biotite granites, which occur as domal outcrops. Intrusive NE trending quartz-reefs and NW trending mafic dykes are important features of the basement. The quartz reefs as well as mafic dykes are of pre-Gwalior age. Systematic mapping carried out during course of present study along basement-Gwalior contact shows that the reefs and the dykes continue below the Gwalior cover and appears to have been peneplained before Gwalior sedimentation started. The NE trending quartz reefs constitute an important physiographic feature as they occur as sharp ridges and could be even traced below the Morar Formation (Upper Gwalior Group), particularly in the eastern part of Gwalior basin. Even Morar sediments also could not cover them as these quartz reefs are projected over it. Another important feature is presence of Archean supracrustal enclaves within the granites. These supracrustal of Archean crust are composed of cratonic sediments of quartzite-phyllite association along with minor metabasics. This is evident from their occurrence as remnant/enclave within the granitic massif (Plate 1.1). The remnants of amphibolite enclave are noticed near village Bilaua (Plate 1.2) and east of Sidhpura Village. Biotite-schist has also been observed in some localities. A northwest-

Plate1.1: Out crop of Archean quartzites in Pichhor village. Note very large out crop forming a hillock that are enclosed within basement granite terrain. Also see telephone tower for scale.

Plate1.2: Ambhibolite enclave within Bundelkhand Granite.

Plate1.3: Tight folding within Archean quartzites, photograph from (A) Near Ladera Village and (B) Pichhor village

Plate1.4: Archean quartzites engulfed within Bundelkhand Granite (Gijora Area). From the outcrop pattern it is evident that granites were emplaced along the fracture/weak planes of the pre-granite crust.

Plate1.5: BIF pebble bearing conglomerate at the base of Archean quartzites. Note matrix supported conglomerate with BIF/Chert clasts

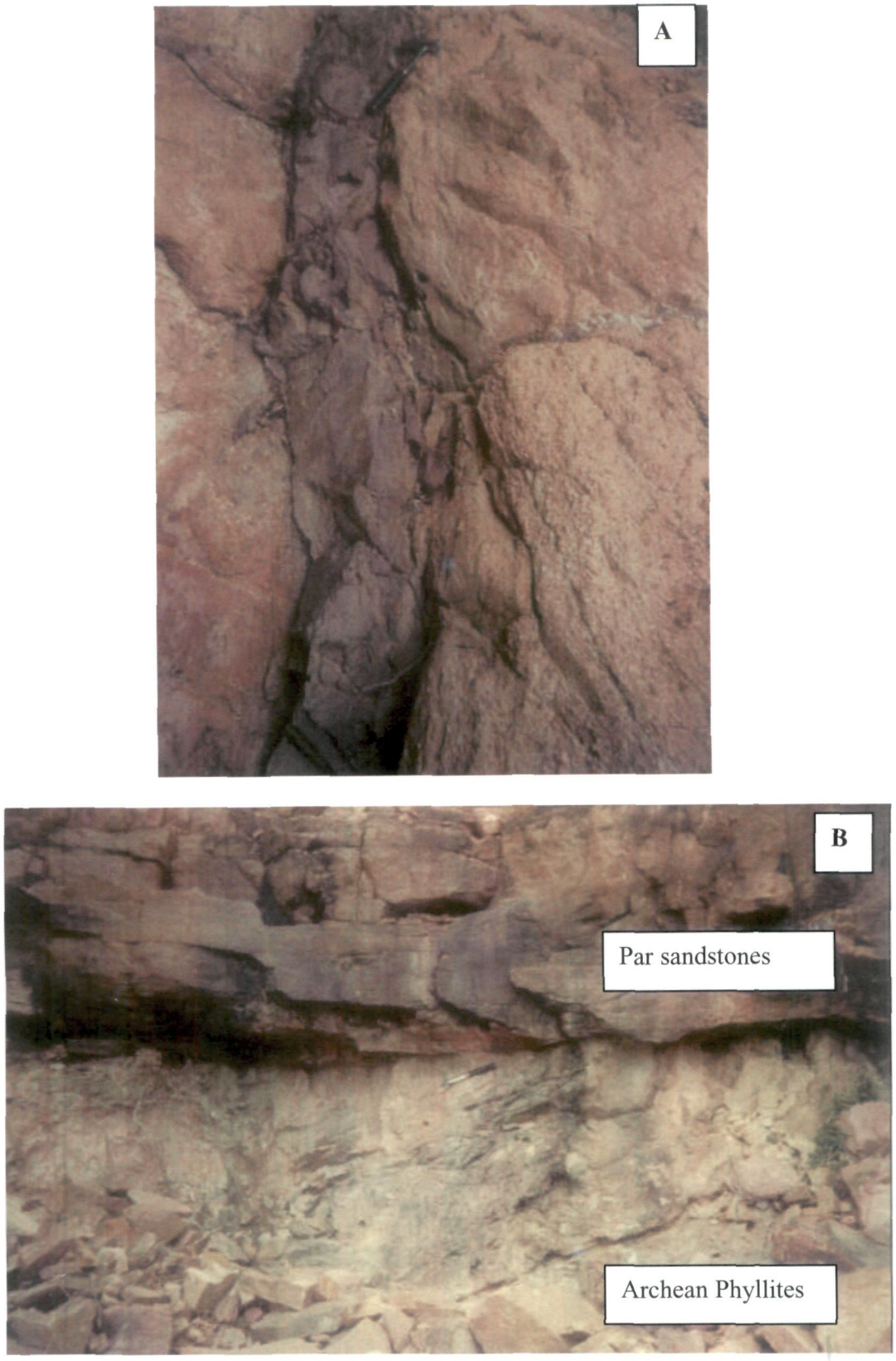

Plate1.6: Archean phyllite enclaves within Bundelkhand granite. (A) Red Phyllite xenoliths and (B) outcrop of green phyllites that form the base of Gwalior Group near Sidhpura village.

Plate1.7: Typical ball like fabric of the weathering surface of the Archean quartzites.

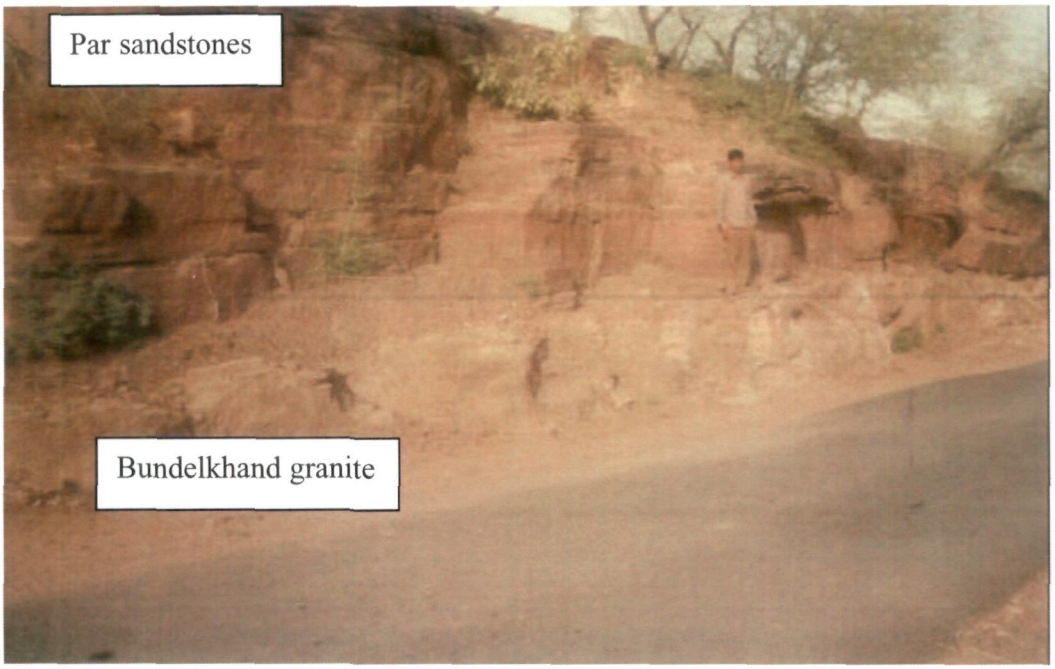

Plate1.8: Unconformable contact between the basement Bundelkhand Granite and Gwalior Group sediments. Note subhorizontal strata of Gwalior Group lying over basement complex.

southeast trending ridge of quartzite is found at Ladera, which can be intermittently traced back to the Pichhor village in the southeast and extended up to Jarga through Bastari in the northwest where it is projected over the cover rocks of Morar Formation. In Pichhor and Bansi-Ladera area, these quartzites are steeply dipping and highly deformed. Nevertheless the sedimentary beddings can be readily recognized as compositional banding. Tight folding is generally observed within these rocks (Plate 1.3). The peculiarity of the quartzite is the presence of rounded, ball like fabric (Plate 1.7), which is an undiagnosed feature. About 5m thick conglomerate horizon has been observed at the base of this Archean quartzite that is polymictic (matrix supported) in nature and contains angular clasts of BIF and cherts. In Gijora area these quartzites occur as thin elongated body surrounded by granite (Plate 1.4), and sometimes contains BIF-chert clasts. There are pockets of green and red coloured Phyllites with limited dimension (Plate 1.5). Significantly, near Sidhpura the Par sediments directly overlie the weathered phyllites of Archean age (Plate 1.6). These quartzite-phyllite assemblages are thought to be of pre-granite eternity as evidenced from their contact relationship with the granites. It is to be mentioned that detrital zircons of similar quartzitic rock of Banded Gneissic Complex (BGC), Aravalli block have been dated at 3230 Ma on the basis of zircon evaporation $^{207}Pb/^{206}Pb$ data (Roy et al., 2001). The depositional age of these quartzites are bracketed between the maximum age of deposition i.e. 3230 Ma and age of amphibolite that intrude these quartzitic rock i.e.2828 ± 46 Ma (Gopalan et al., 1990, Roy et al., 2001). Roy et al., (2001) interpreted that there is not much age difference between the depositional age of quartzites and intrusion of amphibolites; thus it is reasonable to believe that these quartzites were deposited at ~2.9 Ga.

A porphyry acidic dyke is emplaced into basal gritty Par sandstone of Gwalior Group at Sidhpura. The breadth of this dyke is 1 to 2 m and extends for about 500 m in ENE-WSW direction. Based on chemical data and petrographic observation these are altered rhyolite. This is the first ever report of post Gwalior acid magmatic activity in the massif.

The Bundelkhand block is now geochronologically fairly well defined. K-Ar ages of hornblende and biotite from enclaves of amphibolite and mica schist within the granitoids vary between 2520 and 2187 Ma (Sarkar and Miller 1996). Crawford (1970) assigned the Rb-Sr isochron age of 2555 ± 55 Ma of the granitoid as the stabilization of the Archean crust in this part of Indian shield. Sarkar *et al.* (1984)

reported the whole rock Rb-Sr isochron age as 2359 ± 53 Ma to 2246 ± 78 Ma for different granitic phases of the massif. The Rb-Sr age of 3503 ± 99 Ma of TTG Gneisses of Babina area is the oldest reported age of the BGGC (Sarkar et al., 1996). The ion microprobe studies on $^{207}Pb/^{206}Pb$ of zircons separated from Bundelkhand granitoid suggested major phase of granitoids intrusion at 2.5 Ga with an older granitic component of 2.7 Ga (Mondal et al., 2002). The zircons of gneissic rocks have been assigned at 3.3 Ga, which dates the oldest TTG magmatism of the massif. The age of 2.5 Ga has been interpreted as the over all stabilization of the massif (Mondal et al., 1997, 1998, 2002). Based on recent $^{40}Ar/^{39}Ar$ age data, the mafic dyke swarms of BGGC were emplaced in two phases at 2150 Ma and 2000 Ma (Mallikharjuna Rao et al., 2005).

1.3 Geology of cover sequences

The Paleoproterozoic sedimentation in Bundelkhand Craton in Central India is represented in three discrete basins, viz. Gwalior basin, Bijawar basin and Sonrai Basin (inset Fig.1.2). All of these basins are homotaxial in nature and characterized by intracratonic siliciclastic sediments in basal formations followed by platformal sequence of chemical sediments like carbonates and BIFS in the upper formations. While the Gwalior basin was developed at the northwestern fringe of the Bundelkhand massif, the other two occupy southern fringe. The basal rift related volcanics which are preserved in type areas of Bijawars, are non-existent in Gwalior basin. Mafic magmatism in Gwalior basin is represented only by post Gwalior intrusive sills and dykes. During the whole episode of Proterozoic sedimentation the Bundelkhand massif appears to have remained as basement high and provided detritus to the sedimentary basins developed at its peripheries.

1.3.1 Bijawar Group:

The Bijawar basin is situated in the southern part of the Bundelkhand massif. The basal Moli Subgroup is comprised of coarse grained clastic sediments like conglomerate, grits and cross bedded sandstones with two vesicular volcanic flows (Kawar Formation). The Kawar Formation is overlained by Malhera Chert Breccia Formation (MCBF) consisting of chert, jasper bands and chert breccia. The Bajno Dolomite Formation that predominantly comprised of white to pink colour dolomite

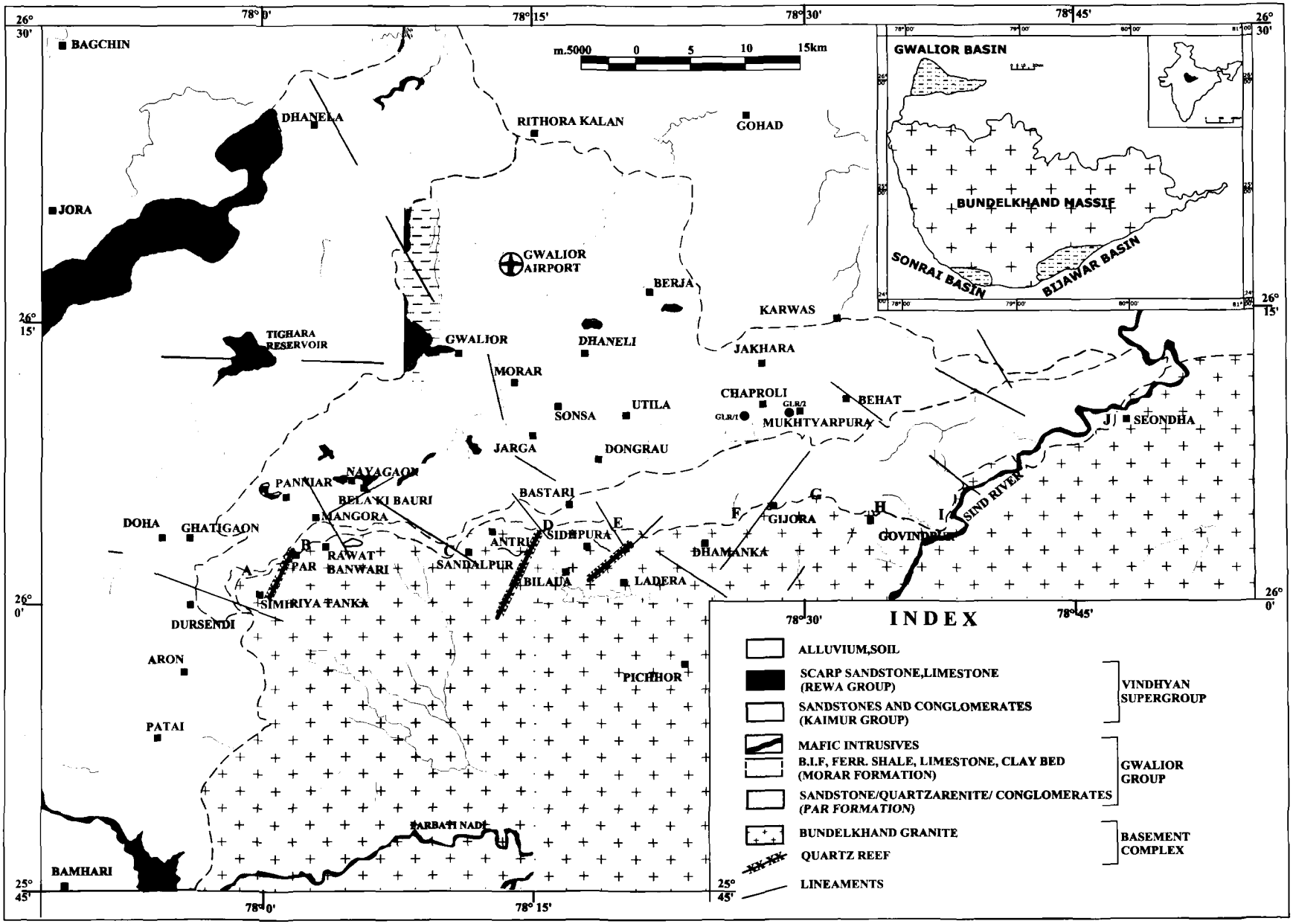
m.5000 0 5 10 15km
BAGCHIN
DHANELA
RITHORA KALAN
GOHAD
JORA
GWALIOR AIRPORT
BERJA
KARWAS
TIGHARA RESERVOIR
GWALIOR
DHANELI
JAKHARA
MORAR
CHAPROLI
BEHAT
SONSA
UTILA
MUKHTYARPURA
SEONDHA
JARGA
DONGRAU
NAYAGAON
PANNIAR
BASTARI
BELA KI BAURI
MANGORA
DOHA
GHATIGAON
SIDHPURA
ANTRI
GIJORA
GOVINDPUR
SIND RIVER
DHAMANKA
RAWAT
PAR
BANWARI
SANDALPUR
BILAUA
LADERA
SIMHRIYA TANKA
DURSENDI
ARON
PICHHOR
PATAI
PARBATI NADI
BAMHARI
GWALIOR BASIN
BUNDELKHAND MASSIF
SONRAI BASIN
BIJAWAR BASIN
INDEX
ALLUVIUM,SOIL
SCARP SANDSTONE,LIMESTONE (REWA GROUP)
SANDSTONES AND CONGLOMERATES (KAIMUR GROUP)
VINDHYAN SUPERGROUP
MAFIC INTRUSIVES
B.I.F, FERR. SHALE, LIMESTONE, CLAY BED (MORAR FORMATION)
SANDSTONE/QUARTZARENITE/ CONGLOMERATES (PAR FORMATION)
GWALIOR GROUP
BUNDELKHAND GRANITE
QUARTZ REEF
BASEMENT COMPLEX
LINEAMENTS

with minor chert bands overlies the MCBF, which is intruded by mafic sills of Dargawan Intrusive Formation. Gangau Subgroup of rocks unconformably overlie Moli Subgroup and consist of basal Hirapur Phosphorite Formation and upper Karri Ferruginous Formation. The Karri Ferruginous Formation is predominantly consisting of ferruginous shale, sandstone with minor hematite bands (Kumar et al., 1990, Mathur, 1982).

1.3.2 Sonrai Group:

The western part of the Bijawar basin is known as the Sonrai basin and is broadly divided into the basal Sonrai Formation and upper Solda Iron Formation. The Sonrai Formation is consisting of basal phosphorite bed, clastic sandstone with interbedded lava flows (Kurrat volcanics) and carbonates (Rohini carbonates). The Solda Iron Formation is predominantly comprised of ferruginous shale, jasper and BIFs.

1.4 Geology of Gwalior Group:

Gwalior basin is situated on the northwestern fringe of Bundelkhand massif (Fig.1.2). The Gwalior group sediments were deposited over the denudated, irregular surface of Bundelkhand Granite-Gneiss Complex (BGGC), which is marked by intense gravity low (Verma & Banerjee, 1992). The Gwalior basin is an east-west trending basin with a exposed strike length of about 80 km and a down dip northward extension of about 35 km, spreading over an area of about 2400 sq.km (Fig.1.2). Majority of the basin to the north and west is blanketed by Mesoproterozoic Kaimur Group of Vindhyan Supergroup. The Gwalior group of rocks are exposed in a prominent E-W trending escarp section, which mark the unconformity contact with basement complex (Plate2.1). While the western most boundary of the basin is concealed under Kaimur sandstones, the eastern most boundary is truncated against the northeast - southwest flowing Sind river. The river probably represents a regional fault. In the east of the Sind river the outcrops of Gwalior Group are scanty and covered by thick alluvium. Thus the original dimension of Gwalior basin might be quite extensive than presently exposed area. The evidence of continuance of Gwalior strata in west below Kaimurs has been found in Atomic Minerals Directorate for Exploration and Research (AMD) drillholes near Doha area, where thick Gwalior Group sediments have been intercepted below the Kaimur Group sediments.

The Gwalior basin remained poorly studied. The data generated so far are of preliminary nature both in quality as well as in quantity. Very early studies, carried out by Hacket (1870), Meddlicott (1875) and Heron (1922), suggested two fold stratigraphic nomenclature for the whole sequence. The lower most arenaceous unit has been described as Par Subgroup and the upper chemogenic iron formations are described as Morar Subgroup. The later studies were mainly confined to the study of mafic rocks (Dubey, 1930; Bajpai, 1935; Varadarajan & Verma, 1971,1973). While Mathur (1982) attempted to correlate these rocks with other Precambrian basins of India, Adil (1999) carried out preliminary sedimentological work in a limited area.

During the present study mapping has been carried out along specific sections to establish the detailed stratigraphy of the basin. The revised stratigraphy is given on table 1.1 and stratigraphic relationship between different lithounits of Gwalior Group is diagrammatically presented in Figure 1.3. The lithofacies examined along and across the strike in escarp sections are discussed as follows:

Table 1.1: Stratigraphic succession of Gwalior basin, Gwalior district, M.P.

Group	Formation	Rock unit
Kaimur Group of Vindhyan Super group		Matrix rich sandstone, quartzarenite, Shale BIF Pebble Breccia conglomerate
---------- Unconformity----------		
Gwalior Group	***Morar***	Mafic Intrusive rock Banded Iron Formation with impersistent limestone horizons. Clay bed Black siliceous shale
	Par	Quartzarenite, Black shale Arkosic sandstone, Lithic sandstone, Ferruginous sandstone, Intercalated sand-mud Quartz pebble conglomerate
---------- Unconformity----------		
Bundelkhand Granite-Gneiss Complex (BGGC)		Pink granites, grey granites, Quartz reefs and mafic dykes with xenolithic older gneisses and metasedimentary enclaves

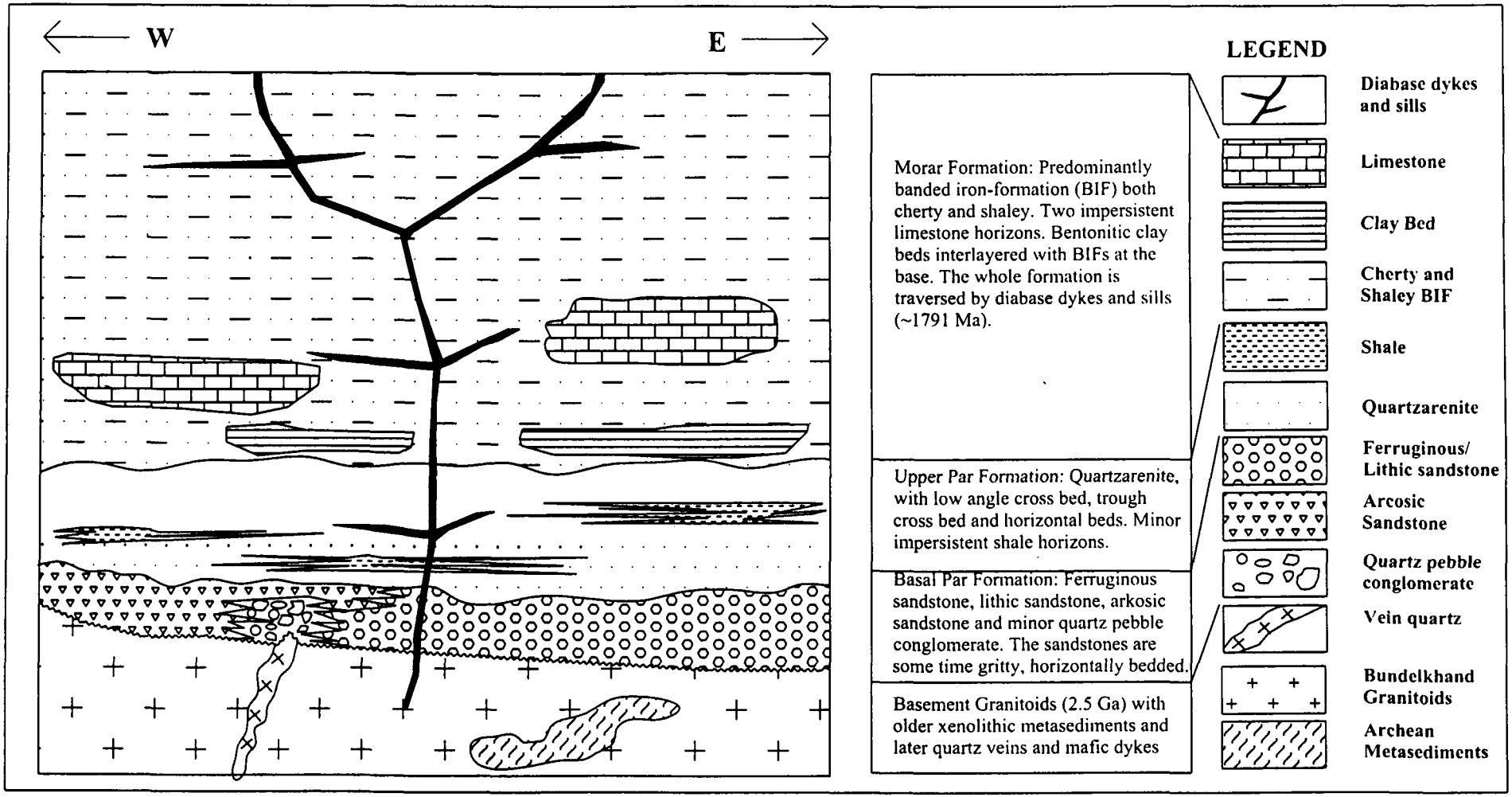

Fig.1.3: Diagram illustrating the stratigraphic relationships of different litho-units of Gwalior Group.

1.4.1 Par Formation:

The name of Par Formation has been derived from Par village and is the type area of Par Formation. The basal Par formation unconformably overlies the basement Bundelkhand granite complex (Plate1.8), and is represented by variety of siliciclastic sediments. For the sake of convenience, the whole strike line from east to west is divided herein into six representative sections and is described accordingly as members. The original basinal setting is very well preserved as the strata is unmetamorphosed and structurally undisturbed with a gentle sub-horizontal dip (2^{o}-5^{o}). The thickness of sediment increases from fraction of meters to several meters in down dip direction (toward north) along the N-S stream cutting section. Similar situation has been found in the borehole lithology where the thickness of Gwalior sediment increases toward north, thus preserving the original basin slope. The different members from west to east are described in the following paragraphs.

Arkosic Sandstone Member:

The Par sandstones in the western part are represented by arkosic sandstones. The sandstones are coarse grained, poorly sorted, silica cemented with angular grains of abundant K-feldspars and quartz. No graded bedding has been observed, instead the pebbly coarser grained layer occur as pulses and contain well-rounded grains. The feldspars are generally fresh indicating nearness of provenance. This unit also contains the lenticular quartz pebble conglomerate (QPC) with highly well rounded to subrounded quartz pebbles of variable size. These QPCs are local in nature and appear to have been derived from basement quartz reefs as they occur in the close vicinity to it. The arkosic unit grades into fine grained siliceous quartzarenite upwards. In down dip direction it contains considerable shaley intercalations. The arkosic sandstone unit is quite extensive and traced upto Par village in the east, where it grades to lithic sandstone in eastern part.

Conglomerate Member :

This member is represented by oligomictic quartz pebble boulder conglomerate (QPBC) and quartz pebble conglomerate (QPC). These are clast supported conglomerates, forming about 2-6m thick beds and contain pebbles and boulders of quartz probably derived from basement quartz reefs. The boulder size quartz clasts are angular and very local in nature, which probably filled the depressions in the basement flanked by the quartz reefs. The smaller pebble size clasts are subrounded to very well rounded, indicating substantial reworking probably along

a shoreline. The basal bouldery unit, upto 4m thick, also contains rare granite clasts. This unit is overlain by pebbly and granule unit of about 2m thickness, having well rounded quartz clasts set in a sandy matrix. The granules are extremely well rounded and sorted representing extreme reworking along shore. The pebbly unit is best developed around Rawat-Banwari village and is radioactive. The radioactivity is due to presence of thorium, bounded in heavies like zircon and monazite. Lithologically this unit resembles modern day beach placers with heavy refractory minerals. The arkosic sandstone member is occurring above this unit, with comparatively lesser thickness, is inturn overlain by well-sorted quartzarenite member that shall be described in the later part of this chapter.

Lithic Sandstone Member :

The arkosic sandstone member pinches towards east and is laterally merged towards a matrix rich moderately ferruginous sandstone unit near Sandalpur. This unit is about 20-30m thick and composed of clay matrix rich sandstone with variable grain size. The granule size layers are thin (few cm thick) with extremely well rounded quartz granules. These are generally flat-bedded stacked sand bodies. Each flat bedded unit internally consisting of low dip cross-bedded units. Wave ripple trains and ladder ripples are very well preserved. This feature in combination with low dip cross beds indicates deposition in shallow water conditions. In the down dip direction this unit contains considerable shale intercalations. The typical exposure of intercalated shale and sandstone can be seen along railway cutting near Sandalpur. This unit is overlained by well washed quartzarenite unit, which occur as overlapping transgressive sheets.

Ferruginous Sandstone Member:

In the central and eastern part of the basin the basal members of Par Formation are extremely ferruginised, cherry red in colour. This member is persistent and thickens toward the east. In the type areas near Gijora village it is about 30m thick, whereas in the eastern part of the basin near Seondha it attains a thickness of about 80m. Lithologically it is similar to lithic sandstone member but is affected by pervasive ferruginisation. The sandstones of this unit are of variable grain size but medium grained sandstones are most common. The granules and coarse sands are extremely well rounded, embedded in clay matrix. This unit is generally flat bedded with characteristic sheet like geometry. Low dip cross beds, both tabular and trough type have been observed. In general, these sandstones are matrix rich, some time

minority sand (quartz) grains are dispersed in clay matrix and are petrographically identified as quartzwacke. The tops of individual beds are characterized by the presence of well preserved wave ripples. The ripple crests are straight continuous to bifurcated. Ladder ripples are also very well preserved. The wave interference is clearly depicted as ripple train interferences. Crude graded bedding is observed at few outcrops. Fining upward sequences are common, each topped by rippled unit with mud drapes. There are shale units of 5-6m thick at the top of this member. This ferruginous sandstone member is capped by flat bedded, well washed sheet like quartzarenite member. The sedimentological aspects are dealt in detail in chapter-II.

Intercalated Sand-Mud member:

This unit is similar to Ferruginous sandstone member with respect to lithology and sedimentary features. It is characterized by additional intercalated muds and sandstones similar to rhythmites. Individual mud and sand layer are rippled, about 1-2cm thick. The muds as well as sandstones are green coloured, affected by later ferruginisation event.

Quartzarenite Member :

The basal Par members described in the earlier paragraphs vary across and along the strike. The basal unit is overlained by transgressive well washed mature quartz arenite. This unit is monotonous, extensive, cropping out through out the basin and overlaps the basal unit. The outcrops of the above described basal members are available only along the E-W trending escarpment section in the southern most margin of the basin where it displays an unconformable contact with the basement granites. In rest of the areas the basal members are capped by quartzarenite member. These quartzarenites are fine grained, very well sorted, mineralogically and texturally mature silica cemented quartzarenites. The quartz grains are sub angular to angular in nature because of their extreme fine-grained nature. This unit is occasionally topped by mega ripples. Dune like large bedforms are observed in Bhadona section (about 2 km south of Utila), where at least 25m thick quartzarenites unit is exposed along contact of Par and Morar Formation because of post Gwalior faulting. The lee side of this dune contains small-scale longitudinal ripples, crest line of which is oriented perpendicular to the larger bed form, thereby resembles with the classic ladder ripples. Considerable shale intercalations are associated with this unit at several locations.

The above lithofacies has been identified on the basis of outcrop examination. As the Gwaliors are subhorizontal strata, only the topmost arenitic unit is exposed.

The boreholes drilled by Atomic Minerals Directorate (AMD) in the central and western parts of the basin, revealed the lithofacies in the deeper part of the basin. Par Formation contains huge thickness of alternating shale and sandstone sequences. The scale of alternation varies from few cm to several meters. The shale/mud intercalations are of three types (i) Red ferruginous shale (ii) Green shale and (iii) Black carbonaceous shale. Considerable thickness of black shale has been observed in the deeper horizons of borehole cores, which is totally absent in surface exposures. The thickness of upto 150m of Par Formation has been intercepted in boreholes drilled in the periphery of the basin (Fig.1.2), implying much more thicker Par Formation and Gwalior Group as computed by earlier workers.

1.4.2 Morar Formation:

Chemogenic Morar Formation of Gwalior Group conformably overlies the clastic Par Formation. Although there is marked change in style of deposition, composition of chemical Morar Formation to that of clastic Par Formation, a depositional break (unconformity) is not recognized. Both Par and Morar formations maintain same depositional strike with similar basinal configuration. It is obvious that there may be little time gap in deposition, but an unconformity or a depositional hiatus cannot be ascertained. Subsurface lithological data obtained from boreholes drilled in central and western part of the basin shows occurrence of similar type of black shales at different depths, both in the upper part of Par Formation as well as in the lower part of Morar Formation. This indicates fluctuating redox fronts are common attributes of the both formations, substantiating the field observation of continuous sedimentation through out the Par-Morar formations.

Morar Formation consists of about 800m thick volcano-sedimentary sequences, which overlap the basal Par arenite as transgressive sheet, and occupies most of the basin except the southern most margin where Par Formation is exposed (Fig1.2). The chief constituents of Morar Formation include banded iron-formation (BIF), ferruginous shale, Black shale/cherty shale, two thin impersistent limestone units and a conspicuous kaolinitic clay bed at the base. Mafic dyke swarms intrude into the Gwaliors succession (Fig.1.3). The lithological details of different lithounits are described in the following paragraphs:

Banded Iron Formation (BIF) member:

The Fe-rich rocks are the major constituent (>90%) of Morar Formation. These are Superior type BIFs consisting of rhythmic Fe rich and silica rich cherty bands. These are predominantly oxide facies BIF with hematite as major mineral constituent of Fe rich bands. Alteration of hematite to goethite is common. Carbonate and sulfide facies BIFs are not observed. However in few thin sections rhomb shaped goethite has been found which could be alteration product of siderite. The silica bands are composed of cryptocrystalline spherulitic chert. Minor iron impurity some time give bright red colouration to cherts. Colour of chert bands varies from normal grey to red (jasper) and black.

The compositional banding in BIF is observed in outcrop scale (macrobands), hand specimen scale (mesobands) and microscopic scale (microbands, aft varves). Mesobands can be observed in individual macrobands. The contacts between compositional bands are sharp.

The iron formations can be typified according to the clastic material content as (a) Cherty BIF, (b) Shaley BIF and (c) Ferruginous shale.

(a) Cherty BIF: These are composed of alternate iron and silica bands with little or no shaley material content (Plate2.23). Due to their indurated nature they provide fresh outcrops. They often grades to pure chert or pure hematite within a single macroband. Reworked chert fragments are rarely present in some out crops. A conspicuous feature of these BIFs is that in many outcrop the top surface of individual bed occur as inverted bowl (pod shaped). In cross section they appear to be lenticular body with quartz occupying the central portion rimmed by chert or hematite bands. This remained an undiagnosed feature and may owe their origin due to biogenic activity. Central quartz rich portion may be related to silica secreting organism like diatoms.

(b) Shaley BIF: These contains considerable shaley material and can be readily identified in outcrop as they do not form ridges and have weathered shale like appearance (Plate2.24). The overall high abundance of clastic shaley material in BIF and ferruginous shales indicate that a carbonate barrier reef was absent during Morar sedimentation which is common in other Proterozoic BIF related basins of Canadian and Australian shields (Trendall and Morris, 1983). The carbonate reef hinders the clastic material's entry to the basin. That is why, Morar BIFs contains lot of shaley clastic material except the cherty BIF facies.

(c) Ferruginous Shale: Ferruginous shales are quite abundant lithofacies. They occur as thick units that provide individual outcrop and as well as thin layer within BIFs. These shale units probably represent sedimentation during periods of regression.

Black Shale Member:

Black shales / black siliceous shales constitute the basal Morar Formation in the deeper part of the basin. As Gwaliors are undisturbed subhorizontal strata, the black shale facies are found only in boreholes drilled in relatively deeper parts of the basin (plate 2.21 & 2.22). The surface exposures are found near Bela Ki Bauri, immediately below the cherty limestone unit. The black shales are quite thick (~30m), fine grained and contain organic carbonaceous material. Globular migratory type carbonaceous material has been identified in few thin sections. Black shales are often pyritiferous indicating that euxinic acidic environment prevailed in the deeper parts of the basin.

Within these Black shales a few cm thick cherty BIFs are observed, indicating that the BIF deposition occurred in pulses due to fumarolic activity near vents/fissures. The availability of oxygen for precipitation of iron in an otherwise anoxic environment is not clear. However the majority of the BIF appears to have been deposited in a raised sea level over this black shale unit.

Similar type of black shales are found at different stratigraphic levels within quartzarenites of Par formation. As black shales represent deposition in anoxic condition under a thick water column below the photic level, the presence of black shale at different stratigraphic level implies wide fluctuation of redox front because of sea level changes. Redox front moves basin ward with sea level rise and vice versa. The normal green shales grades to grey and black shales with the increase in carbonaceous material content. It appears that the microorganisms flourished at shallow oxygenated part with abundant nutrient supply. The petrographic study indicates that carbonaceous materials in these black shales are probably transported organic detritus.

Limestone Member:

The two impersistent limestone horizons of 5 to 15m thicknesses are sandwiched within the BIF member. Outcrops of limestone are available in central part of the basin near village Utila and in Chaproli-Dangora area, north of Behat. The Utila-Chaproli limestones are micritic type with microsparites as the major mineral

constituent. Some of thin layers/beds (few cm thick) are dolomitic, characterized by elephant skin weathering. Dolomitic limestones are comparatively hard and compact than micritic variety. Within these limestones calcareous shales are observed along bedding planes, especially in Utila area (Plate2.26). The limestones in the western part of the basin near Bela Ki Bauri are thin with about 5m thickness and are impure cherty limestones. Crystalline calcites are found along with cherts, because of their proximity to basic intrusives. Field setting shows that the limestones units are thin and impersistent in nature. These may have been deposited during minimal volcanic/fumarolic activity, when pH of basinal water increased due to silicate weathering flux other wise in the dominant BIF depositional regime. In chaproli area, the limestones are banded in nature with rhythmic bands (mesobands) of jasper and black cherts (Plate2.25). This phenomenon also indicates localized carbonate precipitation as volcanic activity did not die out completely.

Clay Bed member:

Kaolinitic clay beds are an important constituent of Morar Formation. Fresh white kaolinitic clay layers of varying thickness (5-15m) occur at the base of Morar Formation near Par-Morar contact (plate2.27). These are persistent units though out the basin and occur at particular stratigraphic level. This implies that clay beds were deposited due to explosive acid volcanic activity within a restricted time frame. Their absolute fine grained nature and freshness indicate that they were deposited as ash fall out of wind blown material from distal volcanic source. Due to their extreme fine grained nature, identification of glass shards is minimal. However in few thin sections glass shard like feature and bipyramidal quartz has been observed. Recently volcanic cauldron like structure has been discovered in Bundelkhand massif (Jain et al., 2001), representing the volcanic activity of Pre-vindhyans age. This explosive acid volcanism may be the source of felsic clay beds of Gwalior basin. The thin mm scale layers of Fe rich laminae are continuous for several meters within these clay beds, indicating very slow rate of deposition of these clay beds which did not disturb the Fe precipitation. This phenomenon rule out their normal clastic origin, and substantiate the view of their volcanic ash fall out nature.

Mafic Intrusive member:

The Gwalior sediments are intruded by massive dolerite intrusives. The intrusive bodies occur as sills and dykes. They are medium to coarse grained dolerite with ophitic to gabbroic texture. Graphic texture also observed in few thin sections.

The intrusive bodies occur at two distinctive stratigraphic levels. The lower horizon crops out near Nayagaon -Chora area, are relatively finer grained, thin, having ophitic texture and can be traced at considerable distance along strike. The upper horizon is quite thick, coarser grained, exposed extensively along E-W trending line around Gwalior, Morar, Dhaneli, Karwas and Jakharas area (Fig1.2). The mafic rocks crop out as isolated bodies showing east-west extension and locally they occur as sills running parallel to the bedding planes. The outcrop pattern of mafic bodies suggests that they may be east-west trending dyke, which radiates from common source and intrudes Gwalior sediments at two different stratigraphic horizons. This is corroborated by their chemistry (Unpublished data of AMD). Both of horizons have similar major, trace and rare earth element chemistry. The intrusive activity in the Par sandstones is also observed in lithocore of few boreholes.

1.5 Geology of Kaimur Group:

The western and northern boundaries of Gwalior basin are covered by Kaimur Group sandstone-shale sequence of Vindhyan Supergroup (Fig.1.2). In the study area Kaimur group of rocks strike in NNE-SSW direction and display 2^{o}-5^{o} dip towards WNW. Their outcrop boundary in NNE-SSW direction probably demarcates the land ward boundary of Kaimur sea. Kaimur sediments unconformably overlie the BGGC basement in the southern part and Gwalior Group of rocks in the northern part (Fig.1.2).

Kaimur Group starts with BIF pebble bearing sedimentary breccia (BPSB) in the western part of the Gwalior basin near Dursendi village. The BPSB are local units cropping out around the present day E-W trending southern most Gwalior escarp section. The BIF pebble were derived from Morar highlands and dumped without major reworking. The BIF clasts are generally set in ferruginous clay matrix. The BPSB unit is succeeded by regionally established clay matrix rich sandstones, well washed quartzarenitic sandstones and shales. The sandstones show small to medium scale tabular and trough cross beds. However the plane bedded sandstones are most common. The sand bodies have simple sheet like geometry. Flaser bedding and lenticular bedding are also observed at few outcrops. Although shales are scantily exposed at the surface, substantially thick units of shale are frequently found in borehole. The lithological interpretation of two representative boreholes indicate (unpublished AMD report) siliciclastic sedimentation in a stable shelf. The deeper

series borehole intercepts thick black shale horizons, which are thought to be deposited in deep-water anoxic environments.

1.6 Present Status of Age and Correlation:

The age of Proterozoic sequences, especially Paleoproterozoic sequences of the Bundelkhand craton are poorly constrained. The basal Bijawar volcanics have been dated at 2780 ± 365 Ma based on Rb-Sr errorchron age (Crawford and Compston, 1970), are of serious suspect as the basement complex itself is very well constrained at ~2.5Ga (for e.g. Mondal et al., 2002; Mathur, 1982). The upper age limit of Bijawar-Gwalior Group is constrained at 2000 Ma on the basis of $^{40}Ar/^{39}Ar$ age determination of basement mafic dykes (Mallikharjuna Rao et al., 2005). Crawford and Compston (1970) reported an Rb-Sr isochron age of 1830 ± 200 Ma for the mafic sill that intrude the Morar Formation of Gwalior Group. Recalculation of the data by using new Rb-Sr decay constant yield an isochron age of 1791± 200 Ma. The lower age limit of Gwalior Group is thus constrained at 1791 Ma. The mafic sill from Dargawan Intrusive formation of basal Bijawar Group is dated at 1789 ± 71 Ma by using Rb-Sr whole rock isochron (Sarkar et al., 1997). This age is similar to the age of mafic sill of Gwalior Group, indicating that the Gwalior Group and Basal Moli Subgroup of type Bijawar sequence are equivalent while the Gangau subgroup is younger. Rb-Sr isochron age of 1691 ± 180 Ma is reported for the Kurrat volcanics of basal Sonrai Group (Pandey et al., 1995). This implies that Sonrai Group may be equivalent to Gangau Subgroup of type Bijawar sequence and were deposited at around ~1.7Ga.

The age of basal Semri Group of Vindhyan Supergroup is now very well constrained at ~1.6 by U-Pb zircon dating of volcaniclastic bed (Rasmussen et al., 2002; Ray et al., 2002) and Pb-Pb systematics of carbonates (Ray et al., 2003; Sarangi et al., 2004). The lower age limit of Kaimur Group is constrained at 1140 ± 12 Ma by the age of Kimberlite that intrude Kaimur Group (Crawford and Compston, 1970). But with new precise radiometric data of Semri Group, the depositional age of Kaimur Group is inferred as ~1.4Ga.

CHAPTER-II

Sedimentological analysis of Gwalior Group: An example of shoreline and stable shelf deposition

2.1 Introduction

Sedimentary basins are commonly considered to be the products of isostatic compensation due to tectono-thermal processes operating at the lithospheric scale (Allen and Allen, 1990). The formation and evolution of the Precambrian sedimentary basins was primarily governed by magmatism and plate tectonics with secondary controls of processes like eustasy and paleoclimates (Eriksson et al., 2001). From a sedimentological perspective, the formation of the basin involves complex interplay between sediment supply and basin floor subsidence. The sedimentological attributes are key to the understanding of Precambrian plate tectonics and crustal evolution model, as it offers the reconstruction of paleophysical systems in terms of modern analogues and are far more informative than gathered by other means. In the present study the sedimentary facies analysis were carried out for the Gwalior Group sediments to establish their depositional environment and paleotectonic setting.

2.2 Sedimentology: Depositional systems

Facies studies have been carried out along the southern most escarpment section (Fig.1.2, Plate 2.1) and gully section orthogonal to the escarpment section, where excellent exposures are available. The present study is based on ten (10) measured sections along the total 80 km E-W trending basinal strike line and two borehole core data. The locations of the sites are shown in the Fig.1.2 and measured sections are illustrated in Fig.2.1 & Fig.2.2. The litho-exposures were examined all along the 80 km strike line, out of which ten representative sections are selected for discussion. Good dip sections are few and were studied wherever available. The vertical sectional thickness was computed from RL difference as the RL gradually rise from south to north along escarpment section. The sub-horizontal dip of strata permits this computation, thus a vertical measured log presented herein contains a considerable dip component, strictly not a vertical log. They are presented as vertical log instead of dip section for the sake of simplicity.

Fig.2.1: Measured lithologs of different representative sections of Par Formation of Gwalior Group. The locations of these sections (A-J) are shown in Fig.1.2. Also shown the facies no., sedimentary structures and the paleocurrent arrows. Note fining upward facies patterns and wide reversals of paleocurrent directions.

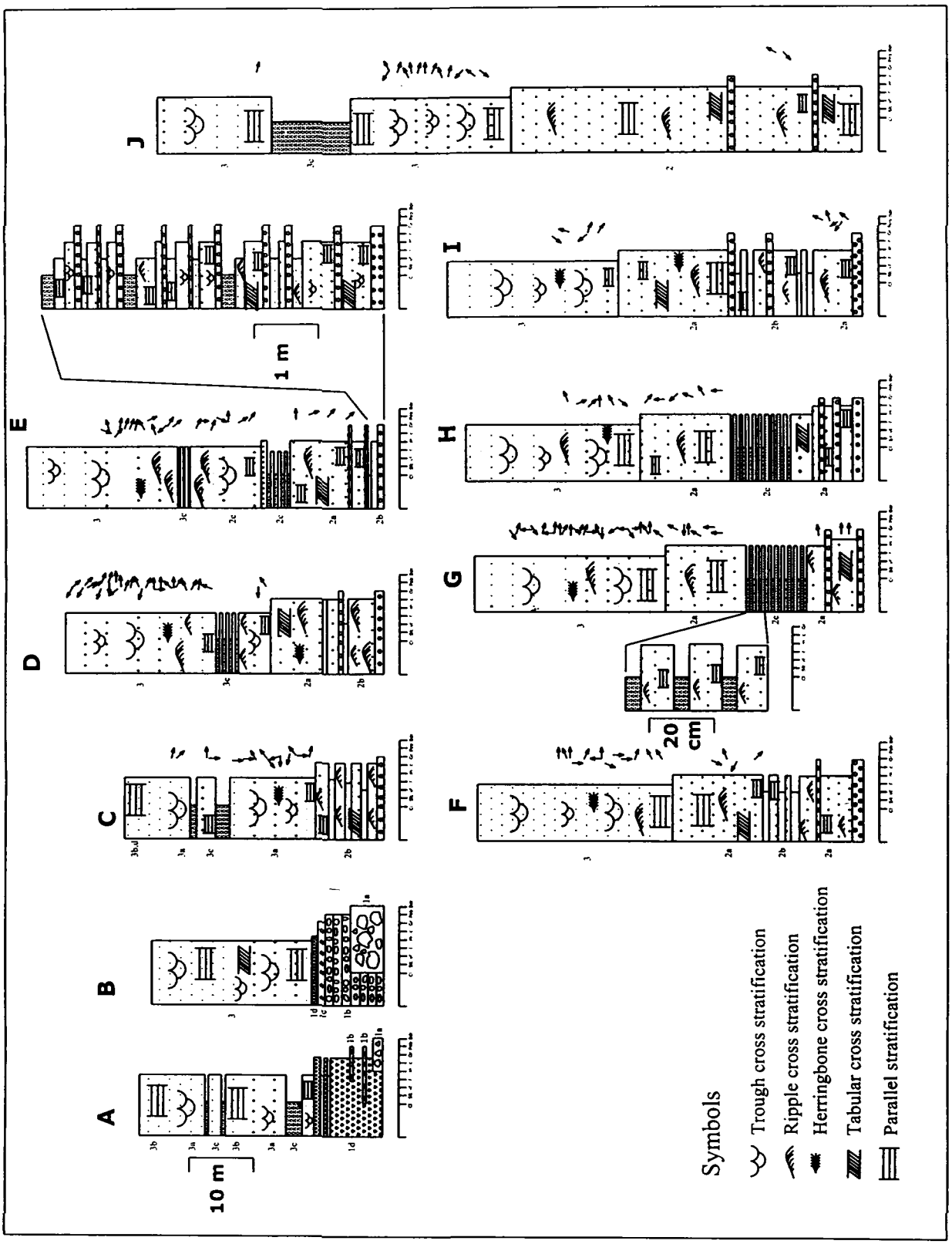
A
B
C
D
E
F
G
H
I
J
10 m
1 m
20 cm
Symbols
Trough cross stratification
Ripple cross stratification
Herringbone cross stratification
Tabular cross stratification
Parallel stratification

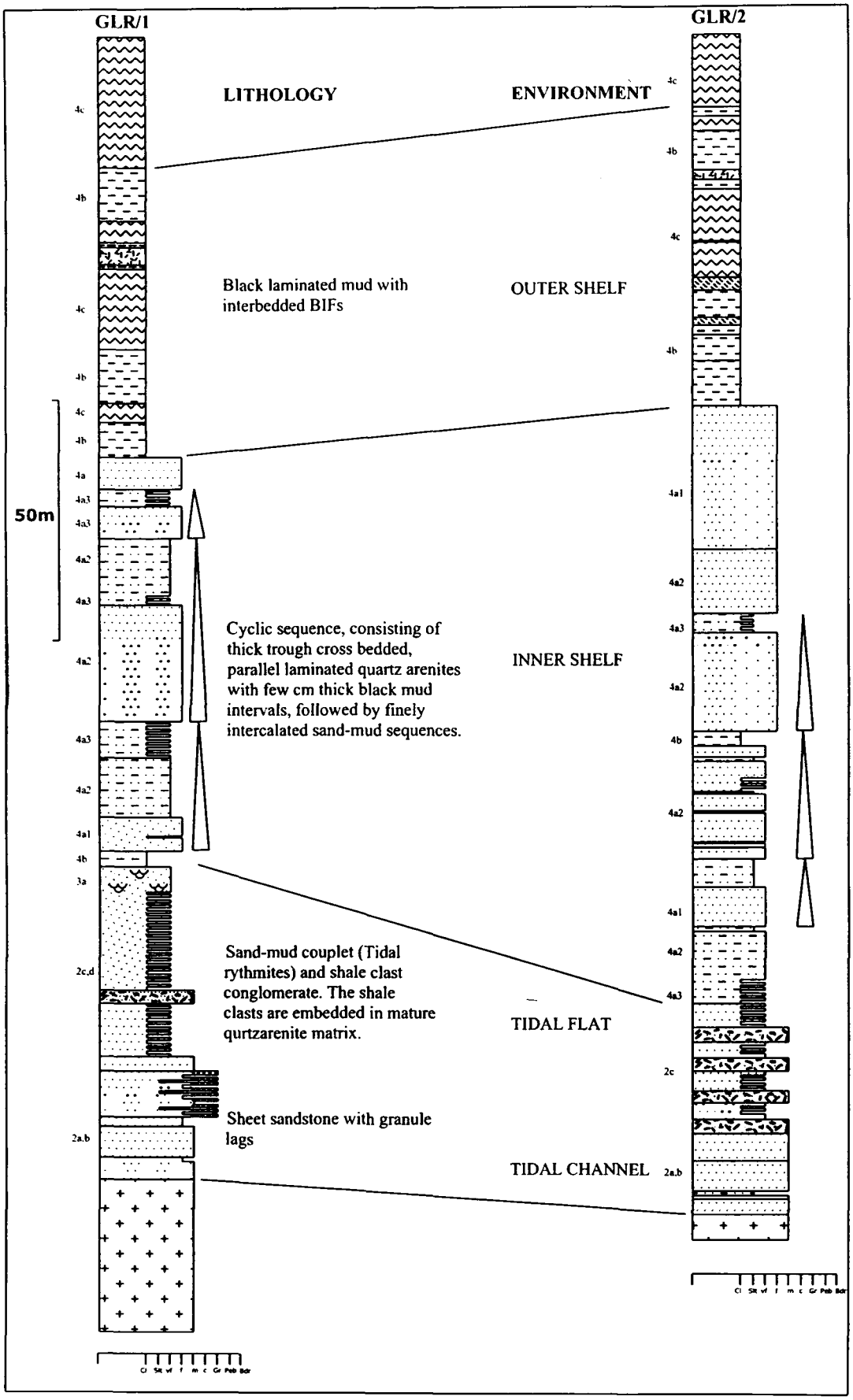

Fig.2.2: Sedimentary litholog interpretation of two boreholes. For location of boreholes refer figure 1.2. Different facies are marked and depositional environments are also indicated.

By careful examination of facies, five facies system of a broadly shorezone-shelf association are recognized viz. alluvial system, back barrier lagoonal system, shoreface-foreshore system, inner shelf and outer shelf system. The facies are described below.

2.2.1 Alluvial System

Alluvial system (facies 1) is developed locally in the western part of the basin in basal Par Formation. This system consists of four facies. Viz. 1. Boulder conglomerate confined to the base, overlying the basement granite. 2. Horizontally bedded sheet like pebble conglomerate. 3. Horizontally bedded mature clast supported granule stone. 4. Medium to coarse grained arkosic sandstone. The facies characteristics are as follows:

Facies 1a: Boulder conglomerate

Boulder-cobble conglomerate facies are about 1-3m thick (Fig.2.1, Log. B), best developed near Par village in the western part of the basin (Plate 2.2). These are oligomictic clast supported conglomerate; consisting of assorted sub-rounded to sub-angular clast derived from vein quartz. The clast size varies from 6 cm to 25cm. The boulder bed is generally massive to vaguely stratified and developed locally along the paleo-depressions. Thus these rocks are laterally impersistent and occur as gully filling in the flanks of the basement ridges of quartz reefs.

Facies 1b: Horizontally bedded pebble conglomerate

The pebble conglomerate unit generally lies over basement granites or seldom over boulder conglomerate facies (f1a), where boulder conglomerate facies is developed (Fig.2.1, Log A&B). These are 2-6m thick, bedded oligomictic conglomerates (Plate 2.3) containing well rounded to very well rounded pebble size quartz clasts (1cm to 5cm). They range from matrix supported to clast supported type while the former is being dominant. In the matrix supported conglomerates, the quartz pebbles float in the matrix of well sorted mature quartzarenite. The conglomerates are horizontally stratified and normally graded. They have sheet like geometry and can be traced for several tens of meters along depositional strike, lenticularity index are thus very high (Clifton, 1973). Some of these conglomerates often contain heavy minerals like monazite, zircon and thorite towards the top and show radioactivity.

Facies 1c: Horizontally bedded granule stone

The pebbly unit is overlained by horizontally stratified, mature, grain supported granule stone (Fig.2.1, Log B). The granule size (2-3mm) clasts are extremely well rounded and sorted (Plate 2.4). The thickness of this unit varies from about ½ m to 2m, with wide lateral extension.

Facies 1d: Arkosic sandstone

Arkosic sandstone facies is about 2-8m thick and occur in basal Par formation (Fig.2.1, Log A, B). This facies is restricted locally in western part of the basin and best developed in north of Simiriya Tanka village. These are coarse grained sandstones comprising angular coarse sand size fresh K-feldspar (upto 50%) and quartz grains. Horizontal bedding is the dominant sedimentary structure. The feldspar content diminishes laterally towards east and towards the top. At few locations boulder conglomerates (facies 1a) are developed at the base of this unit. The pebbly conglomerate bodies (facies 1b) are sometime intercalated in these sandstone units. Towards the top, the rocks of this facies are often intercalated with well washed quartzarenite facies of beach-shoreface association.

Interpretation

Massive to vaguely stratified boulder-cobble conglomerates are similar to deposits attributed to hyper concentrated flow in which clasts are supported by turbulent suspension (Nemec and Muszynski, 1982; Nemec and Steel, 1984). The presence of stratification indicates transition to tractive processes associated with increase in fluid concentration and high flow velocity (Nemec and Muszynski, 1982). The vertical and lateral gradation of this facies to pebble conglomerate (f1b) and granule stone (f1c) suggests waning of flow through time and/or consequence of shift from debris flow to sheet flood process (Nemec and Steel, 1984, Mial, 1977, 1985) from proximal to distal areas.

The broad sheet like geometry of arkosic sandstone is also comparable to sheet flood facies. The angularity of clasts and presence of fresh K-feldspar (upto 50%) indicate nearness of provenance and minimal reworking by fluvial processes. However horizontal stratification indicates channelised deposition in a near horizontal pavement. The feldspar content, as well as thickness of the units decreases toward east. These indicate a Granitic provenance in the southwestern territories and transportation of sediments towards east and north. Intercalation of pebbly conglomerate unit (f1b) as thin broad lenticular unit within this facies (Fig.2.1 logA)

suggests that the pebbly units were deposited either as a lag in a channel floor or at the top of a braided bar (Nemec and Postma, 1993).

The pebble conglomerate (f1b) and granule stone (f1C) facies are also compatible with shoreface origin, as they have sheet like geometry and are horizontally bedded. The alluvial interpretation is preferred because of their intimate association with immature arkosic sandstone facies (f1d). Nevertheless, basinal reworking of alluvial sediments is indicated by several phenomenons. The intercalation of arkosic sandstone facies with mature quartzarenitic sandstone (Fig.2.1 Log-A) of beach-foreshore association suggests transgressive reworking of these sediments during a gradual relative sea level rise (Swift 1968). The Pebbly matrix supported conglomerate facies (f1b) towards top are thin (0.5m-2m thick) horizontally bedded with considerable extent along basinal strike (3-4 km). The high lenticularity index (constant thickness vs. extensive lateral continuity, Clifton 1973) is similar to that of shoreface conglomerates (Bourgeois and Leithold, 1984). These units often contain radioactive heavy minerals like monazite, zircon and thorite, showing similarity with beach placers of modern day. Thus the parts of pebble conglomerate facies (f1b) are akin to shoreface processes.

2.2.2 Back Barrier Lagoonal System

Back barrier lagoonal system (Facies 2) is extensively developed in central and eastern part of the basin in the basal Par formation (Fig.2.1, Log C-J). The outcrops are available immediately over basement granites. Several sub-environments of lagoonal facies system have been identified as described below:

Facies 2a: Medium to coarse grained horizontally stratified sandstone

This facies developed extensively in central and eastern part of the basin (Fig.2.1, Log C-J) in basal Par Formation, directly resting on basement granite. These sandstones are generally consisting thinly horizontal bedded units. The thickness of each set ranges from few cm to 20 cm and are often characterized by granule lags of few pebble thickness. The erosional surfaces are planar to concave curvilinear with very small gradient (Plate 2.5). The relatively finer grained sets contains trough to tabular cross beds (set thickness ~5cm) which often indicate a southward current direction. Tabular sets of cross bedding with less than 20cm set thickness are seen, which are characterized by concave or rarely sigmoidal fore sets and common reactivation surfaces (Plate 2.6). Some of the sets have rippled top. Herringbone type

bi-directional features are commonly found in 3D exposures, which are not apparent from current rose diagrams. The thin granule layers (5-10 mm thick) and bed sets continue for several meters along strike. The extreme length to breadth ratio is indicative of deposition in horizontal surface. The low dips of cross beds corroborate the interpretation that they were deposited under extreme low bottom gradient. Plane bedded coarse-grained sandstone with very well rounded sand/granule grains, are also important component of this facies. Coarse sand and granules are set in clay matrix and are generally grain supported. Occasionally they are matrix supported in which minority sand/granule grains float in clay matrix, thereby producing distinct bimodality of grain size.

Interpretation

The sheet like geometry of sand beds resembles to shoreline facies. Extreme roundness of coarse sands and granules was achieved in high energy swashing condition. A back barrier tidal channel sheet flood facies model has been envisaged for these sand bodies. This is preferred over foreshore-shoreface facies because of bimodality of grain size, presence of herringbone structures and land ward directed paleocurrent direction and also close association of this facies with tidal rhythmites. The well rounded sand/granule grains indicate that the roundness maturity was achieved in a shoreline environment and were deposited in low energy back barrier environment by tidal channels during a flood tide, thus resulting in mixing of high energy (well rounded grains) and low energy (clay matrix) sediments. The grain size bimodality of fine grained sandstones are observed under microscope, identified as quartzwacke. The bimodality is typical of tidal environment (Taira and Scholle, 1979), and also the close association of this facies with tidal rhythmites and tidal bundles are consistent with the tidal channel interpretation. The low dip foreset indicates migration of smaller bedforms on a sand dominated sediments.

Facies 2b: Alternate fining upward sequence

Alternate fining upward sequence from coarse sand to silt-mud has been found in several out crops (Fig.2.1, Log E-H). Each fining upward sequence is 8-50cm thick and necessarily not complete. Ten such cycles are observed in section E (Fig.2.1, Log-E inset). Each cycle starts with granules gradually fining upward to mud in completed cycle and to fine sand-silt in most of the cycles. The medium to fine grained sands are ripple cross laminated, tabular-trough cross laminated and

occasionally horizontally laminated. The cross bed show southward (landward) directed paleocurrent direction.

Interpretation

Each coarse sand to mud cycle is related to tidal current action in a tidal channel. The granule beds indicate high energy traction current in bottom channel. The fining upward sequences indicate drop of energy in ebbing condition and deposition of mud in the top. The intimately associated high and low energy stratification is typical of tidal setting (De Raaf and Boersma, 1971). The cyclicity of the pattern is akin to tidal processes during a high-low tide cycle. Paleocurrent directions from the foreset suggest southward flow in most of the area. Predominance of flood-oriented current suggests deposition in back barrier flood tidal delta environment. The evidence of delta is, in part, speculative but essential to account sheet-like geometry of Facies 2a and 2b. Because of high wave energy condition in coastal setting, ebb tidal delta did not develop. Most of the sediment was transported through the inlet into the back-barrier. As a result the lagoon was dominated by flood-tidal sands which are characteristic of wave dominated barrier islands (Hubbard, 1977; Cheel and Leckie, 1990).

Facies 2c: Horizontally bedded alternate sand-mud sequence

Horizontally laminated finely intercalated sandstone-mudstone sequence (Plate 2.7) is very well preserved in central and eastern part of the basin (Fig.2.1, Log F-J). Individual sand layers are few cm (1-5cm) thick. Internally they are consisting of plane lamination with wave rippled top. The sands are topped by few mm (2-5mm) thick mud drapes. In general mud drapes covers up the ripple trough of underlying sand bed. These alternate sand-mud layers are stacked to give rise thickness of individual bed upto 15m, which are excellently preserved in most of the outcrop. In borehole cores, within these unit mud rip up clasts are found embedded in mature quartzarenite matrix (shale clast conglomerate).

Facies 2d: Trough cross bedded coarse sand-silt-mud couplet

Beside horizontally laminated sand-mud couplets, there are also found trough cross bedded sand-silt-mud couplets with concave-sigmoidal bounding surfaces. Grain size variations of these couplets range from sand-mud couplet to that of granule-silt couplets. A strong reversal of current is indicated in some sand-mud couplets as sand layer show oppositely directed cross stratification (Plate 2.8). The ebbing current is indicated by mud drapes. The granule-silt couplets constitute about

15-20cm thick sets. The bottom set is comprised of granule size sediment with the grain size gradually decreases upto silt size towards the top. These make up granule-silt couplets which are inclined on the foresets and flatten out along the toesets where they extend as horizontal layer for several meters in the flow direction (Plate 2.9). Granule layer occurring within these couplets are upto 10-15cm thick and gradually become thinner towards the foreset dip direction, while silt-fine sand layers thicken.

Interpretation

Silt-mud draped sand-granule foresets are tidal bundles which are widely reported in shallow intertidal to sub tidal deposits (Boersma, 1969; Visser, 1980; Ulhir et al., 1988; Cheel and Leckie, 1990). The bundles represent alternating slack water deposition from suspension (mud/silt) and current deposition from bed load (sand/granule) on the lee surface of advancing bed form that produced cross stratification. Horizontal sand-shale couplet (facies2c) represents similar style of deposition but on a flat surface, commonly the surface over which the bedform was migrating. The thin wave rippled sandstone of facies 2c suggests migration of 2D longitudinal ripple trains under extreme shallow water cover. These are characteristics of high tidal flats with mixed sand-mud sediments and is similar to those described by Visser (1980). Formation of tidal bundles and horizontal couplets requires strongly reversing currents (Boersma, 1969; Visser, 1980) with major sand deposition during a competent dominant flow and only minor sand deposition during subordinate flow. The shale clast conglomerates found within these units represent tidal channel deposits which dissect the tidal flats, similar to those described by Kumar and Sanders (1974), and Hoyt and Henry (1967).

Facies 2e: Medium to Fine grained rippled sheet sandstone

These are horizontally bedded sandstones. Each unit, 1-2 cm thick, can be traced several meters along strike. Preservation of ripples are excellent as almost each and every unit is topped by ripples (Plate 2.10). The wave ripples are of symmetrical to slightly asymmetrical longitudinal type, with wavelength of 3-8 cm. The ripples have high symmetry index (<2) compatible with wave generated ripples (Reinick and Singh, 1980). Chevron ripples (Plate 2.11) are also found. The grain size of the topmost rippled unit is relatively finer (silt). The crest lines of the ripples are often bifurcated and interference of ripples is common. Ladder back ripples are also found in several outcrops. The flat topped ripples (Plate 2.12) and ripples with broken crest line (Plate 2.13) are among the modified types.

Interpretation:

The successive thin-bedded rippled sandstone units indicate sedimentation in protected environment with shallow water cover. The wave ripples indicate predominance of wave over current flow. The absence of mud in these units may be due to absence of mud in the source, as sediments were derived from granitic sand rich basement. This resembles sedimentation in a lagoon or a lower tidal flat environment. Muds were probably deposited as drapes in upper tidal flats; could not be deposited in lower flats, as receding water leaves no time for flocculation of mud and may be genetically similar to the facies 2c. The modified ripples like flat crested ripples and ripples with broken crest line indicate intertidal environment (Reinick and Singh, 1980). The widely preserved ladder back ripple are also indicative of intertidal depositional environment (Tankard and Hobday, 1977; Klein, 1977; Wunderlich, 1970).

Facies 2f: Horizontally stratified quartzarenite

The lithofacies 2a to 2e are overlained by horizontally stratified 1-5 m thick quartzarenite unit at most of the places. These quartzarenites are fine grained, very well sorted and mature with high silica content. Internal structures are dominated by parallel laminae with subordinate current ripple laminae with individual sets of 5-20 cm thickness.

Interpretation

The lagoonal tidal system of facies 2a to 2e was inundated by coalescing beds of washover fans to produce thin sheet like sandstone facies dominated by parallel lamination. The high maturity of the sandstone indicates reworking in high energy swashing conditions of a foreshore beach environment and are part of barrier island system. Wash over fan resulted because of erosion of barrier island sediments from seaward side and transportation of the debris to the lagoon during storm periods (Reinson, 1984; Reading and Collinson, 1996; Cashyap et al., 2002).

2.2.3 Shoreface-foreshore system

Shoreface–foreshore facies (facies 3) are recognized on the basis of mineralogical and textural maturity of quartzarenite and wave produced sedimentary structures. These deposits form transgressive sheets which covers the back barrier lagoonal facies (Fig.2.1, Log. A-J). In fact they are thick (15-60m), monotonous

quartzarenite bodies occurring at the top of the Par formation and are most abundant facies. Different facies variations are described in following paragraphs.

Facies 3a: Trough cross stratified sandstone

These facies are composed of well sorted medium to fine grained sandstones which sharply overlie the back barrier facies system. The trough cross stratified sandstone forms discontinuous 5-20 cm thick sets and extend laterally for about 1-2 m (Plate 2.14). Asymmetrical to symmetrical rounded crest ripples with straight crest, sometime cap the trough cross stratified sandstones (Plate 2.15). The ripple symmetry index (<2) suggests that the ripples are compatible to wave origin (Reinick and Singh, 1980). Occasional sets of sigmoidal cross bedding suggest high angle of climb of mega ripple which produced them (Allen, 1968). Intricately interwoven trough cross stratification are also found in some outcrop similar to described by De Raaf et al., (1977). This unit often shows herringbone type cross bedding (Plate2.16) which is genuine in 3D exposure. Cross bed dip azimuths indicate current direction towards east, south and north.

Facies 3b: Parallel laminated sandstone

Parallel laminated sandstone contains internal flat to undulating laminae with a 1-4 mm thickness and exhibits low angle discordance and are intercalated within trough cross stratified quartz-arenite.

Facies 3c: Parallel laminated thin sand-silt alternation

This facies is made up of alternating fine to medium grained quartz-arenite and siltstone, constituting 1-4 m thick beds (Plate 2.17). Arenite intervals are 1-5 cm thick and contain wave ripple cross laminae and horizontal stratification. Silt/mud intervals are generally less than 1 cm thick but may thicken upto 0.5 m at places.

Facies 3d: Plane bedded sandstone

This facies comprises fine to medium grained quartz arenite with variable set size, and overlies the above described lithofacies (facies 3a, 3b&3c). The intrasets within horizontal bedding are apparently massive, plane bedded to laminated (Plate 2.19). There are occasional intrasets of planar trough cross bedding.

Interpretation:

The cross beds of facies 3a indicate unidirectional tractive flow, with dominant current direction towards east, showing shore parallel accretion of shoreface sands (Fig.2.1, Log C-J). The moderate in-shore and off-shore components suggest tidal currents. Form discordant symmetrical wave ripples are found capping

the trough cross stratified sets, similar to those described by De Raaf et al., (1977) and indicates storm-wave activity probably in outer shoreface. This unit sharply overlies back barrier facies, indicate transgression of sea.

The parallel laminated sandstone (facies 3b) was generated by combined flow processes because of intense bed shear due to storm-wave activity (Nottvedt and Kreisa, 1987; Harris and Errikson, 1990).

In some sections, parallel laminated sandstone (facies 3b) grades upwards to cross stratified sandstone (facies 3a) and finally to wave ripple laminated sandstone (Plate 2.18). This feature indicates gradual decrease in flow strength, probably follows a quiescence period (fair weather), after a storm event. The wave ripple capping suggests that these facies were modified by or were a product of wave activity.

The intercalated mudstone-siltstone layers (facies 3c) represent fine grained sedimentation during the periods of low energy or fair weather condition (Levell, 1980a, b; Harris and Errikson, 1990; Jackson, Simpson and Erriksson, 1990).

Foreshore and swash deposits are represented by facies 3d that suggest plane bed movement and/or wash out ripple under upper flow regime. The complete sequence of 3a-3d reflect transgression followed by shoaling from lower shoreface to foreshore environment along a wave dominated coastline, comparable to that as documented by Clifton et al., (1971).

2.2.4 Shelf Depositional System

Shelf depositional systems are identified only in borehole lithologies. Surface exposures of these facies are not found as Gwalior Group sediments constitute subhorizontal strata, thus these facies are overlapped (onlap) by younger strata.

Facies 4a: Quartzarenite and black mud intercalation

This facies assembly consists of cyclic assemblage (Fig.2.2) of thick fine grained, plane bedded quartz-arenite, upto 6-22 m thick (facies 4a1), followed by quartz-arenite with few black mud laminaes (5-20m thick, facies 4a2), and finally thinly intercalated quartzarenite and black mud (facies 4a3)with individual bed set thickness of 2-5 cm (f-4a3, Plate 2.20). Generally mud and sand proportion is equal in the facies 4a3, but some time sand proportion exceeds the mud content.

Interpretation

The above lithofacies are similar to Bouma type bed (Bouma, 1962) with intervals of black mudstone, that record deposition from waning suspension current. Horizontally stratified fine grained quartz-arenite comprises lower most division of T_{bde} beds. Bouma type beds are separated by black mudstone. The finely intercalated sand-muds (f4a3) are T_{de} beds of Bouma sequence. These Bouma type beds (Tempestites) are similar to that of Mesozoic rocks of Canada and south-west US (Leckie and Walker, 1982; Swift et al., 1987). These facies are comparable to those from modern and ancient shelf deposits that are attributed to alternate storm and fair weather process (Johnson and Baldwin, 1986). The thick quartzarenite deposition is related to prolonged storm activity. On the other hand the thin mud laminae represent limited short period fair weather suspension deposits. The finely intercalated sand sequence with equal sand-mud ratio suggests frequent storm and fair weather couplets. The quartz-arenites are sometime carbonaceous. The black colour of mudstone and quartzarenite indicates that sedimentation took place in anoxic environment.

Parallel lamination of the T_b interval are the product of deposition on a plane bed (Blatt et al., 1980) or generated by migration of low amplitude bed form, as a function of bed load traction and sediment fall out during passage of an over-riding turbulent suspension current (Paola et al., 1989; Harris and Errikson, 1990). Offshore transport of sand was possibly carried out by turbidity current or more likely by geostrophic flows which are considered to be related to storm surge ebb flows (Hayes, 1967; Nelson, 1982; Aigner, 1985).

The prevalence of sand over mud implies that these sediments were deposited near (below/above) storm wave base in an inner shelf setting (Definition of Harm's et al., 1982).

Facies 4b: Black mud facies

This facies consist of pyritic, often siliceous (cherty) black mudstone of several meter (~10m) thickness (Fig.2.2). The mudstones are finely laminated (Plate 2.21). The pyrites are tabular and aligned to bedding planes.

Interpretation:

Black pyritic mudstone reflects slow sedimentation in an environment relatively starved of siliciclastic influx. This facies is thus interpreted as outer-shelf deposition (Jackson et al., 1990). The black muds represent maximum flooding

surface, condensed section of a transgressive system tract. The pyrites and carbonaceous material indicate deposition in anoxic acidic condition. The absence arenites and wave produced structure indicate deposition below storm wave base during quiescence period.

Facies 4c: Banded Iron Formation (BIF) Facies

BIFs do not have modern analogues and are chemical sediments that lack sedimentary structures; therefore it is difficult to establish their depositional environment. Although this work is mainly concentrated on clastic rocks, the intimate associations of BIFs with clastic sedimentary rocks provide an opportunity to trace the sedimentary depositional environment of BIFs of Proterozoic age.

The BIFs are of oxide facies showing two major varieties, i.e. 1. cherty BIF with no shaly material content, containing rhythmic chert and hematite bands (Plate 2.22 & 2.23); 2.shaley BIF with shaley material, often grades to shale (S-band) and at places show clastic contamination (Plate 2.24).

The basal BIFs are interbedded within black siliceous mud (f-4b) indicating their deposition at outer shelf (Fig.2.2, Plate 2.22) during initial stage of deposition. This character account for periodic hydrothermal exhalations within a regional anoxic outer shelf setting. However, most of the BIFs appear to have been deposited with much elevated sea level in an open shelf with dominant hydrothermal exhalation of iron-silica rich solution in an oxygenated environment, thus they overlap previous sediments. The shale bands (S-band) and shaley BIF represent entrance of clastic sediments in the shelf probably due to storm activity or due to local sea level regression.

Facies 4d: Limestone facies

There are thin (5-10 m) impersistent limestone horizons sandwiched within the basal BIFs. These are micritic limestone and indicate temporary quiescence of iron-rich volcanic exhalations. However, the hydrothermal activity did not die out completely as indicated by occurrence of thin chert and hematite bands within the limestone units (Plate 2.25). At some places in central part of the basin, thin mud layers (few mm) are observed along the bedding planes of limestones (Plate 2.26). Appearance of these muds are similar to the facies 4e and may be of pyroclastic origin.

Facies 4e: Clay bed facies

This facies is comprised of extremely fine-grained white kaolinitic clay that is about 5-10 m thick and occurs in basal part of Morar Formation BIFs (Plate 2.27). These clay beds occur as marker horizon and persistent throughout the strike line of the basin. These clay beds are interpreted as volcanic ash fallout deposits and owe their origin to the explosive acid volcanic activity, which probably occurred in distal south within Bundelkhand provenance. Absence of any wave related structure in these beds indicates that these were deposited in the outer shelf below storm wave base. Very thin (1-2 mm) Fe-rich laminae occur within these clay beds that are laterally persistent for several meters. This phenomenon suggests extreme slow deposition of clay by gravity settlement that did not even disturb the hematite precipitation. Extreme fine grained nature of clay beds, their distinctive white colour, low specific gravity and visual difference with normal clastic shales are the features which indicate that they are not a product of normal weathering erosion related processes but are volcanic ash fallout deposits. Recently volcanic cauldron structure has been reported from the interior of Bundelkhand craton that is of pre-Vindhyan age (Jain et al., 2001). The occurrence of these clay beds within BIFs of Morar Formation suggests the possibility of explosive acid volcanic activity during sedimentation of Gwalior Group. It is possible that physico-chemical conditions of the sea water and atmosphere changed drastically during that volcanic episode which resulted in increase of atmospheric f_{CO2} and thereby facilitating carbonate precipitation.

2.3 Paleocurrent & Paleogeography

Foreset dip azimuthal data of cross-bedded sandstone of facies 2 and 3 were measured where cross bedding surface is properly exposed in 3-D space. Most of the data were collected where ac and bc surfaces are exposed, some data comes from ab plane in the topmost surface [a, b and c axes are in the sense of Potter and Pettijohn (1963)]. The data comprising 404 readings were recorded from numerous outcrops along the basinal strike over a stretch of 80 km. Because Gwalior Group sediments are represented by subhorizontal strata with dip less than 5° (2°), no tilt correction is required. The data are plotted as rose diagram to represent paleocurrent map of Gwalior sandstones (Fig.2.3), and as current arrows on measured sections (Fig.2.1). The rose diagrams are plotted as per locations with number of observations made.

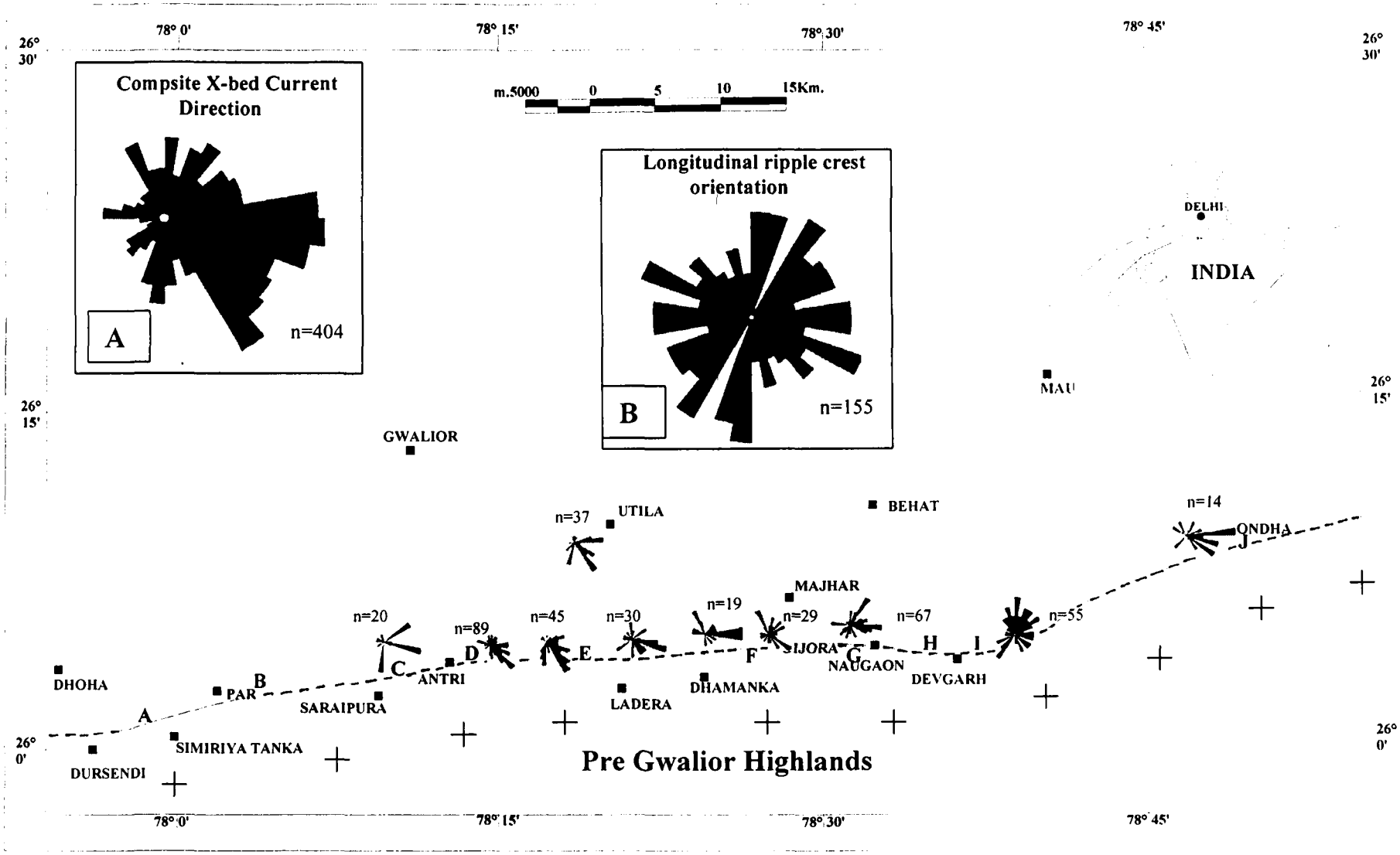
78° 0'
78° 15'
78° 30'
78° 45'
26° 30'
26° 15'
26° 0'
Compsite X-bed Current Direction
A
n=404
m.5000 0 5 10 15Km.
Longitudinal ripple crest orientation
B
n=155
DELHI
INDIA
MAU
GWALIOR
BEHAT
n=37
UTILA
n=14
ONDHA
MAJHAR
n=20
n=89
n=45
n=30
n=19
n=29
n=67
n=55
SIJORA
NAUGAON
DEVGARH
ANTRI
DHAMANKA
LADERA
SARAIPURA
PAR
DHOHA
SIMIRIYA TANKA
DURSENDI
A
B
C
D
E
F
G
H
I
J
Pre Gwalior Highlands

The rose diagrams exhibit complex set of orientation, as most of the data come from shoreface facies (facies2). They show bimodal-bipolar to polymodal patterns with modal axes and subsidiary modes oriented towards SSE, E, and NNE with few reversals. The bi-directional-bipolar bedforms like herringbone cross bed show current reversal at 60^{o}-120^{o} apart, 180^{o} reversal was not observed.

The Gwalior Group sandstones strike in E-W direction and directly rest over basement granite. The basal sandstone unit is well preserved along the E-W directed southern most escarpment section, which also mark the unconformity contact with the basement granite. The basement rocks gradually slope towards north and corresponding thickness of the sedimentary strata increases towards this direction. This feature is evident from the outcrop in the dip sections along the gully cuttings and also confirmed from subsurface borehole data. The sediments are thus seems to be representative of the ancient shoreline profile and the present outcrop limit of basin boundary roughly indicates the paleocoast line, which was oriented in E-W direction with open sea towards the north (Fig.2.3) ward side.

The presence of immature arkose in western part of the basin (Dursendi, Simiriyatanka area) suggests that sediments were derived from pre-Gwalior Granitic highlands from west and south. The decreasing content of feldspar from west to east also supports westerly provenance and transportation of the sediments towards east under fluvial regime. These fluvial sediments are overlained by shoreface sediments, indicating encroachment of sea towards land (south). The intercalations of arkoses with shoreface quartzarenites provide evidence for transgression and rising of sea level. The overall transgressive sequence is also interpreted by studying the pattern of vertical stacking of different facies. The arkosic sandstone and monocrystalline quartz rich quartzarenite are indicative of granitic provenance, which occur in south of Gwalior basin. It appears that the sediments were derived from granitic highlands of southern, western localities and were transported by river system to the shore line where the sediments were subsequently modified by complex basinal hydrodynamic system. This interpretation accounts for the observed complex polymodal rose diagrams.

In most of the rose diagram three modes are most important. (i). Oriented toward north with few reversal toward NNE or NNW, (ii). Current directed toward south with minor SSW, SSE component and (iii). a major eastward component. The northward paleocurrent indicates sea oriented ebb tidal current, southward current

direction broadly corresponds to landward flood tidal current direction, whereas the eastward current corresponds to longshore current (Hayes and Boothroyd, 1969; Klein, 1970; Oomkens, 1974; Reading and Collinson, 1996). The prevalent southward (inset, Fig.2.3) current in composite rose diagram indicates that flood tidal current was dominated over ebb tidal current as expected in wave dominated shore line and also indicative of gradual transgression of sea and basin expansion. The prevalence of easterly directed longshore current is indicative of shore parallel accretion of shoreface sands by storm/wave activity and/or eastward migration of barrier island by tidal inlet migration. It is interesting to note that composite cross bed current direction is near orthogonal to wave ripple crest orientation (inset Fig.2.3). This probably indicates that the bottom currents and surface waves were closely related, suggesting that wind drift currents were responsible for deposition (Levell, 1980a).

2.4 Depositional model

The deposition of Gwalior clastics can be explained by clastic shelf system with zonation from inshore to offshore facies (Johnson and Baldwin, 1986; Eriksson et al., 1998). On the basis of vertical and lateral facies associations four distinctive facies associations are recognized. These are (i) the inshore back barrier lagoonal complex, (ii) shoreface system, (iii) inner shelf and (iv) outer shelf system. The relation between different facies are explained in the block diagram (Fig.2.4) and columnar diagram (Fig.2.5). The facies association indicates a gradual sea level rise because of transgression.

The Gwalior sedimentation appears to have been initiated in a graben like depression which was possibly created due to extensional tectonics by plume activity (Sharma, 1998) and subsequent normal block faulting of Bundelkhand cratonic block. Presence of compositionally and texturally immature sandstone indicates initiation of basin in western part, which is characterized by fluvial facies association. With passage of time, basin opened up and sea encroached the granitic terrain with shore line oriented in E-W direction. Along the shore line, barrier island complex was established in a meso-microtidal setting. In the landward side (south) of barrier island shore parallel lagoonal system was developed and in sea ward (north) side open shelf was developed. The tidal inlets were acting as funnel between basinal water and back barrier lagoonal system (Kumar and Sanders, 1974; Galloway and Hobday, 1983; Reading and Collinson, 1996).

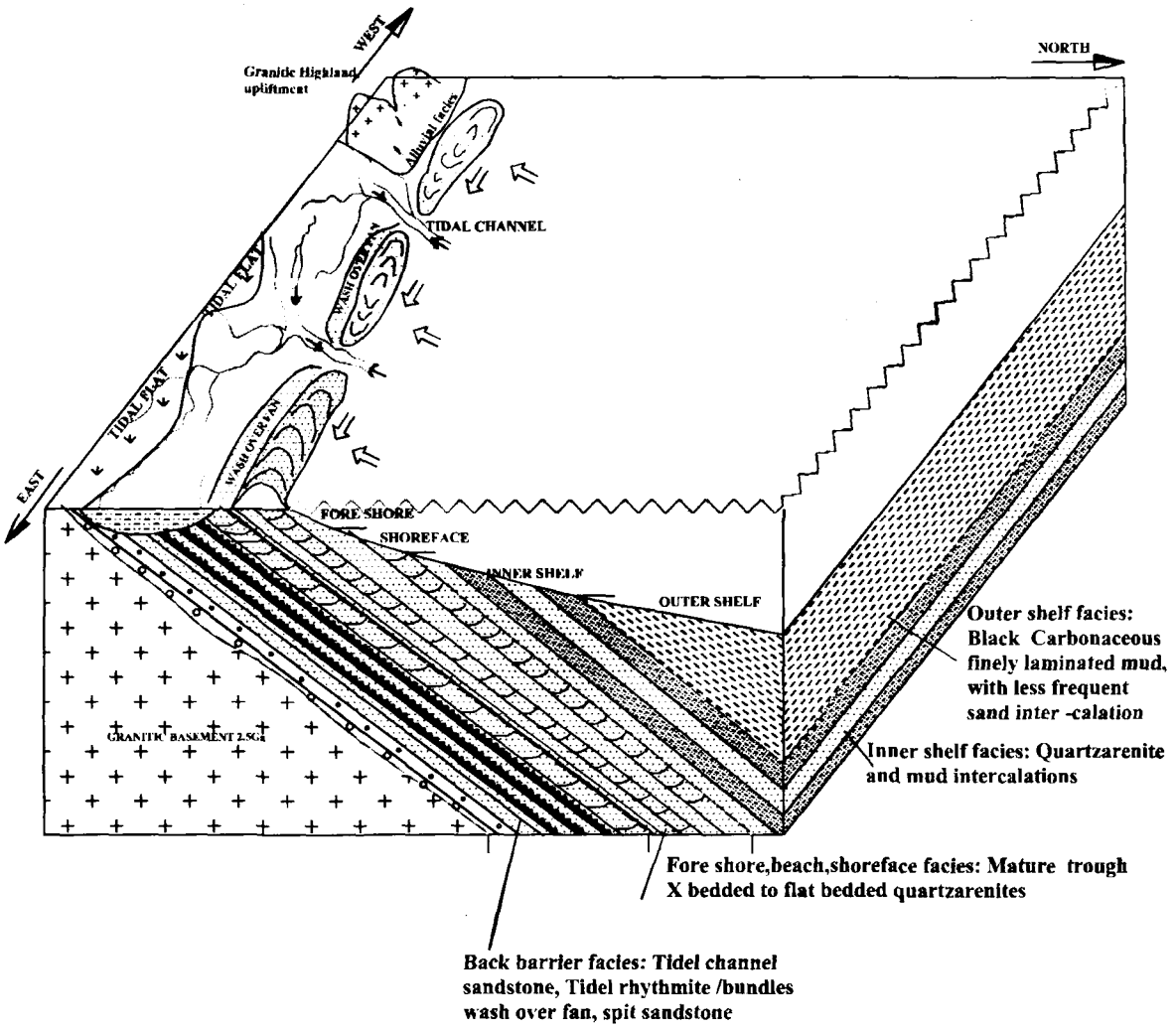

Fig.2.4: The schematic depositional model for Gwalior group sediments showing *simultaneous deposition in shore zone and in deeper shelfs.* East-west trending barrier island complex separates the back barrier lagoonal facies from the open sea. Note predominant southerly and easterly current directions. Also note presence of alluvial facies towards the southwest. The sediments were supplied to the open sea via tidal inlets, and subsequently were reworked by basinal processes.

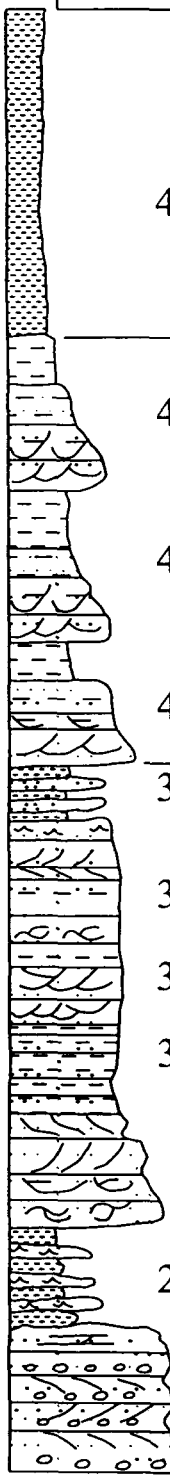

Facies No.	Description	Interpretation
4b	Finely laminated black mud, devoid of wave produced structures	**Outer Shelf** Deposition by suspension below storm wave base.
4a 4a 4a	Cyclic fining upward sequences (Bouma type).Each sequence consist of cross-stratified, parallel laminated quartzarenie with thin black mud intervals. Frequency of sand is much higher than the mud. Towards the top of the sequence mud proportion increases to upto 50%.	**Inner Shelf** Coarse grained sedimentation during storm events followed by mud deposition during fair weather.
3c 3d 3a 3b 3a	Mature, very well sorted quartzarenites: Trough cross bed, tabular cross bed, wave ripple lamination and parallel laminations are among the sedimentary structures. the sandstone units are often capped by symmtrical to asyymmetrical megaripples.	**Shoreface & Foreshore** Wave dominated shoreline is indicated by prevalence of wave produced structures. Predominant east ward paleocurrent show shore-parallel accretion of shoreface sands.
2c,d,e	Intercalated sand and mud -sequence, with rippled top. Each sand-mud intervals are few mm to few cm thick.	**Back-barrier complex** Tidal flat (tidal rythmites)
2a,b	Medium to coarse grained, highly ferruginised plane bedded sandstone with granule lags.	Tidal channel (Sheet flood sandstone)

Fig.2.5: Generalised columner diagram of Gwalior Group sediments, explaining the associations of different lithofacies and their environment of deposition. Note that lithofacies of outer shelf association overlie the lithofacies of shore zone environment indicating transgression of sea.

The back barrier system is characterized by facies association of tidal channel and tidal flat facies, which was inundated by sheet sandstones of washover fans of barrier islands. The wave dominated shoreface facies and foreshore sands overlapped the back barrier system with rising sea level. The outer shelf and inner shelf facies are found in deeper part of the basin toward north, as indicated by borehole core logs. This arrangement provides a unique example of preservation of complete shoreline profile i.e. inshore and offshore facies. The pattern of vertical stacking of facies as evidenced from borehole data and surface measured log, indicates upward fining sequence. The deeper water outer shelf facies overlie shorezone facies and back barrier facies (Fig.2.4 & 2.5). The data indicate that sediments were deposited with a gradual sea level rise. Although sequence boundaries are not identified, the overall association of facies suggests deposition in a transgressive system tract. The abundance of black carbonaceous muds of outer shelf facies indicates starvation of clastic flux and maximum flooding surface. These are similar to condensed section of a transgressive system tract. The clastic sands could not pass littoral energy barrier except during the storm events. The stacking pattern of sand bodies across the basinal strike as conceptualized from the subsurface borehole data and surface outcrops are presented in figure 2.6. The data suggests an accommodation dominated shelf where sediments were supplied to the shelf by shoreface bypassing mechanism (Johnson and Baldwin, 1986). As depicted in figure 2.6 sedimentation started in central bottom portion of basin where a complete profile of shorezone facies, outer and inner shelf facies was developed. With rising of sea level the shore line shifted southward and the shorezone facies were overlained by shelf facies. Repeated transgression can account for the present facies stacking pattern and facies association (Fig.2.6).

The fluvial signature is only found in basal Par formation in southwestern fringe of the basin (Fig.2.1 & 2.4). This regime prevailed during initiation of the basin and was ceased with encroachment of sea with rising of sea level. The sediments, transported by river system, were reworked by basinal system.

With major sea level rise, the clastic sedimentation of Gwalior Basin ceased and chemical environment prevailed leading to the deposition of BIF. The BIF deposited in a raised sea level conditions with minor clastic influx, and overlapped the earlier formed facies.

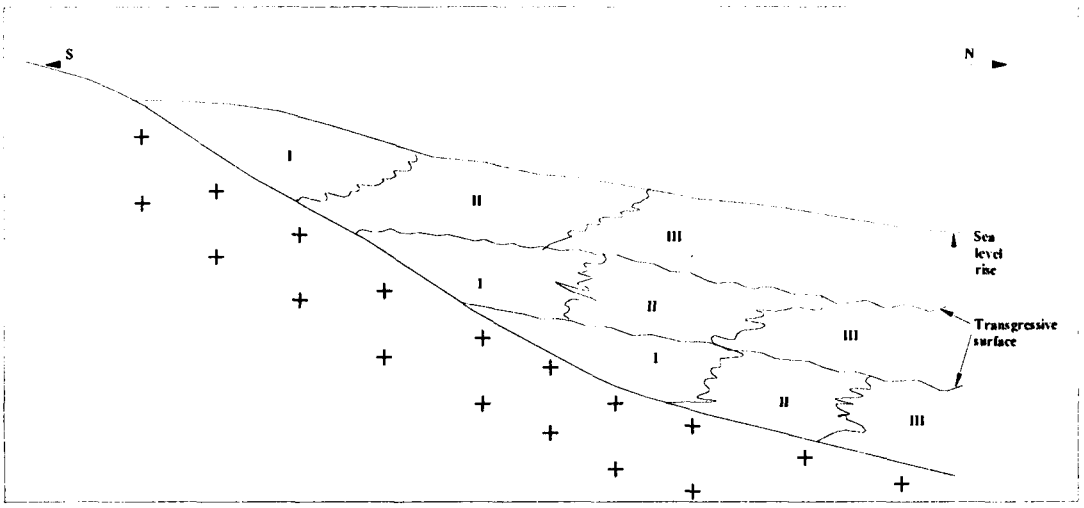

Fig.2.6: Conceptualised stacking pattern of lithofacies of different sub-environments of Gwalior Group. The diagram indicates gradual transgression of sea resulting in shifting of shorezone towards south and opening of the basin.

Plate 2.1: Aerial view of the unconformable contact between Gwalior Group and basement granite, represented by the east-west trending escarpment section. The area south of the escarpments (towards the viewer) is occupied by basement rocks (BGGC).

Plate 2.2: Boulder-conglomerate with capping of quart pebble conglomerates at the base of Par Formation, Gwalior Group, near Par village. Note lenticular shape of pebble-conglomerate unit. Hammer length 35cm

Plate 2.3: Quartz pebble conglomerate (QPC) that overlie the boulder-conglomerate. Note very well rounded quartz clasts float in sandy matrix. Diameter of camera cap is 5cm.

Plate 2.4: Plane bedded grain supported granule stone that is capping the QPC. Camera cap diameter is 5cm.

Plate 2.5: Highly ferruginised sheet sandstone, photograph from Gijora area. Person in top left corner for scale.

Plate 2.6: Plane bedded sandstone with cosets of low angle cross beds, note concave to sigmoidal reactivation surfaces. Pen length 13.5cm.

Plate 2.7: Tidal rhythmite with horizontal sand mud couplet. Hammer length 35cm.

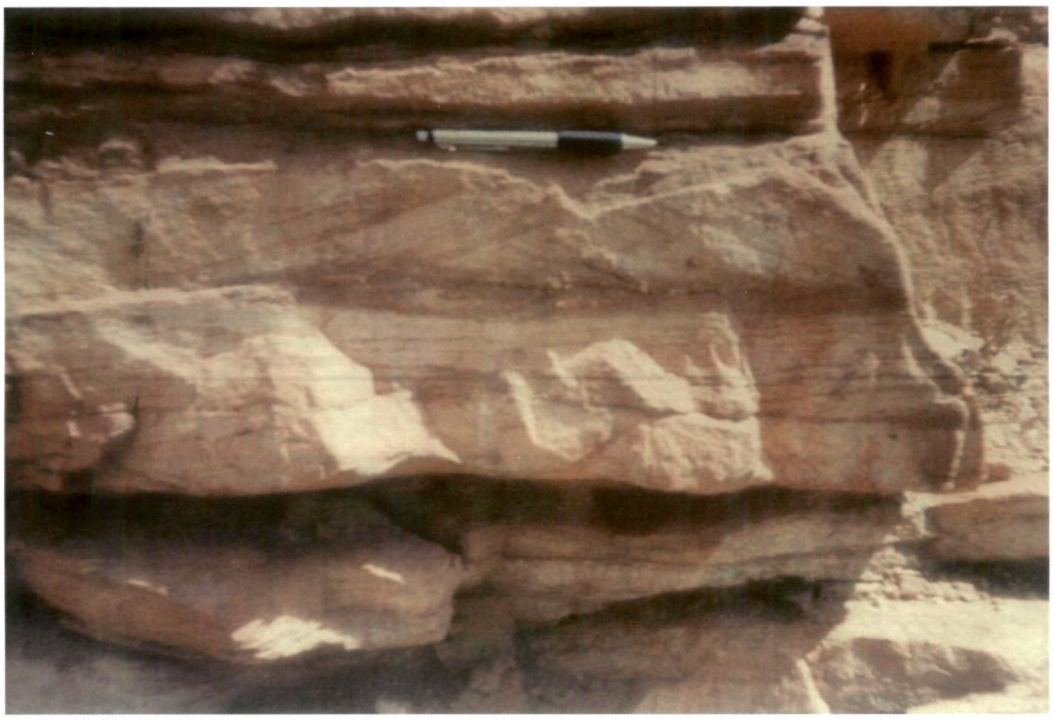

Plate 2.8: Cross stratified sandstone with mud drapes, note that the cross bed foresets indicate strongly reversing currents. Pen length -13 Cm.

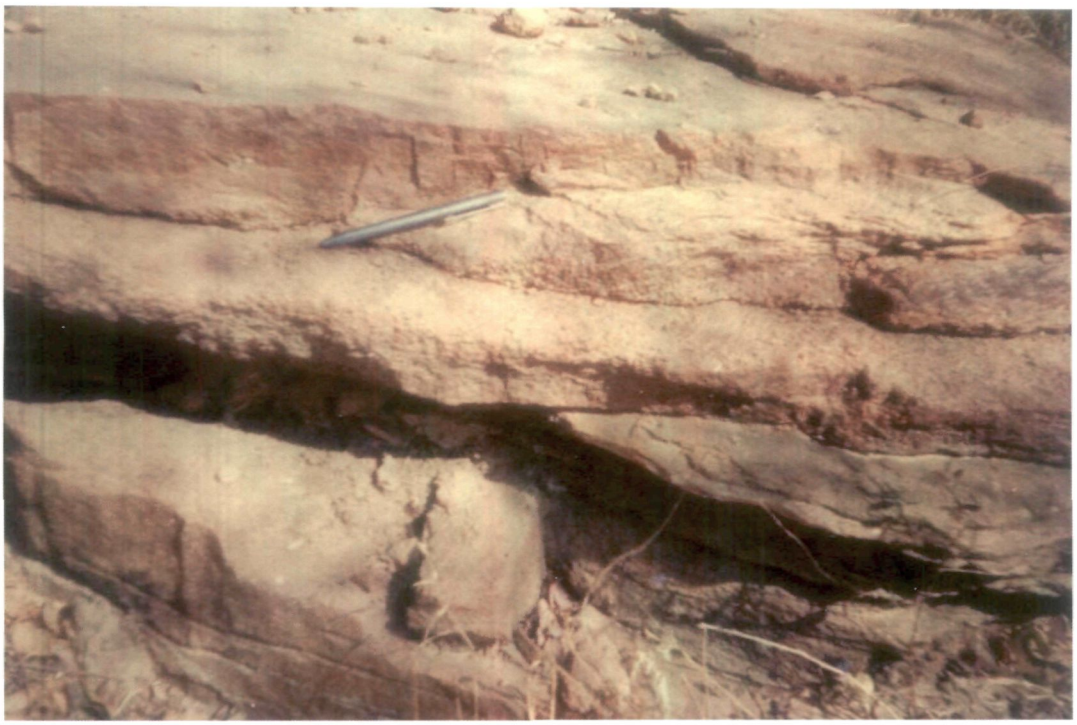

Plate2.9: Trough cross stratified granule-silt couplet, beds are elongated towards toesets. Pen length 13.5cm.

Plate 2.10: Rippled sandstone. Note that that almost every bed is capped by longitudinal wave ripples.

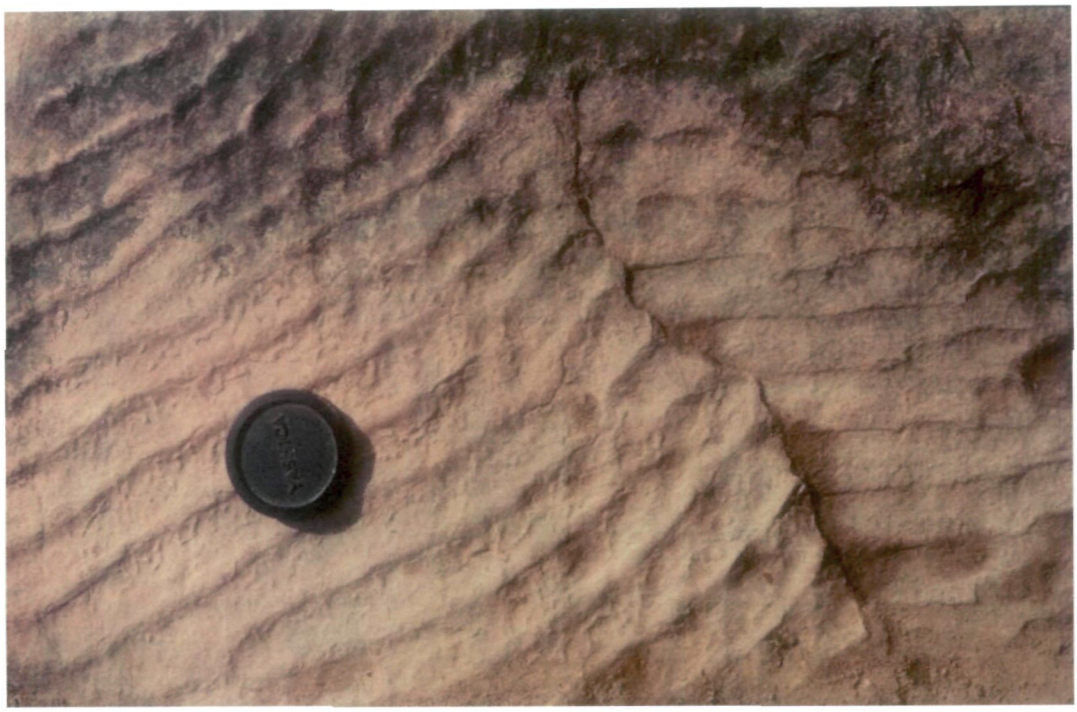

Plate 2.11: Longitudinal chevron ripples. Diameter of camera cap is 5cm.

Plate 2.12: Flat crested ripples, Brunton compass for scale

Plate2.13: Longitudinal ripples with broken crest line.

Plate 2.14: Amalgamated cross stratified sandstone. Note predominant foreset dip (current directions) toward right (east) and occasional bi-directional sets (arrowed)

Plate 2.15: Plane to cross-stratified sandstone with slightly asymmetrical megaripple capping. Internal structure of the ripple is compatible with their wave origin.

Plate 2.16: Herringbone cross bedding.

Plate 2.17: Spectacular sets of plane bedded sandstone with intercalations of mud laminae. Person for scale (height-1.65m)

Plate 2.18: Ripple cross laminated sandstone. Note transitions from plane bed to current ripple lamination and finally to wave ripple lamination from bottom to top of the photograph. Pen length 13 Cm.

Plate 2.19: Horizontally laminated quartzarenites of foreshore association (Swashing zone). Some sets show low angle discordance.

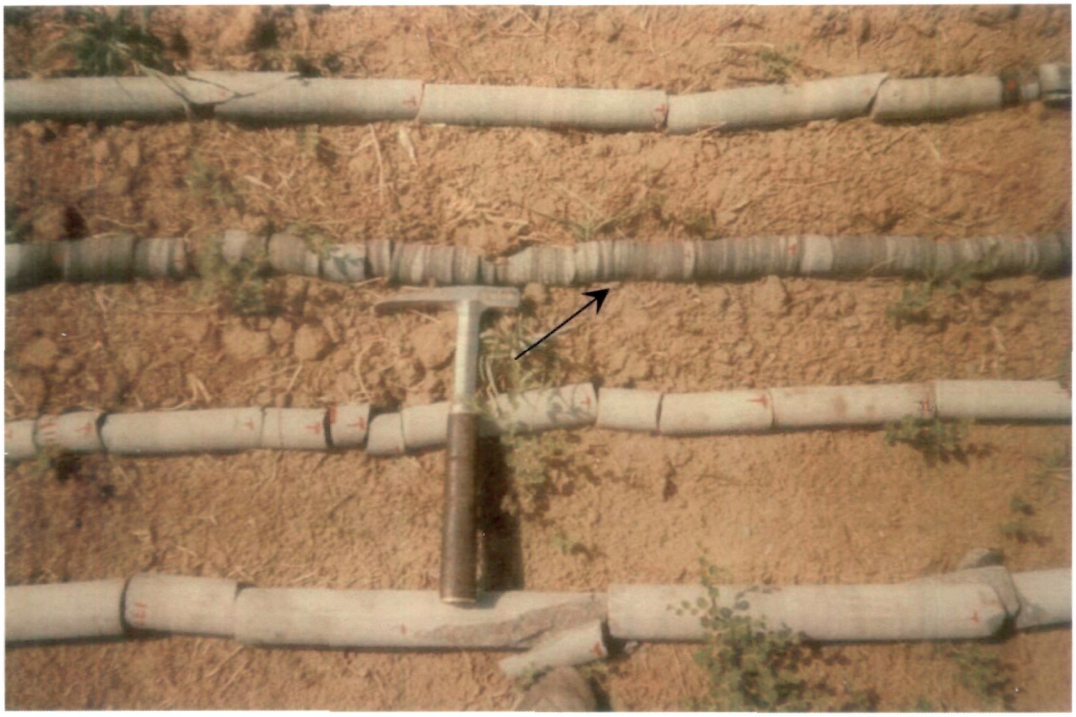

Plate 2.20: Finely intercalated sand and black muds (arrowed) of inner shelf association, rests are mature quartz arenites.

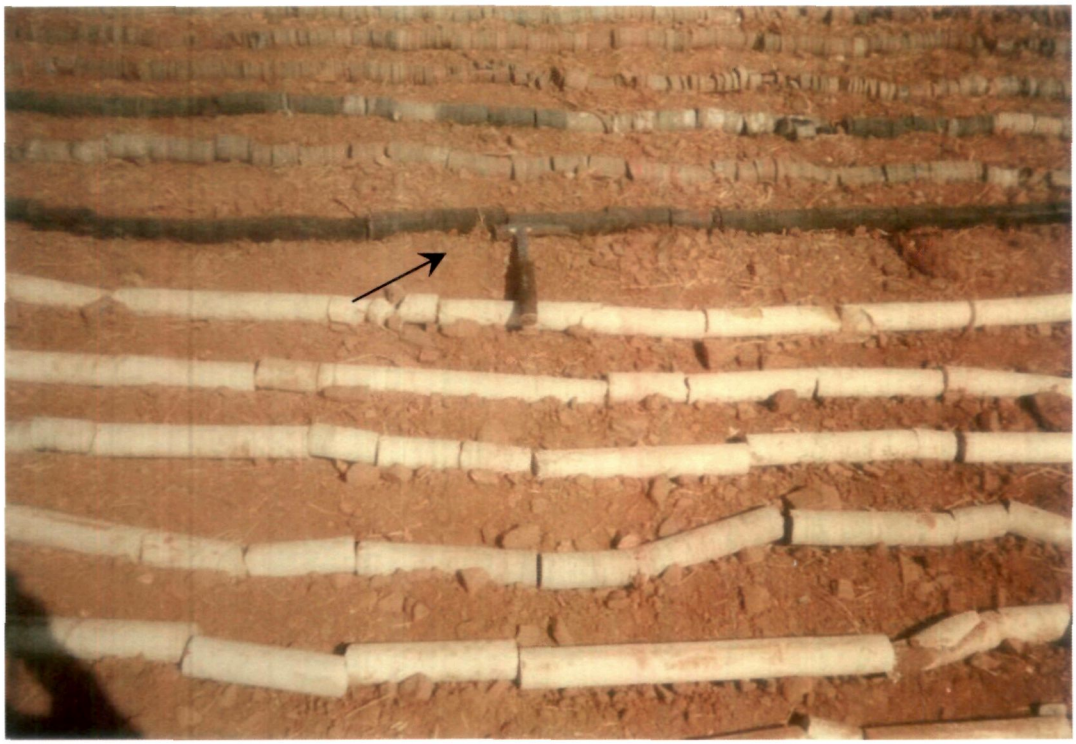

Plate 2.21: Laminated black siliceous muds (arrowed) of outer shelf association.

Plate 2.22: Oxide facies BIFs with interbedded black muds

Plate 2.23: Oxide facies BIFs with hematite and chert mesobands.

Plate 2.24: S-bands within shaley BIFs as indicated by the person (height-1.8m) in the photograph.

Plate 2.25: Micritic limestone with jasper and black chert bands.

Plate 2.26: Micritic limestone with shaley layers.

Plate 2.27: Clay beds of Morar Formation.

CHAPTER-III

Sampling procedures and analytical techniques for geochemical analyses

3.1 Introduction

The present work is the first attempt to carry out a detailed geochemical study of the sedimentary rocks of Bundelkhand block of Indian shield ranging in age from Mesoarchean to Mesoproterozoic. One of the major aim of present study was to generate high quality geochemical database on these sedimentary formations and to utilize the generated data to draw meaningful conclusions regarding provenance characteristics, paleoweathering conditions and tectonic setting during the process of sedimentation. Geochemical data-derived interpretations are utilized to asses the evolutionary history of continental crust and Archean-Proterozoic transition in this part of Indian shield. An attempt is also made to compare the observed evolutionary trend of Indian shield with those of other shield areas of the world. In addition, the Pb, Sr and Nd isotopic data on chemically precipitated sediments of Gwalior Group are also generated and utilized to find out the age of sedimentation and nature of exposed crust during Paleoproterozoic. The whole geochemical work is presented in five chapters i.e. Chapter-3, 4, 5, 6 and 7. In the present chapter the procedure adopted for collection of samples and techniques used for their geochemical analyses are summerised.

3.2 Sampling

Fresh homogenous samples representative of various formations were collected from quarries, road/railway cutting and natural outcrops. Weathered surfaces were avoided. While collecting sandstone-shale samples from basal Gwalior Group, emphasis was made to collect samples from different part of whole strike length of the basin as well as sampling of vertical columns within an area, to get better provenance signals. The basement Archean quartzites were collected where good outcrop with bigger dimension were available. The basement phyllites were not collected specifically because they occur as small xenoliths with considerable alterations, because of very high fluid to rock ratio during granite emplacement. The samples of Kaimur Group sandstones come from western and north-western part of

the Gwalior basin. Sampling of BIF from Gwalior basin was mainly dependent on the availability of fresh outcrops. Absolutely fresh BIF samples were collected from quarries in central and western part of the basin. Since the study has been undertaken to reconstruct the chemical evolution of the Precambrian ocean, only pure cherty BIFs were collected and BIFs with detrital clastic contaminant or shaley intercalations were avoided on the basis of visual observation. The sample collection for geochronological and isotopic study of chemical precipitates required special care and is described in the concerned chapter (Chapter VII).

3.3 Sample Preparation and Analytical Techniques

Fresh chips of rock samples were powdered to –200 mesh for maintaining the homogeneity and representativeness of the sample. The major, minor and some selective trace elements of the all the samples were analysed by WD-XRF method at XRF laboratory of Atomic Minerals Directorate for Exploration and Research (AMD), Nagpur. The REE and trace element contents of some selective sandstone samples and all of the BIF samples were analysed by ICP-MS method at geochemistry laboratory, NGRI, Hyderabad. Some the quartzite-sandstone-shale samples were analysed by INAA method, at the INAA laboratory, AMD-Hyderabad. The samples and elements analysed by different methods yield comparable results. The isotopic analysis was carried out at Isotope laboratory, AMD-Hyderabad. The details of sample preparation, instrumental techniques for each method are described separately as given below:

3.3.1 X-ray Fluorescence Spectrometry

Major, minor and a few selected trace elements were determined using the X-ray fluorescence spectrometer.

Sample Preparation: Collapsible aluminium cups were filled with 9 gm of boric acid that acts as a binding material. 1 gm of –200 mesh homogenised sample powder was sprayed upon it by uniformly covering the boric acid and about 15 tons of pressure was applied using a hydraulic press (H/100) to obtain 40 mm diameter pellets.

Instrument: A PHILIPS X'UNIQUE II microprocessor controlled wavelength dispersive, sequential X-ray fluorescence spectrometer with a 100 KVA generator was used for analysis. The system is interfaced to an online PC for preparing

calibration curves relating the concentration and intensity levels in standard as well as the unknown samples after due matrix corrections.

The X 40 version 4.0 software available in the computer is able to take care of dead time, background and line overlap corrections giving the output as directly as concentration in oxide weight percentages (or) in ppm as required, after correcting the counts into concentration with the help of the calibration curves.

The major and minor element data estimated by XRF are reproducible with a precision range of $\pm$ 5%.

3.3.2 Inductively Coupled Plasma – Mass Spectrometer

The concentrations of 18 trace elements and all the 14 rare earth elements were determined by an Inductively Coupled Plasma Mass Spectrometer

Sample Preparation:

0.1 gm of sample was taken in a Teflon beaker to which 7 ml. of HF (48%) and 3 ml of Conc. HNO_3 was added. This mixture was digested by keeping the beaker over hot plate. After confirming complete digestion, 10 ml. of HNO_3 of 1:1 concentration was added and was kept on hot plate till a clear solution was obtained. When the solution was cooled down, volume was made to 100 ml. with double distilled water after adding 10 ml of 1 ppm Rhodium solution as an internal standard (Balaram et al.1996).

Instrument:

ICP-Mass Spectrometer, Model ELAN DRC II (Perkin-Elmer Sciex Instrument, US) was used. The instrument is equipped with the state-of-the-art features such as Dynamic Reaction Cell (DRC) and other technical advancements leading to extremely low background, better sensitivity and precision. The detection limits for most of the elements are in pg/ml (ppt) and fg/ml (ppq) level. The system was optimized for maximum intensity (~40,000 counts/sec) across the mass range 1 ng/ml solution of Mg, Rh, In, Ba, Ce, Pb and U.

The precision of REE and trace element data is better than 5% RSD with comparable accuracies (Balaram et al., 1996, 1999)

3.3.3 Neutron Activation Analysis

Sample powder weighing 150 mg was sealed in a polythene vial. The sealed samples were irradiated in APSARA research reactor (A swimming pool type reactor) for seven hours, with neutron flux of 10^{11} neutron/cm^2/sec. Counting was done in 4-5 days after irradiation by using high purity Germanium coaxial semiconductor detector at INAA Laboratory, AMD-Hyderabad; with counting time of 100 sec, 500 sec, 1000 sec, 2000 sec, depending upon the element of interest. International rock standards (SY-3, GSN) were used for calibration.

3.3.4 Isotopic Analysis of chemical sediments

Limestone:

Limestones were treated with 2.5M HCl and HCl soluble carbonate fraction was taken for Pb, Sr and Nd isotope ratio measurement. HCl leachates (carbonate fraction) of total ten samples were analysed for Pb isotope ratio. Sr and Nd isotope ratio was analysed for eight and seven samples respectively. The non soluble residue was completely dissolved using HF and HNO_3 in teflon digestion bomb, these parts were taken as detrital component. The amount of detrital component varies from 24% to 36%. Detrital component of four samples were analysed for Sr isotope ratio.

BIF:

The Pb isotope data was obtained for different leach fraction from four BIF samples. Sequential leaching was done using 1N HBr in four steps. In step A whole rock powders was treated with 10ml acid for ten minutes. Following steps involve lesser volume of acid with longer time interval. In Step B the rock powder was treated with 7ml acid for 30 minute, Step C involve treatment for two hours with 5ml acid. The residue was digested using concentrated HF and HNO_3 followed by HCl in teflon digestion bomb (Step D).

Sr isotope ratios, Rb, Sr concentration were measured for 1N HCl soluble fraction for five samples and residue portion (HF +HNO_3 + HCl digestion) was analysed for two samples.

Nd isotope ratios and Sm, Nd, concentrations were measured for whole rock fraction after digestion with HF, HNO_3 and HCl.

Analytical procedure:

The elemental abundances of Sm, Nd, Rb, and Sr were determined by isotope dilution using tracers enriched in ^{87}Rb, ^{84}Sr, ^{149}Sm, and ^{146}Nd by using the procedure of Pandey et al. (1997). The isotopic ratios of Pb, Sr and Nd were determined on separately dissolved unspiked powders. Ion exchange techniques were used to separate the elements for isotopic analyses. Rb, Sr, REE were separated using Bio-Rad AG50x12 cation exchange resin. Sm and Nd were further separated from the REE group using biobeads coated with 10% HDEHP. Separation of Pb was carried out using Bio-Rad AG1x8 anion exchange resin. All isotopic analyses were carried out on a VG-354 multicollector mass spectrometer. The Sr and Nd isotopic ratios were normalized to $^{86}Sr/^{88}Sr$ = 0.1194 and $^{146}Nd/^{144}Nd$ = 0.7219, respectively. SRM987 standard gave a mean $^{87}Sr/^{86}Sr$ ratio pf 0.710241 ± 23 (N=15). JM Nd_2O_3 spec pure solution (NDN-1) from Cambridge gave a mean $^{143}Nd/^{144}Nd$ ratio of 0.511122 ± 10 (N=15) and La Jolla Nd standard gave mean $^{143}Nd/^{144}Nd$ ratio of 0.511875 ± 10 (N=5). USGS rock standard G-2 gave the following mean values (N=3): Rb = 170 ± 0.5 ppm, Sr = 480.5 ± 1 ppm, Sm = 7.18 ± 0.02 ppm, Nd = 53.88 ± 0.05 ppm, $^{87}Sr/^{86}Sr$ = 0.70995 ± 8, and $^{143}Nd/^{144}Nd$ = 0.512219 ± 13. The Pb isotopic ratios were corrected for mass fractionation of 0.15% per AMU based on routine measurements on SRM981 isotopic standard (Pandey et al., 1997). The 2σ analytical errors based on a number of duplicate analyses are 2 % in $^{87}Rb/^{86}Sr$, 1 % in $^{147}Sm/^{144}Nd$, 0.01 % in $^{87}Sr/^{86}Sr$, 0.005 % in $143Nd/^{144}Nd$, 0.1 % in $^{206}Pb/^{204}Pb$ and $^{207}Pb/^{204}Pb$, 0.15 % in $^{208}Pb/^{204}Pb$ and 2% in elemental abundances. The total procedural blanks were Rb< 3 ng, Sr < 5 ng, Sm < 0.1 ng, Nd < 0.1 ng, U < 3 ng and Pb < 5 ng. Errors in age and initial ratios are reported at 2σ and the value of MSWD was used for testing the goodness of fit after Wendt and Carl (1991). For the calculations of single stage model μ_1 the following values were used: age of earth (T) + 4.55 Ga, $^{206}Pb/^{207}Pb(a_0)$ = 9.307, $^{207}Pb/^{204}Pb(b_0)$ = 10.294 and , $^{208}Pb/^{204}Pb$ (c_0) =29.476 for the initial Pb isotopic composition. The decay constants used were $\lambda_{Rb} = 1.42 \times 10^{-11}\ a^{-1}$, $\lambda_{Sm} = 6.54 \times 10^{-12}\ a^{-1}$, $\lambda_{U238} = 1.55125 \times 10^{-10}\ a^{-1}$, $\lambda_{U235} = 9.8485 \times 10^{-10}\ a^{-1}$, $\lambda_{Th232} = 4.9475 \times 10^{-11}\ a^{-1}$. The Pb-Pb isochron regressions were performed out using the software ISOPLOT, version 2.2 (Ludwig, 1999).

CHAPTER-IV

Geochemistry of clastic sediments of Paleoproterozoic Gwalior Group: Implications for provenance, paleoweathering conditions and tectonic setting

4.1 Introduction

Geochemical composition of terrigenous clastic rock has been widely used to decipher the composition of source area (Wronkiewicz and Condie, 1987, 1990; Naqvi et al., 1988, 2002; McLennan et al., 1995; Sambasiva Rao et al., 1999; Cullers, 2000; Cullers and Podkovyrov, 2000; Bhat and Ghosh, 2001; Condie et al., 2001; Saha et al., 2004), to evaluate weathering processes and paleoclimate (Nesbit and Young, 1982; Sreenivas and Srinivasan, 1994; Fedo et al., 1995, 1996), to reconstruct the tectonic setting of depositional basin (Bhatia, 1983; Bhatia and Crook, 1986; Roser and Korsch, 1986, 1988; McLennan et al., 1990), to quantify the secondary processes like post depositional metasomatism (Fedo et al., 1995, 1997) and to evaluate the composition and evolution of continental crust (Taylor and McLennan, 1985, 1995; McLennan and Taylor, 1991;Condie, 1993; Lahtinen, R., 2000). In this regard fine grained sedimentary rocks like shales, mudstones and phyllites are more useful as they are thoroughly homogenized before deposition and acquire debris from wide area thus provide crustal scale sample, enabling study of crustal-scale processes (Taylor and McLennan, 1985). Although chemical changes may take place during sedimentary processes like weathering, erosion, sediment transport, deposition and diagenesis; certain insoluble elements with short residence time in sea water are transferred almost quantitatively to clastic sediments (Taylor and McLennan, 1985; Fedo et al., 1996). Of these, the rare earth elements (REE), Th, Sc and Cr (Condie and Wronkiewicz, 1990) are most useful for inferring crustal composition as they are not seriously affected by secondary processes like diagenesis, metamorphism (as are Fe, Mn, Pb), and are least affected by heavy mineral fractionation (such as Zr, Hf, Sn). Amongst these elements some are highly incompatible (e.g. Th, La) during magmatic processes and thus are enriched in residual silicate melts. On the other hand others are compatible (e.g. Sc, Cr) and concentrate in early crystallizing minerals such as pyroxene. Thus the relative abundances of these two groups of elements provide an index for the relative proportion of felsic to mafic rocks in the source terrain of the

sediments. Furthermore the rare earth elements (REE) are the most thoroughly studied group of trace elements in geochemistry (Taylor and McLennan, 1988). They have a considerable range of ionic radius, so that overall shape of the REE pattern is sensitive to igneous fractionation processes. The REE patterns hence provide best indicator for crustal differentiation processes and can distinguish mantle from intracrustal sources (McLennan and Taylor, 1991). The temporal evolution of composition of upper continental crust can be deciphered from study of clastic rocks of similar tectonic association of different geological ages (Gibbs et al., 1986; Lahtinen, 2000).

In India most of the work on geochemistry of sedimentary rocks has been carried out on the Archean rocks of Dharwar craton (Naqvi and Hussain, 1972, Naqvi and Rogers 1987, Arora and Naqvi, 1993; Manikyamba et al., 1997; Naqvi et al., 1988, 2002 and references therein). Such studies have been restricted on Archean sedimentary rocks because early Proterozoic sequences are not found in south Indian shield suggesting a gap of sedimentary records between 2.7 Ga and 1.7 Ga. Despite an early beginning by Naqvi and his co-workers the application of geochemistry on sedimentological studies did not catch up widely. Although some sedimentary rock formations of Aravalli (Banerjee and Bhattacharya, 1993; Raza et al., 2002) and Singhbhum (Sengupta et al., 1991; Sharma et al., 1994; Saha et al., 2004) cratons have been studied for geochemistry in recent years, the sedimentary rock formation of Bundelkhand craton have not attracted the attention of geoscientists and thus no geochemical data of these rocks are available at present.

Since the composition of clastic rocks is strongly related to provenance which is largely controlled by source rock composition, climate and relief; the geochemical studies of sediments in recent years have been carried out to resolve the problems related to provenance characteristics such as rock types, unroofing, sediment recycling, paleoweathering and also the rate, frequency and mechanism of juvenile mantle additions into the crust. The geochemical studies are also helpful to understand the tectonic setting of the sedimentary basins. However, such studies are hampered by lack of continuous sedimentary records particularly in Precambrian terrains. One of the major objective of the present study is to generate geochemical data on sedimentary rocks of Gwalior Group and utilize it for constraining provenance characteristics, composition of upper continental crust, paleoweathering conditions and tectonic setting of the basin. However, keeping in view the availability of a

complete sedimentary record ranging in age from Mesoarchean to Mesoproterozoic in the area of study, the BGGC metasedimentary enclaves of Archean age and Kaimur sandstone of Mesoproterozoic age are also studied for their geochemistry along with clastic sediments of Gwalior Group. As such study primarily involves chemical features over time, any variation in them should; as such be a reflection of changes in source lithology by means of upliftment of provenance and resultant exposure of newer lithologies or addition of Juvenile mantle or both, and also climate attended during weathering.

Therefore the objective of the present geochemical study of Bundelkhand block is two fold: (i) to study the geochemistry of clastic sediments of Gwalior Group for constraining provenance, upper crustal composition, weathering conditions during Paleoproterozoic in this part of Indian shield and (ii) to study the geochemistry of Mesoarchean sedimentary enclaves and Mesoproterozoic Kaimur Group sediments and to determine temporal changes in upper crustal composition by comparing geochemical characteristics of Paleoproterozoic Gwalior sediments with those of above mentioned older and younger sedimentary sequences of the area.

The geochemistry of Gwalior Group clastic sediments is discussed in this chapter and the geochemical characteristics of underlying and overlying sedimentaries are discussed and presented in Chapter-V.

4.2 Geochemistry

4.2.1 Major elements

The geochemical data of Gwalior group shale and sandstones are presented in table 4.1 and 4.2 respectively. The Gwalior Group sediments define a linear trend on SiO_2-Al_2O_3 graph (r = 0.92, Fig.4.1) with shales containing less than 70% SiO_2 and more than 15% Al_2O_3. Quartz-arenitic sandstones define other extremity of the graph containing 89-98% SiO_2 and <1-5% Al_2O_3, while quartzwackes has intermediate chemistry with 7-11% Al_2O_3 content and 81-83% SiO_2 content. In general these detrital sediments can be considered as mixtures of quartz and illite end members (Fig.4.1).

The K_2O/Na_2O ratios of Gwalior shales ranges from 8.50 to 12.18, that is 3 to 4 times to the value of different post Archean shale standards (3.1-3.5, Condie, 1993). However the SiO_2/Al_2O_3 ratio of these shales varies from 2.58 to 3.63. In $K2O/Na_2O$ vs. SiO_2/Al_2O_3 plot (Fig.4.2) the Gwalior shales are comparable to different

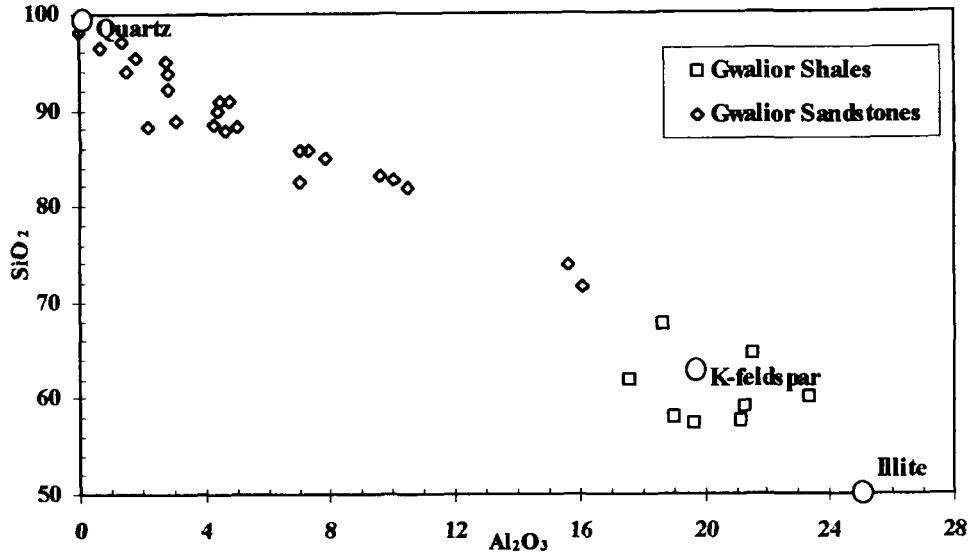

Fig.4.1: Al2O3-SiO2 graph showing Gwalior group of shale and sandstones. The smooth graph suggests that the sediments can be considered as the product of mixing of quartz and illite.

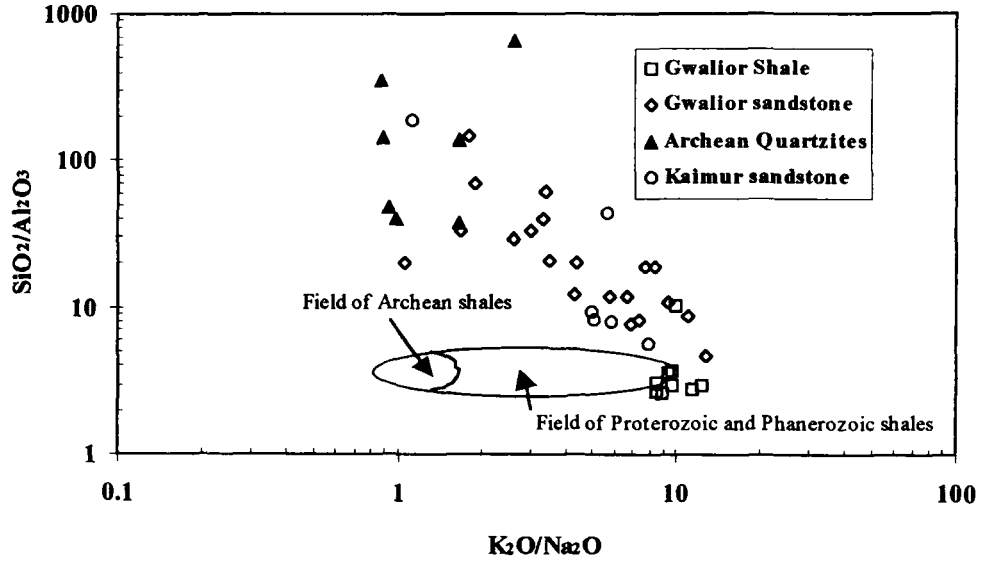

Fig.4.2: SiO2/Al2O3 vs. K2O/Na2O plot for the Gwalior Group shale and sandstones. Also plotted are the data of Kaimur Group sandstones and Archean quartzites. Boundaries of Archean, Proterozoic-Phanerozoic shales from Wronkiewicz and Condie (1987)

Table 4.1: Geochemical composition of Gwalior Group shales[$]

Sample No	TUN-1[#]	TUN-2	TUN-3	JSX-2[#]	JSX-3[#]	NGN-1	BDE-1[#]	SDL-2[@]	MHG-1
SiO_2	57.39	58.04	57.54	61.86	59.15	64.58	67.79	60.11	73.94
TiO_2	0.78	0.84	0.89	0.59	0.91	0.64	0.43	0.97	0.36
Al_2O_3	19.64	19.01	21.16	17.58	21.31	21.55	18.67	23.33	15.64
$FeO^{(T)}$	9.04	9.08	7.18	7.03	6.69	2.59	2.26	7.94	1.67
MgO	1.47	1.42	1.55	1.20	1.60	0.65	0.77	0.81	0.51
MnO	0.03	0.02	0.01	0.05	<0.01	<0.01	<0.01	0.01	<0.01
CaO	0.50	0.48	0.64	0.42	0.56	0.13	0.07	0.06	0.06
Na_2O	0.89	1.00	0.99	0.86	0.77	0.80	0.89	0.66	0.53
K_2O	8.64	8.50	8.42	7.98	8.73	9.74	8.60	5.90	6.70
P_2O_5	0.05	0.02	0.03	0.02	0.03	0.05	0.04	0.05	0.02
Total	98.43	98.41	98.41	97.59	99.75	100.73	99.52		99.43
Sc	13.62			11.08	17.69		9.27	22.00	
V	55.82			44.61	97.16		36.01	44.00	
Cr	137.80	137.00	168.00	108.94	165.06	78.00	60.68	257.00	56.00
Co	15.86			14.10	17.70		3.49	38.00	
Ni	44.05	43.00	59.00	44.59	54.45	23.00	28.74	55.00	24.00
Cu	5.03			5.24	8.82		5.28	40.00	
Zn	50.22			38.92	54.28		20.69		
Ga	22.86	23.00	24.00	19.46	26.93	24.00	20.28	26.00	23.00
Rb	325.17	274.00	322.00	285.07	362.62	335.00	335.70	189.00	203.00
Sr	58.12	32.00	27.00	60.64	52.58	71.00	57.86		43.00
Y	14.88	16.00	27.00	14.41	14.59	19.00	27.28	31.00	12.00
Zr	197.38	188.00	137.00	237.34	193.13	465.00	832.14	264.00	269.00
Nb	13.74	8.00	17.00	10.21	14.27	18.00	10.31	14.00	
Cs	9.92			7.50	18.44		3.51	6.40	
Ba	844.62	921.00	772.00	836.57	813.91	791.00	537.26	434.00	570.00
Hf	6.18			7.35	5.95		26.96	12.80	
Ta	1.67			1.35	1.42		1.48	2.20	
Pb	11.43	18.00	23.00	5.98	1.78	22.00	13.92	56.00	18.00
Th	20.04	13.00	32.00	19.53	22.10	40.00	56.58	39.00	27.00
U	2.05		21.00	1.94	3.01		11.18	7.00	26.00
La	43.44			33.15	54.18		59.99	72.00	
Ce	71.09			55.17	84.99		147.56	139.00	
Pr	8.23			6.36	10.18		14.87		
Nd	27.49			21.51	34.30		52.41	50.00	
Sm	4.89			4.14	5.90		8.27	8.80	
Eu	1.14			0.99	1.30		1.26	1.30	
Gd	3.83			3.39	4.51		6.66	9.26	
Tb	0.57			0.53	0.64		1.02	1.50	
Dy	3.03			3.00	3.31		5.66		
Ho	0.58			0.56	0.61		1.16		
Er	1.61			1.54	1.70		3.52		
Tm	0.27			0.26	0.28		0.69		
Yb	1.53			1.53	1.65		4.72	3.20	
Lu	0.26			0.25	0.27		0.85	0.50	

T.6858*

Table 4.1: (Continued)

Sample No	TUN-1#	TUN-2	TUN-3	JSX-2#	JSX-3#	NGN-1	BDE-1#	SDL-2@	MHG-1
La_N	184.83			141.05	230.54		255.29	306.38	
Ce_N	117.89			91.50	140.94		244.71	230.51	
Pr_N	92.52			71.51	114.36		167.06		
Nd_N	60.81			47.59	75.88		115.95	110.62	
Sm_N	33.29			28.16	40.11		56.24	59.86	
Eu_N	20.39			17.68	23.18		22.54	23.21	
Gd_N	19.46			17.22	22.89		33.81	47.02	
Tb_N	15.81			14.81	17.72		28.33	41.67	
Dy_N	12.48			12.36	13.64		23.28		
Ho_N	10.34			9.96	10.93		20.66		
Er_N	10.15			9.66	10.66		22.13		
Tm_N	11.04			10.71	11.75		28.92		
Yb_N	9.36			9.39	10.10		28.93	19.63	
Lu_N	10.63			10.50	11.13		35.58	20.83	
$(La/Yb)_N$	19.74			15.03	22.83		8.83	15.61	
$(Gd/Yb)_N$	2.08			1.83	2.27		**1.17**	2.39	
$(La/Sm)_N$	5.55			5.01	5.75		4.54	5.12	
Eu/Eu*	0.80			0.80	0.76		0.52		
SiO_2/Al_2O_3	2.92	3.05	2.72	3.52	2.78	3.00	3.63	2.58	4.73
K_2O/Na_2O	9.71	8.50	8.51	9.28	11.34	12.18	9.66	8.94	12.64
Al_2O_3/TiO_2	25.18	22.63	23.78	29.80	23.42	33.67	43.42	24.05	43.44
La/Sc	3.19			2.99	3.06		6.48	3.27	
Th/Sc	1.47			1.76	1.25		6.11	1.77	
Ba/Co	53.24			59.32	45.99		153.85	11.42	
Sc/Th	0.68			0.57	0.80		**0.16**	0.56	
Cr/Th	6.88	10.54	5.25	5.58	7.47	1.95	1.07	6.59	2.07
Co/Th	0.79			0.72	0.80		**0.06**	0.97	
La/Th	2.17			1.70	2.45		**1.06**	1.85	
Rb/Sr	5.59	8.56	11.93	4.70	6.90	4.72	5.80		4.72
Rb/Ba	0.38	0.30	0.42	0.34	0.45	0.42	0.62	0.44	0.36
Zr/Y	13.27	11.75	5.07	16.47	13.24	24.47	30.51	8.52	22.42
CIA	62.62	61.87	63.99	61.91	64.49	64.05	63.14	75.48	65.51
PIA	81.26	79.58	81.18	80.41	83.85	87.64	85.47	93.41	89.53
CIW	89.22	88.30	88.34	88.98	90.32	93.28	92.15	95.13	94.10

$ Major elements in oxide wt.%, trace elements in PPM; total Fe as $FeO^{(T)}$; <, below detection; -, not analyzed; Eu/Eu* = $Eu_N/(Sm_N \times Gd_N)^{1/2}$; # REE and trace element analyses by ICP-MS; @ REE analyses by INAA, Gd values are extrapolated after Condie (1993), $Gd_N = (Sm_N \times Tb_N \times Tb_N)^{1/3}$.

Table 4.2: Geochemical composition of Gwalior Group sandstones[$]

Sample No	BDE-2[#]	BDE-3[#]	GJG-1[#]	GJE-2	SDL-1[@]	JRS-1[@]	LR-2[@]	DK-1[@]	DK-1A[@]	DK-2[@]
SiO_2	82.76	89.91	85.83	90.97	97.05	98.10	96.56	93.98	88.18	98.08
TiO_2	0.29	0.10	0.11	0.08	0.06	0.03	0.04	0.05	0.09	0.03
Al_2O_3	10.06	4.41	7.01	4.45	1.41	<0.01	0.66	1.52	2.18	<0.01
$FeO^{(T)}$	0.96	1.55	2.77	1.91	0.71	0.70	0.63	0.93	7.45	0.67
MgO	0.37	0.18	0.12	<0.01	0.07	0.02	0.09	0.10	0.15	0.03
MnO	<0.01	<0.01	<0.01	<0.01	0.01	<0.01	<0.01	<0.01	0.01	<0.01
CaO	<0.01	<0.01	0.01	<0.01	<0.01	<0.01	<0.01	<0.01	0.03	<0.01
Na_2O	0.66	0.54	0.73	0.53	0.40	0.47	0.48	0.58	0.61	0.57
K_2O	4.87	2.35	3.16	0.56	0.75	0.62	0.86	1.95	2.03	0.55
P_2O_5	<0.01	<0.01	<0.01	<0.01	0.05	0.03	0.03	0.03	0.05	0.03
Total	99.97	99.04	99.74	98.50	100.51	99.97	99.35	99.15	100.78	99.96
Sc	3.25	2.30	2.55		1.80	<0.5	<0.5	1.20	1.90	<0.5
V	15.31	12.72	17.73		9.00			8.00	36.00	
Cr	47.51	43.49	61.46	47.00	77.00	117.00	96.00	93.00	66.00	100.00
Co	2.88	1.61	1.97		1.10	1.40	1.20	1.30	1.80	1.50
Ni	22.92	38.22	42.67	41.00	63.00	79.00	73.00	72.00	38.00	76.00
Cu	3.64	3.80	5.44		28.00	35.00	18.00	20.00	5.00	32.00
Zn	10.67	7.38	8.34							
Ga	8.12	4.40	5.77	22.00						
Rb	146.58	75.96	96.74	29.00	36.00	37.00	42.00	71.00	73.00	23.00
Sr	27.75	18.16	19.56	<5	21.00	5.00	<5	13.00	5.00	<5
Y	32.59	15.36	10.81	20.00	12.00	<5	7.00	<5	<5	<5
Zr	1015.91	493.11	388.84	213.00	129.00	48.00	68.00	88.00	96.00	44.00
Nb	7.01	2.07	2.38	14.00			6.00		6.00	
Cs	1.95	0.99	1.37		<0.5	<0.5	<0.5	0.60	0.80	<0.5
Ba	280.06	143.35	196.23	90.00	250.00	61.00	<50	159.00	95.00	88.00
Hf	36.23	17.50	13.47		2.60	0.90	1.50	2.80	3.10	0.80
Ta	1.08	0.45	0.52		<0.1	<0.1	<0.1	<0.1	0.30	<0.1
Pb	21.83	19.51	8.44	23.00	123.00	19.00	12.00	9.00	13.00	13.00
Th	21.58	8.91	8.01	7.00	5.20	0.70	2.50	5.60	9.20	0.70
U	6.67	3.33	2.48	<2.0	<2.0	<2.0	≤2.0	3.00	5.50	<2.0
La	22.34	17.92	15.78		13.00	2.50	6.00	11.00	30.00	<1
Ce	57.97	45.53	40.61		25.00	5.00	11.00	26.00	68.00	<1
Pr	5.56	4.39	4.02							
Nd	19.61	15.36	14.57							
Sm	3.56	2.54	2.50		2.80	0.80	1.20	1.80	2.70	0.40
Eu	0.71	0.41	0.43		0.50	<0.2	0.20	0.30	0.40	<0.2
Gd	3.92	2.51	2.15							
Tb	0.86	0.45	0.38		0.40	<0.2	0.30	0.30	0.50	<0.2
Dy	5.35	2.59	2.05							
Ho	1.21	0.57	0.44							
Er	3.61	1.70	1.38							
Tm	0.70	0.32	0.28							
Yb	4.36	2.10	1.74		0.50	<0.5	<0.5	0.60	0.90	<0.5
Lu	0.80	0.38	0.30		0.10	<0.1	<0.1	0.10	0.20	<0.1

Table 4.2: (Continued)

Sample No	BDE-2#	BDE-3#	GJG-1#	GJE-2	SDL-1@	JRS-1@	LR-2@	DK-1@	DK-1A@	DK-2@
La_N	95.08	76.27	67.14		55.32	10.64	25.53	46.81	127.66	
Ce_N	96.13	75.50	67.35		41.46	8.29	18.24	43.12	112.77	
Pr_N	62.44	49.37	45.18							
Nd_N	43.38	33.97	32.24							
Sm_N	24.21	17.27	16.97		19.05	5.44	8.16	12.24	18.37	2.72
Eu_N	12.75	7.39	7.73		8.93		3.57	5.36	7.14	
Gd_N	19.88	12.76	10.90		13.30		8.28	9.47	15.24	
Tb_N	23.83	12.50	10.44		11.11		8.33	8.33	13.89	
Dy_N	22.00	10.67	8.44							
Ho_N	21.61	10.11	7.88							
Er_N	22.71	10.66	8.70							
Tm_N	29.08	13.25	11.46							
Yb_N	26.72	12.85	10.64		3.07			3.68	5.52	
Lu_N	33.13	15.67	12.54		4.17			4.17	8.33	
$(La/Yb)_N$	3.56	5.93	6.31		18.03			12.72	23.12	
$(Gd/Yb)_N$	0.74	0.99	1.02		4.34			2.57	2.76	
$(La/Sm)_N$	3.93	4.42	3.96		2.90	1.95	3.13	3.82	6.95	
Eu/Eu*	0.58	0.50	0.57		0.56		0.43	0.50	0.43	
SiO_2/Al_2O_3	8.23	20.39	12.24	20.44	68.83		146.30	61.83	40.45	
K_2O/Na_2O	7.38	4.35	4.33	1.06	1.88	1.32	1.79	3.36	3.33	0.96
Al_2O_3/TiO_2	34.69	44.10	63.73	55.63	23.50		16.50	30.40	24.22	
La/Sc	6.89	7.81	6.19		7.22			9.17	15.79	
Th/Sc	6.65	3.88	3.14		2.89			4.67	4.84	
Ba/Co	97.18	88.93	99.66		227.27	43.57		122.31	52.78	58.67
Sc/Th	0.15	0.26	0.32		0.35			0.21	0.21	
Cr/Th	2.20	4.88	7.67	6.71	14.81	167.14	38.40	16.61	7.17	142.86
Co/Th	0.13	0.18	0.25		0.21	2.00	0.48	0.23	0.20	2.14
La/Th	1.04	2.01	1.97		2.50	3.57	2.40	1.96	3.26	
Rb/Sr	5.28	4.18	4.95		1.71	7.40		5.46	14.60	
Rb/Ba	0.52	0.53	0.49	0.32	0.14	0.61		0.45	0.77	0.26
Zr/Y	31.17	32.11	35.97	10.65	10.75		9.71			
CIA										
PIA			74.65							
CIW			85.19					60.99	67.33	

$ Major elements in oxide wt.%, trace elements in PPM; total Fe as $FeO^{(T)}$; <, below detection; -, not analyzed; $Eu/Eu^* = Eu_N/(Sm_N \times Gd_N)^{1/2}$; # REE and trace element analyses by ICP-MS; @ REE analyses by INAA, Gd values are extrapolated after Condie (1993), $Gd_N = (Sm_N \times Tb_N \times Tb_N)^{1/3}$.

Table 4.2: (Continued)

Sample No	TUN-4[£]	MHG-2[£]	MHG-3[£]	GJ-A[£]	GJ-B[£]	GJR-1[£]	GJR-2[£]	GJR-3[£]
SiO2	95.14	83.23	88.41	81.83	88.30	85.76	82.59	95.39
TiO2	0.04	0.09	0.09	0.22	0.08	0.08	0.18	0.06
Al2O3	2.78	9.59	4.30	10.46	5.04	7.30	7.00	1.79
FeO(T)	1.41	0.78	2.07	1.47	2.39	1.21	4.74	1.42
MgO	<0.01	0.20	0.06	0.24	0.04	0.08	0.11	<0.01
MnO	<0.01	<0.01	<0.01	<0.01	<0.01	0.03	<0.01	<0.01
CaO	<0.01	0.02	<0.01	0.03	0.01	0.01	0.05	<0.01
Na2O	0.48	0.56	0.47	0.70	0.05	0.59	0.52	0.50
K2O	0.01	6.14	1.65	4.77	2.45	3.89	2.99	0.03
P2O5	<0.01	<0.01	<0.01	<0.01	<0.01	<0.01	0.01	<0.01
Total	99.86	100.61	97.05	99.72	98.36	98.95	98.19	99.19
V								
Cr	77.00	31.00	36.00	53.00	91.00	32.00	35.00	66.00
Co								
Ni	63.00	28.00	34.00	36.00	57.00	33.00	29.00	50.00
Cu								
Zn								
Ga	26.00	25.00	19.00	24.00	25.00	24.00	30.00	28.00
Rb	18.00	184.00	69.00	161.00	79.00	131.00	105.00	8.00
Sr	10.00	55.00	<5	36.00	37.00	37.00	56.00	<5
Y	8.00	14.00	6.00	<5	13.00	18.00	19.00	15.00
Zr	63.00	188.00	107.00	211.00	146.00	100.00	254.00	90.00
Nb	9.00	10.00	<5	<5	9.00	<5	9.00	16.00
Ba	<50	650.00	160.00	289.00	282.00	481.00	196.00	<50
Pb	44.00	17.00	27.00	22.00	24.00	22.00	20.00	22.00
Th	<5	19.00	<5	5.00	<5	13.00	17.00	<5
U	<5	<5	5.00	<5	5.00	<5	<5	<5
SiO_2/Al_2O_3	34.22	8.68	20.56	7.82	17.52	11.75	11.80	53.29
K_2O/Na_2O	0.02	10.96	3.51	6.81	46.23	6.59	5.75	0.06
Al_2O_3/TiO_2	69.50	106.56	47.78	47.55	63.00	91.25	38.89	29.83
Cr/Th		1.63		10.60		2.46	2.06	
Rb/Sr	1.80	3.35		4.47	2.14	3.54	1.88	
Rb/Ba		0.28	0.43	0.56	0.28	0.27	0.54	
Zr/Y	7.88	13.43	17.83		11.23	5.56	13.37	6.00
CIA		55.78		62.15	64.64	58.40	62.60	
PIA		75.46		81.45	95.77	75.76	79.91	
CIW		90.92		89.66	97.95	88.07	88.09	

[$] Major elements in oxide wt. %, trace elements in PPM; total Fe as $FeO^{(T)}$; <, below detection; -, not analyzed. [£] All the elements were analysed by WD-XRF method.

Table 4.2: (Continued)

Sample No	SND-1[£]	GJE-1[£]	REG/6[£]	REG/7[£]	RB/12[£]	P/12[£]	REG/5[£]
SiO2	92.25	84.98	90.92	93.77	88.95	71.70	87.88
TiO2	0.09	0.12	0.13	0.01			0.24
Al2O3	2.81	7.82	4.76	2.85	3.06	16.06	4.63
FeO(T)	1.78	1.78	2.13	2.63	6.79	2.43	4.69
MgO	<0.01	0.14	0.44	0.28	0.14	0.23	0.45
MnO	<0.01	<0.01	<0.01	<0.01	0.01	<0.01	0.01
CaO	<0.01	0.01	0.19	0.09	0.14	0.12	0.26
Na2O	0.42	0.52	0.10	0.10	0.10	0.10	0.10
K2O	0.71	4.82	0.77	0.30	0.26	8.56	0.83
P2O5	<0.01	<0.01	0.23	<0.01	0.27	0.04	0.07
Total	98.06	100.19	99.67	100.03	99.72	99.24	99.16
V					66.00	34.00	8.00
Cr	88.00	41.00	79.00	96.00	63.00	37.00	70.00
Co			10.00	10.00	11.00	10.00	11.00
Ni	57.00	27.00	106.00	155.00	58.00	53.00	103.00
Cu			17.00	24.00	97.00	11.00	45.00
Zn			17.00	17.00	48.00	22.00	30.00
Ga	22.00	23.00					
Rb	45.00	157.00	58.00	47.00	40.00	248.00	55.00
Sr	10.00	51.00	144.00	35.00	67.00	69.00	48.00
Y	18.00	19.00	14.00	<5	149.00	24.00	32.00
Zr	152.00	246.00	352.00	34.00		359.00	
Nb	<5	<5	8.00	5.00	57.00	22.00	13.00
Ba	153.00	606.00	481.00	124.00	189.00		149.00
Pb	30.00	15.00	21.00	15.00	320.00	50.00	53.00
Th	16.00	9.00	41.00	<5	1869.0	129.00	199.00
U	<5	12.00	9.00	<5	46.00	7.00	24.00
SiO_2/Al_2O_3	32.83	10.87	19.10	32.90	29.07	4.46	18.98
K_2O/Na_2O	1.69	9.27	7.70	3.00	2.60	85.60	8.30
Al_2O_3/TiO_2	31.22	65.17	36.62	285.00			19.29
Cr/Th	5.50	4.56	1.93		0.03	0.29	0.35
Rb/Sr	4.50	3.08	0.40	1.34	0.60	3.59	1.15
Rb/Ba	0.29	0.26	0.12	0.38	0.21		0.37
Zr/Y	8.44	12.95	25.14		0.00	14.96	0.00
CIA		56.22	77.99	81.36	81.37	62.47	75.09
PIA		74.87	88.51	88.50	86.90	94.67	85.41
CIW		89.95	90.32	89.68	87.96	97.67	87.90

[$] Major elements in oxide wt.%, trace elements in PPM; total Fe as $FeO^{(T)}$; <, below detection; -, not analyzed. [£] All the elements were analysed by WD-XRF method.

Precambrian shales with little more K_2O/Na_2O ratios. The associated sandstones contain higher SiO_2/Al_2O_3 values at a given K_2O/Na_2O ratio than shale indicating quartz dilution. The average Gwalior shales are compared with standard averages of Archean, Proterozoic and Phanerozoic shales (Condie, 1993) and average Archean and post Archean upper crust (McLennan, 1982) in Figure 4.3. The composition of Gwalior shales is comparable to different shale standards in terms of their SiO_2, Al_2O_3, TiO_2 and FeO contents; however they are strongly depleted in mobile constituents like CaO, Na_2O and MgO and are enriched in K_2O contents. The depletion in CaO and Na_2O content in Gwalior shale are more conspicuous when compared with Archean upper crust and post Archean upper crust (Fig.4.3E & F). The strong depletion of these elements suggests strong chemical weathering of their protoliths. The enrichment in K_2O and depletion in MgO refers to more felsic provenance of these rocks and also possible post depositional introduction of K_2O during diagenesis (Fedo et al., 1995). A similar pattern is also observed for Gwalior sandstones when compared to average Proterozoic cratonic sandstone (Fig.4.3D, Condie, 1993); characterized by severe CaO, MgO depletion and K_2O enrichment.

As Gwalior Group shale-sandstone assemblage defines a smooth graph in SiO_2, Al_2O_3 space (Fig.4.1), they are considered as single population for statistical calculation to identify the mineralogical control of major and trace elements chemistry. The SiO_2 shows a strong negative correlation with Al_2O_3 ($r = -0.98$) as expected, because in sedimentary rocks the contents of Al2O3 and SiO_2 are controlled by aluminous clay and quartz contents respectively. On the basis of these ratios the whole sandstone-shale assemblage of Gwalior Group can again be seen as mixing of illite and quartz end members with quartzwackes define the intermediate position. The illite control is evident as Al_2O_3 is strongly correlated with K_2O ($r=0.94$). Na_2O and $FeO^{(T)}$ are also appears to be bounded in clay mineral as they are moderately correlated with Al_2O_3 ($r=0.61$ and 0.60 respectively). This indicates that the weathering was an important factor in the source area controlling the abundances of these elements. Probably the clays may have been more aluminous and later enriched in K to form illite (Fedo, 1995). The highly weathered nature of source terrain is evident as Al_2O_3 and TiO_2 are strongly correlated ($r=0.86$, Fig.4.4). In different source rocks Al_2O_3-TiO_2 ratios vary, thus they form scatter in unweathered sediments. Being an immobile element both Al and Ti are enriched in residual weathering profile and binary mixing of these components in sediments give rise to their strong positive

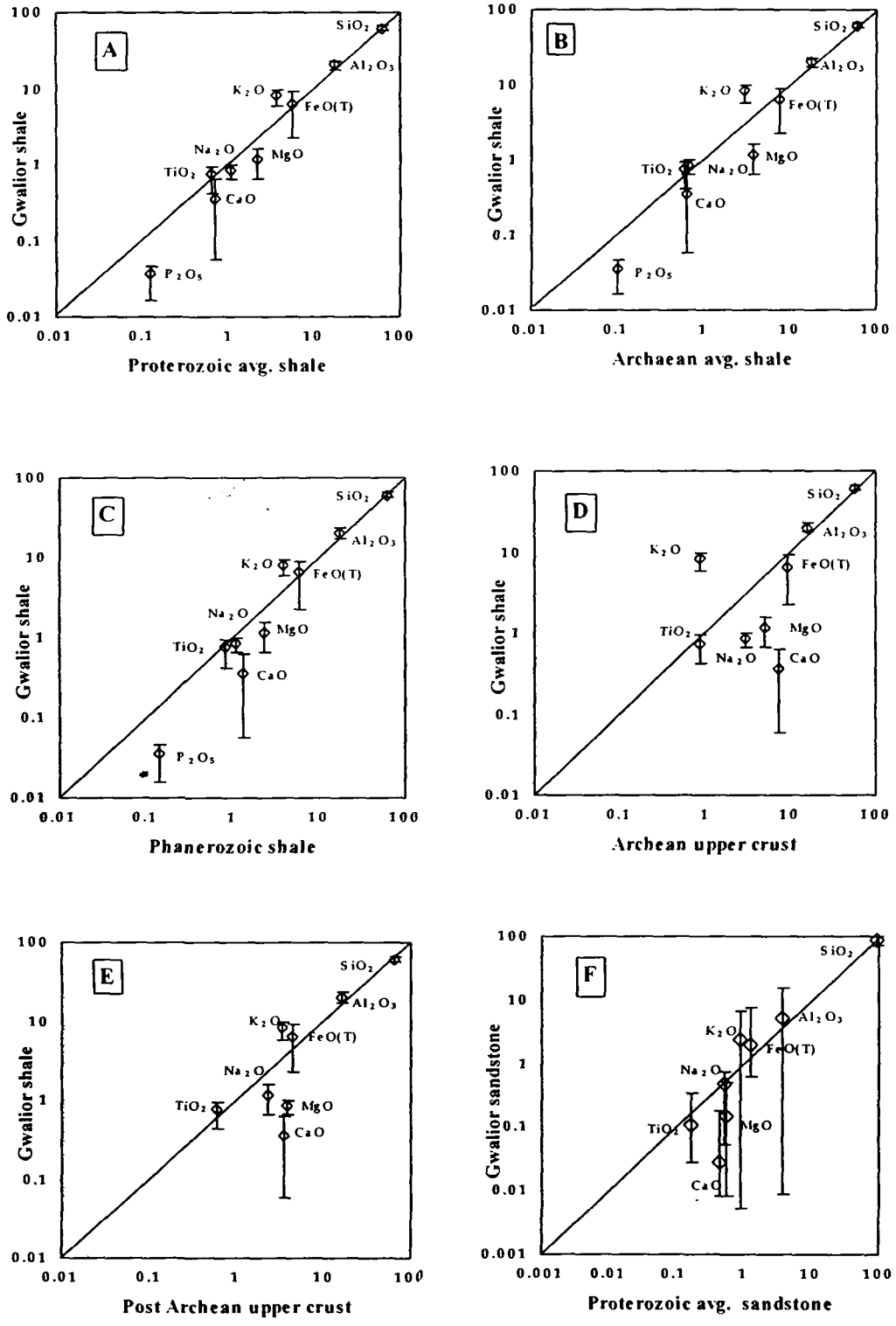

Fig.4.3: Log-log plots for major elements of Gwalior Group shales with reference to: (A) average Proterozoic shale; (B) average Archean shale; (C) average phanerozoic shale; (source Condie, 1993) (D) Archean upper crust; (E) post Archean upper Crust (source McLennan, 1982); and for Gwalior Group sandstones with reference to (F) average Proterozoic sandstone (source Condie,1993). The compositional variations of Gwalior clastics are shown as error bars.

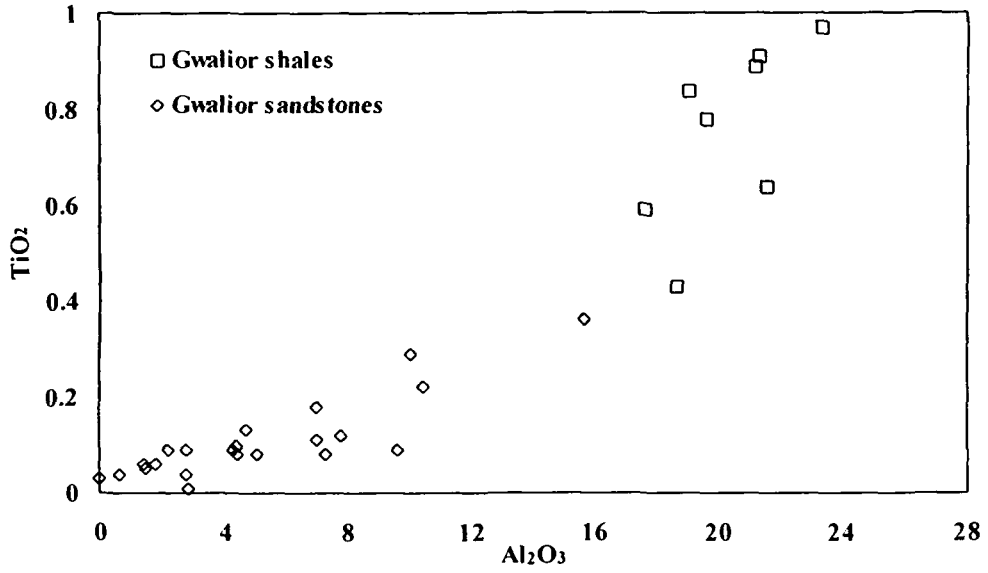

Fig.4.4: Al_2O_3 vs. TiO_2 plot of the Gwalior Group shales and sandstones. Note strong positive correlation.

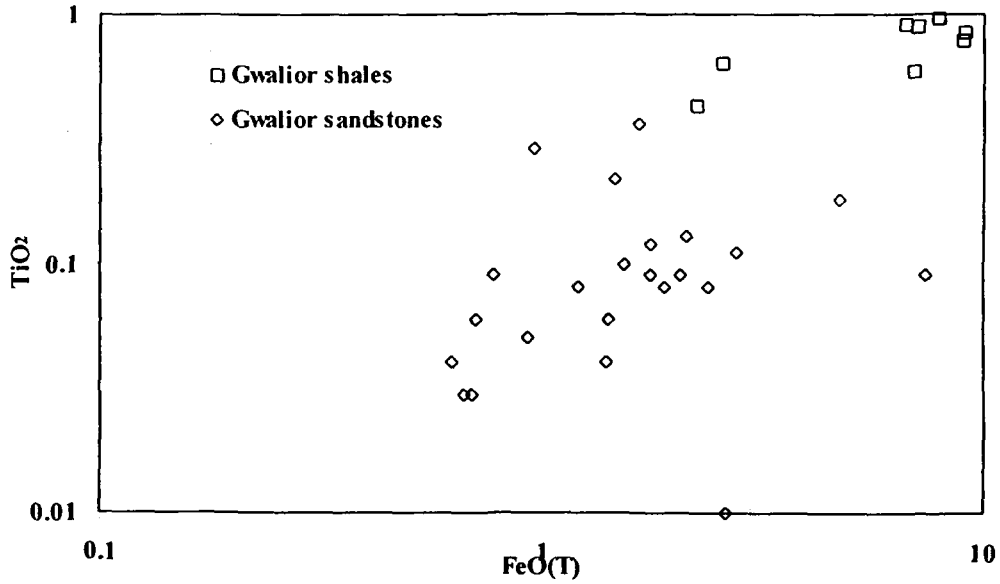

Fig.4.5: $FeO^{(T)}$ vs. TiO_2 plot of the Gwalior Group shales and sandstones. The broad co-linearity between the two elements indicates iron retention during weathering.

correlation (Young and Nesbitt, 1998). $FeO^{(T)}$ covary with TiO_2 (r=0.77, Fig.4.5) indicating that iron was also enriched during weathering and chlorite may be important constituent among clays in case of relative mafic provenance. The positive correlation between $FeO^{(T)}$ and TiO_2 can be attributed to the iron retention in paleoweathering profiles (Young and Nesbitt, 1998) in an oxygenated atmosphere (Holland et al., 1989; Holland and Beukes, 1990)

4.2.2 Trace elements

Like major elements, trace element contents in Gwalior shales are also quite variable. In comparison to shale standards like Post Archean Australian Shale (PAAS, Taylor and McLennan, 1985) and North American Shale Composit (NASC, Gromet et al., 1984), they are enriched in large ion lithophile elements (LILE) and depleted in alkaline earth elements. Ba, Rb, K, Th are highly enriched whereas Sr and Ca are depleted. These relationships are demonstrated on Archean Upper Crust (AUC) normalized spider plot (Fig.4.6). Among the high field strength elements (HFSE), Zr and Hf is enriched (Av. Zr - 314 ppm) while Y is depleted (Av. 20 ppm) in comparison to NASC or PAAS. Gwalior shales are comparable with PAAS and NASC in terms of transition metal contents e.g. Sc, Cr, Co, Ni and also Fe but slightly depleted in V (Fig.4.6A). Gwalior sandstones have similar trace element distribution as shales except low total metal content because of quartz dilution. However similar geochemical patterns are displayed by shales and sandstones as shown in Figure 4.6A and 4.6B. In comparison to average Proterozoic sandstone (Condie, 1993) Gwalior sandstones are highly enriched in LILE such as Th (Av. 115 ppm, Proterozoic sandstone – 4.2 ppm), Rb (Av. 8.6 ppm, Proterozoic sandstone – 30 ppm), Ba (Av. 258 ppm, Proterozoic sandstone – 190 ppm) and HFSE such as Zr (Avg. 214 ppm, Proterozoic sandstone – 89 ppm) and Y (Av. 23 ppm, Proterozoic sandstone – 10.3 ppm); and nearly similar in transition metal contents e.g. Sc, V and Co but slightly enriched in Cr and Ni. The total overall abundance of most of the elements in Gwalior sandstones is higher in comparison to average Proterozoic sandstone.

All the trace elements are negatively correlated with SiO_2, indicating decrease in elemental abundances with quartz dilution. Al_2O_3 is positively correlated with K_2O (r=0.98), Rb (r=0.94), Ba (r=0.82) and Cs (r=0.75), indicating that these elements are fixed in K-rich clays (i.e. illites). The transition elements like, Sc(r=0.93), V (r=0.76),

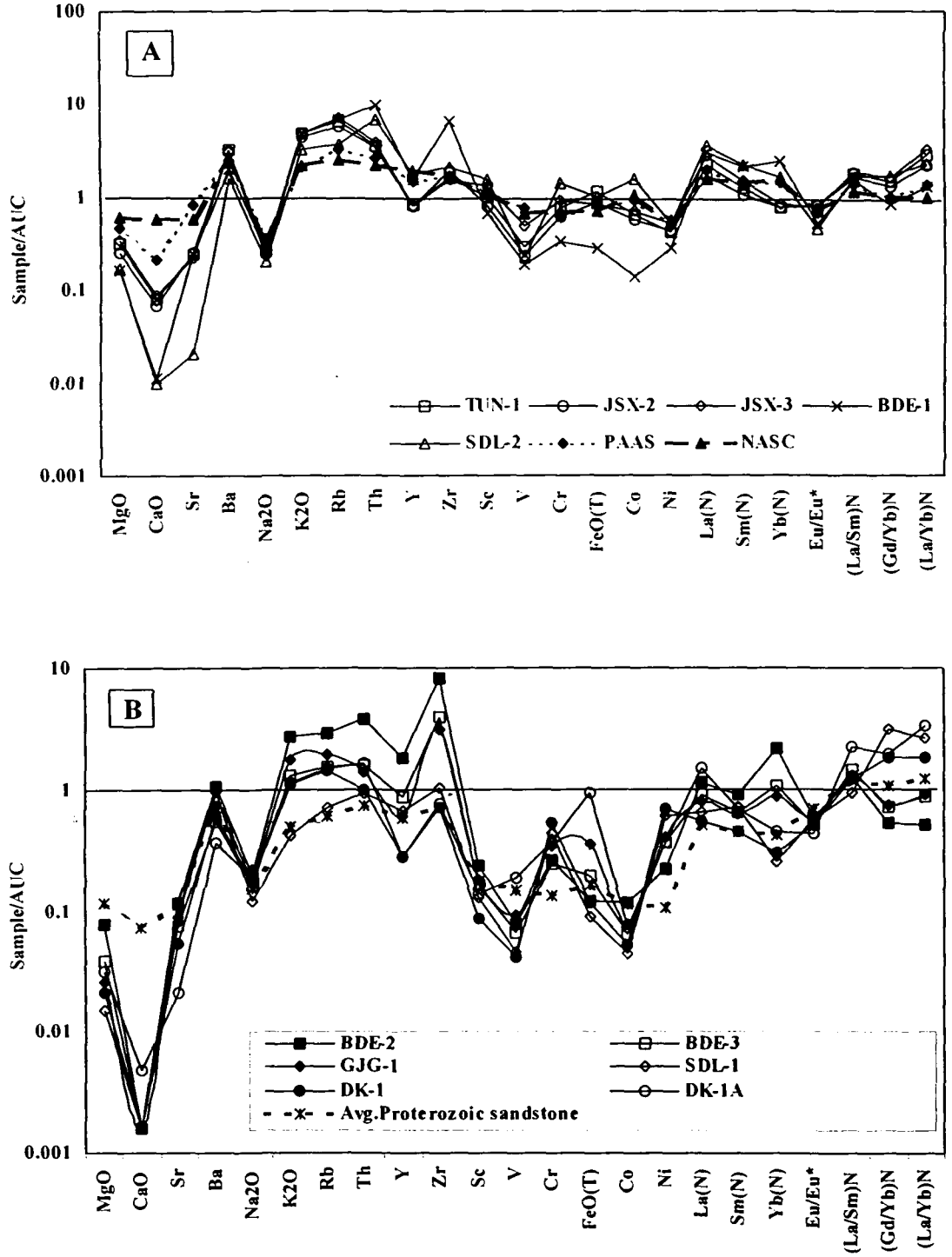

Fig.4.6: Archean upper crust (AUC) normalized spider plot of Gwalior Group shales (A) and sandstones (B) (Normalisation values after Taylor and McLennan, 1985). Note strong depletion in CaO, Na_2O, Sr and also conspicuous negative anomaly for Y. For reference also plotted the data of NASC (Gromet et al., 1984), PAAS (Taylor and McLennan, 1985) and Proterozoic cratonic sandstone (Condie, 1993).

Cr (r=0.54) and Co (r=0.71) show a strong to moderate correlation with Al_2O_3. Also, these elements are strongly correlated with FeO, TiO_2 and MgO. These relationships signify that transition elements are fixed in clay mineral like chlorite and are related to tholeiitic mafic components enriched in Fe, Ti and Mg.

The high field strength elements (Zr, Y, Nb, Ta) do not covary with Al_2O_3, instead they are strongly correlated with each other and positively correlated with P_2O_5 and Th. This indicates that HFSEs are not bounded in clay minerals but are controlled by accessory minerals like zircon and monazite. Indeed, rounded zircon and monazite are identified in thin section and mineral separates of sandstones and conglomerates of Gwalior Group, which are characterized by high order radioactivity due to thorium. These characteristics suggest a granitic provenance of these sediments. Since these elements are strongly fractionated in heavies, they should be considered with caution for provenance modelling.

4.2.3 Rare earth elements

Out of eight shale samples and twenty-two sandstone samples, five shale samples and nine sandstone samples were analysed for rare earth elements. The REE data are presented in table 4.1 & 4.2 and their chondrite normalized patterns are presented in Figures 4.7 and 4.8. The Gwalior shales exhibit sub-parallel REE pattern with La abundance ranging from 141 to 306 x chondrite (Mean = 223) and Yb from 9.36 to 28.93 x chondrite (Mean = 16.41). All the shale samples are characterized by highly fractionated REE pattern where $(La/Yb)_N$ ranges from 8.83 to 22.83 with a mean of 16.41, which is more than two times of NASC (=7.17) and PAAS (=8.2). LREEs are highly fractionated [avg. $(La/Sm)_N$ = 5.19], while HREEs are slightly fractionated [avg. $Gd/Yb)_N$ = 1.95] compared to NASC (=1.39) and Proterozoic Shale Standard (=1.62) (Condie, 1993). The shale samples display variable negative europium anomaly, Eu/Eu* value ranges from moderate (0.76-0.80) to strong (0.44-0.52). The highly fractionated REE pattern and Eu anomalies calls for felsic source rock for these shales.

The sandstones of Gwalior Group exhibit parallel REE patterns similar to shales with lower REE abundances. La abundance in sandstone ranges from 10.64 to 127.66 x chondrite (mean = 63.06) and Yb ranges from 3.07 to 26.72 x chondrite (mean = 10.41). Sandstones characteristically show more strong negative europium anomalies in comparison to shales (Eu/Eu^* = 0.43 to 0.58, mean = 0.51). LREE

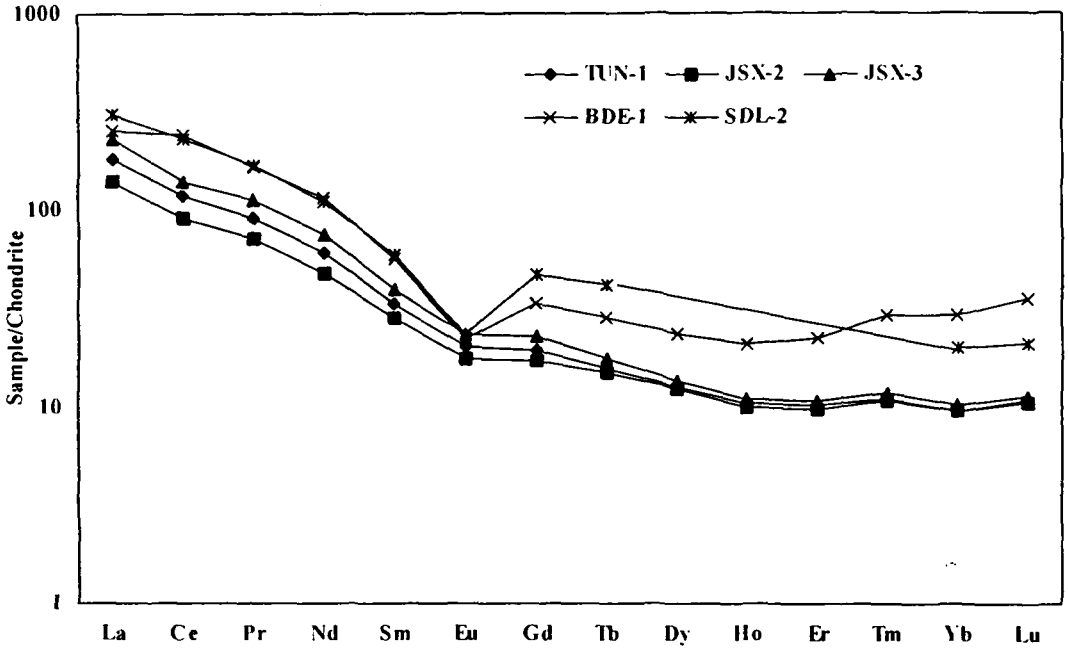

Fig.4.7: Chondrite normalised (Taylor and McLennan, 1985) rare earth element plot for Gwalior shales. Note fractionated REE patterns and mild negative Eu anomaly for three samples (i.e. TUN-1, JSX-2 and JSX-3); other two (i.e. BDE-1 and SDL-2) have strong negative Eu anomaly and comparatively less fractionated REE patterns.

fractionation $[(La/Sm)_N]$ ranges from 1.95 to 4.42 (mean = 3.88), while HREE fractionation $[(Gd/Yb)_N]$ ranges from 0.74 to 4.34 (mean = 2.07). Total REE fractionation $[(La/Yb)_N]$ ranges from 3.56 to 23.12 (mean = 11.61), that is strikingly lesser than that of shales. This characteristic along with strong europium anomaly calls for different source characteristic of sandstones and shales.

The REEs are positively correlated with Al_2O_3. While the LREEs and MREEs are strongly correlated, HREE are moderately correlated. The tune of correlation coefficient with Al_2O_3 is quite high for La (r=0.90), Ce (r=0.79), Pr (r=0.74), Nd (r=0.78), Sm (r=0.88), Eu (r=0.98), Gd (r=0.67), Tb (r=0.49), and moderate for Yb (r=0.48) and Lu (r=0.41). The rest of the HREEs do not yield good correlation coefficient with Al_2O_3 because of few analyses of these elements. These indicate that the REEs are chiefly housed in clays. Since REEs are also positively correlated with K_2O with same intensity, illite seems to be the host of REEs. However, this do not appear to be the entire story, the HREEs are strongly correlated with Zr and Y and upto some extent with Th, thus indicating partial zircon control over HREEs. Small

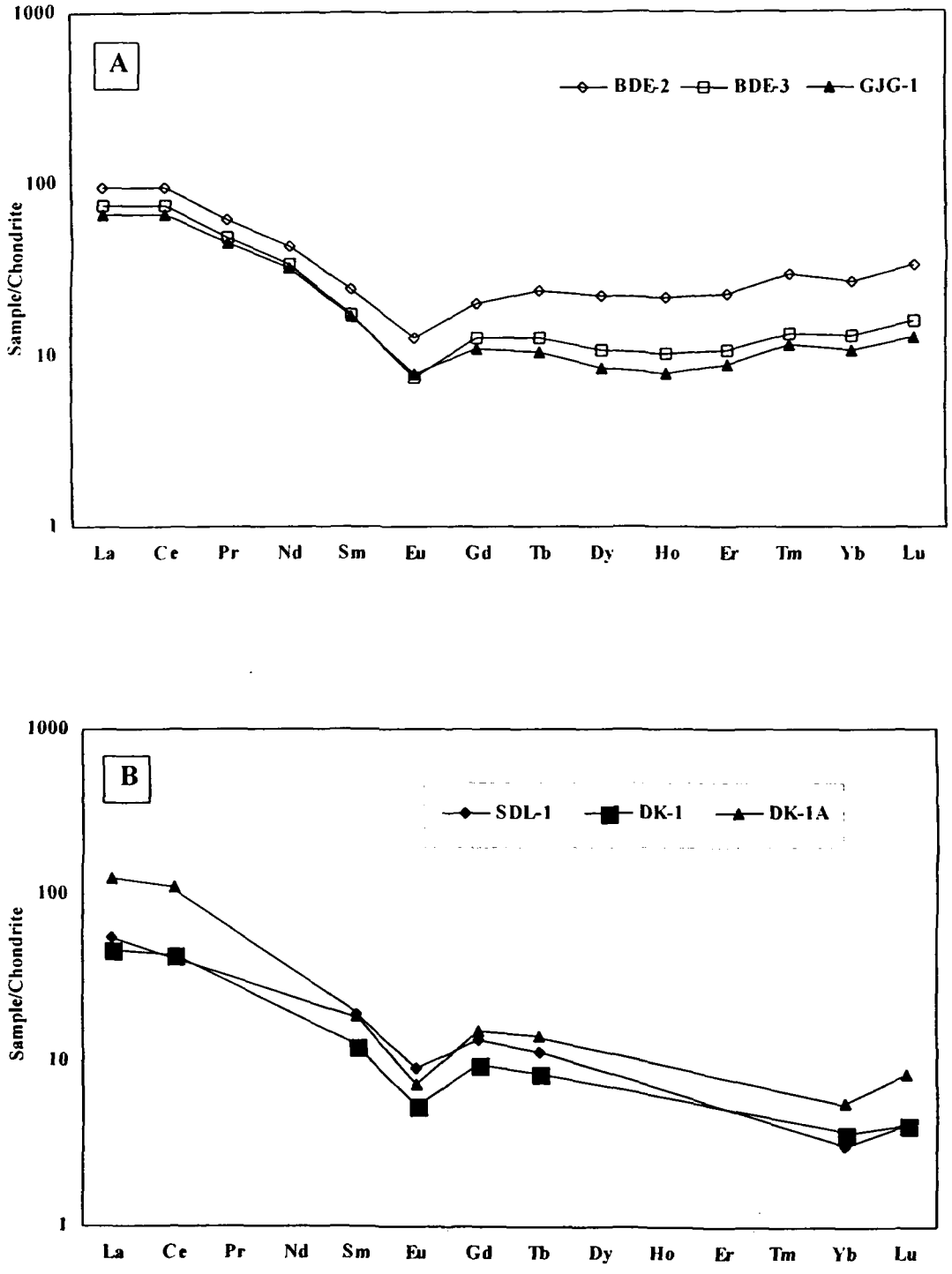

Fig.4.8: Chondrite normalised rare earth element plot for Gwalior sandstones. Note strong negative Eu anomaly compared to shales. Data is plotted in two diagrams to avoid crowding.

depletion in Ho-Er relative to Yb-Lu in some samples also support that HREEs are hosted by zircon. As shales have high REE abundances, the overall REE patterns do not change with changing zircon content. But in case of sandstone, REE patterns with low REE abundances could seriously be affected (McLennan, 1989) with increased zircon content. These samples can be readily recognized because of their unusual elevated Zr abundances. The REE patterns of some samples are indeed modified by zircon e.g. samples BDE-1and BDE-2 typify the situation. The Archean quartzite sample Son-A and Kaimur sandstone sample AMP-1 are similarly contaminated by zircon as discussed in the next chapter. Overall REE abundances in Gwalior shale and sandstones are housed in illitic clay, with small contribution from zircon towards HREE. Since the REEs are bound in clay minerals, the REE patterns could be reasonably used for deducing source area composition with caution toward unusual modified patterns.

4.3 Discussion

4.3.1 Provenance characteristics

Numerous factors including source area composition, source area weathering conditions, hydraulic sorting, adsorption, diagenesis, and metamorphism affect the overall composition of clastic sediments (Wronkiewicz and Condie, 1987; Fedo et al., 1996; Nesbit et al., 1996, 1997). In order to characterize the provenance of terrigenous sediments, it is necessary to rely on elements that are the least mobile during these processes. Taylor and McLennan (1985) and McLennan and Taylor (1991) have suggested that the REEs, Th, Sc, Co and high field strength elements are especially useful elements for monitoring source area composition. These elements have very short residence times in sea water and are transferred almost quantitatively into the sedimentary record. Additionally, this array includes both incompatible and compatible elements, ratios of which are useful in differentiating felsic from mafic source components. However, the HFSEs are strongly partitioned in sand size grains and can be decoupled from other element groups because of heavy mineral fractionation, owing to their high specific gravity and resistance to weathering (Taylor and McLennan, 1985). Similar situation is observed in case of Gwalior clastics and thus use of HFSE is avoided in provenance modelling. Therefore, our discussion on provenance characteristics chiefly relies on immobile elements such as REE, Sc, Th

and Co contents, their ratios and overall REE patterns which are most useful provenance indicators (Taylor and McLennan, 1985).

A broad hint of felsic plutonic source rock is indicated for Gwalior siliciclastics, by features such as extreme mineralogical maturity of quartz arenites and stable heavy mineral population of zircon, monazite and/or sphene in these rocks. Reworked sedimentary source is unlikely as lithic fragments are sparse, quartz is chiefly monocrystalline and fine quartz grains are texturally immature showing angular to subangular grains. The presence of fresh K-feldspars in arkosic sandstone also indicates a granite source. The available paleocurrent data (Chapter II) indicate a predominant north directed paleocurrent. The sedimentological data also indicate transportation of sedimentary debris from south and south-west and reworking of these sediments along an E-W trending shore line. The Archean basement rock of Bundelkhand craton in south of Gwalior basin are chiefly composed of late Archean (2.5 Ga) high-K granite; with minor components of Archean TTG (3.2 Ga), Archean metasedimentary rocks and mafic rocks (Basu, 1986). As the Gwalior basin itself is floored by Bundelkhand granite gneiss complex (BGGC), it is reasonable to assume that BGGC is the main source component of Gwalior sediments.

In a discriminant function plot based on major element data (after Roser and Korsch, 1988), the Gwalior clastics falls in area of felsic igneous provenance and quartzose sedimentary provenance (Fig.4.9). Interestingly all the shale samples fall on felsic igneous provenance and most of sandstone samples fall on quartzose sedimentary provenance. In this diagram the shale data indicate original source signature but sandstone chemistry indicates a recycled sedimentary provenance. It may be recalled that the petrographic study does not favour a recycled nature of sandstone thus the quartz richness may be a consequence of extreme sorting, achieved in a shore zone environment; coupled with extreme chemical weathering condition in source area.

AUC normalized spider plot (Fig. 4.6a, 4.6b) shows almost similar patterns of Gwalior clastics, shale standards like NASC and PAAS and Proterozoic cratonic sandstone of Condie (1993). However, a detailed comparison suggests that Gwalior shales are enriched in Th, Rb and K relative to these standards whereas transition elements such as Sc, V, Cr, Fe, Co, Ni are comparable or slightly depleted. These are consistent with felsic sources for Gwalior shales. The Gwalior shales are also enriched in LREE [$(La)_N$], depleted in HREE [$(Yb)_N$] and have comparable MREE

$[(Sm)_N]$ content with respect to NASC and PAAS. They are also characterized by strong negative Eu anomaly, high total REE $[(La/Yb)_N]$ fractionation in comparison to NASC or PAAS. The higher total REE fractionation calls for a HREE depleted high-Al TTG source component. This interpretation is corroborated by strong depletion of Y over Th and Zr, as the Y is marked by conspicuous trough on the spidergram (Fig. 6a, 6b). It has been suggested that HREEs along with Y are partitioned into residual garnet and amphibole during partial melting of amphibolite or eclogite source (Martin, 1987, 1993) during TTG magma generation. The negative Y anomaly that is characteristic feature of Gwalior clastics is not observed in case of PAAS, NASC or Proterozoic sandstone standard, thus suggesting that the source rock of Gwalior clastics were quite different from those of shale/sandstone standards and point toward their TTG type felsic source component. Gwalior sandstones display similar pattern to those of Gwalior shale but are characterized by lower elemental abundances.

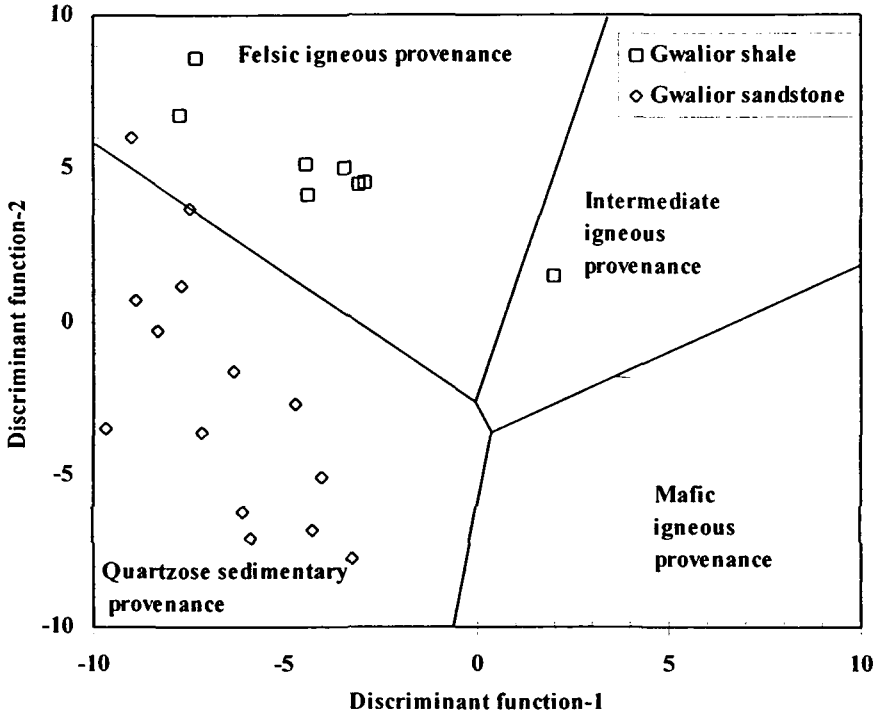

Fig.4.9: Discriminant function diagram of Gwalior clastics (after Roser and Korsch, 1988), indicating felsic provenance and reworked sedimentary provenance.

Although the Gwalior clastics are characterized by low transition element contents, a Fe, Ti rich tholeiitic mafic component can be visualized in the source terrain. This idea is supported by positive correlation of Sc, V, Co and Cr with FeO, TiO_2 and MgO. The relative contribution of felsic to mafic input into the sedimentary basins can be established in the ratio-ratio plot of different compatible to incompatible element pairs. For this purpose Th/Sc-Sc, La/Sc-Sc/Th and Co/Th-La/Sc systematics (Taylor and McLennan, 1985; Condie, 1993; Bhatt and Ghosh, 2001) has been proved more robust and widely used in characterizing the source lithology of clastic sediments. The data of Gwalior clastics are plotted in various diagram (Fig. 4.10, 4.11, 4.12) involving these elements along with the available data of TTG (Sharma and Rahman, 1995), Granite (Mondal and Zainuddin, 1996) and mafic rock (Mondal and Ahmad, 2001) of the Bundelkhand massif (BGGC). In these plots the Gwalior clastics are plotted at an intermediate position between granite and mafic end members supporting their role as the end member components of the Gwalior sediments. Compared with BGGC granites, the BGGC mafic rock lie far away from the Gwalior samples, indicating a minor contribution from the latter. It is interesting to note that Gwalior shales plots nearer to mafic end member compared to sandstones implying more mafic source of shales than sandstones. In a ternary plot involving La-Th-Sc (Fig.4.13) a similar situation can be observed, as most of the Gwalior clastics are consistent with granitic source, with a minor component from mafic source. Here also the shale show characteristically more mafic source than sandstones and plot nearer to the mafic end member.

As discussed in the earlier section of this chapter, the REE pattern of Gwalior Group shales are variable; out of five analysed samples, three (TUN-1, JSX-2, JSX-3) show similar pattern (Fig.4.7). These samples exhibit high total REE fractionation with $(La/Yb)_N$ ranging from 15.03 to 22.83. These samples are also characterized by relatively higher HREE fractionation with $(Gd/Yb)_N$ ranging from 1.83 to 2.27 and mild negative europium anomaly ($Eu/Eu^* = 0.76$-0.80) compared to Proterozoic shale standards. The HREE depletion, high $(La/Yb)_N$ ratio and mild negative europium anomaly are unlikely to be generated from sole granite source, a TTG component is required to explain this type of REE pattern as discussed in the earlier paragraph. The sample SDL-2 is characterized by higher REE abundance, with similar total REE ($La/Yb_N = 15.61$) fractionation and HREE fractionation ($Gd/Yb_N = 2.39$) to previous one but strong negative Eu anomaly ($Eu/Eu^* = 0.44$). The sample BDE-1 show lower

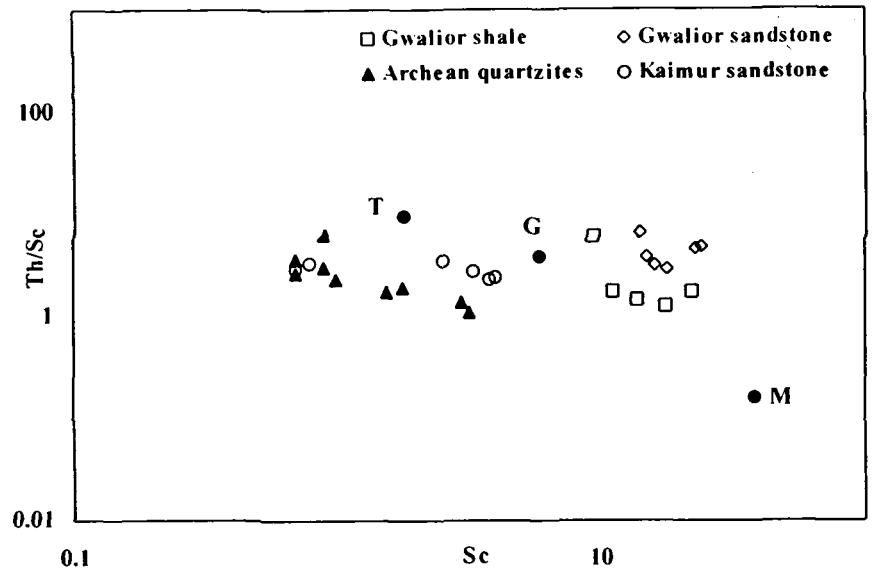

Fig.4.10: Th/Sc vs. ppm Sc plot of Gwalior Group shales and sandstones, Archean basement quartzites and Kaimur Group sandstone. For reference the data of basement end members are also plotted as solid dots. T=TTG after Sharma and Rahman, 1995; G= Granite after Mondal and Zainuddin, 1995, 1996, Mondal, 2002 and M= Mafic end member after Mondal and Ahmad, 2001. The data source and symbols are same in subsequent diagrams.

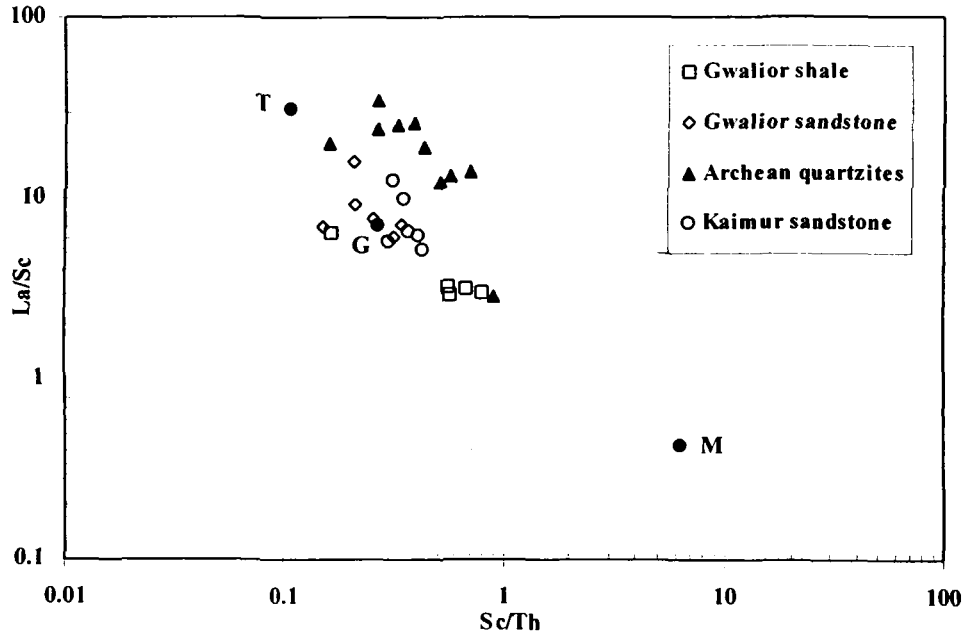

Fig.4.11: La/Sc vs. ppm Sc/Th plot of Gwalior Group shales and sandstones, Archean basement quartzites and Kaimur Group sandstones. Basement end members are also plotted for reference.

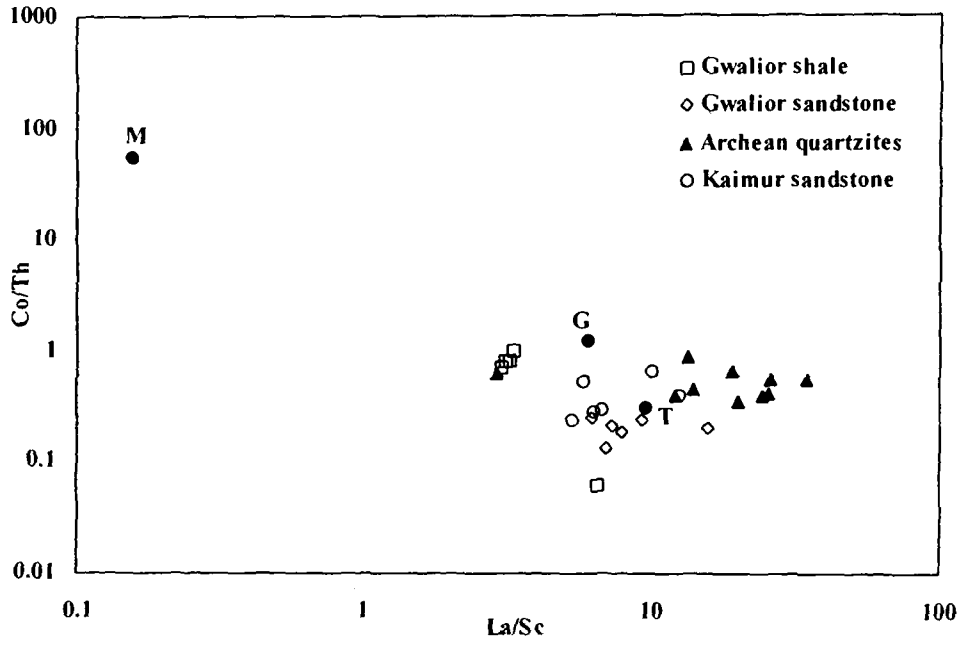

Fig.4.12: Co/Th vs. La/Sc plot of Gwalior Group shales and sandstones, Archean basement quartzites and Kaimur Group sandstones. For reference the data of basement end members are also plotted.

total REE (La/Yb_N = 8.83) and HREE (Gd/Yb_N = 1.17) fractionation, chiefly because of elevated HREE content probably hosted in zircons that is readily identified because of elevated Zr content.

As far as the Gwalior sandstones are concerned they exhibit parallel REE patterns (Fig. 4.8), with obvious lesser total REE abundance than shales. These sandstones are also characterized by lesser total REE (La/Yb_N = 3.56-23.12, mean 11.61) fractionation and strong negative europium anomaly (Eu/Eu* mean = 0.51). This is consistent with a granite source component. Out of six sandstone samples, REE pattern of two samples are unique. The sample BDE-2 show flat pattern because of elevated HREE content probably housed in zircons. The REE pattern of sample no. SDL-1 is interesting, it shows relatively mild negative europium anomaly (Eu/Eu* = 0.56) than adjoining samples (DK-1, DK-14), (Fig.4.8b), and is characterized by lesser Th/.Sc, La/Sc ratio and higher Cr/Th ratio compared to other sandstone samples, indicating possible mafic input.

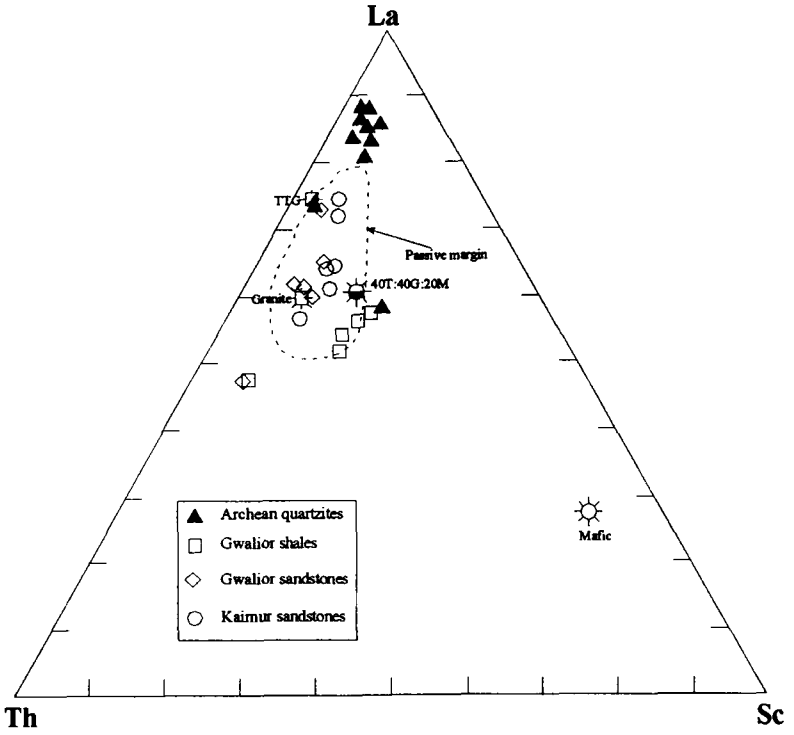

Fig.4.13: La-Th-Sc ternary plot of Gwalior clastics, Kaimur sandstones and basement Archean quartzites. For reference the TTG, Granite and mafic end members of basement complex are plotted. Also plotted are the model upper crust composition (40T:40G:20M; 40% TTG, 40% granite and 20% mafic rock) as derived from REE modelling of Gwalior Group clastic rocks. The Proterozoic clastics plot near granite end member, while the Archean quartzites plot near TTG end member that signify the control of the basement end members in the composition of these sediments. The field of passive margin (Bhatia and Crook, 1986) is also shown. Proterozoic sediments as well as the Archean sediments indicate deposition in passive margin tectonic setting.

Therefore with the identification of several likely source components it is possible to quantitatively model the relative contribution of granite, TTG and mafic source types to generate average Gwalior clastics. In this regard mass balance has to be taken into consideration before attempting such calculation. The consideration of only shale or sandstone component may give rise erroneous result; while shale contains more abundances of REE and other trace element than source rock, the sandstones are relatively depleted. It is well established that fine grained terrigenous sediments (shale and siltstones) comprise 70% of sedimentary mass, while coarse grained sediments (sandstone) contribute 30% to the sedimentary mass (Garrels and Mackenzie, 1971; Taylor and McLennan, 1985). It is reasonable to consider that 70:30 ratio of shale and sandstone is representative of source composition and hence

mixture of 70% shale and 30% sandstone is taken as model composition of Gwalior clastic rocks. The paleocurrent data as discussed in Chapter-II indicates derivation of Gwalior clastics from south of the basin where Bundelkhand granite-gneiss complex (BGGC) is exposed. The BGGC massif is composed of late Archean (2.5 Ga) high K-granites, with subordinate mafic rock and minor Mesoarchean (3.2 Ga) TTG and Archean metasedimentary rocks (~2.9 Ga). The REE data of basement granite (Mondal and Zainuddin, 1995, 1996; Mondal, 2002), tholeiitic mafic rock (Mondal and Ahmad, 2001) and TTG (Sharma and Rahman, 1995) of Bundelkhand massif occurring to the south of Gwalior basin are taken as end members for modelling purpose. To determine the contribution of these components of BGGC to the overall composition of Gwalior clastic sediments the mixing calculations are performed. Parameters and results of mixing calculations are shown in Table 4.3 and Fig.4.14. REE modelling reveals that average Gwalior clastics represent mixture of sediments derived from a provenance consisting of 40% granite (G), 40% TTG (T) and 20% mafic rocks (M). The total individual REE abundances and ratios like $(La/Sm)_N$, $(La/Yb)_N$ and $(Gd/Yb)_N$ are in excellent agreement with model values. The average Gwalior clastics shows little bit more negative europium anomaly (Eu/Eu* = 0.60) than modeled value (Eu/Eu*=0.74), which is within analytical uncertainty. The discrepancy in Eu anomaly can be explained from the fact that the Archean source terrain also contained Low-K granite with low K2O/Na2O ratio, large negative Eu anomaly and highly fractionated HREE depleted REE pattern along with TTG as discussed in the next chapter. Since only TTG (due to lack of data of Mesoarchean Granite of BGGC) is considered as modelling end member the resulting data show discrepancy in Eu anomaly. Thus the negative europium anomaly of source rock are not properly represented in modelling end members, as higher negative europium anomaly is expected where source is dominated by felsic component (80%).

The significant conclusion of the modeling is that Archean-TTG comprised an important part (40%) of the exposed Paleoproterozoic upper crust. Such rocks are not commonly exposed in Bundelkhand craton at present. The present day Bundelkhand massif is composed predominantly of (80-90%) high-K late Archean granite (2.5 Ga, Mondal et al., 1998, 2002) with minor components of mafic rock, caught up blocks of TTG rocks and metasedimentary enclaves. This simply indicates the phenomenon of erosion, where upper TTG crust was eroded and entered to the Paleoproterozoic sedimentary records thereby exposing the deep level granite batholiths.

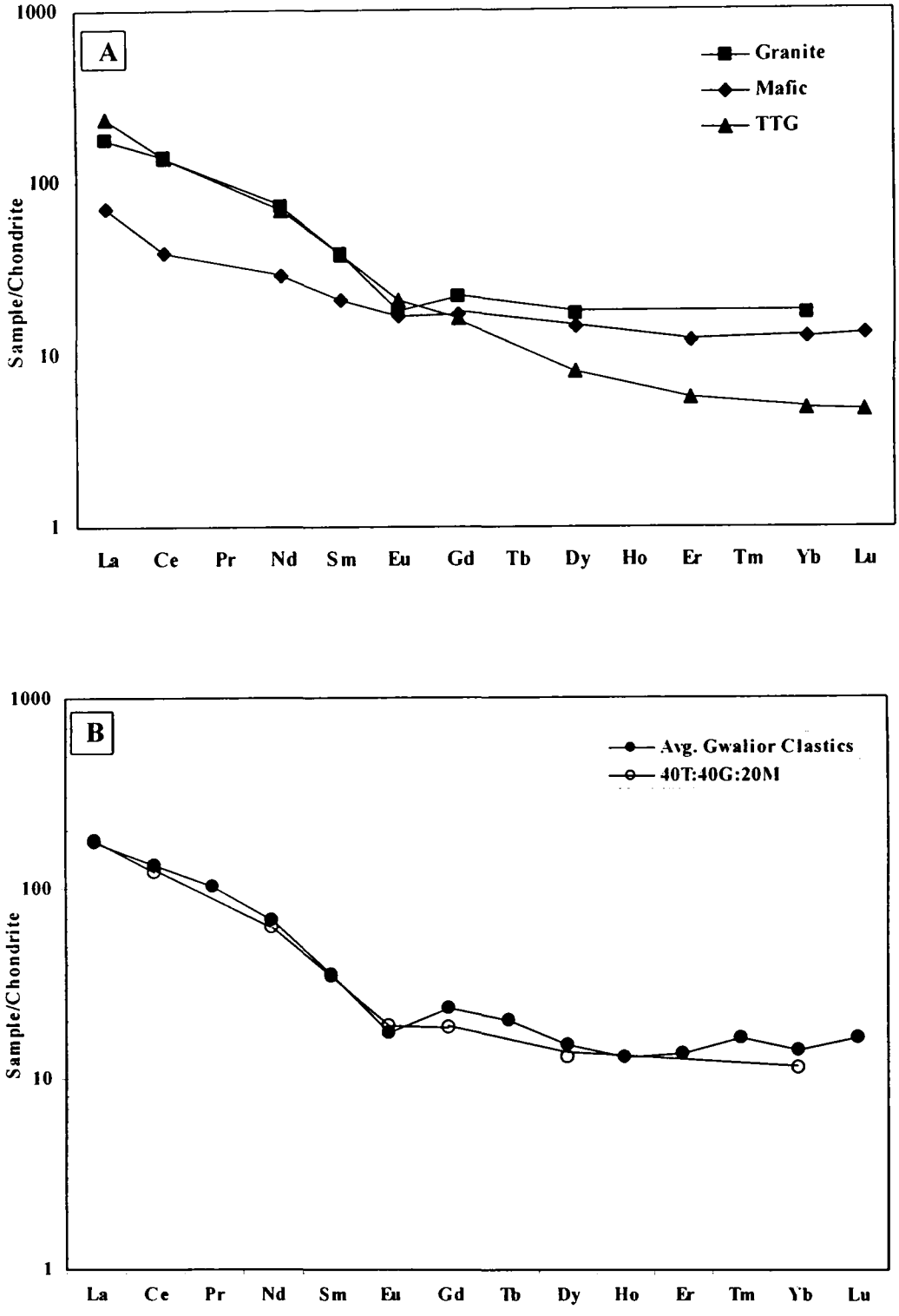

Fig.4.14: Results of REE modelling for estimating provenance of Gwalior clastics. (A) Chondrite normalised REE patterns for basement end members such as TTG (T), Granite (G) and mafic rock (M), the data sources is same as given in figure 4.10. (B) REE patterns of average Gwalior clastics (mixture of 70% shale and 30% sandstone) and estimated provenance after mixing the end members in the proportion of 40T:40G:20M. The REE pattern of average Gwalior clastic is in excellent agreement with the mixing results.

Table 4.3: Results from mixing calculations of basement end members compared with average Gwalior clastics.

Elements	Avg. Gwalior Shale (A)	Avg. Gwalior sandstone (B)	Avg. Gwalior clastics (70A:30B)		Mixing end members						Mix results 40T:40G:20M	
					TTG (T)[#]		Granite (G)[@]		Mafic (M)[$]			
	N*	N	ppm	N	ppm	N	ppm	CN	ppm	N	ppm	N
La	223.62	63.06	41.23	175.45	55.50	236.17	41.32	175.83	16.60	70.64	42.05	178.93
Ce	165.11	57.86	80.16	132.94	84.00	139.30	85.34	141.52	23.60	39.14	72.46	120.16
Pr	123.20	52.33	9.07	101.94								
Nd	82.17	36.53	30.95	68.48	31.00	68.58	32.77	72.50	13.16	29.11	28.14	62.26
Sm	43.53	15.21	5.15	35.04	5.60	38.10	5.63	38.27	3.07	20.89	5.10	34.73
Eu	21.40	7.55	0.97	17.25	1.15	20.54	1.01	18.09	0.93	16.58	1.05	18.77
Gd	28.08	12.83	4.63	23.51	3.20	16.24	4.27	21.68	3.37	17.11	3.66	18.59
Tb	23.67	12.63	0.73	20.36								
Dy	15.44	13.70	3.63	14.92	1.95	8.02	4.20	17.28	3.56	14.64	3.17	13.05
Ho	12.97	13.20	0.73	13.04								
Er	13.15	14.03	2.13	13.41	0.90	5.66			1.90	11.95		
Tm	15.60	17.93	0.39	16.30								
Yb	15.48	10.41	2.28	13.96	0.80	4.91	2.79	17.09	2.03	12.45	1.84	11.29
Lu	17.73	13.00	0.39	16.31	0.12	4.79				13.10		
(La/Sm)N	5.14	4.14		5.01		6.20		4.59		3.38		5.15
(Gd/Yb)N	1.81	1.23		1.68		3.31		1.27		1.38		1.65
(La/Yb)N	14.44	6.05		12.57		48.12		10.29		5.68		15.85
Eu/Eu*	0.61	0.54		0.60		0.83		0.63		0.88		0.74

*N represents chondrite normalised values (normalisation values after Taylor and McLennan, 1985)
Data sources of basement end members: [#] Sharma and Rahman (1995); [@] Mondal and Zainuddin (1996, 1997), Mondal, (2002); [$] Mondal and Ahmad (2001).

4.3.2 Paleoweathering conditions

The effect of variable degree of weathering in source area can be important in influencing alkali and alkaline earth element contents of terrigenous sediments (Nesbitt et al., 1980; Schau and Henderson, 1983; Reimer, 1985). Cations with large ionic radius as Cs, Ba and Rb remain fixed in weathering profile by preferential exchange and adsorption on clays, whereas smaller cations such as Ca, Na, and Sr are selectively leached from weathering profile (Nesbitt et al., 1980). These chemical trends may be transferred to the sedimentary records (e.g. Nesbitt and Young, 1982; Wronkiewicz and Condie, 1987; Fedo et al., 1996), thus provide a useful tool for monitoring source area weathering conditions. This relationship is demonstrated in an AUC normalized spider plot (Fig.4.6A & 4.6B). In this diagram the CaO, Sr and Na_2O contents are strongly depleted both in Gwalior shale and sandstones whereas Ba, Rb and K are enriched. Similar pattern has been identified in Torongo granodiorite weathering profile (Nesbitt, 1980), indicating high chemical weathering of source area. The relative depletion of CaO in Gwalior shale compare to other Proterozoic and Phanerozoic shales (Fig.4.3) indicates more severe weathering than these shale standards. As stated in previous section, a positive linear correlation between Al_2O_3 and TiO_2 also supports strong chemical weathering of source rock (Young and Nesbitt, 1998; Sreenivas and Srinivasan, 1994).

The intensity of chemical weathering of source terrain can be evaluated by computing Chemical Index of Alteration (CIA) of derived clastic rocks (Nesbitt and Young ,1982) that is defined by the equation: CIA = $[Al_2O_3/(Al_2O_3 + CaO^* + Na_2O+K_2O]$ x 100. Where all elements are in molecular proportion, and CaO* represent Ca in silicate fraction. CIA values for average shales range from 70 to 75 which reflect composition of muscovite, illites and smectites. Intensely weathered rock yields mineral compositions trending towards kaolinite or gibbsite and a corresponding CIA that approaches to 100. CIA values of unweathered rock are about 50. The CIA values (Table 4.1) of Gwalior shale (61.81-75.48, mean = 64.78) and sandstones (55.78-81.37, mean = 67.10), do not indicate substantial weathering in the source terrains as depicted by severe CaO, Na_2O and Sr depletion. This can be evaluated by plotting the data in Al_2O_3-CaO^*+Na_2O-K_2O (A-CN-K) compositional space (molecular proportion, Fig.4.15A). Also shown on the diagram are idealized minerals; possible source rocks such as granite, TTG and mafic rocks and model upper crust composition (40% Granite, 40% TTG and 40% Mafic rock;

40G:40T:20M) as deduced herein from REE modelling. The dashed line represent the limit of weathering, to the right of which is the field of K-enrichment. The solid arrow emanating from model upper crust represents weathering trend of source rock (predicted weathering path). The theoretical background of this diagram (Nesbitt and Young, 1982, 1984; Fedo et al., 1995) is that the weathering of bed rock produces Al-rich sediments, that results in the movement of plots of weathered samples sub-parallel to A-CN join from their unweathered source composition on the feldspar join. Majority of Gwalior clastics are enriched in K_2O and plot right side of "limit of weathering" line. These indicate that the Gwalior clastics have suffered post depositional potash metasomatism, which accounts for their low CIA values. The Gwalior clastics followed the predicted weathering path for model upper crust composition until virtually all Na and Ca were removed (Trend1, Fig.4.15A). At some later time, the samples suffered K-metasomatism as a result of which their composition shifted toward K_2O apex (Trend 2, Fig.4.15A). It is possible to assess the pre-metasomatised CIA values of the sediments in A-CN-K space when K is introduced in aluminous clays to form illite (Fedo et al., 1995). The backward projection of tie line between the K apex and sample point to the predicted weathering path give rise pre-metasomatic CIA of that particular sample (Fedo et al., 1995). Using this principle, the premetasomatic CIA values obtained for Gwalior sandstones ranges from 74 to 98 and pre-metasomatic CIA values of shales range from 76 to 84. This is in conformity with the observation of severe weathering of source rocks during their sedimentation.

A quantitative estimate of K-enrichment can be determined by difference from the pre-metasomatised CIA and current values (Fedo et al., 1995). The extraneous K_2O addition in Gwalior clastics ranges from near zero to as high as 38%. The majority of shale samples are characterized by about ~30 % K_2O addition. The quartzarenites with high silica content is least affected by K-metasomatism, whereas clay matrix rich quartzwackes have suffered severe K-metasomatism with value as high as 38% K_2O addition. This is because of absence of K-metasomatism site (kaolinite clay) in former and abundance of aluminous clay in wackes. The very high linear correlation of Al_2O_3 with K_2O ($r=0.94$) may partly be governed by K-metasomatism along with weathering.

The intense nature of chemical weathering can also be portrayed by Chemical Index of Weathering (CIW, Harnois, 1988) and Plagioclase Index of Alteration (PIA,

Fedo et al., 1995). The CIW index eliminates affect of K-metasomatism and defined as: CIW = $Al_2O_3/(Al_2O_3 + CaO^* Na_2O)$ x 100 where the elements are represented in mole proportion. The Chemical Index of Weathering (CIW) of Gwalior shale (table 4.1) varies from 88 to 95 indicating severe weathering of source rock. But CIW is as much as a function of source rock composition as it is a function of weathering intensity, thus could not be used strictly where basement compositions vary (Fedo et al., 1995). Plagioclase Index of Alteration (PIA, Fedo et al., 1995) is better index, as it portrays weathering of plagioclase feldspars, which are abundant in Archean basement terrains. The PIA is defined by the equation: PIA = $[(Al_2O_3 - K_2O) / (Al_2O_3 + CaO^* + Na_2O - K_2O)$ x 100, where all elements are in molecular proportions and CaO* represent CaO in silicate fractions. The above equation can be plotted in $(Al_2O_3-K_2O)$-CaO*-Na_2O (A-C-N) compositional space (Fig.4.15B). The maximum PIA value is 100 (kaolinite, gibbsite) and unweathered plagioclase has PIA value of 50. Gwalior shales have average PIA value of 85 (79.57-93.41, Table 4.1), and Gwalior sandstone have average PIA value of 84 (74.64-94.66, Table 4.1). The high PIA values of Gwalior clastics indicate strong chemical weathering as depicted by severe depletion of CaO, Na_2O and Sr in AUC normalized spider plot (Fig. 4.6A & 4.6B) and strong Al_2O_3-TiO_2 (Fig. 4.4) correlation. Such intense chemical weathering condition, as indicated by Gwalior clastics are in conformity with world wide humid warm climate during the Paleoproterozoic period (Eriksson et al., 1998). The positive correlation between $FeO^{(T)}$ and TiO_2 indicates that the iron was retained in paleoweathering profiles. The conservative behavior of Fe suggests that Fe was chiefly in ferric oxidation state and will require oxygenated atmosphere. Evolution of atmospheric oxygen from <1 to ~15% of the present atmosphere level (PAL) between 2.2 and 1.9 Ga is indicated by the geochemical studies of iron retention in the Paleoproterozoic paleosols (Holland et al., 1989; Holland and Beukes, 1990; Macfarlane et al., 1994; Rye and Holland, 1998).

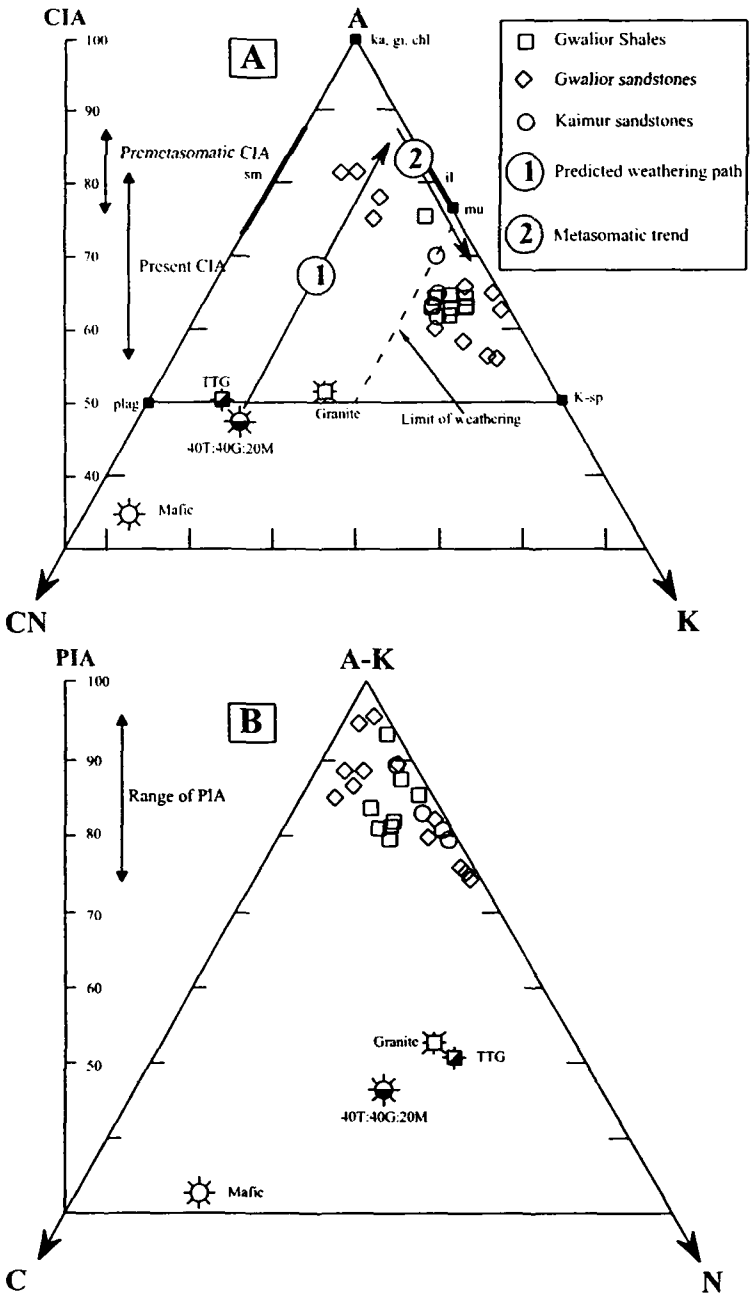

Fig.4.15. (A) A-CN-K diagram (in molecular proportion) for Gwalior and Kaimur clastics. Note that the enrichment of K lowers the CIA value. Samples initially follow the predicted weathering path (trend-1) and subsequently follow the metasomatic trend (trend-2). Mineral abbreviations: ka=kaolinite, gi=gibbsite, chl=chlorite, sm=smectite, il=illite, mu=muscovite, K-sp=potassium feldspar, plag=plagioclase. (B) A-C-N diagram (in molecular proportion) for Gwalior clastics and Kaimur clastics. Note high average PIA values indicative of intense chemical weathering. Only top 70% of triangle is shown.

4.3.3 Tectonic Setting

The sedimentological analysis of Gwalior clastic rock reveals sedimentation in shallow shelf with a range of sedimentary facies from high-energy shore zone to low-energy outer shelf (Chapter II). These sedimentological characteristics show deposition in a classical platformal setting in a craton interior. The extreme quartz richness indicates stable continental regime. Very low feldspar content and absence of lithic components only strengthen the view of craton interior platformal association of sediments with low uplift and high insitu weathering. The local arkosic sandstones may represent local upliftment or reactivation of wrench faults during the course of sedimentation. The tectono-sedimentary association of sediments can also be cross-validated by geochemical data.

The Gwalior clastics are especially rich in silica and have high K_2O/Na_2O ratio. The K_2O/Na_2O vs. SiO_2 plot is strong discriminant of tectonic setting (Roser and Korsch, 1986). In this diagram (Fig.4.16) the Gwalior clastics data invariably fall in passive margin field in the discriminant plot, indicating their passive margin tectonic setting. In discriminant function diagram (Fig.4.9) of Roser and Korsch (1988), the quartzose sedimentary provenance indirectly addresses the passive margin association. Interestingly, most of Gwalior sandstones fall on area of quartzose sedimentary provenance, although they are infact first cycle sediments derived from felsic igneous provenance. This is because of extreme reworking (sorting) of sediment in a stable cratonic regime, thereby enriched in SiO_2 and have abnormally high SiO_2/Al_2O_3 ratio (Fig.4.2). Bhatia (1983) observed close correlation between the major element composition of sandstones and their relative tectonic setting. Based on geochemical parameters $Fe_2O_3^{(T)}$ + MgO, TiO_2, Al_2O_3/SiO_2, K_2O/Na_2O, $Al_2O_3/CaO+Na_2O$ and SiO_2, possible tectonic setting association of sediment such as oceanic island arc (OIA), continental island arc (CIA), active Continental Margin (ACM) and passive margin (PM) can be identified. These parameters are summarized in table 4.4. All these geochemical parameters of Gwalior sandstones closely match to that of sandstones of passive margin setting. The Gwalior sandstones are characterized by SiO_2 (avg.89.30%) enrichment, very high K_2O/Na_2O ratio (avg. 10.08), Low Al_2O_3, $Fe_2O_3^{(T)}$ and TiO_2 contents, all these data are in conformity with passive margin tectonic setting of Gwalior sandstones.

La-Th-Sc systematics is proved to be strong discriminant of tectonic setting (Bhatia and Crook, 1986). In this plot (Fig.4.13) Gwalior clastics are plotted

near La vertex in field of passive margin. The other discriminant plot developed by Bhatia and Crook (1986) involving HFSEs cannot be used to test the tectonic setting of Gwalior Group sediments because of their heavy minerals enriched nature, which have resulted in elevated HFSE contents. The overall REE pattern of Gwalior clastic also matches well with the pattern of passive margin trailing edges of McLennan et al. (1990).

Therefore the geochemical data are in collaboration with sedimentological observations of Gwalior Group, overwhelmingly suggests stable craton interior platformal setting of deposition for the sediments of Gwalior Group.

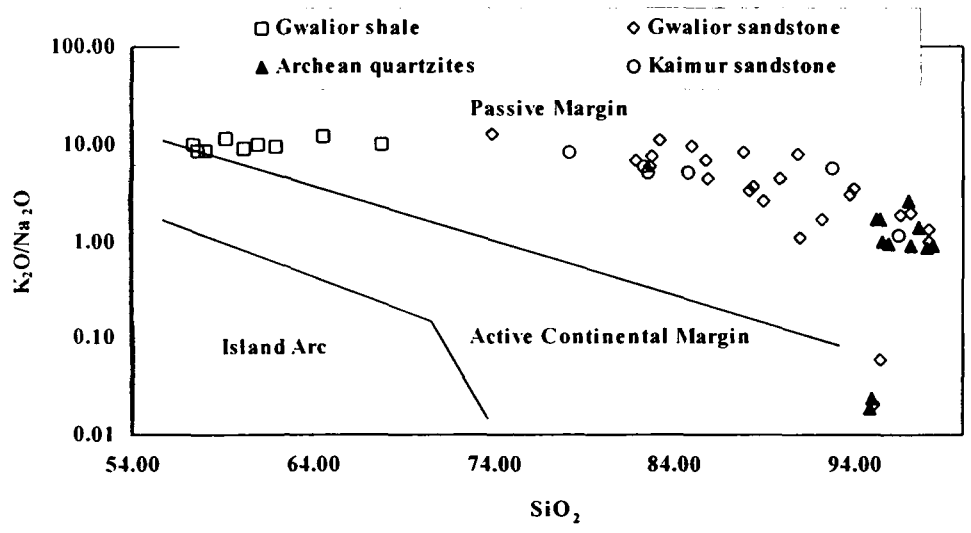

Fig.4.16: SiO_2 vs. K_2O/Na_2O discrimination diagram (after Roser and Korsch, 1986) showing deposition of Gwalior sediments in a passive margin tectonic setting. Note that the Archean quartzites and Kaimur sandstones also indicate deposition in passive margin tectonic setting.

Table 4.4: Geochemical parameters for sandstones of different tectonic settings (after Bhatia, 1983) along with the parameters for Gwalior sandstones.

	$Fe_2O_3^{(T)}$	TiO_2	Al_2O_3/SiO_2	K_2O/Na_2O	$Al_2O_3/CaO+Na_2O$	SiO_2
OIA	8-14 (11.73)*	0.8-1.4 (1.06)	0.24-0.33 (0.29)	0.2-0.4 (0.39)	(1.72)	(58.83)
CIA	5-8 (6.79)	0.5-0.7 (0.64)	0.15-0.22 (0.20)	0.4-0.8 (0.61)	(2.42)	(70.69)
ACM	2-5 (4.63)	0.25-0.45 (0.46)	(0.18)	(0.99)	(2.56)	(73.86)
PM	(2.89)	Depleted	(0.10)	(1.60)	(4.16)	(81.95)
Gwalior Sandstone	(2.41)	(0.10)	(0.033)	(9.11)	(10.39)	(89.30)

* Averages are given in the parenthesis. OIA = Oceanic Island Arc, CIA = Continental Island Arc, ACM = Active Continental Margin, PM = Passive margin.

CHAPTER-V

Geochemistry of underlying Archean quartzites and overlying Mesoproterozoic Kaimur Group sandstones: Implications for evolution of upper continental crust

5.1 Introduction

Evolutionary changes of upper continental crust across Archean-Proterozoic Boundary (APB) can be traced through geochemical examination of sedimentary rocks of different ages but of similar tectonic association (Taylor and McLennan, 1985; Gibbs et al., 1986; Condie, 1993, 1997; Gao and Wedepohl, 1995). Several geochemical parameters like K_2O/Na_2O ratio, Ni-Cr content, europium anomaly and REE fractionation are found to be distinctive in Archean and Proterozoic sedimentary rocks (Reference above cited). Several significant changes in the chemistry of sedimentary rocks across the APB have been observed world over, e.g. (i) Increase in total REE content and magnitude of negative Eu anomaly, (ii) increase in Th/Sc ratio and (iii) increase in $^{87}Sr/^{86}Sr$ ratio in carbonate rocks. The Archean crust formation was dominated by greenstone tectonics and the crust was predominantly mafic in nature. The Archean-Proterozoic transition is characterized by intrusion of high-K intracrustal granite and voluminous production of upper crust. Taylor and McLennan (1985) suggested that Archean sedimentary rock are characterized by flat REE pattern with no europium anomaly and high Ni-Cr content in comparison to their Proterozoic counterpart, which shows fractionated REE patterns with significant negative europium anomaly and low Ni-Cr content. Voluminous production of high-K intracrustal granites and widespread crust formation at 2.5 Ga has been suggested for above geochemical changes in expense of komatiitic magmatism of greenstone association of the Archeans. However, this has been challenged by several workers (Gibbs et al., 1986; Condie, 1993, 1997: Gao and Wedepohl 1995) who have suggested tectonic setting artifacts for such geochemical changes. These authors emphasized that comparison should be made on rocks of similar tectonic associations. Condie (1993, 1997) suggested that upper crustal compositional changes at the APB can be related to four evolutionary changes of earth history viz. i) komatiite effect, ii) TTG effect, iii) subduction effect, iv) weathering effect. Out of these, first three changes are direct consequence of cooling of mantle through time. Komatiite effect resulted from relatively large production rate of komatiitic magmas during the

Archean. This effect is preserved in sedimentary rock records in term of high Ni-Cr content and flat REE pattern with moderate positive Eu anomaly in Archean sediments relative to those of Proterozoic. The TTG effect resulted from voluminous production of TTG in Archean from partial melting of amphibolite/eclogite, where amphibole and garnets were left in residue. The subduction effects were important during late Archean-Early Proterozoic where huge amounts of granitic magma were produced due to partial melting of metasomatised mantle wedge and are characterized by distinct subduction geochemical component i.e. LILE enrichment over Nb and Ta. During the Proterozoic period, TTG magma was generated from fractional crystallization of basaltic magma at shallower depths (Martin, 1994), unlike the Archean TTG magma which was the product of partial melting of wet mafic crust. These changes are recorded in terms of HREE and Y depletion in Archean TTG and LILE enrichment in Proterozoic granites. The Archean TTG is characterized by steep fractionated REE pattern and LILE depletion in comparison to Proterozoic granite and TTG. Some geochemical changes across APB seems to be related to paleoweathering effects since intensity of chemical weathering decreased after the Archean.

In the study area, complete sedimentary record from Mesoarchean to Mesoproterozoic has been preserved. The Archean sediments (~2.9 Ga) of quartzite-phyllite-BIF assemblage, occurring as enclaves within 2.5 Ga Bundelkhand granite, forms the basement for Proterozoic sedimentary successions. The Paleoproterozoic Gwalior Group comprises cratonic sediments of sandstone-shale-BIF association and overlie the basement complex, which inturn overlain by sandstone-shale association of Mesoproterozoic Kaimur Group (~1.4 Ga) of Vindhyan Supergroup. The sequences represent a long part of earth's early history. Moreover this part of Bundelkhand craton is least deformed and unmetamorphosed; thus provide unique opportunity to compare the sediments of different ages with similar tectonic association and to trace the temporal geochemical changes in upper crustal composition. With these objective geochemical characteristics of Archean sandstones and Kaimur sandstones are compared with those of Gwalior sediments and discussed to draw interpretations in the light of modern concepts on crustal evolution.

5.2 Geochemistry of Archean quartzites

Thirteen quartzite samples were analysed for major and trace elements, out of which ten samples were selected for REE analysis. The results are given in Table 5.1.

These quartzites are enriched in SiO_2 (Av. 95.73) and depleted in other major elements in comparison to Archean cratonic sandstone of Condie, 1993. The K_2O/Na_2O ratios of these quartzites vary from 0.02 to 2.62 with a mean value of 1.07. This is distinctive in comparison to Proterozoic sediments of Gwalior and Kaimur Group, which are characterized by K_2O/Na_2O ratio of ~10. This feature is also mimicked by Rb/Sr ratios which vary from 0.12 to 4.73 with a mean value of 1.78 in these quartzites. The difference of these quartzites with their Proterozoic counterpart in terms of K_2O/Na_2O and Rb/Sr ratio is demonstrated in Fig.5.1. The distinctive low Rb/Sr and K_2O/Na_2O ratio of these Archean quartzites calls for Na-rich TTG type source rocks. The Na-rich TTG has been reported in Bundelkhand massif by Sharma and Rahman (1995), which is dated at 3.2 Ga (Sharma, 1998, Mondal et al., 2002,).

In terms of trace elements, these quartzites are characterized by near similar abundances of Rb (Av. 29.95ppm), Sr (Av. 17.39 ppm) and Th (Av. 3.68 ppm), and low Ba (Av. 79.89 ppm), higher Zr (Av. 137.93 ppm) and Y (Av. 8.93 ppm) in comparison to cratonic Archean sandstone reported by Condie (1993) as shown in Figure 5.2.

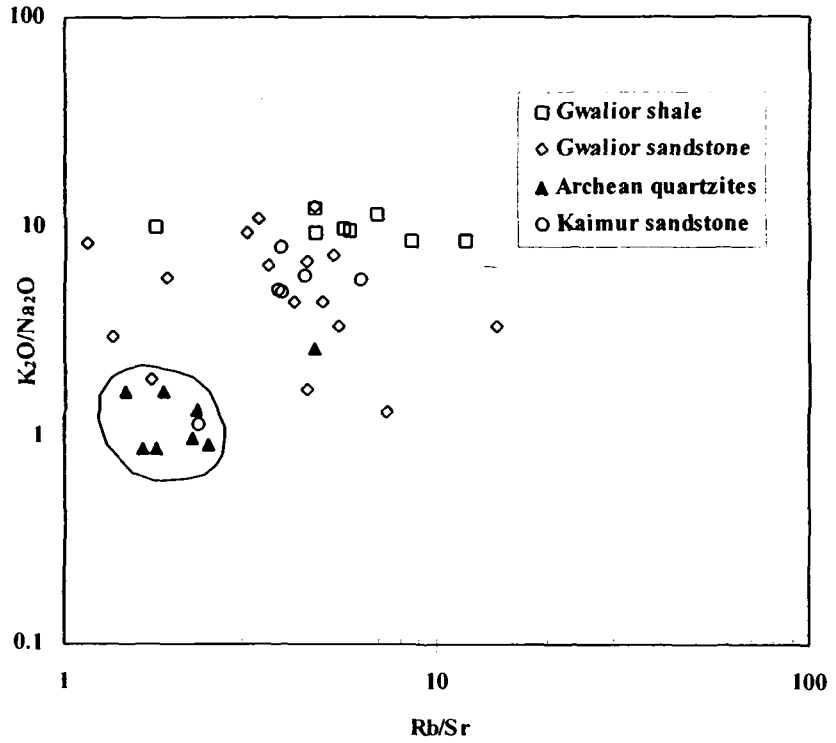

Fig.5.1: Rb/Sr vs. K2O/Na2O plot for Gwalior clastics, Kaimur Group sandstones and basement Archean quartzites. Note distinct position of Archean quartzites with low K2O/Na2O and Rb/Sr ratios compared to Proterozoic clastics.

Table 5.1: Geochemical composition of the basement Archean quartzites[S]

Sample No	BNS-1*	BNS-2	PC-1	PC-2	PC-3*	SON-A*	LD-3*	LD-4*	LD-5*	BNS-3*	LDR-1*	BST-1*	BST-2*
SiO_2	95.48	95.93	94.94	94.84	92.15	92.40	98.38	95.54	97.97	95.17	96.99	97.55	97.11
TiO_2	0.09	0.05	0.13	0.08	0.14	0.17	0.08	0.12	0.06	0.07	0.07	0.06	0.08
Al_2O_3	2.51	2.00	3.77	3.52	4.74	6.25	0.69	2.43	<0.01	0.69	0.15	0.09	0.28
$FeO^{(T)}$	0.53	0.90	0.59	0.78	1.74	0.48	0.57	0.63	0.85	0.41	0.65	0.57	0.73
MgO	<0.01	<0.01	<0.01	<0.01	<0.01	<0.01	0.04	0.08	0.04	0.03	0.04	0.01	0.01
MnO	<0.01	<0.01	<0.01	<0.01	0.01	0.03	<0.01	<0.01	<0.01	<0.01	<0.01	<0.01	<0.01
CaO	<0.01	<0.01	<0.01	<0.01	<0.01	0.03	<0.01	<0.01	<0.01	<0.01	<0.01	<0.01	<0.01
Na_2O	0.43	0.51	0.43	0.54	0.48	0.59	0.59	0.63	0.86	0.43	0.50	0.38	0.61
K_2O	0.71	0.47	0.01	0.01	<0.01	<0.01	0.52	0.62	0.72	0.71	1.31	0.51	0.53
P_2O_5	<0.01	<0.01	<0.01	<0.01	<0.01	<0.01	0.03	0.03	0.03	0.03	0.03	0.03	0.03
Total	99.75	99.86	99.87	99.77	99.26	99.95	100.90	100.08	100.53	97.54	99.74	99.20	99.38
Sc	1.55				2.96	3.16	1.00	1.80	0.90	0.70	0.70	0.70	0.90
V	9.06	<5	<5	<5	19.77	7.55	<5	6.00	37.00	<5	<5	<5	<5
Cr	117.97	119.00	37.00	68.00	38.88	49.12	65.00	75.00	141.00	86.00	135.00	80.00	93.00
Co	2.34				1.86	2.20	1.50	1.40	1.90	1.40	1.00	1.00	1.10
Ni	83.67	119.00	22.00	49.00	23.55	31.55	46.00	51.00	70.00	46.00	86.00	47.00	61.00
Cu	7.31		<5	<5	28.97	7.10	25.00	31.00	22.00	32.00	22.00	24.00	28.00
Zn	8.77	<5			20.65	10.99							
Ga	1.53		26.00	28.00	3.27	2.59	<5	7.00	6.00	<5	<5	<5	<5
Rb	25.17	39.00	<5	33.00	1.76	2.51	32.00	40.00	43.00	35.00	52.00	25.00	31.00
Sr	17.29	16.00	11.00	48.00	14.75	5.61	18.00	18.00	<5	19.00	11.00	11.00	19.00
Y	4.43	<5	<5	<5	9.49	17.60	10.00	<5	8.00	8.00	<5	5.00	<5
Zr	188.63	16.00	77.00	101.0	323.5	608.04	73.00	63.00	60.00	67.00	69.00	69.00	78.00
Nb	2.09	15.00	<5	20.00	7.76	3.46	<5	6.00	6.00	<5	<5	<5	7.00
Cs	0.94				0.19	0.20	<0.5	0.60	<0.5	0.60	1.10	<0.5	<0.5
Ba	113.00	81.00	117.0	<50	20.56	65.47	<50	130.00	<50	<50	53.00	59.00	80.00
Hf	6.53				10.73	19.98	1.50	1.60	1.10	1.60	1.90	1.70	1.90
Ta	0.39				1.87	0.82	<0.1	<0.1	<0.1	0.50	<0.1	<0.1	<0.1
Pb	14.13	29.00	18.00	32.00	17.92	7.84	23.00	35.00	24.00	53.00	30.00	30.00	48.00
Th	2.73	<5	<5	9.00	4.15	3.50	2.30	3.50	5.60	2.60	2.60	1.80	2.70
U	1.01	<5	<5	7.00	2.20	1.17	<2.0	<2.0	<2.0	<2.0	<2.0	<2.0	<2.0
La	20.71				41.56	9.09	19.00	22.00	18.00	24.00	17.00	18.00	23.00
Ce	27.03				49.29	15.90	29.00	36.00	27.00	32.00	23.00	24.00	31.00
Pr	2.44				5.48	2.22							
Nd	6.91				14.94	8.44	<25	<25	<25	<25	<25	<25	<25
Sm	0.86				1.83	1.53	1.60	1.90	2.30	1.20	1.20	1.30	1.70
Eu	0.16				0.31	0.35	0.30	0.40	0.50	0.20	0.20	0.20	0.30
Gd	0.88				1.86	1.50							
Tb	0.14				0.30	0.42	0.30	0.40	0.30	0.20	0.20	0.30	0.30
Dy	0.79				1.61	3.13							
Ho	0.16				0.34	0.72							
Er	0.53				1.07	2.30							
Tm	0.10				0.21	0.48	<0.5	<0.5	<0.5	<0.5	<0.5	<0.5	<0.5
Yb	0.63				1.35	2.98	0.50	0.60	0.50	0.50	<0.5	<0.5	0.50
Lu	0.11				0.23	0.49	0.10	0.10	0.10	0.10	<0.1	<0.1	0.10

Table 5.1: (continued)

Sample No	BNS-1#	BNS-2	PC-1	PC-2	PC-3#	SON-A#	LD-3#	LD-4#	LD-5#	BNS-3#	LDR-1#	BST-1#	BST-2#
La_N	88.11				176.83	38.68	80.85	93.62	76.60	102.13	72.34	76.60	97.87
Ce_N	44.83				81.74	26.36	48.09	59.70	44.78	53.07	38.14	39.80	51.41
Pr_N	27.39				61.57	24.99							
Nd_N	15.28				33.06	18.68							
Sm_N	5.84				12.41	10.37	10.88	12.93	15.65	8.16	8.16	8.84	11.56
Eu_N	2.86				5.61	6.21	5.36	7.14	8.93	3.57	3.57	3.57	5.36
Gd_N	4.48				9.46	7.61	9.11	11.69	10.28	6.32	6.32	8.50	9.30
Tb_N	3.94				8.28	11.58	8.33	11.11	8.33	5.56	5.56	8.33	8.33
Dy_N	3.23				6.64	12.86							
Ho_N	2.88				6.13	12.93							
Er_N	3.31				6.74	14.45							
Tm_N	4.21				8.54	20.08							
Yb_N	3.88				8.25	18.30	3.07	3.68	3.07	3.07			3.07
Lu_N	4.50				9.50	20.38	4.17	4.17	4.17	4.17			4.17
$(La/Yb)_N$	22.69				21.43	2.11	26.36	25.43	24.97	33.29			31.91
$(Gd/Yb)_N$	1.15				1.15	0.42	2.97	3.17	3.35	2.06			3.03
$(La/Sm)_N$	15.08				14.24	3.73	7.43	7.24	4.90	12.51	8.86	8.66	8.46
Eu/Eu*	0.56				0.52	0.70	0.54	0.58	0.70	0.50	0.50	0.41	0.52
SiO_2/Al_2O_3	38.04	47.97	25.18	26.94	19.44	14.78	142.58	39.32		137.93	646.60	1083.89	346.82
K_2O/Na_2O	1.65	0.92	0.02	0.02			0.88	0.98	0.84	1.65	2.62	1.34	0.87
Al_2O_3/TiO_2	27.89	40.00	29.00	44.00	33.86	36.76	8.63	20.25		9.86	2.14	1.50	3.50
La/Sc	13.34				14.06	2.87	19.00	12.22	20.00	34.29	24.29	25.71	25.56
Th/Sc	1.76				1.40	1.11	2.30	1.94	6.22	3.71	3.71	2.57	3.00
Ba/Co	48.21				11.05	29.83		92.86			53.00	59.00	72.73
Sc/Th	0.57				0.71	0.90	0.43	0.51	0.16	0.27	0.27	0.39	0.33
Cr/Th	43.15			7.56	9.37	14.02	28.26	21.43	25.18	33.08	51.92	44.44	34.44
Co/Th	0.86				0.45	0.63	0.65	0.40	0.34	0.54	0.38	0.56	0.41
La/Th	7.57				10.02	2.59	8.26	6.29	3.21	9.23	6.54	10.00	8.52
Rb/Sr	1.46	2.44		0.69	0.12	0.45	1.78	2.22		1.84	4.73	2.27	1.63
Rb/Ba	0.22	0.48			0.09	0.04		0.31			0.98	0.42	0.39
Zr/Y	42.58				34.08	34.54	7.30		7.50	8.38		13.80	
CIA						85.78							
PIA						85.89							
CIW						85.91							

$ Major elements in oxide wt.%, trace elements in PPM; total Fe as $FeO^{(T)}$; <, below detection; -, not analyzed; $Eu/Eu^* = Eu_N/(Sm_N \times Gd_N)^{1/2}$; # REE and trace element analyses by ICP-MS; @ REE analyses by INAA, Gd values are extrapolated after Condie (1993), $Gd_N = (Sm_N \times Tb_N \times Tb_N)^{1/3}$.

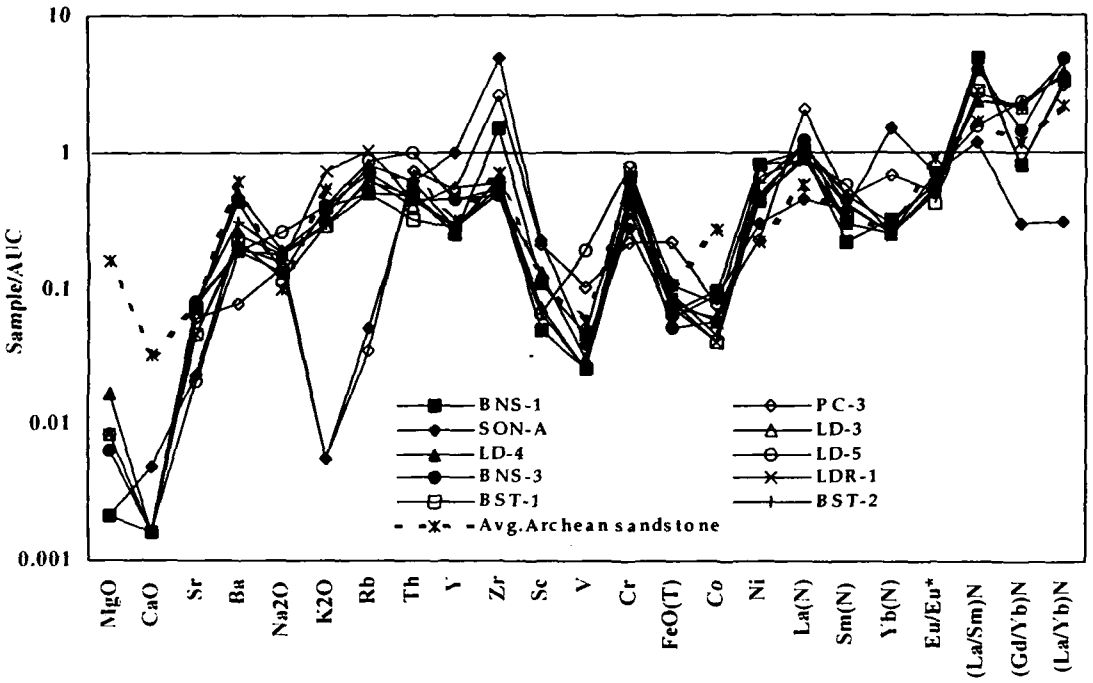

Fig.5.2: Spider plot of Archean quartzites, normalised against average Archean upper crust (values from Taylor and McLennan, 1985). Note strong depletion in CaO, Na_2O, K_2O, Y and high $(La/Yb)_N$ ratios. The average Archean cratonic sandstone (Condie,1993) is also plotted for reference.

In compatible vs. incompatible element ratio-ratio plot such as Th/Sc-Sc, La/Sc-Sc/Th, Co/Th-La/Sc and La-Th-Sc systematics (Fig.4.10, 4.11, 4.12, 4.13), these samples plot nearer to TTG end member and does not indicate any mafic component. In conjunction with their low K_2O/Na_2O, Rb/Sr ratios overall composition of these quartzites is consistent with Na-rich, K-poor source rock like TTG, as reported by Sharma and Rahman (1995). The La/Th ratio of these quartzites are higher (av. 7.22) than that of granite and Proterozoic sandstones. In La-Th-Sc ternary plot (Fig.4.13) these sandstones define distinct space near La apex, indicating a source enriched in La, depleted both in Th and Sc.

The quartzites exhibit near parallel REE patterns (Fig.5.3) with high total REE fractionation [Av. $(La/Yb)_N$ = 26.58], and relatively less fractionated HREE [$(Gd/Yb)_N$ = 2.06-3.03] patterns. One sample (SON-A) shows flat pattern because of high HREE content probably housed in zircon (Zr content 608 ppm). REE pattern of this sample appears to be modified due to presence of high zircon content, therefore the sample SON-A has not been considered for petrogenetic interpretations. The entire set of samples show strong negative europium anomalies with Eu/Eu* values

ranging from 0.41 to 0.70 with a mean of 0.55. The HREE depletion and total REE fractionation can be tested in $(La/Yb)_N$ vs. $(Yb)_N$ plot (Fig.5.4A). The samples clearly fall on high $(La/Yb)_N$ and low $(Yb)_N$ space, that is a characteristics feature of TTG. The Proterozoic sediments plots on distinctively different area of the diagram with low $(La/Yb)_N$ and high $(Yb)_N$ compared to Archean quartzites which is characteristics field for granite. In a La/Th – $(Yb)_N$ plot (Fig.5.4B), the Archean quartzites occupy distinctive place with higher La/Th value and low $(Yb)_N$ content. The high La/Th ratio of these sediments results from both La enrichment and Th depletion, which are characteristics of Archean TTG (Condie, 1993). In AUC normalized spider plot (Fig.5.2) conspicuous depletion of Y is noted with respect to Zr and Th, except the sample SON-A which is contaminated by zircon. All these parameters such as K_2O/Na_2O and Rb/Sr ratios, La/Sc-Sc/Th plot (Fig.4.11), REE patterns and Y depletion are collectively indicative of TTG source rock for these quartzites. The near flat HREE pattern {Av. $(Gd/Yb)_N$ = 2.16} however can arise in case of mafic source component, but such a source is not indicated in incompatible element ratio-ratio plots (Fig. 4.10, 4.11, 4.12, 4.13). Since these rocks exhibit large negative europium anomalies, it is reasonable to assume that HREE pattern is not primary and predominantly governed by heavy minerals. The high negative europium anomalies in these sandstones however are not in coherence with sole TTG source. This will require a granite source component having high negative europium anomalies. Archean granites with low K_2O/Na_2O ratio (1.56), large europium anomalies (Eu/Eu*=0.48) and fractionated REE patterns (La/Yb_N = 15.2), as reported by Condie (1993) may be a source component of these sandstones along with TTG. Therefore the geochemical changes across APB in this region appear to be a consequence of TTG effect (Condie, 1993).

As discussed above, flattening of REE patterns is observed across APB. The BGGC Archean quartzites show very steep REE patterns with average $(La/Yb)_N$ ratio of 26.58 and high negative europium anomalies (Eu/Eu* = 0.55), contrary to the Paleoproterozoic Gwalior Group clastic rocks which display relatively less fractionated REE patterns with average $(La/Yb)_N$ ratio of 12.57 and nearly similar negative europium anomaly (Eu/Eu* = 0.60). This phenomenon is not compatible to that as reported by Taylor and McLennan (1985, 1995). These authors and their coworkers (Taylor and McLennan, 1985, 1995; McLennan et al., 1990; McLennan and Taylor, 1991) have long been maintained that the Archean clastic rocks are

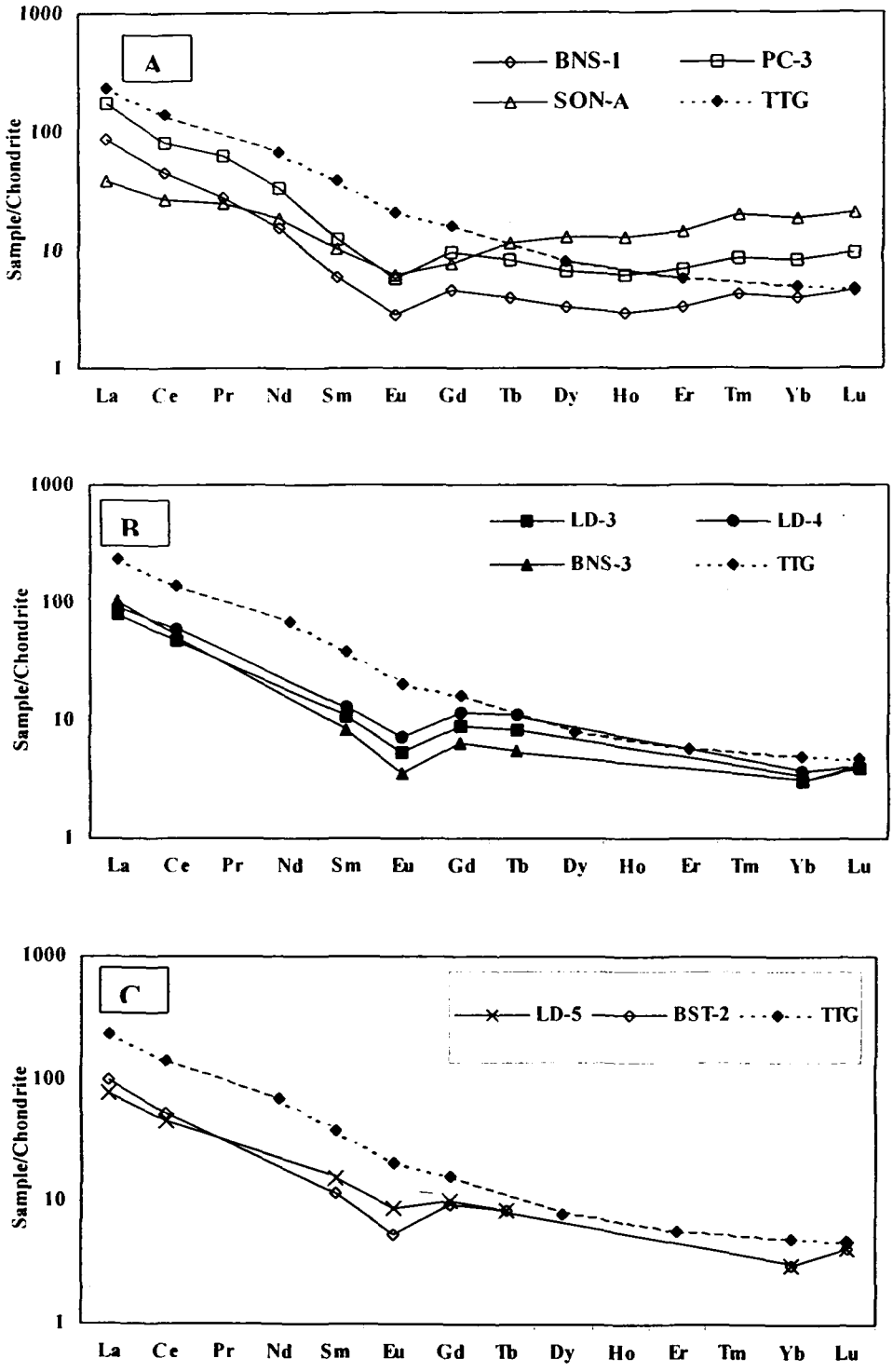

Fig.5.3: Chondrite normalised rare earth element patterns of Archean quartzites. The data of Bundelkhand TTG (Sharma and Rahman, 1995) is also plotted for reference. Note that REE patterns of these quartzites are grossly parallel to that of TTG. Also note high total REE fractionation and flat HREE patterns in first diagram (A) and both high total REE and HREE fractionation in the rest of the two diagrams (B&C). Data is plotted in three diagrams to avoid crowding.

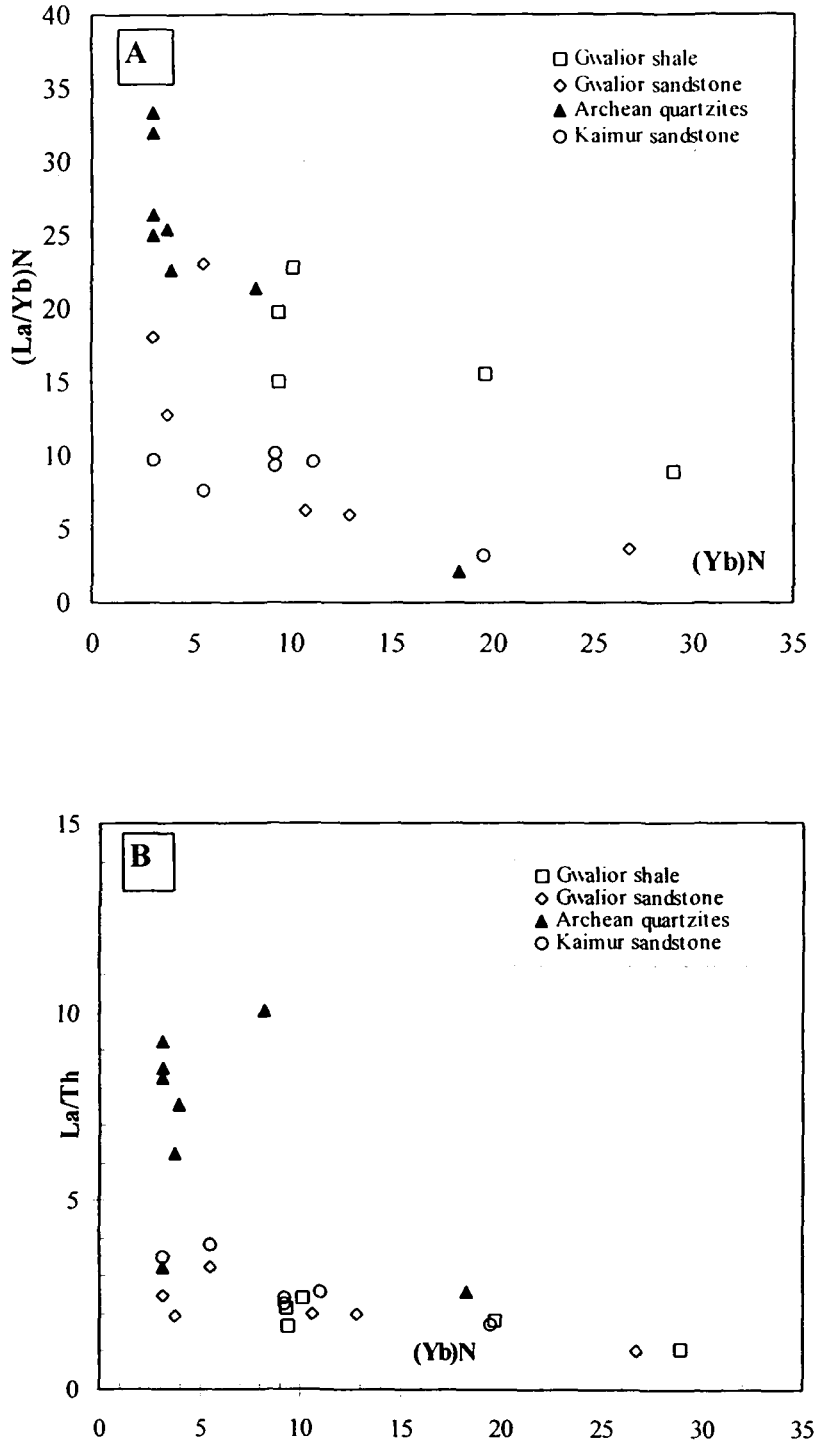

Fig.5.4: (A) $(La/Yb)_N$ vs. $(Yb)_N$ and (B) La/Th vs. $(Yb)_N$ diagrams for Gwalior clastics, Kaimur clastics and basement Archean quartzites. The Archean quartzites plot in high $(La/Yb)_N$, La/Th and low $(Yb)_N$ fields that is characteristics feature of TTG. Whereas the Proterozoic sediments plot in low $(La/Yb)_N$, La/Th and high $(Yb)_N$ fields which is characteristics of post Archean granites.

characterized by flat REE patterns with positive to no europium anomalies, whereas the post Archean clastic rocks are characterized by fractionated REE patterns with presence of high negative europium anomalies. These features have been grossly attributed to the over all mafic nature of Archean upper crust and importance of intracrustal granites in post Archean upper crust. However, this generalization has been objected by several researchers (Gao and Wedepohl, 1995; Gibbs et al., 1986; Condie, 1993, 1997; Naqvi, 2002) as they suggested that these geochemical changes across the APB are observed because the clastic rocks of Archean greenstone belts are compared with cratonic sediments of Proterozoic age and thus attesting the tectonic bias of sampling. Condie (1993, 1997) opined that the first order geochemical changes across the APB is the direct consequence of secular cooling of the earth and three major effects controlling the geochemical changes across APB have been suggested viz. (i) 'komatiite effect', (ii) 'TTG effect' and (iii) 'subduction effect', which are already discussed in the earlier section. The first two effects signify the considerable proportion of komatiites and TTG in the Archean upper crust. The 'komatiite effect' is perhaps governed the geochemical composition of Archean upper continental crust in case of greenstone belts which contain significant amount of mafic volcanic rocks. The 'TTG effect' is perhaps more important in controlling upper crustal composition of Archean cratonic terrains. The broad generalization made by Taylor and McLennan (1985) is appears to be valid only on Archean greenstone sediments and seems to be untenable in case of Archean cratonic sediments. The present geochemical study of BGGC Archean quartzites shows that TTG was the major component of source terrain. The overlying Paleoproterozoic cover rocks of Gwalior Group display considerable flat REE pattern compare to those of Archean quartzite. Moreover the Gwalior sediments are extremely enriched in LILE such as K, Rb, Ba and Th. Thus 'TTG effect' along with 'subduction effect' govern the geochemical changes across APB in Bundelkhand craton.

5.3 Geochemistry of Kaimur sandstones, Vindhyan Supergroup

Six sandstone samples of Kaimur Group were analysed for major, trace and rare earth elements in order to identify temporal changes of upper crustal composition. The results are listed in the table 5.2. The Kaimur sandstone samples vary from quartzarenite to quartzwacke and exhibit negative correlation between Al_2O_3 and SiO_2, indicating quartz dilution or enrichment in clay matrix. Al_2O_3

exhibit positive correlation with K_2O, FeO and MgO indicating clay mineral and weathering control. The Al_2O_3 and TiO_2 are strongly positively correlated, indicating severe weathering of source rocks. In A-CN-K compositional plot (Fig.4.15A), the samples indicate mild potash metasomatism, as they fall right side of "limit of weathering line". The source terrain of Kaimur sediments are relatively less weathered in comparison to Gwalior clastics as indicated by PIA values (Fig. 4.15B) which ranges from 79.99 to 89.48 with an average value of 83.74. In AUC normalized spidergram Kaimur sandstones display parallel patterns to that of Gwalior clastics, NASC and PAAS (Fig.5.5). They are severely depleted in Sc, V, Cr, Fe, Co, Ni and enriched in K, Rb, Th, Zr and Y relative to AUC. In comparison with Proterozoic cratonic sandstone standard (Condie, 1993), the Kaimur sediments exhibit nearly similar transition element contents, while they are strongly enriched in LILEs

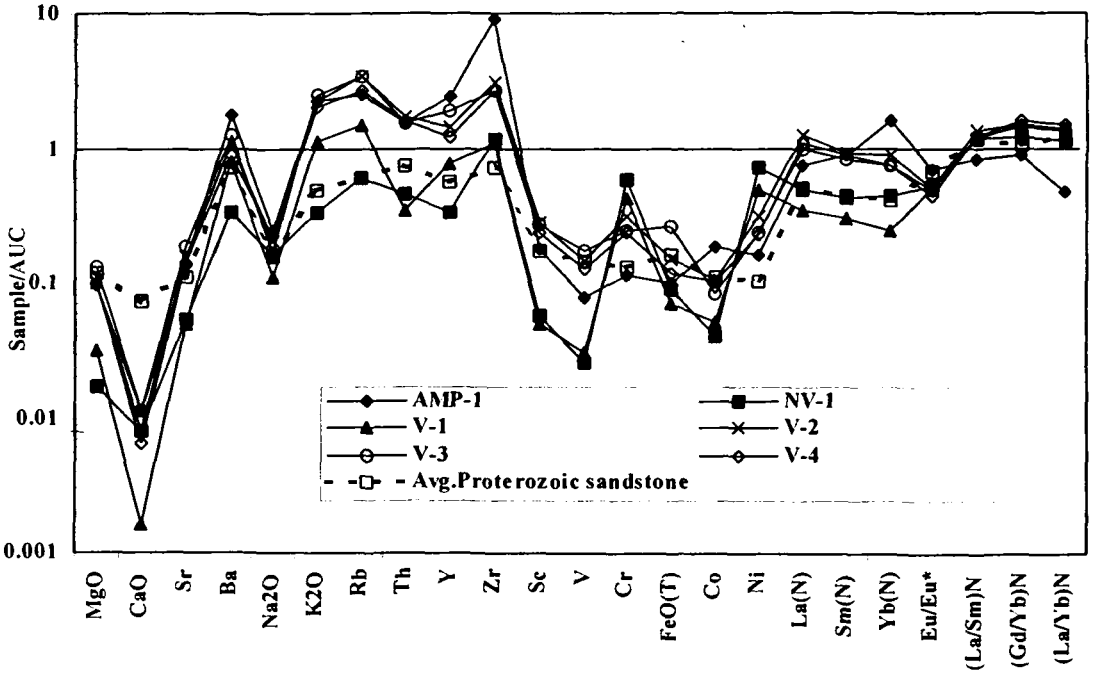

Fig.5.5: Spider plot of Kaimur Group sandstones normalised against average Archean upper crust (values from Taylor and McLennan, 1985). Note strong depletion in CaO, Na_2O, Sr, absence of Y anomaly and lesser $(La/Yb)_N$ ratios. The average Proterozoic cratonic sandstone (Condie, 1993) is also plotted for reference.

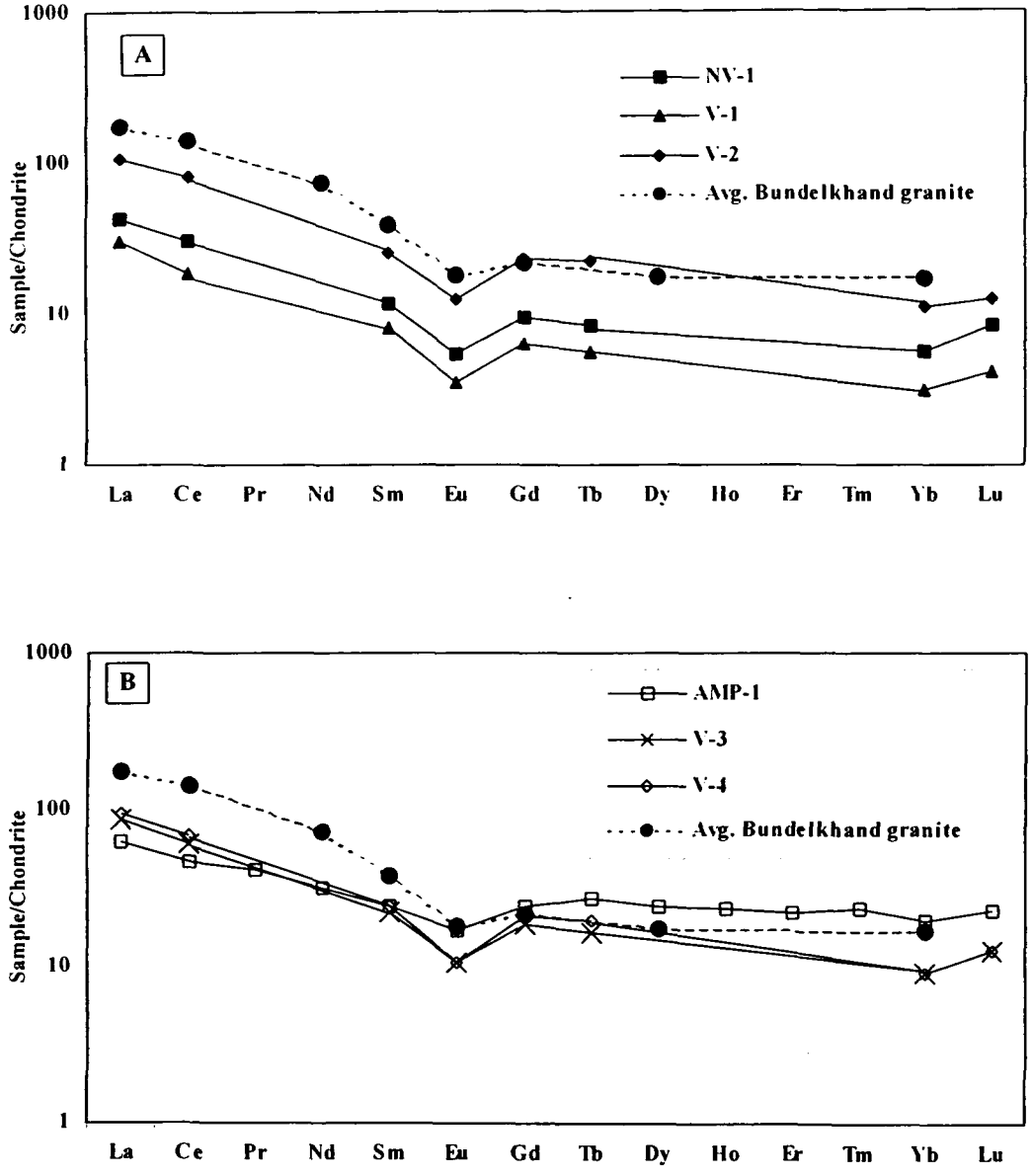

Fig.5.6: Chondrite normalised rare earth element patterns of Kaimur sandstones of Vindhyan Supergroup. Samples show lesser total REE fractionation compared to Gwalior clastics and Archean quartzites. Also note that the REE patterns are sub-parallel to basement Bundelkhand granite (Mondal and Zainuddin, 1995, 1996, Mondal, 2002). Data is plotted in two diagrams to avoid crowding.

Table 5.2: Geochemical composition of the Kaimur sandstones[$]

Sample No	AMP-1[#]	NV-1[@]	V-1[@]	V-2[@]	V-3[@]	V-4[@]
SiO_2	82.52	96.49	92.75	82.32	78.14	84.75
TiO_2	0.32	0.19	0.09	0.39	0.51	0.37
Al_2O_3	9.91	0.51	2.15	10.22	13.75	8.99
$FeO^{(T)}$	0.80	0.73	0.56	1.20	2.08	0.95
MgO	0.46	0.08	0.15	0.47	0.61	0.47
MnO	<0.01	<0.01	<0.01	<0.01	<0.0.1	<0.01
CaO	0.07	0.05	<0.01	0.05	0.07	0.04
Na_2O	0.82	0.53	0.36	0.69	0.56	0.73
K_2O	4.11	0.60	2.03	4.01	4.46	3.60
P_2O_5	<0.01	0.03	0.03	0.04	0.04	0.03
Total	99.01	99.21	98.12	99.39	100.22	99.93
Sc	2.55	0.80	0.70	4.00	3.80	3.30
V	15.41	<5	6.00	29.00	34.00	25.00
Cr	21.02	107.00	76.00	57.00	45.00	43.00
Co	4.65	1.00	1.30	2.70	2.10	2.60
Ni	16.81	75.00	52.00	33.00	25.00	24.00
Cu	10.29	22.00	15.00	16.00	10.00	31.00
Zn	14.05					
Ga	5.63	5.00	<5	10.00	17.00	8.00
Rb	124.59	30.00	75.00	169.00	171.00	132.00
Sr	32.88	13.00	12.00	38.00	45.00	34.00
Y	44.08	6.00	14.00	26.00	34.00	22.00
Zr	1108.89	148.00	134.00	388.00	334.00	332.00
Nb	7.36	<5	<5	8.00	12.00	11.00
Cs	3.79	<0.5	1.40	5.80	5.00	5.60
Ba	474.03	90.00	215.00	287.00	328.00	237.00
Hf	37.75	3.80	3.20	10.00	7.30	8.60
Ta	1.59	0.90	<0.1	0.50	<0.1	<0.1
Pb	10.61	13.00	17.00	23.00	24.00	15.00
Th	8.66	2.60	2.00	9.70	8.90	9.00
U	1.72	<2.0	<2.0	<2.0	<2.0	2.20
La	14.83	10.00	7.00	25.00	20.00	22.00
Ce	28.23	18.00	11.00	48.00	36.00	41.00
Pr	3.70					
Nd	14.44	<25	<25	<25	<25	29.00
Sm	3.61	1.70	1.20	3.70	3.30	3.60
Eu	0.94	0.30	0.20	0.70	0.60	0.60
Gd	4.77					
Tb	0.98	0.30	0.20	0.80	0.60	0.70
Dy	5.83					
Ho	1.31					
Er	3.57					
Tm	0.57	<0.5	<0.5	<0.5	<0.5	<0.5
Yb	3.17	0.90	0.50	1.80	1.50	1.50
Lu	0.56	0.20	0.10	0.30	0.30	0.30

Table 5.2: (continued)

Sample No	AMP-1#	NV-1@	V-1@	V-2@	V-3@	V-4@
La_N	63.11	42.55	29.79	106.38	85.11	93.62
Ce_N	46.82	29.85	18.24	79.60	59.70	67.99
Pr_N	41.54					
Nd_N	31.95					64.16
Sm_N	24.52	11.56	8.16	25.17	22.45	24.49
Eu_N	16.80	5.36	3.57	12.50	10.71	10.71
Gd_N	24.19	9.30	6.32	23.16	18.41	21.00
Tb_N	27.19	8.33	5.56	22.22	16.67	19.44
Dy_N	24.01					
Ho_N	23.45					
Er_N	22.45					
Tm_N	23.83					
Yb_N	19.47	5.52	3.07	11.04	9.20	9.20
Lu_N	23.17	8.33	4.17	12.50	12.50	12.50
$(La/Yb)_N$	3.24	7.71	9.71	9.63	9.25	10.17
$(Gd/Yb)_N$	1.24	1.68	2.06	2.10	2.00	2.28
$(La/Sm)_N$	2.57	3.68	3.65	4.23	3.79	3.82
Eu/Eu*	0.69	0.52	0.50	0.52	0.53	0.47
SiO_2/Al_2O_3	8.33	189.20	43.14	8.05	5.68	9.43
K_2O/Na_2O	5.01	1.13	5.64	5.81	7.96	4.93
Al_2O_3/TiO_2	30.97	2.68	23.89	26.21	26.96	24.30
La/Sc	5.81	12.50	10.00	6.25	5.26	6.67
Th/Sc	3.39	3.25	2.86	2.43	2.34	2.73
Ba/Co	101.99	90.00	165.38	106.30	156.19	91.15
Sc/Th	0.29	0.31	0.35	0.41	0.43	0.37
Cr/Th	2.43	41.15	38.00	5.88	5.06	4.78
Co/Th	0.54	0.38	0.65	0.28	0.24	0.29
La/Th	1.71	3.85	3.50	2.58	2.25	2.44
Rb/Sr	3.79	2.31	6.25	4.45	3.80	3.88
Rb/Ba	0.26	0.33	0.35	0.59	0.52	0.56
Zr/Y	25.16	24.67	9.57	14.92	9.82	15.09
CIA	62.58			64.74	70.06	63.49
PIA	78.7218			82.7463	89.4847	79.9969
CIW	87.0351			89.2889	92.9149	87.591

$ Major elements in oxide wt.%, trace elements in PPM; total Fe as $FeO^{(T)}$; <, below detection; -, not analyzed; $Eu/Eu^* = Eu_N/(Sm_N \times Gd_N)^{1/2}$; # REE and trace element analyses by ICP-MS; @ REE analyses by INAA, Gd values are extrapolated after Condie (1993), $Gd_N = (Sm_N \times Tb_N \times Tb_N)^{1/3}$.

and HFSEs. This indicate felsic provenance for these rocks. Th/Sc-Sc (Fig.4.10), La/Sc-Sc/Th, (Fig.4.11), Co/Th-La/Sc (Fig.4.12), La-Th-Sc (Fig.4.13) systematics are in conformity with granitic provenance of Kaimur sediments. This can be further tested by examining REE patterns. The Kaimur sandstone exhibit parallel REE patterns (Fig.5.6) with moderate total REE fractionation and strong negative Eu anomalies. $(La/Yb)_N$ ranges from 7.71 to 10.17 with a mean of 8.29 and Eu/Eu* values range from 0.47 to 0.53 with a mean of 0.54. The REE data of sample AMP-1 is not considered because the REE pattern is extremely modified by high HREE content and interpreted to be housed in zircons (Zr = 1109ppm). The REE patterns of Kaimur sandstone are sub-parallel to the 2.5 Ga high-K granites of the basement as reported by Mondal and Zainuddin (1995, 1996) and Mondal (2002) (Fig.5.6). In AUC normalized spidergram (Fig. 5.5) Kaimur sandstones do not show depletion of Y relative to Zr and Th, as in the case of Gwalior clastics and Archean sandstones. HREE enrichment of Kaimur sandstones as evidenced from REE patterns, do not support a TTG component of source rock. These characteristics along with LILE enrichment indicate that granite was dominant or sole source component for the sediments of Kaimur Group.

5.4 Geochemical changes across APB

The geochemical data and detailed discussion presented in the present work have important implications on change of upper crustal composition from Mesoarchean to Mesoproterozoics period in Bundelkhand block of north Indian shield. As evidenced from the geochemistry of Archean clastic rocks from this terrain, the Archean crust was dominated by TTG and possibly with a low K-Archean granite component. The mixing modelling of REE data of Gwalior clastics indicates that the Paleoproterozoic upper crust was consisting of 40% TTG, 40% high-K granites (~2.5 Ga) and 20% mafic rocks. The geochemical data of Gwalior clastics suggest a significant contribution from high K-granitic rocks, as well as an equal contribution from TTG. The Mesoproterozoic Kaimur sandstone geochemistry points towards a dominantly high-K granitic (~2.5 Ga) upper continental crust. At present, the Bundelkhand massif predominantly composed of high K-granite (~90%, Basu 1986). Therefore the present study suggests that in this part of Indian shield the upper crust evolved from TTG composition during Archean period (~2.9Ga) to a granitic composition during the Mesoproterozoic period. This phenomenon can be explained

simply by erosional processes. It is suggested that the TTG upper crust was completely eroded during the Paleoproterozoic and its debris entered into the sedimentary record of that period. The erosion of upper TTG cover exposed the deep level granite batholiths which significantly contributed detritus to Gwalior basin. By the end of Paleoproterozoic the TTG upper crust was probably completely eroded, thus no signatures of its presence is available in geochemistry Mesoproterozoic Kaimur Group sediments.

Therefore the compositional changes of upper crust across APB in Bundelkhand craton is characterized by evolution from TTG crust of Mesoarchean to a granitic crust during the Paleoproterozoic. In summary following parameters signifies the change and illustrated in Fig.5.7:

i) K_2O/Na_2O ratio changed dramatically from Archean to Proterozoic: K_2O/Na_2O ratio of ~1 at Archean was shifted to around ~10 during the Proterozoic. The Rb/Sr ratio mimics the K_2O/Na_2O ratio, and show similar change in upper crust (Fig.5.7).

ii) LILEs along with Th are enriched in Proterozoic sediments compared to those of Archean sediments. This signifies the importance of intra-crustal granite during Proterozoic. The metasomatic addition of LILEs is governed by "subduction effect" where excess LILEs are introduced in metasomatised mantle wedge.

iii) Total REE fractionation $(La/Yb)_N$ was changed and flattened with time (Fig.5.7). The average $(La/Yb)_N$ of Archean sediment is 26.58, which evolved to a value of 12.57 for Gwalior sediments, and changed eventually to a value of 8.29 in Kaimur sediments. The temporal evolution of REE patterns is exactly opposite to that reported by Taylor and McLennan (1985). These signify that "TTG effect" was the dominating factor instead of "Komatiite effect".

iv) La/Th ratio also changed temporally (Fig.5.7): the Archean sediments are characterized by higher values (avg. 7.22), declined with increase in Th content in Proterozoic (Av. Gwalior sandstone: 2.34, Avg. Kaimur Sandstone: 2.72). The data indicate systematic unroofing of granite batholiths during the Proterozoic by upliftment and erosion of upper TTG cover.

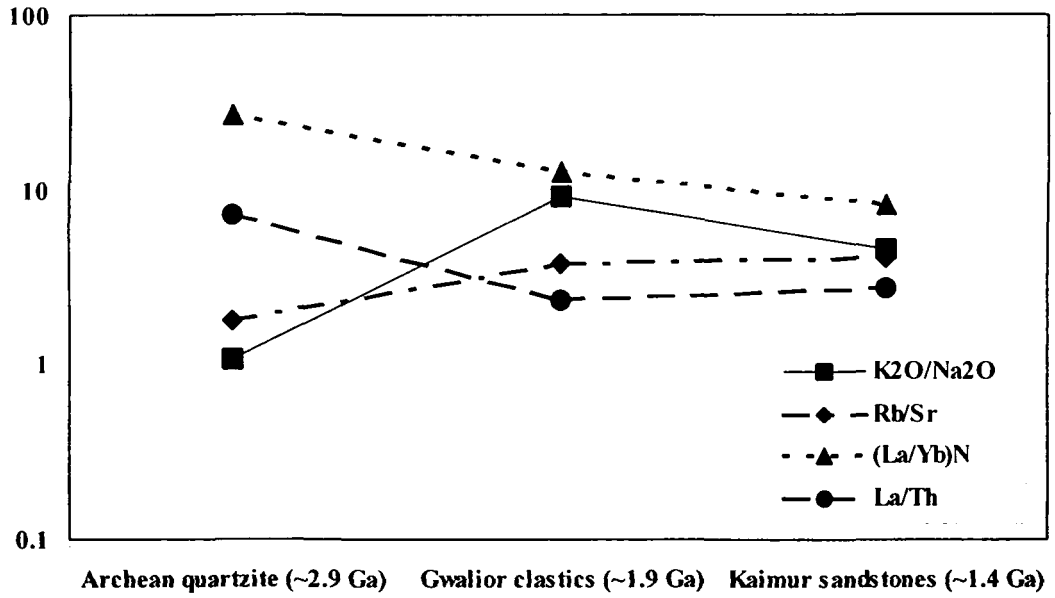

Fig.5.7: The Geochemical parameters showing compositional evolution of upper continental crust during 2.9 Ga and 1.4 Ga. The decreasing temporal $(La/Yb)_N$ ratios suggests Yb enrichment with time and importance of subduction related granites at the expense of HREE depleted Archean TTG in the Proterozoic upper continental crust. La/Th also indicates similar processes. The temporal change of K_2O/Na_2O and Rb/Sr ratios suggests importance of high-K granites over Na-rich tonalites in the upper continental crust during the Proterozoic period. All these data, together suggest evolution of upper continental crust of Bundelkhand craton from TTG composition during the Mesoarchean to granitic composition during the Mesoproterozoic. Note the data are in logarithmic scale and still the temporal variations can be distinguished.

CHAPTER-VI

Geochemistry of Banded Iron Formation of Gwalior Group: Implications for sources of Fe and composition of Precambrian seawater

6.1 Introduction:

Geochemical features of chemical sediments are believed to reflect those of water from which the sediments precipitate. Therefore, chemical sediments like BIF, chert and limestone of Precambrian age would provide important insights into the chemistry of Precambrian sea water (Veizer and Compston, 1976; Fryer et al., 1979; Veizer et al., 1982, 1989, 1990; Fryer, 1983; Miller and O'nions, 1985; Jacobsen and Pimentel-Klose, 1988a, b; Derry and Jacobsen, 1990; Shimizu et al., 1990; Denielson et al., 1992; Bau and Möller, 1993; Bau et al., 1997; Khan et al., 1996). In absence of preserved samples of old sea water itself, this record offers a chance to infer some of the important chemical characteristics of ancient oceans. The trace element chemistry of seawater is governed by erosional fluxes from continental crust and hydrothermal flux of materials from oceanic crust (Derry and Jacobsen, 1990). The present day sea water chemistry is chiefly controlled by fluvial and eolion erosional flux from continent as dissolved load and as particulate which are extremely modified by estuarine processes (De Baar et al., 1985a; Goldstein and Jacobsen, 1987,1988a,b,c; Sholkovitz, 1988; Derry and Jacobsen, 1990). However a higher hydrothermal contribution to the Precambrian ocean is expected because this era of geological past was characterised by higher surface heat flow, which in turn should result in higher sea-floor production rates. This would result in an increase in the hydrothermal water flux through ocean ridges and/or higher exiting temperature of water. Thus the patterns of trace elements and isotopic abundances preserved in ancient chemical sediments can be used to constrain relative magnitude of crustal and mantle fluxes to the ocean during that period. Banded Iron Formations (BIF) constitute one of the most common type of marine chemical precipitates found in Precambrian sequences. The two major types of BIFs, identified in geological record, viz. (a) "Lake Superior" – type of shallow-continental shelf association (cratonic) chiefly restricted to Paleoproterozoic; and (b) "Algoma" –type BIF of greenstone association, restricted to middle Archean age. The sources of iron and rare earth elements (REE) and redox conditions of Precambrian seas have been studied through geochemical pattern and

Nd isotopic study of BIFs of various shield areas. Contrasting sources of Fe and REE of Precambrian BIFs have been proposed. For example, Miller and O'nions (1985) reported Nd isotopic composition of Precambrian BIFs, concluding that iron and REE of Precambrian BIFs were supplied by continental weathering, and in this respect the water masses in which iron-formations formed were analogues to modern sea water. On the other hand, many researcher (e.g. Jaocobsen and Pimental-Klose,1988 a, b; Shimizu et al., 1990; Alibert and McCulloch, 1993; Isley, 1995; Bau et al., 1997; Isley and Abott, 1999, Frei et al., 1999) on the basis of Nd isotopic data suggested that positive and mantle like εNd values of Precambrian oceans contrast strongly with the negative and continent-like εNd values of the phanerozoic sea water. Furthermore, these authors also suggested that the REE budget of the oceans during the deposition of iron-formations (2.5-3.7 Ga) was probably dominated by hydrothermal circulation of sea water through mid-ocean ridge basalts and not by continent derived river water, as is the case today. However in all these studies, the data of late Paleoproterozoic BIFs are grossly unrepresentative as emphasis have been given to Archean and early Paleoproterozoic (2.5 –3.7 Ga) BIFs. Although significant amount of BIF of geological record has been precipitated during late Paleoproterozoic (~1.9 Ga) (James, 1983; Klein and Beukes,1992a), baring the data of Gunflint and Sokoman BIF of Canada (Jacobsen and Pimentel-Klose, 1988a, Derry and Jacobsen, 1990) detailed studies have not been carried out on late Paleoproterozoic BIFs. It is well established that significant changes occurred in upper crustal composition and style of tectonics during Archean-Proterozoic (AP) transition (Taylor and McLennan, 1985; Condie, 1997). For example, the Archean-Proterozoic transition is marked by evolution of upper continental crust from mafic to felsic composition with the production of huge amount of high-K intracrustal granite at ~2.5 Ga. The greenstone tectonics, which dominated during the Archeans diminished with time and cratonic assemblages became dominated during the Proterozoic. These changes should be reflected in geochemistry of chemical sediments like BIFs. The early Paleoproterozoic (~2.5Ga) BIFs represent the immediate Archean-Proterozoic transition era and still can inherit the chemical signatures of Archean sea. The late Paleoproterozoic chemical precipitates unambiguously represent post Archean-Proterozoic transition era, and thus comparison of late Paleoproterozoic BIFs with Archean BIFs will allow to infer some of the temporal changes in sea water and upper

crustal composition. The late Paleoproterozoic (~1.9 Ga) Gwalior Group BIFs of central India are subjected to geochemical study in this chapter with objective to deduce the sources of iron and REE, to infer the relative contribution of continental to hydrothermal flux to the ocean and to study the temporal changes of sea water chemistry by comparing them with their Archean counterparts.

6.2 Geochemistry:

6.2.1 Major elements

Seven samples of the BIFs from Morar Formation, Gwalior Group were analysed for major, trace, and rare earth elements, and five of them were analysed for Nd-isotopic composition. The data are given in the table 6.1. Major element compositions show significant variations in iron and silica contents depending upon the thickness of rhythmic hematite rich and silica rich meso bands. The FeO content varies from 5.53 to 48.70 percent and is antipathetically related to SiO_2 content, with a corresponding value of 90.88 and 48.31 percent respectively (Fig.6.1). Al_2O_3 content of these BIFs, which varies from 1.37 to 1.74 percent, are less than 2 % and similar to Cherty banded iron-formation (CBIF) described by Khan and Naqvi (1996) for BIFs of Dharwar craton. The BIFs are of oxide facies with hematites are being sole Fe mineral, that is also reflected in their chemistry. Fe and Si, the major constituents, together comprise about 97% of bulk chemistry and other elements are present only in negligible quantity.

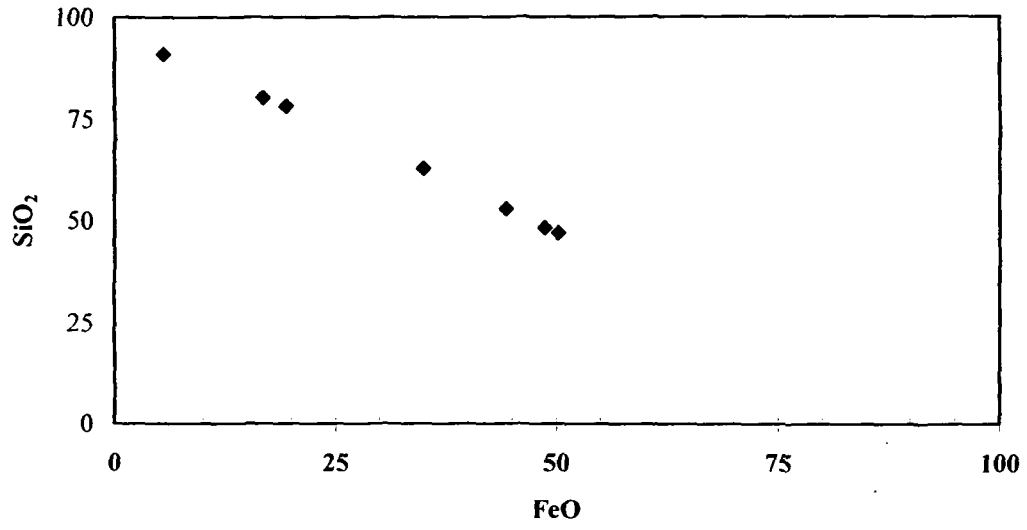

Fig.6.1: Binary relationships between FeO and SiO_2 showing antipathetic relationship. The antipathetic relationship is because of relative abundances of hematite and chert mesobands of BIFs.

6.2.2 Trace elements

Since the samples were preferentially drawn from pure cherty BIF fraction, the abundances of elements such as Sc, Th, Zr, Hf, Rb, Cs, are very low (Table 6.1), indicating minimal detrital aluminosilicate clastic contamination and near pure chemical fraction. The samples exhibit very high Y/Ho (26.59-41.51, Average ~ 32.09) and Y/Zr (12-64) ratios that supports this inference (Bau et al., 1997). However, positive correlation (Fig.6.2) between Al_2O_3 and TiO_2 (r=0.62), Zr and Hf (r=0.77), Nb and Ta (r=0.67), Zr and Th (r=0.83) possibly indicate minor clastic control over trace elements as well (Gnaeshwar Rao and Naqvi, 1995; Khan and Naqvi, 1996).

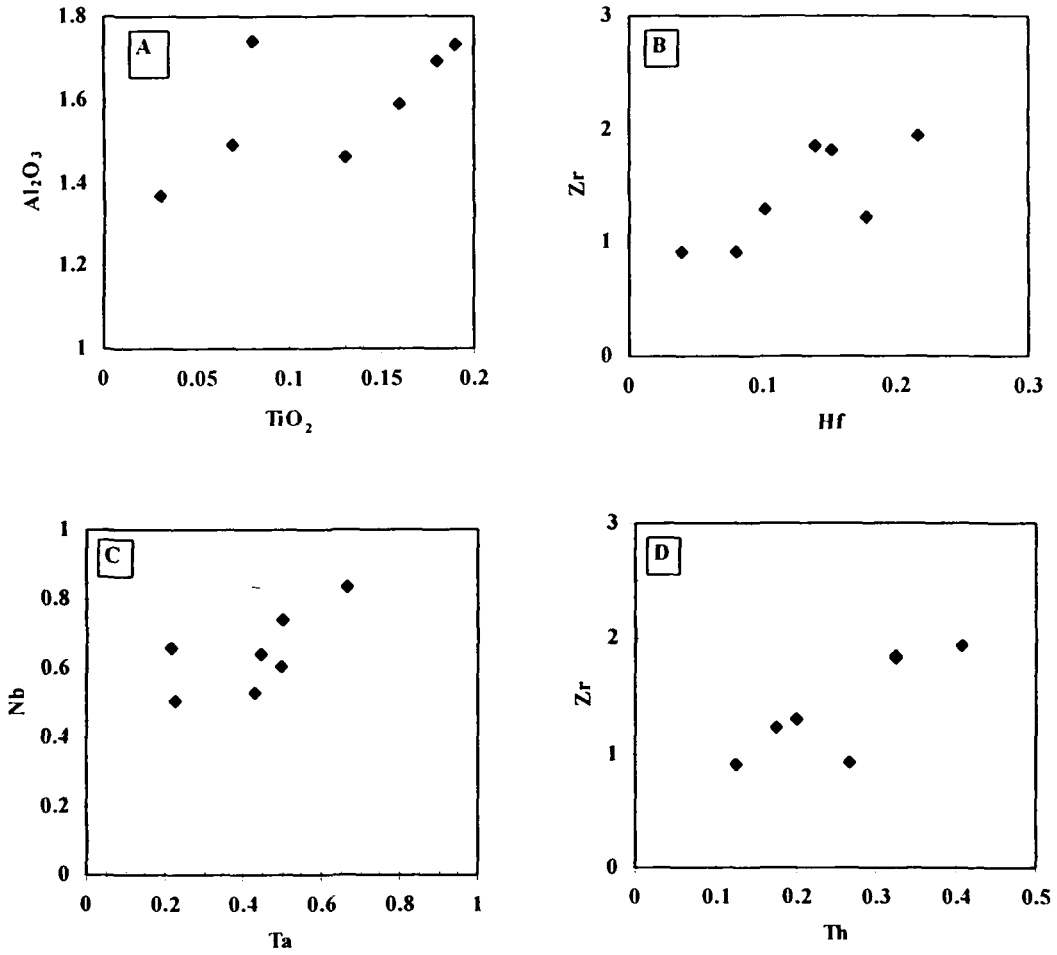

Fig 6.2: Sympathetic relationships between different characteristic elements indicating contribution from terrigenous inputs as particulate and colloidal loads.

Table 6.1: Geochemical composition of BIFs of Gwalior Group[S]

Sample No	SNS1	SNS3	SNS2	MGR1	MGR2	STL1	MHS1
SiO_2	48.31	52.92	62.84	46.89	90.88	78.13	80.17
TiO_2	0.19	0.16	0.13	0.18	0.03	0.08	0.07
Al_2O_3	1.73	1.59	1.46	1.69	1.37	1.74	1.49
$FeO^{(T)}$	48.7	44.33	34.95	50.19	5.53	19.38	16.79
MgO	0.17	0.12	0.08	0.14	<0.01	0.03	0.04
MnO	0.022	0.05	0.015	0.006	0.006	0.01	0.007
CaO	0.02	<0.01	<0.01	<0.01	<0.01	0.03	0.04
Na_2O	0.38	0.37	0.47	0.16	0.43	0.29	0.55
K_2O	<0.01	<0.01	<0.01	<0.01	<0.01	<0.01	<0.01
P_2O_5	0.04	0.08	<0.01	0.01	<0.01	<0.01	<0.01
Total	99.56	99.62	99.95	99.36	98.25	99.69	99.16
Sc	0.27	0.28	0.24	0.20	0.17	0.21	0.17
V	3.25	3.57	2.76	2.31	0.93	2.23	1.79
Cr	33.41	52.72	51.44	73.01	69.33	43.60	78.88
Co	10.25	10.97	14.02	3.71	2.63	1.58	3.21
Ni	93.66	105.50	95.12	117.76	108.02	64.32	116.69
Cu	30.31	22.68	26.97	39.80	19.48	6.63	8.54
Zn	26.05	28.94	22.43	24.75	13.21	12.11	14.29
Ga	0.96	1.08	0.86	0.85	0.25	0.87	0.48
Rb	1.01	0.96	0.41	0.88	0.69	2.52	1.44
Sr	2.96	3.80	2.23	2.27	5.31	5.49	10.12
Y	12.39	38.58	65.75	7.43	2.81	5.30	9.95
Zr	0.92	1.94	1.23	1.84	0.91	1.82	1.29
Nb	0.65	0.83	0.64	0.74	0.53	0.51	0.61
Cs	0.09	0.09	0.04	0.10	0.06	0.17	0.18
Ba	4.49	10.31	2.84	3.79	3.87	4.18	5.10
Hf	0.08	0.22	0.18	0.14	0.04	0.15	0.10
Ta	0.22	0.67	0.45	0.50	0.43	0.23	0.50
Pb	3.85	4.04	3.89	3.91	4.53	4.15	4.59
Th	0.27	0.41	0.18	0.32	0.13	0.33	0.20
U	0.61	0.43	0.16	0.26	0.07	0.08	0.07
La	5.96	21.95	7.15	1.42	1.25	4.55	7.52
Ce	9.64	35.33	14.47	2.99	2.42	6.41	11.94
Pr	1.33	4.82	1.71	0.38	0.29	0.86	1.28
Nd	6.14	23.59	8.63	1.93	1.45	3.70	5.86
Sm	1.51	4.88	2.40	0.51	0.39	0.65	1.07
Eu	0.45	1.39	0.80	0.17	0.13	0.19	0.36
Gd	2.06	6.64	5.28	0.76	0.47	0.80	1.40
Tb	0.33	0.98	0.89	0.13	0.08	0.11	0.18
Dy	2.30	6.35	6.52	0.98	0.48	0.72	1.25
Ho	0.47	1.31	1.58	0.24	0.10	0.17	0.28
Er	1.46	3.84	4.66	0.80	0.29	0.52	0.84
Tm	0.19	0.47	0.54	0.11	0.04	0.06	0.10
Yb	1.24	2.89	3.03	0.65	0.25	0.35	0.51
Lu	0.17	0.40	0.45	0.09	0.03	0.05	0.06
ΣREE	33.25	114.83	58.12	11.16	7.64	19.14	32.65
ΣLREE	24.58	90.57	34.36	7.22	5.78	16.17	27.68
ΣHREE	8.22	22.87	22.96	3.76	1.73	2.78	4.61

Table 6.1: (Continued)

Sample No	SNS1	SNS3	SNS2	MGR1	MGR2	STL1	MHS1
La_{SN}	0.19	0.69	0.22	0.04	0.04	0.14	0.24
Ce_{SN}	0.13	0.48	0.20	0.04	0.03	0.09	0.16
Pr_{SN}	0.17	0.61	0.22	0.05	0.04	0.11	0.16
Nd_{SN}	0.19	0.71	0.26	0.06	0.04	0.11	0.18
Sm_{SN}	0.27	0.86	0.42	0.09	0.07	0.11	0.19
Eu_{SN}	0.37	1.12	0.64	0.14	0.10	0.16	0.29
Gd_{SN}	0.40	1.28	1.02	0.15	0.09	0.15	0.27
Tb_{SN}	0.39	1.15	1.05	0.15	0.09	0.13	0.21
Dy_{SN}	0.40	1.09	1.12	0.17	0.08	0.12	0.21
Y_{SN}	0.46	1.43	2.44	0.28	0.10	0.20	0.37
Ho_{SN}	0.45	1.26	1.52	0.23	0.09	0.16	0.27
Er_{SN}	0.43	1.13	1.37	0.24	0.08	0.15	0.25
Tm_{SN}	0.38	0.94	1.08	0.22	0.07	0.12	0.19
Yb_{SN}	0.40	0.93	0.98	0.21	0.08	0.11	0.16
Lu_{SN}	0.35	0.83	0.94	0.20	0.07	0.10	0.13
$(La/Nd)_{SN}$	1.00	0.96	0.85	0.76	0.89	1.27	1.32
$(La/Yb)_{SN}$	0.47	0.74	0.23	0.21	0.49	1.25	1.43
$(La/Sm)_{SN}$	0.70	0.80	0.53	0.50	0.58	1.25	1.25
$(Gd/Yb)_{SN}$	0.99	1.37	1.04	0.70	1.15	1.34	1.64
$(Pr/Yb)_{SN}$	0.42	0.65	0.22	0.23	0.46	0.96	0.99
$(Nd/Yb)_{SN}$	0.47	0.77	0.27	0.28	0.55	0.99	1.08
$(Eu/Sm)_{SN}$	1.38	1.31	1.53	1.57	1.55	1.38	1.55
Eu/Eu*	1.13	1.07	0.98	1.23	1.34	1.19	1.30
La/La*	1.41	1.72	1.75	1.69	1.82	1.38	1.78
Ce/Ce*	0.75	0.75	0.90	0.89	0.88	0.70	0.84
Gd/Gd*	1.03	1.07	1.04	1.05	0.95	1.08	1.3201
Y/Y*	1.09	1.22	1.86	1.39	1.18	1.39	1.54
Pr/Pr*	1.06	1.02	0.94	0.96	0.94	1.09	0.95
Y/Ho	26.59	29.40	41.51	30.57	28.92	31.76	35.91
Y/Zr	13.44	19.90	53.45	4.03	3.08	2.91	7.69
Zr/Hf	11.38	8.94	6.95	13.26	23.38	11.99	12.68

$ Major elements in oxide wt.%, trace elements in PPM; total Fe as $FeO^{(T)}$; <, below detection. All the trace and rare earth element analyses were performed by ICP-MS. The subscript SN refers to the NASC (Gromet et al., 1984) normalized values; Eu/Eu*, La/La*, Ce/Ce*, Gd/Gd*, Y/Y*, Pr/Pr* are calculated after Bolhar et al., (2004).

6.2.3 Rare earth elements and Nd isotopes

The rare earth element contents are variable in Morar BIFs. Total REE contents show a range of variation from 7.63 ppm to 114.83 ppm. The mineralogical control of REE in these BIFs is difficult to evaluate because of limited amount of data. Nevertheless, total REE content is positively correlated with Fe (r=0.5), Mn (r=0.93), Sc (r=0.71), V (r=0.73) and Co (r=0.70) and all these elements are mutually correlated, thus indicating that these elements are locked in hematite. This is consistent with their mineralogical composition. The abnormally high REE content of the sample SNS-3 (ΣREE=114.83 ppm) corresponds with relatively high P_2O_5 concentration (0.08%), which may be controlled by phosphatic phase. Two different types of REE pattern has been observed (Fig.6.3 & 6.4) Five samples exhibit parallel patterns (Fig.6.3) with HREE enrichment and LREE depletion. NASC normalized (Gromet et al., 1984) $(Nd/Yb)_{SN}$ ratios vary from 0.280 to 0.767. These REE patterns resembles with modern sea water (Goldstein and Jacobsen,1988b; Alibo and Nozaki, 1998), except Ce and Eu anomalies (Fig.6.3). The rest two samples STL-1 and MHS-1 show flat patterns $\{(La/Yb)_{SN} \sim 1.25\text{-}1.43\}$ and are devoid of HREE enrichment $\{(Nd/Yb)_{SN} \sim 0.98\text{-}1.08\}$. This pattern is identical with the pattern of coeval clastic rocks (Fig.6.4). These two samples also contain relatively higher Rb, Sr and Cs contents, indicating clastic flux that may be controlling REE pattern. All the samples exhibit mild positive (Eu/Eu* = 1.13-1.33) to no (Eu/Eu* = 0.98-1.06) europium anomalies and moderate negative Ce anomalies (Ce/Ce*=0.70-0.90) in a NASC normalized REE+Y spider gram (Fig.6.3 and 6.4). The REE patterns are grossly similar to those of late Paleoproterozoic Gunflint and Sokoman BIF of Canada (Jacobsen and Pimentel-Klose 1988a, Derry and Jacobsen 1990). The above all features are consistent with the derivation of the REEs from continental source similar to present day sea water.

The Nd isotopes data of five BIF sub samples are listed in table 6.2 and are plotted in Fig.6.5. The samples of Morar BIF yield εNd value at 1.9 Ga between –6.29 to –13.68. The model ages are not calculated as $^{147}Sm/^{144}Nd$ ratios are more than 0.14 in all the samples. The εNd data of these BIFs indicate derivation of their Nd from very old crustal sources.

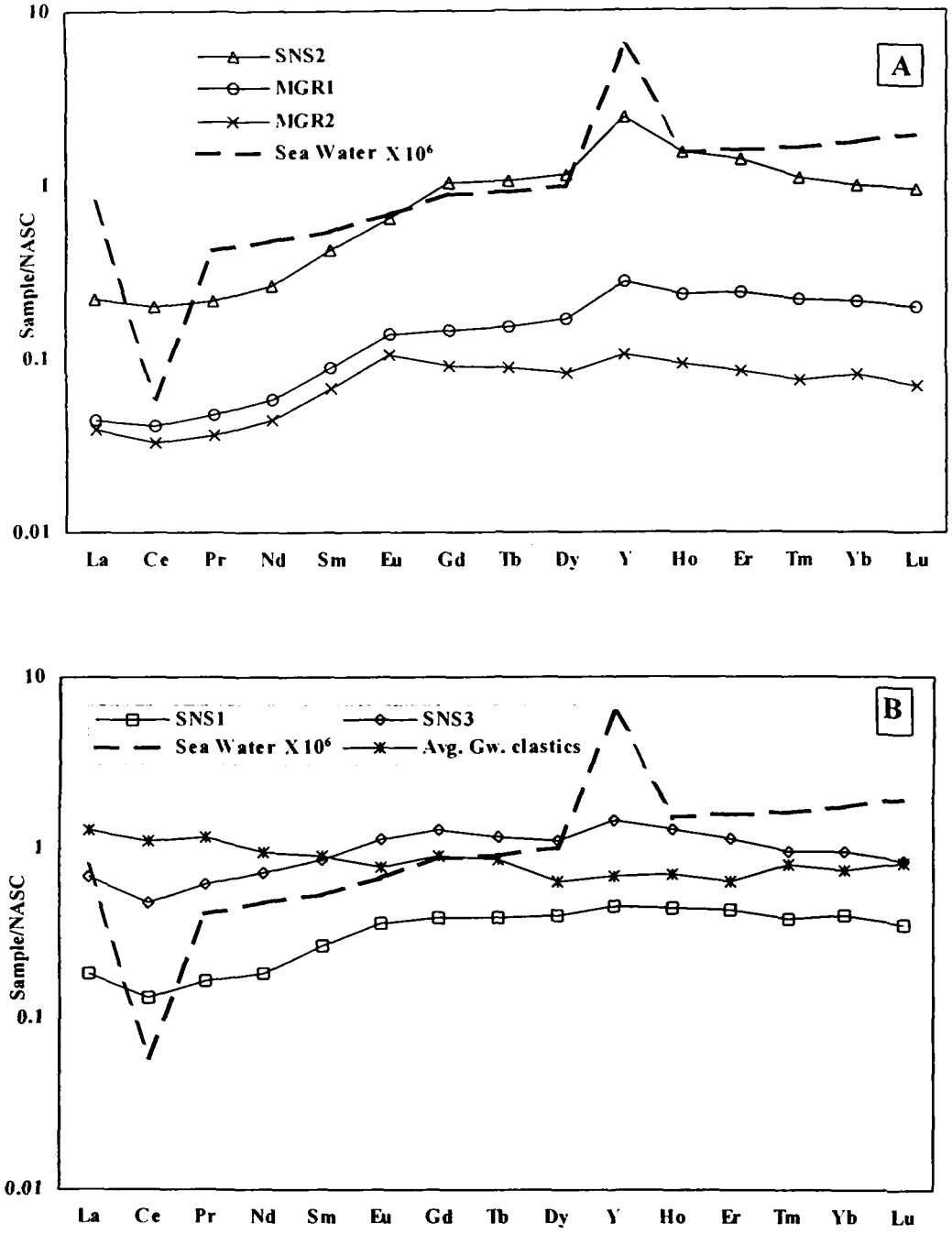

Fig 6.3: NASC normalized REE+Y spidergram of some BIF samples of Gwalior Group. The BIFs show similar HREE enriched pattern to that of sea water (North Pacific deep sea water, Alibo and Nozaki, 1988), except positive Eu anomalies and less magnitude negative Ce anomalies.

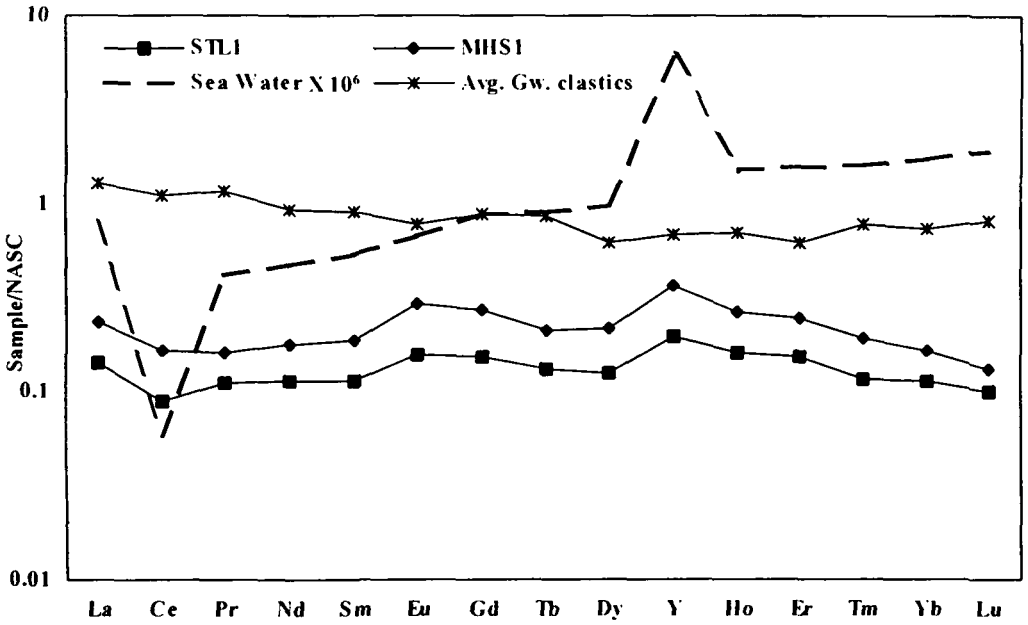

Fig.6.4: NASC normalized REE+Y spidergram of some BIF samples of Gwalior Group. The patterns are sub-parallel to the coeval clastic rocks, indicating control of particulate and colloidal pools over REE composition in these samples.

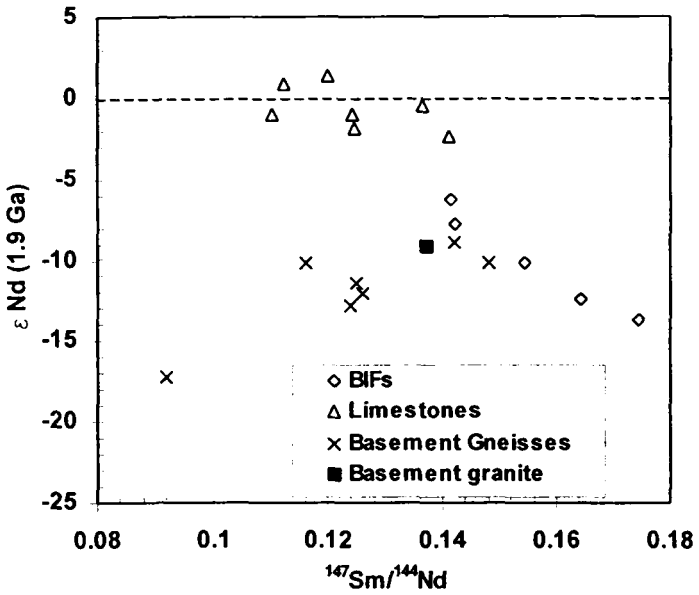

Fig.6.5: Plot of εNd (1.9 Ga) vs. $^{147}Sm/^{144}Nd$ for the BIFs of Gwalior Group, also plotted in the diagram are the data of basement granites, gneisses and coeval limestones. The plot demonstrates the influence of basement chemistry over Nd isotope compositions of the BIFs. The limestones show significantly more radiogenic εNd at 1.9 Ga indicating juvenile inputs from depleted mantle. The differences in Nd isotope compositions of BIFs and carbonates exist, because they are not strictly contemporaneous. Pb-Pb data indicates the limestones were deposited 64 Ma before the deposition of BIFs.

Table-6.2: Sm-Nd isotope data of BIFs from Sonsa and Mangora area

Sample No	Sm ppm	Nd ppm	$^{147}Sm/^{144}Nd$	$^{143}Nd/^{144}Nd$	εNd at 1.9 Ga
SNS-1 A	1.315	5.17	0.1547	0.511607	
SNS-1 B	1.32	5.189	0.1542	0.511572	
SNS-1 Avg.	**1.317**	**5.179**	**0.1545**	**0.511589**	**-10.21**
SNS-2 A	2.336	8.687	0.1638		
SNS-2 B	2.332	8.63	0.1644	0.511596	-12.41
SNS-2 Avg.	**2.334**	**8.658**	**0.1641**		
SNS-3 A	3.902	16.72	0.1417	0.511559	
SNS-3 B	3.863	16.53	0.1423	0.511547	
SNS-3 Avg.	**3.883**	**16.63**	**0.142**	**0.511553**	-7.89
MGR-1	1.265	5.44	0.1415	0.511627	-6.32
MGR-2 A	0.182	0.6367	0.1736	0.51166	-13.64
MGR-2 B	0.181	0.63	0.175		
MGR-2 Avg.	**0.1815**	**0.6334**	**0.1743**		
Errors (2σ)	1%	1%	1%	0.01%	

6.3 Discussion:

6.3.1 Sources of REE and Fe

Since BIFs of Precambrian age contain a large quantity of Fe, the source should be able to provide this vast amount of iron. Different sources of iron in BIFs have been proposed; e.g. (a) Fe carried in solutions by rivers into the ocean (Garrels 1987), (b) Fe leached from suspended load of rivers after deposition in the deeper, more reducing portion of the ocean (Holland 1984) and (c) volcanic- exhalations from mid oceanic ridges (Derry and Jacobsen 1990). In all these studies (e.g. Miller and O'nions, 1985; Derry and Jacobsen, 1990; Jacobsen and Pimentel-Klose, 1988a, b; Shimizu et al., 1990; Denielson et al., 1992; Alibert and McCulloch 1993; Bau and Möller, 1993; Bau et al., 1997; Khan et al., 1996; Frei et al., 1999) the REE patterns and Nd-isotope systematics are used extensively to trace the source of REEs and by analogy the sources of Fe in Precambrian BIFs, as they represent most robust tracers.

As discussed in the previous section two distinct types of REE pattern have been found in Gwalior Group BIFs (Fig. 6.3 & 6.4). In these REE+Y spidergram also plotted the data of modern seawater from Pacific Ocean (Alibo and Nozaki, 1988) and average data of coeval clastic rock of Gwalior Group as discussed in the previous chapter. Five samples show sub-parallel REE patterns (Fig.6.3) with variable REE content, with prominent HREE enrichment, small negative Ce anomalies and mild positive to no europium anomalies (Fig.6.3). The overall patterns are remarkably similar to modern day seawater (Alibo and Nozaki, 1988; Goldstein and Jacobsen 1988b). The $(Nd/Yb)_{SN}$ ratios in these samples vary from 0.267 to 0.767. This appears

to be result of REE speciation which is dominated by $REECO_3^+$ and $REE(CO_3)_2^-$ (Bryne et al., 1988; Bau and Möller 1993). Due to higher stability of HREE in carbonate complexes (Centrel and Bryne 1987) free LREEs are available for sorption onto the suspended particles. Hence $[CO_3^{2-}]$ is the major parameters which control $(Nd/Yb)_{SN}$ ratio in recent sea water. The same mechanism control REE behavior in rivers (Goldstein and Jacobsen, 1988a; Elderfield et al., 1990) and lake waters (Fee et al., 1992), as well as in the deep oceans (Piepgras and Jacobsen, 1987; Piepgras and Wassserburg, 1980). The REEs are distributed amongst three pools; termed as particulate, colloidal and dissolved pool (Elderfield et al., 1990). Mixing of river water and seawater in estuaries results in coagulation and sedimentation of the REEs related to first two pools and only the dissolved REEs, after loosing most of the LREEs in estuaries reach the open ocean. Thus, decreasing $(Nd/Yb)_{SN}$ ratio indicates near pure chemical precipitate from sea water, and increasing $(Nd/Yb)_{SN}$ ratio (≥ 1) indicate increased tapping of particulate and colloidal pools and possible clastic contamination. Such mechanisms account for the REE patterns of two samples i.e. STL-1 and MHS-1 (Fig.6.4). These samples show flat pattern and parallel to coeval clastic rocks thus indicating that the clastic particulates governed the REE patterns of these samples. This is further corroborated by slightly higher Rb, Sr and Cs content in these samples. The REE pattern of previously described five samples (Fig.6.3) are grossly identical to that of present sea water and rest two (Fig.6.4) as discussed above are identical to coeval clastic rocks. These REE patterns are consistent with dominant supply of REE from continent, both as dissolved load and as particulate-colloidal load. However, mild positive Eu anomaly in NASC normalized pattern could be suggestive of a hydrothermal source also (Michard et al., 1983; Klinkhammer et al., 1983, 1994). Since Gd, the neighboring element of Eu is itself enriched in sea water; the Eu/Eu* index may fail to recognize the anomalous Eu behavior (Bolhar et al., 2004) and in that case the $(Eu/Sm)_{SN}$ ratio can be used for deducing hydrothermal input (Bau and Möller 1993). Since Sm do not show any anomalous behavior in sea water, the $(Eu/Sm)_{SN}$ ratio greater than one would indicate anomalous Eu addition presumably via hydrothermal input. The BIFs of Gwalior Group exhibit mild positive Eu anomaly (Eu/Eu*~ 1.13-1.33) to no Eu anomaly (Eu/Eu*~ 0.98-1.07), while the $(Eu/Sm)_{SN}$ ratios ranges from 1.30-1.57. The $(Eu/Sm)_{SN}$ ratios greater than one and positive Eu anomalies indicate hydrothermal flux in REE budget as well. It has been suggested that the magnitude of positive Eu anomaly is dependent on the thermal

history of the earth, as a result it is much lesser in Proterozoic BIFs compare to their Archean counterparts, because low temperature hydrothermal alteration of ocean floor became important during Proterozoic (Danielson et al., 1992). In the ΣREE vs. (Cu+Co+Ni) plot (Fig.6.6, after Klein and Beukes 1992b) the BIFs of Gwalior Group falls in the field of hydrothermal deposit or near to it, indicating partly hydrothermal derivation of transition elements and REE, thus corroborate the inference based on positive europium anomaly and $(Eu/Sm)_{SN}$ ratios.

The REE source can be further evaluated by Nd-isotopic results (Table 6.2). The εNd value calculated at 1.9 Ga (depositional age of Gwalior Group) show strong continent like negative values and varies from –6.29 to –13.68 (Fig.6.5). The wide range of εNd values (–6.29 - –13.68) are either due to initial isotopic inhomogenity or post depositional disturbances. Such wide variations of εNd are observed for Archean Isua BIFs. Since Gwalior Group of rocks are unmetamorphosed, post depositional disturbances are ruled out. Genetically related samples SNS-1,2,3 and MGR-1,2 also exhibit wide range of εNd within themselves indicating isotopic heterogeneity. The data indicate very old crustal source of Nd, that is unusual when compared to Archean and early Paleoproterozoic BIFs which shows typical mantle like Nd-isotopic signatures. Similar types of high negative □Nd values were obtained by Miller and O'nions (1985) in mid-Archean (3.7 Ga) Isua BIFs. They attributed this feature as a result of disturbance of Sm-Nd systematics due to high grade (upper amphibolite facies) metamorphism. Since Gwalior Group sediments are completely unmetamorphosed, resetting of Sm-Nd systematics is unlikely and Nd-isotopic results probably show source characteristics. The very high negative εNd value can be generated from post depositional crustal fluid activity. Since most natural fluids have very low abundances of REE, a very high fluid to rock ratio is required to alter the REE pattern of chemically precipitated rocks (Banner and Hanson, 1990; Qing and Mountjoy, 1994; Zachariah et al., 1999). Crustal fluid has LREE enriched fractionated REE pattern in contrast to that of LREE depleted, HREE enriched patterns of chemical precipitate like BIF. The mixing of crustal fluid in appreciable quantity will alter the REE patterns, which can not be applied in the present case as the Gwalior BIF still preserve typical chemical sediment like REE patterns and Y/Ho ratios. Although post depositional potash metasomatism occurred in Gwalior sediments as discussed in chapter 4, fluid infiltration in hematite and quartz crystals are unrealistic.

Such a process would also increase the concentrations of Rb, Sr, Ba and K, which is not observed in these samples. The Nd isotope data may, therefore appear to be original in nature and can be used to place constraints on the provenance of REE in BIFs. Nevertheless, the possibility of Nd-isotopic signatures being source derived has to be further evaluated. Based on paleocurrent indicators(Chapter II) and associated clastic sediment geochemistry (Chapter IV), the sediments of Gwalior Group are considered to have been derived from the Bundelkhand massif which lies south of Gwalior basin. The Bundelkhand cratonic block predominantly consists of high K granite (2.5 Ga) with an older 3.3 Ga TTG component and subordinate mafic and metasedimentary rocks (Mondal et al., 2002). The Sm-Nd data of 2.5 Ga granites of Bundelkhand massif (Unpublished data of Atomic Minerals Directorate) yield εNd value of –8.75 at 1.9 Ga. The Sm-Nd isotope data of TTG components (Sharma and Rahman 1996, Mondal et al 2002) of Bundelkhand craton are not available. However similar type of rock in Banded Gneissic Complex (BGC) of Aravalli cratonic block has been dated at 3.3 Ga by Sm-Nd method (Gopalan et al., 1990). It has been suggested (Naqvi and Rogers, 1987; Sharma, 1998; Sharma and Rahman, 2000; Mondal et al., 2002) that both BGGC of Bundelkhand protocontinent and BGC of Aravalli protocontinent evolved together till Paleoproterozoic and represent a single continental mass. If this is true, the Sm-Nd data of 3.3 Ga old BGC gneisses (Gopalan et al., 1990) of Aravalli terrain would provide valid estimate for Nd – isotopic evolution of sediments derived from Bundelkhand block. When Nd-isotopic data of 3.3 old BGC gneisses are taken into consideration, they yield εNd value of order –13 at 1.9 Ga (Fig.6.5). Thus mixture of Nd from 2.5 Ga granites and 3.3 Ga gneisses explain the εNd (1.9 Ga) variability of the present data set. The εNd (1.9 Ga) vs. $^{147}Sm/^{144}Nd$ plot (Fig.6.5) clearly demonstrate the control of basement granites and gneisses for the Nd isotope compositions of BIFs. The geochemistry of coeval clastic rock sedimentary rock also indicates 40% granite, 40% Archean TTG and 20% mafic rocks as the source component for these sediments (Chapter IV). This is consistent with present εNd dataset of BIFs which also indicate an Archean crustal source component for part of the Nd. The εNd data and REE patterns together indicate dominantly crustal source for Nd and other REEs. Similar observation was made by Miller and O'nion (1985) in the studies of Isua BIFs. These authors concluded that, in all post Archean BIFs the Nd could have been derived from an

analogue of modern seawater, dominated by Nd budget typical of average exposed continental crust of that time. Sr and Pb isotopic results also support the evidence of crustal influences as discussed in the next chapter. The initial $^{87}Sr/^{86}Sr$ ratio (Sr_i) calculated at time of deposition are highly radiogenic (0.71348-0.72576) and are much higher than contemporary seawater (0.705, Shields and Veizer, 2002). The model μ_1 ($^{238}U/^{204}Pb$) values are also higher (~8.50) indicating crustal influences. The continental signatures of Nd isotopes are also supported by field evidence. The ridges of quartz reefs and Archean quartzites occur as basement highs and are sometime projected over Morar Formation BIFs, even transgressed sea could not fully cover these basement irregularities during Morar sedimentation. Therefore, indicating shallow nature of the sea and thus crustal overprint in such setting is obvious.

The results of this investigation directly address the source of Nd in BIF and demonstrate the importance of continental sources of Nd in ocean during late Paleoproterozoic. By analogy, Fe could also have been transported from continent. As discussed earlier, Fe can be carried in solution by rivers into the ocean, or Fe can be leached from suspended load (sediment) in deeper reducing part of the basin. The present day Fe in river fluxes are mostly removed in estuaries as they are transported as particulate ferric oxide materials in oxygenated environments (Martin et al., 1976; Goldstein and Jacobsen 1988a,b,c; Jacobsen and Pimentel-Klose 1988). It is suggested that atmospheric oxygen grew from <1 to ~15% of the present atmosphere level (PAL) of oxygen between 2200 and 1900 Ma. (for e.g. Holland et al., 1989; Holland and Beukes, 1990; Sarangi et al., 2004). The oxygenation of atmosphere during the Paleoproterozoic period is evidenced by negative Ce anomalies in Gwalior BIFs and highly ferruginised nature of coeval clastic shore line facies. Thus possibility of transportation of Fe as dissolved load in the continental river water can be ruled out.. The leaching of Fe from suspended load in more reducing condition in deeper part of the basin can also be a viable source (Holland 1984). The occurrence of euxinic black shales in deeper water outer shelf facies in Gwalior basin, adds such a possibility. These sediments represent starved clastic flux rich in carbonaceous matter; as expected in a transgressive shelf facies where most of the suspended load and sand sized grains are removed by shore line wave related processes, and only a fraction of particulate/suspended load cross the littoral energy fence and enters the deeper ocean. Since the source rock for these sediments itself are Fe-poor felsic rocks,

it is difficult to produce huge amount of Fe required to precipitate as BIF. As stated by Jacobsen and Pimentel-klose (1988a) only 10% suspended load reach the deeper ocean and 10% of Fe of these sediment are leached away, giving rise only 1% leaching efficiency, which is unable to account for huge Fe source needed for BIF production. The mass balance considerations of Fe in these BIFs require a different source other than discussed above. The Fe/Nd ratio in continental crust is ~1.5 X 10^3, in river water the ratio ranges from 10^3 to 10^4, whereas the Fe/Nd ratio for Gwalior BIFs is about 10^5. Submarine hydrothermal vent water have similar Fe/Nd ratio (10^5 - 10^6). The mass balance consideration implies that submarine hydrothermal waters are a possible source for Fe budget in these BIFs, along with continental budget. The different sources of Fe and Nd are speculative (Veizer 1983), but required to explain the present field geological setting and mass balance consideration of Fe, as basement comprising of 80% felsic rock and can not yield the Fe required for BIF production. The sudden facies change from shoreline clastic facies to chemical precipitation of BIF will require a sudden sea level rise and subsidence of basin related to tectonic activity. This sedimentary facies gradation can best be explained by rift activation and expansion of basin. If this inference is correct, Fe influx from hydrothermal fissures can be a possible source of Fe in these BIFs. But in absence of other supporting geochemical data, it is only speculative. It is proposed that Nd budget was dominated by continental source and entered into the basin by riverine dissolved flux, whereas the Fe was derived from hydrothermal fissures/vents and leaching of Fe from sediments in reduced deeper part of the basin. The upwelling of these Fe-rich solutions through the chemocline and thermocline gave rise to precipitation of Fe bands. Oxygenated surface layer of seawater was completely buffered with continents in terms of REE systematics. Since the surface run off water drained through the felsic terrain and contained higher REE, the mixing of these waters with fluids from juvenile source with low Nd resulted in continent like REE patterns and the juvenile mantle like signature can be completely masked. Such process can explain the divergence of geochemical data and field geological setting, as is the present case. A hydrothermal component in these BIF is also indicated by mild positive europium anomaly (Fig.6.3 & 6.4), $(Eu/Sm)_{SN}$ ratios (>1) and in LREE vs. (Cu+Co+Ni) plot (Fig.6.6). Some of the Gwalior Group BIF samples yield εNd values (e.g. -6.29 to -7.86) that are 2 to 3 epsilon unit higher than εNd values of youngest basement phase

(-8.75 for 2.5 Ga granites) calculated at the time of deposition of sediments. These features also support the hydrothermal input to the sea water. The idea of different source for Fe and Si was invoked by Hamade et al., (2003) for Hammersely BIFs. Miller and O'nion (1985) also acknowledged the possibility of different sources of Fe and Nd in BIFs. The possible mechanisms of BIF generation are diagrammatically explained in a cartoon (Fig. 6.7) which invoke different source for REE and Fe. A stable continental shelf with density stratified ocean system is envisaged for the deposition of these BIFs. In this model, the surface waters were some what oxic and buffered with continent in terms of REE systematics and the trace elemental and isotopic signatures were governed by continent derived alluvial flux. The deeper water received Fe inputs from hydrothermal exhalations through volcanic fissures. The Fe sources were also probably augmented via leaching of reduced carbonaceous sediments. Strongly reduced deeper waters were buffered with mantle in terms of trace element, REE and isotopic systematics. A low temperature hydrothermal component is favoured as these BIFs lack strong positive Eu anomalies and are characterized by only mild positive anomalies (Danielson et al., 1992). The mixing of Fe rich anoxic bottom water and oxic surface water through the chemocline gave rise the precipitation of BIFs. The oxidized surface water mainly governed the REE and Nd isotopic systematics because of higher REE contents in continent derived run off water.

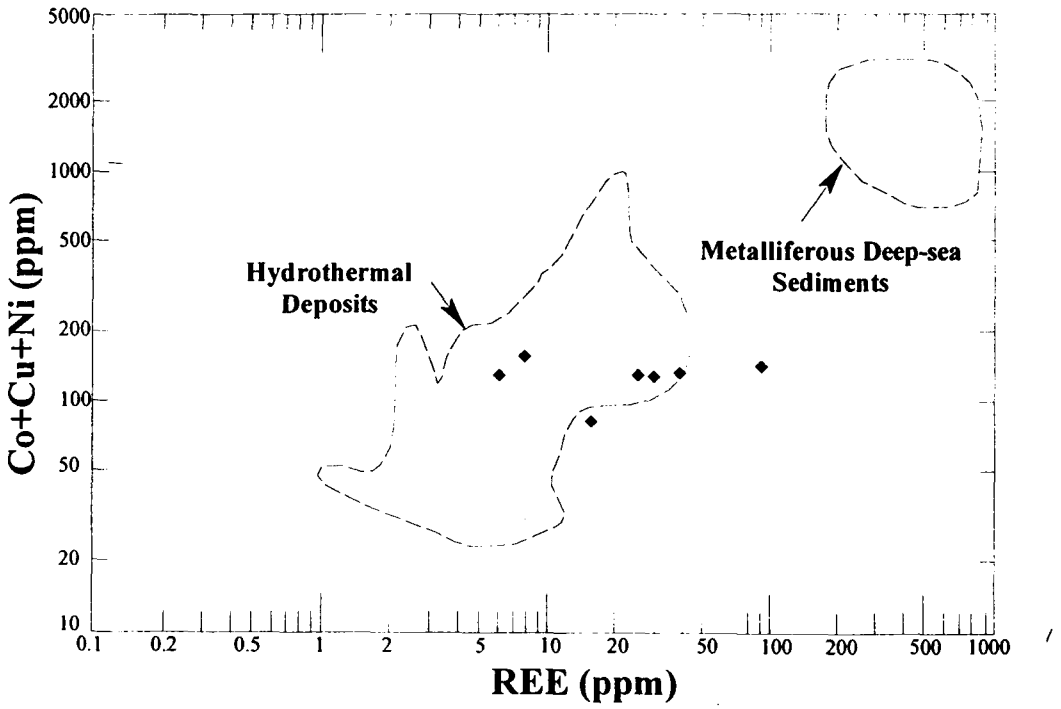

Fig 6.6: The total REE vs. Co+Cu+Ni plot, demonstrating hydrothermal origin of Gwalior BIFs. The data plots in the field of hydrothermal deposits (after Klein and Beukes 1992a)

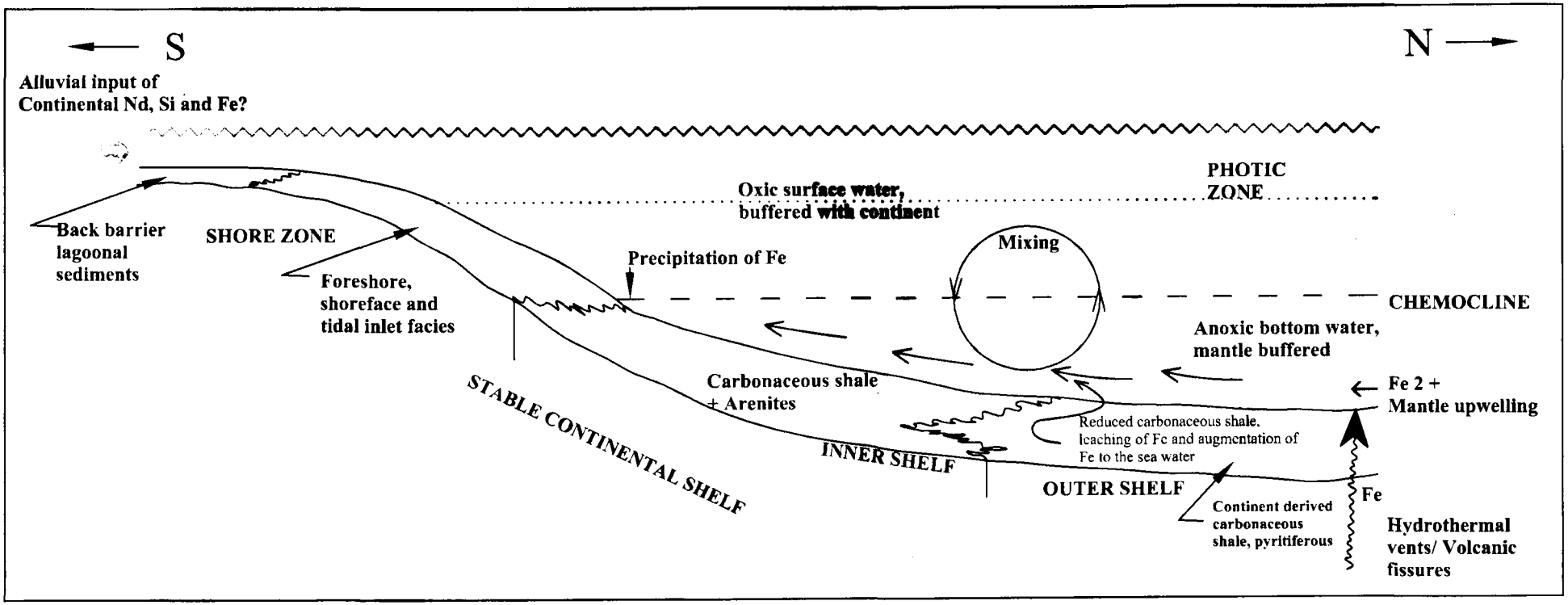

Fig. 6.7: Schematic model for the deposition of banded iron-formation (BIF) Gwalior Group. The BIFs were deposited on a stable continental shelf with permanently density-stratified ocean system, also shown in the diagram are the associated lithofacies.

6.3.2 Implications for chemical evolution of seawater:

The REE+Y systematics of marine chemical precipitates provide strong proxy to that of sea water. The modern sea water are characterized by (i) negative Ce anomalies, (ii) positive La anomalies, (iii) positive Gd anomalies, (iv) positive Y anomalies, and (v) LREE and MREE depletion relative to HREE in shale normalized REE+Y diagram. (Bau and Dulski 1996; Bolhar et al., 2004). The negative Ce anomalies resulted due to oxidation of trivalent Ce to less soluble tetravalent Ce and subsequent removal through scavenging by suspended particles that settles through the water column (Sholkovitz et al., 1994). The relative deficiency of Ce to neighbouring REE is one of the most characteristic feature of modern sea water and indicative of oxidation states (German et al., 1995). Negative Ce anomaly (Ce/Ce* ranges from 0.70 to 0.90) as displayed by Gwalior Group BIFs is also reported for other Proterozoic BIFs (for e.g. Klein and Beukes, 1989). This implies that similar processes were operative during late Paleoproterozoic and would require moderately oxidizing conditions in Proterozoic seas. It is speculated that small negative Ce anomalies, as displayed by late Paleoproterozoic Gwalior Group BIFs, indicate the beginning of a global oxidative process which was considerably less efficient than modern ocean. Interestingly, modern anoxic basins like black sea (German et al., 1991) and Saanich outlet, British Columbia (German and Elderfield, 1989) show considerably less magnitude of negative Ce anomalies than open ocean (Fig.1 of Bolhar et al., 2004). The Archean BIFs do not show such significant anomalous Ce behavior (Fryer, 1983). An equally important feature of modern sea water is La spiking. The elevated La concentration reflects enhanced stability of La in solutions compared to other LREE but similar to HREE and Y. The Gwalior BIFs show strong positive La anomaly and La/La* (calculated after Bolhar et al., 2004) varies from 1.38 to 1.82. The La/La* vs. Ce/Ce* plot (Fig.6.8A) and Ce/Ce* vs. Pr/Pr* plot (Fig.6.8B) demonstrate the presence of negative Ce anomaly and positive La anomaly in these BIFs. Baring one sample (MGR-2), other six samples exhibit positive Gd anomaly (1.03-1.32) similar to that of sea water (De Baar et al., 1985b; Kim et al., 1991). The strong positive Y anomaly and superchondritic Y/Ho ratio are another important features of modern oceans (Bolhar et al., 2004). The Gwalior BIFs are characterized by positive Y anomaly (Y/Y* = 1.08-1.86, Fig. 6.3 & 6.4) and superchondritic Y/Ho ratios (Average 32.09, Fig.6.9). Even the samples (MHS-1, STL-1) with supposed

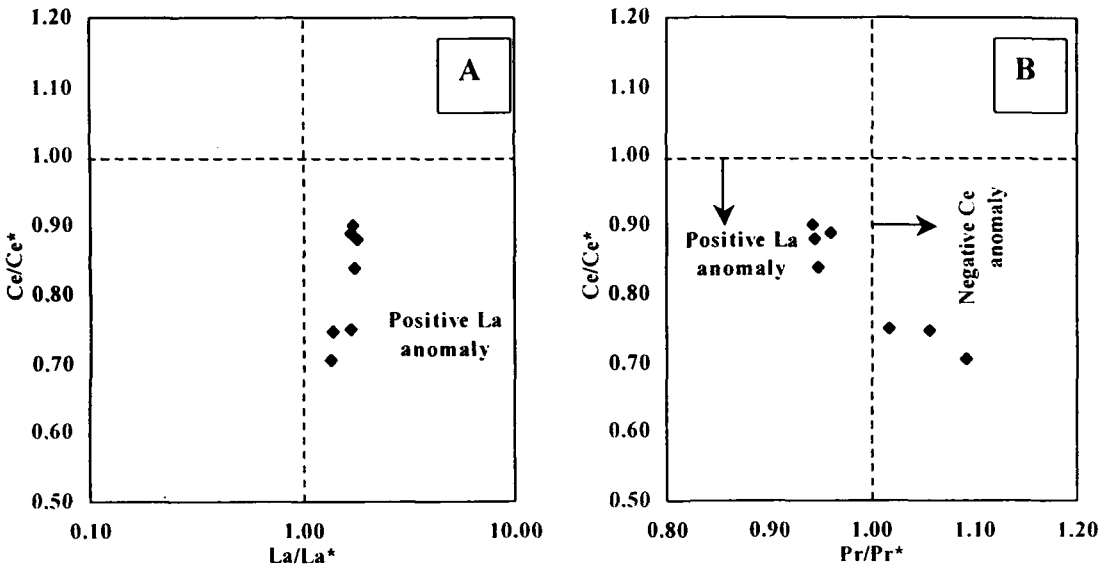

Fig.6.8: Ce/Ce* vs. La/La* (A) and Pr/Pr* (B) plot for the Gwalior Group BIFs. Both the plots demonstrate presence of positive La anomaly and negative Ce anomaly in the Gwalior Group BIFs.

clastic contamination that are devoid of HREE enrichment and characterized by flat patterns, the strong sea water type components like negative Ce anomaly, positive La and Y anomaly, superchondritic Y/Ho ratio (>26) are still preserved. The other five samples exhibit typical sea water like HREE enriched REE patterns (Fig.6.3). These are all consistent with sea water origin of these BIFs which are remarkably similar to modern day sea water. The negative Ce anomaly along with HREE enrichment of Gwalior BIF indicate oxygenated water and the REE abundances appear to be controlled by carbonate complexes possibly in an alkaline pH (Bau and Möller, 1993). The continent like Nd-isotope signature and REE patterns suggest that deposition of BIF took place in an open shelf, where oxygenated surface sea water was completely buffered with continental crust. The absence of high magnitude positive europium anomaly and mantle like εNd in these BIFs suggests that the late Paleoproterozoic sea was not buffered with mantle as is the case of Archean sea (for e.g. Jacobsen and Pimentel-Klose, 1988 a b; Derry and Jacobsen, 1990; Khan et al., 1996). Larger ridge length and higher exit temperature are suggested for generation of Archean BIFs, where Fe was exhalated from Archean mid ocean ridges. Higher heat flow and rapid oceanic crust production in Archean are

consistent with this interpretation. Because of higher ridge lengths and smaller plates in Archeans, the whole sea water was buffered with mantle. In Proterozoic, cratonic tectonics dominated over greenstone tectonics, thus the ocean water acquired continent like signatures. The generation of huge pile of BIFs in late Paleoproterozoic is enigmatic with absence of preserved oceanic crust. Possibly in case of late Paleoproterozoic BIFs, Fe rich hydrothermal solutions were exhalated from fissures produced during subsidence of the basin, some of them were probably extended to the mantle.

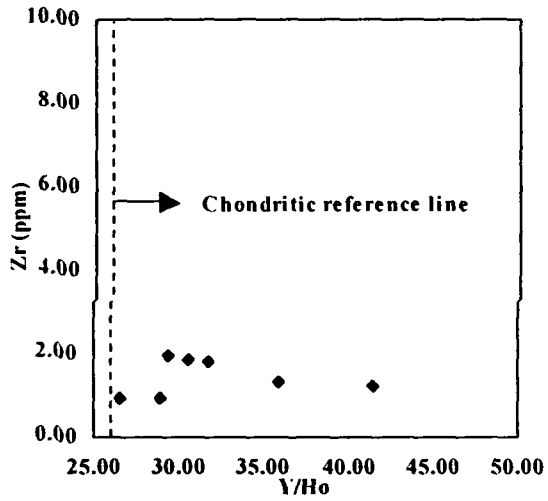

Fig.6.9: Y/Ho vs. Zr plot of BIFs indicating typical marine water like signatures, represented by superchondritic Y/Ho ratios and extremely low zirconium abundances.

CHAPTER-VII

Pb, Sr, Nd isotope systematics of chemical sediments of Morar Formation, Gwalior Group: Implications for age and Provenance

7.1 Introduction:

Direct dating of sedimentary units better constrains the age of sedimentation as compared to dating of associated igneous rocks. As the clastic sedimentary rocks inherit isotopic signals of provenance rocks and are complexly mixed, they do not provide a geochronometer. U-Pb systems of zircon of synsedimentary acid volcaniclastic beds serve as best geochronometer, but are subject to availability. With the advancement of analytical techniques, the chemical precipitates of Precambrian age are progressively more used for dating purpose in recent times (for e.g. Jahn and Cuvellier 1994, Frei et al., 1999) as they constitute important parts of unfossiliferous Precambrian successions. For this purpose, Pb isotope system to date carbonate rocks has been increasingly applied (Babinski et al., 1999, Zachariah et al., 1999; Bolhar et al., 2002; Ray et al 2003; Sarangi et al., 2004) since the pioneering work of Moorbath et al., (1987) who successfully dated Achaean stromatolitic limestone. The only requirement of this method is that the analysed portion should have common initial Pb isotopic composition (for review see Jahn and Cuvellier 1994) which can be met by drawing closely spaced samples from same formation (Ray et al., 2003) or by analyzing sub-samples of single hand-specimen (Zachariah et al., 1999). First direct Pb-Pb dating of randomly collected BIFs from Isua Greenstone belt, West Greenland; was carried out by Moorbath et al., (1973). But recently Pb stepwise leaching (PbSL) method has been adopted (Frei et al 1999, Erel et al 1997), as it offers increasing data spread in uranogenic ($^{207}Pb/^{204}Pb$ vs. $^{206}Pb/^{204}Pb$) and thorogenic ($^{208}Pb/^{204}Pb$ vs. $^{206}Pb/^{204}Pb$) data arrays, and therefore, in principle allows for the calculation of Pb-Pb isochron from phases with less favourable U/Pb concentration ratios. A major advantage of this method is that it can be applied to a single rock-forming mineral, and therefore, does not rely on prerequisite of initial isotopic equilibrium between coexisting phases for dating purpose. It has also been shown to be potentially important to decipher internal mineral complexities and inhomogeneties (such as those introduced by unequilibrated solid inclusions, incomplete metamorphic re-equilibration etc.) by comparing leach data in respectively uranogenic and thorogenic arrays (Nagler et al., 1995a, b, 1996, Frei et al., 1997). In the present study, Pb isotopic study of limestones and BIFs are carried out in an attempt to date the

sedimentation age of Paleoproterozoic intracratonic Gwalior basin, Bundelkhand craton, Central India. In addition to Pb isotopes, Sr and Nd isotope systematics were also analysed to trace the provenance of chemogenic sediments, which would help to constrain the nature of exposed continental crust at the time of their deposition.

7.2 Sample description, Mineral-Textural relationship:

Sampling of carbonate rock for Pb-Pb geochronology is not straightforward; since it is well known that lead isotopic composition (U/Pb ratio) of these can vary on many scales from microscopic to that of many meters. Generally sub-samples from single hand specimen are preferred over widely located samples for constructing an isochron, as widely located hand specimens may introduce variation in initial ratio and thus degrade the isochron. However, this is not always the case and some unit may be isotopically homogenous for many meters; in this case sub-samples may not show sufficient data spread in their U/Pb ratios to define an isochron precisely and also may not have remained close systems due to even weak post depositional remobilization of U and Pb. For this reason, in this study, sampling of different hand specimen from same out crop is preferred in order to maintain homogeneity in initial lead ratios, as well as to get spread in U/Pb ratio for obtaining a meaningful isochron. Ten limestone samples weighing about 8 Kg each were drawn from outcrop near Utila village, central part of Gwalior basin. The limestone unit is 8-10m thick and sandwiched between two successive BIF units of Morar Formation. They constitute sub-horizontal strata, devoid of any tectonic/deformational features. In hand specimen, they look to be unmetamorphosed micritic limestone, within these limestones very thin (few mm thick) shaley layers are observed which probably are of pyroclastic origin. Closely spaced samples were drawn from approximately 200m X 200m area to ensure common initial Pb isotopic composition. Petrographically, the limestone contains equigranular xenotopic mosaic of microsparites; sparry calcite is present as pore filling and as veins sub-parallel to bedding lamination. Quartz and sericite constitute minor accessory minerals. Ilmenite, pyrite, anatase and leucoxenes are found among opaque minerals.

Five BIF sample weighing 5 kg each was collected from central and western part of the basin from the basal Morar BIFs. The samples SNS-1, 2 and 3 are genetically related, stratigraphically corresponds to the top of the above mentioned limestone unit and have been collected from Sonsa area, central part of the basin. The

other two genetically related samples MGR-1 and 2 were drawn from Mangora area, western part of Gwalior basin. These samples are stratigraphically similar to the Sonsa samples. Microscopically, the samples contain alternate Fe rich bands and cryptocrystalline chert bands, while the former being dominant. Fe bands are constituted of hematite and goethite. The megascopic and microscopic features are consistent with their unmetamorphosed nature. The rocks show minor chalcedony veining, thickness varying from 20μm to 1.6mm.

7.3 Results:

7.3.1 Pb isotopes of limestone:

The HCl soluble carbonate fraction Pb-Pb data are presented in the table 7.1, and are graphically illustrated in Fig.7.1. The lead in these samples are moderately radiogenic, showing a small range of variation of $^{206}Pb/^{204}Pb$ from 19.211 to 23.774 and variation of $^{207}Pb/^{204}Pb$ from 15.845 to 16.370. Despite this limited spread, the data defines well-correlated positive array in uranogenic ($^{207}Pb/^{204}Pb$ vs. $^{206}Pb/^{204}Pb$) diagram (Fig.7.1A) while they form scatter in thorogenic ($^{208}Pb/^{204}Pb$ vs. $^{206}Pb/^{204}Pb$) diagram (Fig.7.1B). The linear arrangement of samples in uranogenic diagram indicates that they were compositionally homogeneous. Linear regression of the entire nine samples with a blanket error of 0.1% (2σ) yields an errorchron age of 1926 ± 360 Ma. The mean square of weighted deviates (MSWD) for this regression is of 30, indicating a scatter that is slightly beyond analytical uncertainties. Such high MSWDs are not uncommon in whole-rock Pb measurements of carbonate rocks (Jahn and

Table-7.1: Pb-Pb isotope data of limestones from Utila area

Sample No	$^{206}Pb/^{204}Pb$	$^{207}Pb/^{204}Pb$	$^{208}Pb/^{204}Pb$	$^{207}Pb/^{206}Pb$	$^{208}Pb/^{206}Pb$
UTL1*	20.059	15.893	43.27	0.79215	2.1565
UTL2	19.211	15.845	38.71	0.82506	2.0159
UTL3	23.774	16.37	42.67	0.68869	1.7950
UTL5	22.007	16.182	43.5	0.73348	1.9774
UTL6	20.322	15.957	41.59	0.78532	2.0464
UTL7*	20.443	15.925	44.3	0.77881	2.1666
UTL8*	20.097	15.992	41.35	0.79553	2.0554
UTL9	21.307	16.092	43.04	0.75525	2.0200
UTL10*	21.199	16.033	42.99	0.75617	2.0267
Errors (2σ)	0.001	0.10%	0.20%	0.10%	0.10%

* Samples not considered for isochron calculation.

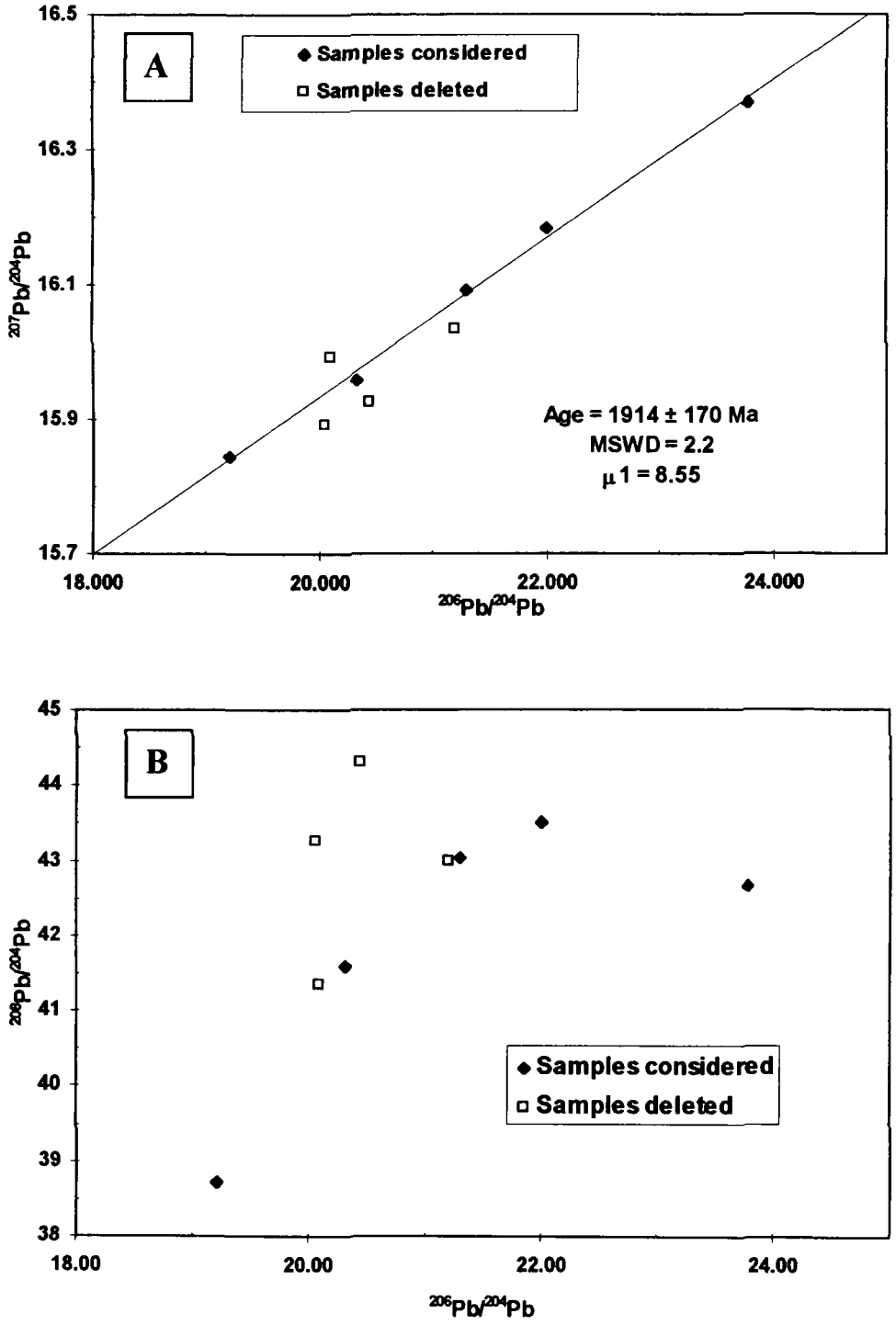

Fig. 7.1: $^{207}Pb/^{204}Pb$ vs. $^{206}Pb/^{204}Pb$ diagram (A) and $^{208}Pb/^{204}Pb$ vs. $^{206}Pb/^{204}Pb$ diagram (B) of HCl leachates of Gwalior limestones. Note scatter of data in thorogenic diagram.

Cuvellier, 1994). Varying amount of Pb and U, incorporated into carbonate minerals (calcite-aragonite) as they precipitate from seawater, show large scatter in Pb-Pb space (Jahn and Cuvellier 1994), which is interpreted as due to inhomogeneous initial Pb isotope composition and/or open system behavior. Deletion of four stray data points, yield better fit and provide a well defined isochron age of 1914 ± 170 Ma with a model μ_1 value of 8.55. The deletion of these data points is justified on two grounds. Firstly, this do not significantly change the slope of the best fit line and at the same time improves the quality of the isochron; the definition of straight line becomes better with mean square of weighted deviates (MSWD) of 2.2. Secondly, the stray data points show strong scatter in thorogenic diagram compare to the other data points (Fig.7.1B), indicating different Th/U ratios in these samples and/or open system behavior. The rest data points conform better to a straight line both in uranogenic as well as thorogenic diagram (Fig.7.1), and presumably refer to the more homogenous portions in initial Pb isotopic compositions. Thus the preferred age of deposition/diagenesis of carbonate rock is 1914 ± 170 Ma. The mean square weighted deviate (MSWD) of this regression is 2.2, indicating that the scattering of data points is mainly due to analytical uncertainties. This implies that outcrop scale volume of carbonate rocks remained closed systems since 1.9 Ga with a common initial lead isotope ratio.

7.3.2 Pb isotopes of BIF:

Bulk Pb and PbSL isotope data from the whole rock samples of Sonsa area (SNS-1, 2, 3) and Mangora (MGR-1, 2) area are listed in table.7.2 and plotted in Figures 7.2 to 7.5. The sequential leaching experiments were carried out in four steps by using 1N HBr acid with different acid volume and time of digestion following Frei et al., (1999) and Erel et al., (1997). In the step A the sample powder was leached with 10 ml of acid for 10 minutes, subsequent steps involved in leaching of the residue material of preceding step with longer leaching interval and lesser volume of acid. The following steps B and C involves in leaching with 7 ml acid for 30 minutes and 5 ml acid for 2 hours respectively. In the step D, the residue was digested by using HF, HNO_3 and HCl. The PbSL data obtained in this study are comparable to sequential leaching results obtained by Erel et al., (1997) on whole rock and magnetite fractions of BIFs of Paleoproterozoic Hammersely Basin, Australia and

Frei et al., (1999) on magnetite fractions of Achaean Isua BIFs. The most radiogenic Pb are leached in first short step and followed by decreasing radiogenic Pb from step to step. This can be explained by partitioning of structurally weakly bound radiogenic Pb from the lattice into the leaching acids which are opposite to the case of silicate minerals (Frei et al., 1999). The data defines linear array in uranogenic diagram (Fig.7.2A-7.5A) for all individual samples, while the thorogenic diagrams (Fig.7.2B-7.5B) show scatter with broad co-linearity.

Table-7.2: Pb-Pb isotope data of BIFs from Sonsa and Mangora area

Sample No	U ppm	Pb ppm	$^{206}Pb/^{204}Pb$	$^{207}Pb/^{204}Pb$	$^{208}Pb/^{204}Pb$
SNS-1 wr[#]	0.566	2.734	18.913	15.989	37.97
SNS-2 wr	1.986	2.704	31.409	17.396	39.2
SNS-2 A[@]			142.71	29.632	38.53
SNS-2 B			91.37	23.94	38.93
SNS-2 C			30.869	17.113	37.49
SNS-2 D			21.399	16.246	39.28
SNS-3 wr	0.859	5.28	19.328	16.087	38.33
SNS-3 A			19.674	16.11	38.51
SNS-3 B			19.143	15.975	38.09
SNS-3 C			18.744	15.943	38.09
SNS-3 D			19.332	16.096	38.41
MGR-1 wr	1.155	5.84	18.948	15.863	37.5
MGR-1 A			20.64	16.053	37.48
MGR-1 B			19.624	15.923	37.32
MGR-1 C			18.669	15.827	37.26
MGR-1 D			18.192	15.736	37.5
MGR-2 wr	0.139	2.145	18.022	15.772	37.05
MGR-2 A			20.24	16.013	38.29
MGR-2 B			19.09	15.877	37.85
MGR-2 C			18.601	15.787	37.36
MGR-2 D			17.367	15.703	36.7
Errors (2σ)	2%	2%	0.20%	0.20%	0.20%

[#] 'wr' refers to the whole rock fraction and [@] 'A-D' refers to the leach fractions in the step A, B, C, D respectively.

The whole rock data of SNS-2 together with three leach and one residual fraction show significant spread in lead-lead space (Fig.7.3). $^{206}Pb/^{204}Pb$ ratios vary from 21.399 to 142.71 while 207Pb/^{204}Pb ratios vary from 16.246 to 29.632. The data from all the fractions conform to straight line in the uranogenic ($^{207}Pb/^{204}Pb$ vs. $^{206}Pb/^{204}Pb$) diagram (Fig.7.3A). The linear regression of these fractions defines an isochron age of 1809 ± 75 Ma with model μ_1 of 8.59 ± 0.48 and MSWD of 31. It is well established that leach fraction represents the most homogenous portion of the

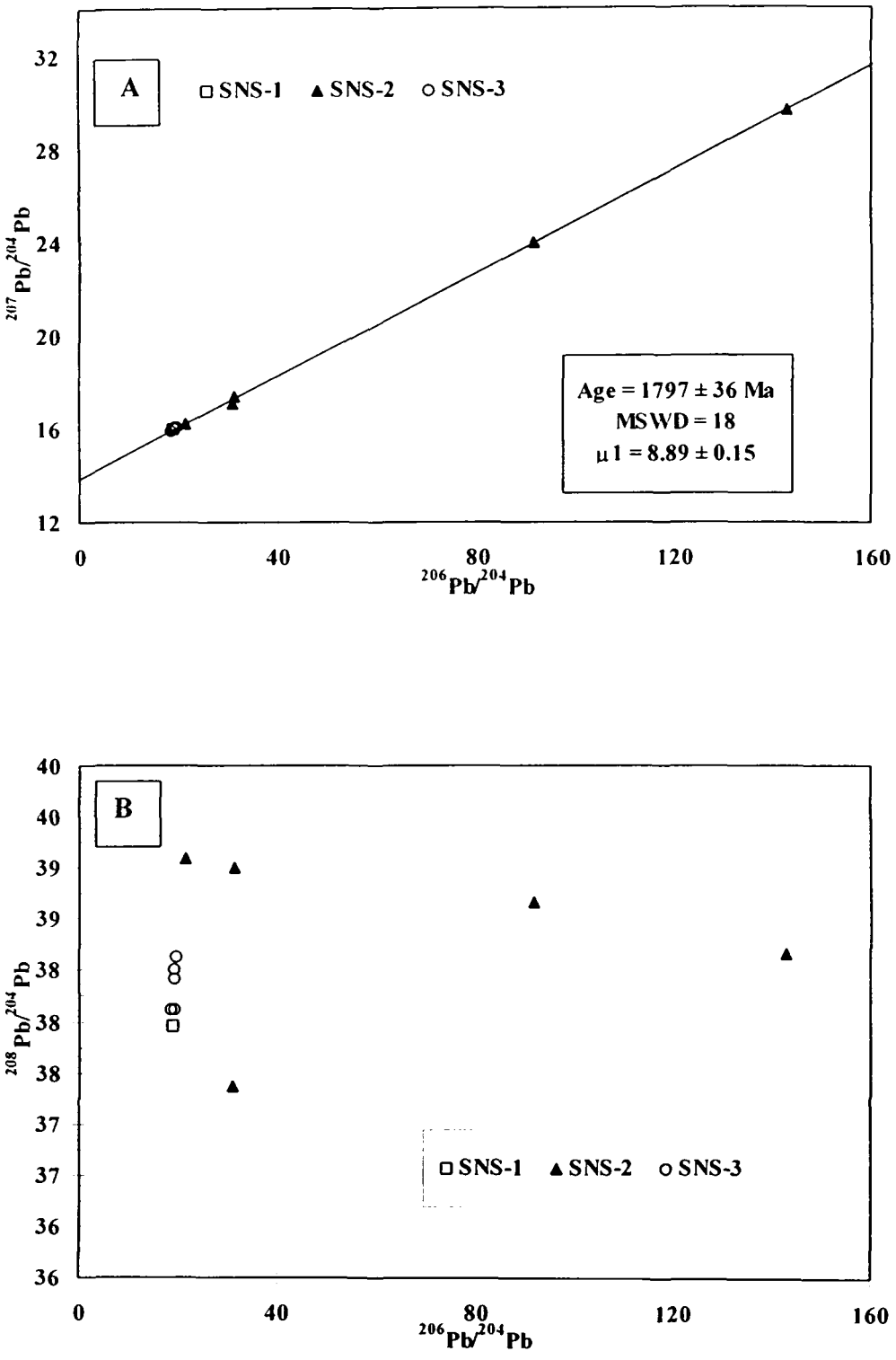

Fig. 7.2: $^{207}Pb/^{204}Pb$ vs. $^{206}Pb/^{204}Pb$ diagram (A) and $^{208}Pb/^{204}Pb$ vs. $^{206}Pb/^{204}Pb$ diagram (B) of various leach and residual portions of some samples of Gwalior BIFs. Note scatter of data in thorogenic diagram (B) for the sample SNS-2.

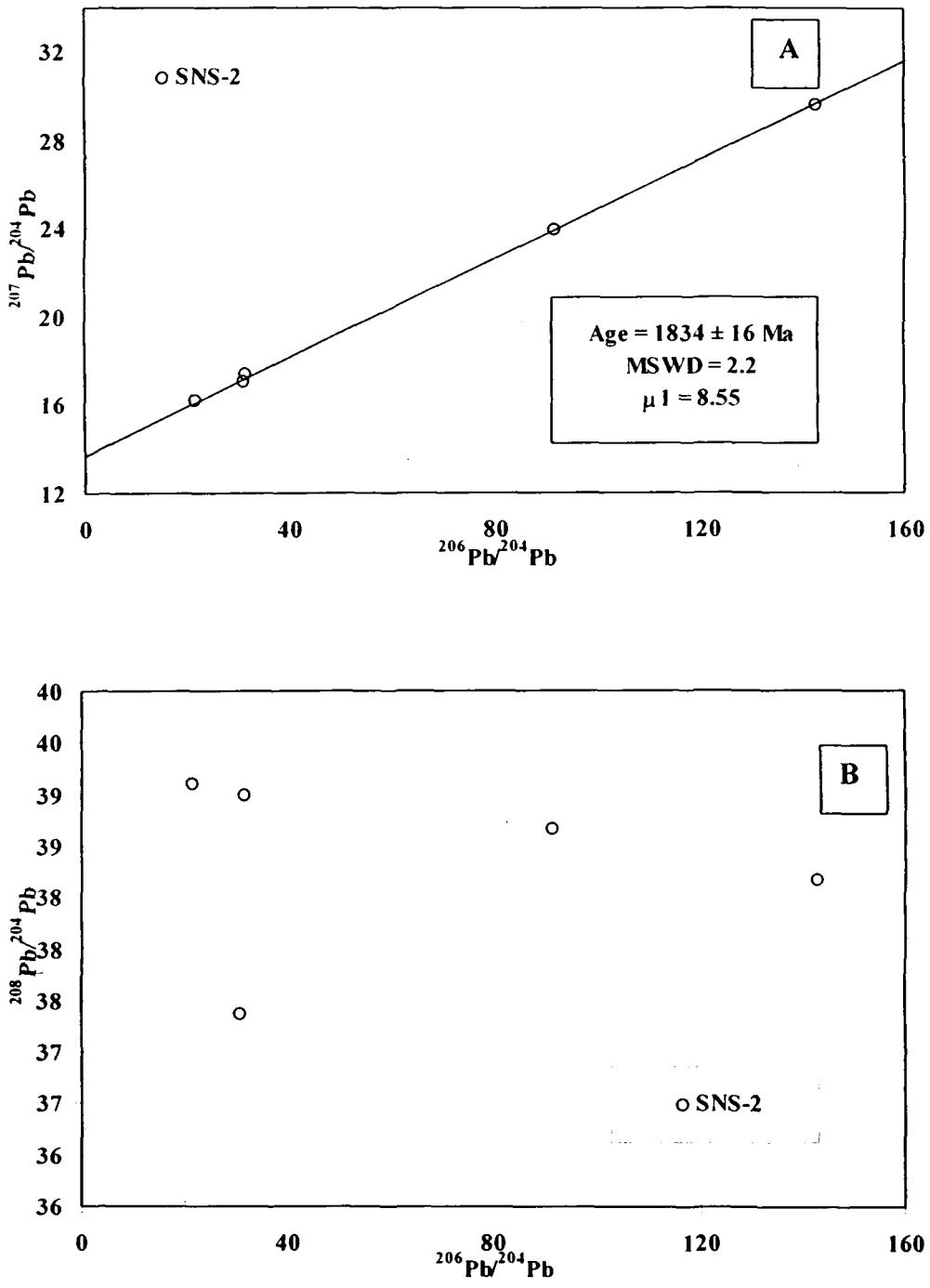

Fig. 7.3: $^{207}Pb/^{204}Pb$ vs. $^{206}Pb/^{204}Pb$ diagram (A) and $^{208}Pb/^{204}Pb$ vs. $^{206}Pb/^{204}Pb$ diagram (B) of various leach and residual portions of BIF sample SNS-2. Note scatter of data in thorogenic diagram. Consideration of three leach fractions define well correlated data array in uranogénic diagram (A) and yields an isochron age of 1834 ± 16 Ma.

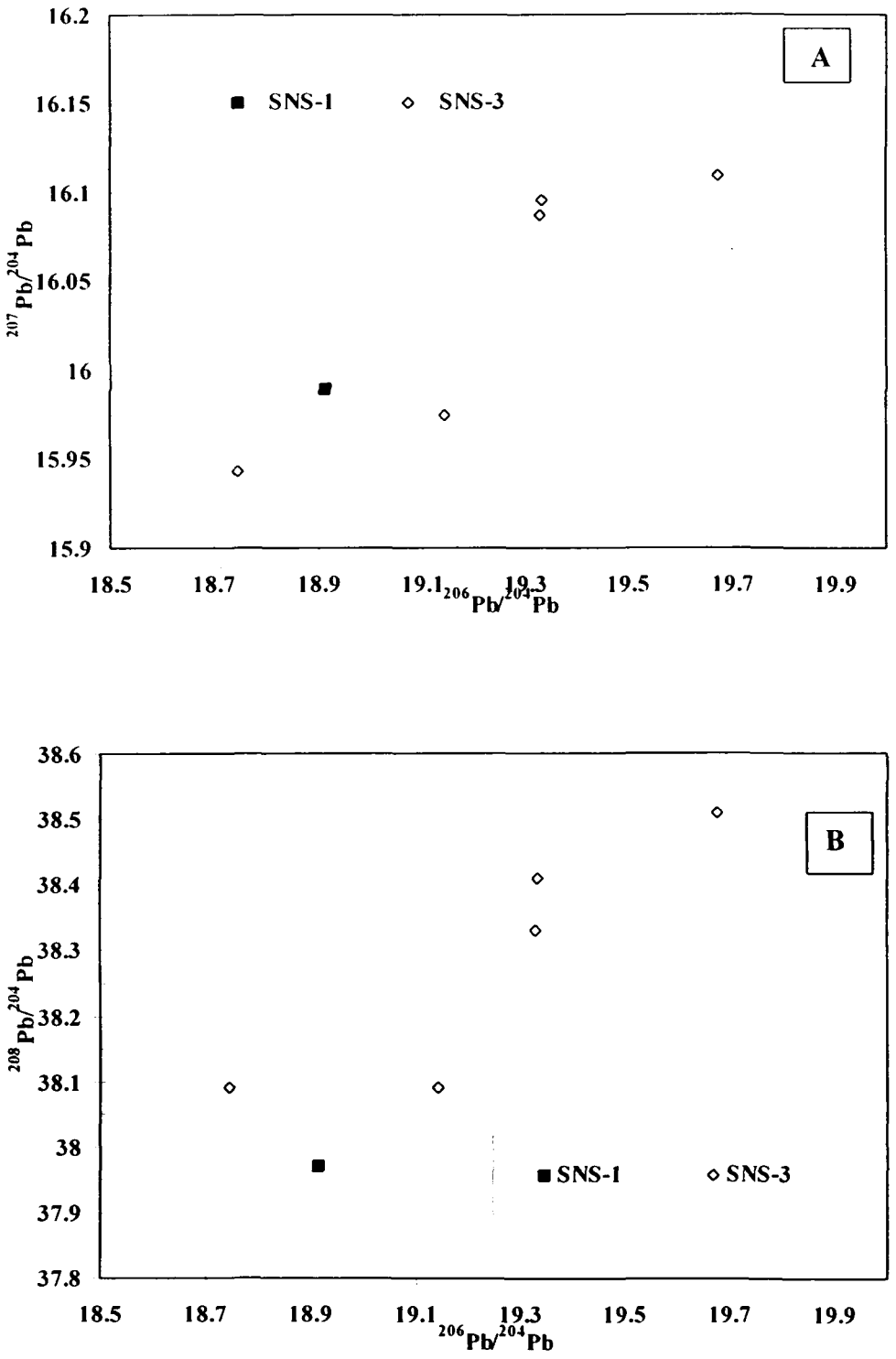

Fig. 7.4: $^{207}Pb/^{204}Pb$ vs. $^{206}Pb/^{204}Pb$ diagram (A) and $^{208}Pb/^{204}Pb$ vs. $^{206}Pb/^{204}Pb$ diagram (B) of various leach and residual portions of BIF sample SNS-1 and SNS-3. Note the data are well correlated in both the diagram.

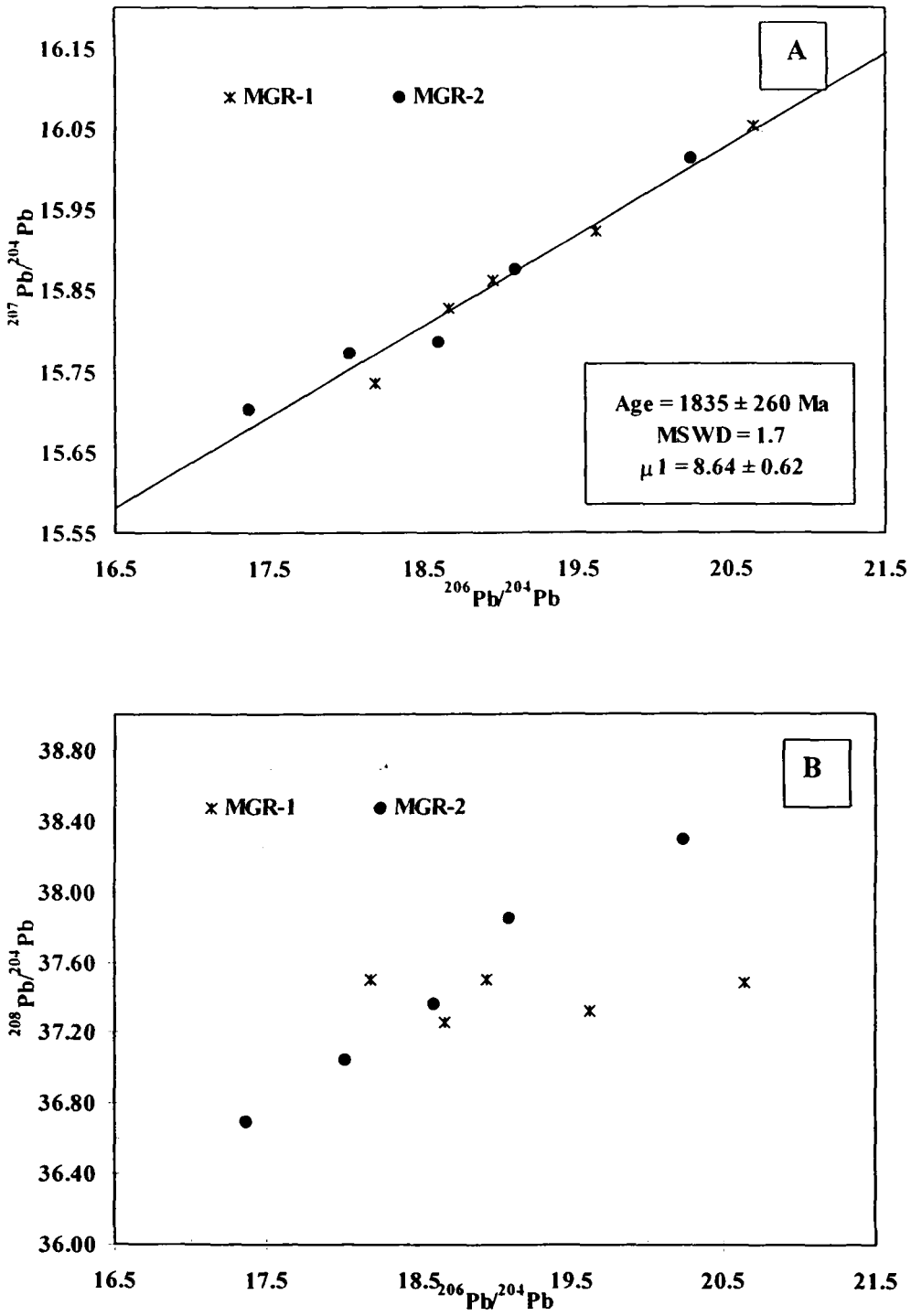

Fig. 7.5: $^{207}Pb/^{204}Pb$ vs. $^{206}Pb/^{204}Pb$ diagram (A) and $^{208}Pb/^{204}Pb$ vs. $^{206}Pb/^{204}Pb$ diagram (B) of various leach and residual portions of BIF sample MGR-1 and MGR-2. Note, the data sample MGR-2 show scatter in thorogenic diagram (b) indicating presence of uranium bearing phase.

statistically well characterized isochron age (Fig.7.3A) of 1834 ± 16 Ma with model μ_1 of 8.50 ± 0.15, the mean square weighted deviates of this regression is 2.8 indicating the scatter of the data points are mainly due to analytical uncertainties. The whole rock, leach and residue fractions of samples SNS-1 and SNS-3 exhibit comparatively lesser variation in Pb-Pb space (Fig.7.4, Table 7.2). The $^{206}Pb/^{204}Pb$ ratios vary from 18.774 to 19.674 and $^{207}Pb/^{204}Pb$ ratios range from 15.943 to 16.110; and do not define any isochron line. Combining of all fractions of all the three samples of Sonsa area (SNS-1, 2 and 3) an isochron age of 1797 ± 36 Ma is obtained (Fig.7.2), with model μ_1 of 8.89 ± 0.15 and MSWD of 18. Higher values of MSWDs indicate that the degrees of scatter are in excess of experimental error, possibly due to slightly inhomogeneous initial isotopic ratios in different leach (mineralogical/structural) fractions. The whole rock, leach and residual fractions of samples from Mangora area (MGR-1, 2) define a well correlated line in uranogenic ($^{207}Pb/^{204}Pb$ vs. $^{206}Pb/^{204}Pb$) diagram (Fig.7.5). The data define limited spread in Pb-Pb space (Table 7.2), the $^{206}Pb/^{204}Pb$ ratios range from 17.367 to 20.640 and $^{207}Pb/^{204}Pb$ ratios range from 15.703 to 16.053. Linear regression of the data points define an isochron age of 1835 ± 260 Ma with model μ_1 of 8.64 ± 0.62 and MSWD of 1.7. Higher error in the age is due to limited spread in $^{206}Pb/^{204}Pb$ ratios, albeit the mean square weighted deviates is close to unity thus indicating that the scatter is due to analytical uncertainties.

The residue fractions and whole rock fractions of all the five BIF samples leached/dissolved with strong acids, conforms to the linear array in uranogenic ($^{207}Pb/^{204}Pb$ vs. $^{206}Pb/^{204}Pb$) diagram and define isochron age within the limits of MSWDs which are accepted/permitted for chemical precipitates (Jahn and Cuvellier 1994). This implies that even the silicate fractions were isotopically homogenous with the hematite fractions and different mineralogical bands of BIF (hematite and chert) remained close system since their deposition, thereby increase the confidence of the Pb-Pb age derived from these BIFs.

All the samples in individual and together define similar ages, as the slope of the best-fit line do not change and agrees within their error limits. As leach fractions represents the most homogeneous phase of the sample (Frei et al 1999), the age defined by three leach fractions of sample SNS-2 alone i.e. 1834 ± 16 Ma is considered to be the best representative of the deposition/diagenesis of BIFs which are also in excellent agreement with age of BIFs from Mangora area (1835 ± 260 Ma).

The thorogenic ($^{207}Pb/^{204}Pb$ vs. $^{206}Pb/^{204}Pb$) data array (Fig.7.2B-7.5B) of these BIF samples are generally positively correlated with few exceptions, indicating U and Th behaved in similar fashion. However in case of samples SNS-2 (Fig.7.3B) and MGR-1 (Fig.7.5B) the $^{206}Pb/^{204}Pb$ ratios vary considerably but corresponding $^{208}Pb/^{204}Pb$ ratios do not change significantly and forms plateau in the graph. This indicates presence of minor uranium bearing phases and is supported by slightly higher uranium abundances in these samples (Table 7.2).

7.3.3 Sr isotopes of limestone:

Sr, Rb abundances and isotopic data of limestones are given in Table 7.3. Sr concentration in these samples (HCl soluble) ranges from 64.8 ppm to 132.1 ppm and Rb concentration vary from 0.45 ppm to 3.04 ppm. The $^{87}Sr/^{86}Sr$ ratios in the carbonate HCl leach fractions show a range of variation from 0.70785 to 0.71004. $^{87}Rb/^{86}Sr$ ratios of HCl leachates are very low and range from 0.0183 to 0.0762. The initial $^{87}Sr/^{86}Sr$ ratios (Sr_i) calculated for an age of 1.9 Ga, for the carbonate fraction, ranges from 0.70718 to 0.70871. These are much higher than 0.705, the value represented by contemporary seawater (Shields and Viezer, 2002). The highly radiogenic nature of Sr isotope systematics is either due to mixing of evolved diagenetic fluids with high initial Sr_i or equilibration with detrital residual phase within the samples. The dolomitisation or other diagenetic features could not be identified in the field or under microscope. The $^{87}Sr/^{86}Sr$ ratios of residual detrital fractions are highly radiogenic (Table-7.3) where $^{87}Sr/^{86}Sr$ ratio ranges from 0.84131 to 0.90842. The current Sr_i of carbonates probably indicates post-depositional equilibration of carbonate and detrital phase of the rock.

Table-7.3: Rb-Sr isotope data of limestones from Utila area

Sample No	Rb ppm	Sr ppm	$^{87}Rb/^{86}Sr$	$^{87}Sr/^{86}Sr$	$^{87}Sr/^{86}Sr$ at 1.9 Ga
UTL1 HCl sol.	1.32	115.7	0.0329	0.70869	0.707779
UTL2 HCl sol.	0.89	66.9	0.0384	0.7087	0.70765
UTL2 Residue	118	63.5	5.415	0.88071	
UTL3 HCl sol.	0.45	71.8	0.0183	0.70921	0.70871
UTL3 Residue	161	42.4	11.21	0.90842	
UTL6 HCl sol.	0.65	76.4	0.0245	0.70785	0.70718
UTL6 Residue	230	101	6.699	0.871116	
UTL7 HCl sol.	3.04	115.5	0.0762	0.71004	0.70796
UTL8 HCl sol.	0.68	64.8	0.0281	0.70829	0.70752
UTL8 Residue	220	117	5.508	0.84131	
UTL9 HCl sol.	0.66	79.9	0.024	0.70826	0.7076
UTL10 HCl sol.	0.96	132.1	0.029	0.70853	0.70796
Errors (2σ)	2%	1%	2%	0.05%	

7.3.4 Sr isotopes of BIF:

Sr isotope systematics were analysed for five BIF whole rocks and HCl soluble portions from two BIF samples (SNS-1 and 3), the data are presented in the table-7.4. The Rb and Sr abundances are very low, ranges from 0.202 ppm to 0.929 ppm and from 2.737 ppm to 4.230 ppm respectively. The $^{87}Rb/^{86}Sr$ ratios are also low and restricted and ranges from 0.138 to 0.741, whereas the $^{87}Sr/^{86}Sr$ ratio ranges from 0.72232 to 0.736314. The Rb-Sr systematics are evidently disturbed and do not define any isochron. The Sr_i ratios calculated at the time of deposition (1.9 Ga) are highly radiogenic, ranges from 0.715 to 0.725. This shows crustal influence on Sr isotope systematics, the large range of Sr_i indicates post depositional contaminations by crustally derived material. As Sr concentrations in these BIFs are very low, small inputs of contaminant are sufficient to bring about the changes in their Sr isotopic composition. Although an originally radiogenic evolved source cannot be ruled out, both the factors together can better explain the present Sr isotope systematics. Such types of high Sr_i are reported from Achaean Isua BIFs (Stecher et al., 1986, Frei et al., 1999).

Table-7.4: Rb-Sr isotope data of BIFs from Sonsa and Mangora area

Sample No	Rb ppm	Sr ppm	$^{87}Rb/^{86}Sr$	$^{87}Sr/^{86}Sr$	$^{87}Sr/^{86}Sr$ at 1.9 Ga
SNS-1	0.698	2.737	0.741	0.73574	0.715476
SNS-2	0.202	4.220	0.138	0.72059	0.716816
SNS-3	0.566	3.960	0.407	0.736314	0.725784
MGR-1	0.929	4.207	0.641	0.73743	0.719900
MGR-2	0.617	4.230	0.424	0.72838	0.716785
SNS-1#	0.068	0.674	0.291	0.72232	0.71479
SNS-1@	0.511	1.626	0.941	0.73785	0.71348
SNS-3#	0.077	1.427	0.734	0.73928	0.72027
Errors (2σ)	2%	1%	2%	0.05%	

HCl soluble fraction, @ Residue fraction.

7.3.5 Nd isotopes of limestone:

The Sm/Nd ratio of carbonate fractions in these rocks shows that they are LREE enriched compare to CHUR. The Nd isotope data and Sm, Nd abundances are presented in the table-7.5. The Sm and Nd content in carbonate fractions varies from 1.69 ppm to 5.25 ppm and 8.31 ppm to 22.67 ppm respectively. The $^{147}Sm/^{144}Nd$ and $^{143}Nd/^{144}Nd$ ratios vary within a range of 0.1103 to 0.14140 and 0.511506 to 0.511864 respectively. The εNd values calculated at 1.9 Ga vary from –2.37 to +1.37. The data

indicate a young basaltic mantle component for positive εNd values, as basement Bundelkhand granite yield εNd value of –8.75 at 1.9 Ga (Unpublished AMD Data).

7.3.6 Nd isotopes of BIF:

The Nd isotope systematics of BIFs are discussed in detail in previous chapter, the data are presented in the table-6.2. The Sm and Nd content in whole rock samples of BIFs range from 0.18 to 3.88 ppm and 0.63 to 16.63 ppm respectively. The $^{147}Sm/^{144}Nd$ and $^{143}Nd/^{144}Nd$ ratios vary within a range of 0.1420 to 0.0.1743 and 0.511553 to 0.511660 respectively. The εNd values calculated at 1.9 Ga range from -7.86 to -13.68. The data indicates very old LREE enriched crustal component for giving rise such high negative εNd values. This is in contrast with Nd isotope systematics of interbedded limestones, which show juvenile signatures.

Table-7.5: Sm-Nd isotope data of limestones from Utila area

Sample No	Sm ppm	Nd ppm	$^{147}Sm/^{144}Nd$	$^{143}Nd/^{144}Nd$	Model Age	εNd at 1.9 Ga
UTL1	3.198	13.25	0.1366	0.511864	2329	-0.56
UTL2	5.251	22.67	0.141	0.511816	2562	-2.37
UTL3	1.699	8.312	0.1245	0.511639	2388	-1.86
UTL7	2.452	12.38	0.1122	0.511623	2119	0.82
UTL8	2.785	15.37	0.1103	0.511506	2254	-1.02
UTL9	1.82	8.582	0.1201	0.511745	2092	1.37
UTL10	1.826	8.96	0.1241	0.511682	2308	-0.98
Errors (2σ)	1%	1%	1%	0.01%		

7.4 Discussion:

7.4.1 Age:

Stratigraphically, the age of deposition of Gwalior Group is bracketed between the minimum age of basement Bundelkhand granites and the age of mafic dyke swarm, which intrude the Gwalior succession. Recently Mondal et al., (2002) reported high precision U-Pb ion microprobe data of zircons separated from different granitoid phase of Bundelkhand massif, concluding that the massif was stabilized at 2.5 Ga and last major phases of granites were intruded within a short span of time around 2.5 Ga. The mafic sill within Morar Formation BIFs was dated as 1830 ± 200 Ma by using Rb-Sr isotope analyses of five whole rocks and three plagioclase separates (Crawford

and Compston, 1970). The recalculation of these data with new Rb-Sr decay constants yields an age of 1791 ± 200 Ma. These sills are confirmed to be a part of major mafic dyke swarm by systematic geological mapping. Intrusive relationships like contact metamorphism and apophyses are recognized in field outcrops and in borehole cores, and are also reported in literature (Vardharajan and Verma, 1971, 1973). This implies that sedimentation in Gwalior basin occurred any time between 2500 Ma and 1791 Ma. However, Bundelkhand massif witnessed series of minor intrusive events such as pegmatite veining, acid volcanism, large scale quartz veining and mafic dyke activity after the last phase of granitic magmatism (Basu, 1986; Mondal et al., 2002). The mafic dyke intrusions in the Bundelkhand massif are recognized as the last phase among these events, on the basis of field geological setting (Basu, 1986). Even these basement mafic dykes predate the Gwalior sedimentation as observed during systematic mapping along the contact of Gwalior Group sediments and basement Bundelkhand Granite Complex during the course of present study. The peneplaination of these units before initiation of Gwalior sedimentation is evident in the field. Moreover, the contact between basement granites and Gwalior groups are marked by pronounce unconformity and development of widespread regoliths (Roy and Saxena, 2000), indicating few hundred million years probably elapsed before formation of Gwalior basin. The upper age limit of Gwalior sedimentation at 2200 Ma, instead of 2500 Ma, is more realistic, on the basis of beginning of rise of atmospheric oxygen and iron retention in the paleosols at about 2200 Ma (Holland et al., 1989; Holland and Beukes, 1990). Recent $^{40}Ar/^{39}Ar$ age determinations (Mallikharjuna Rao et al., 2005) of mafic dyke swarms of BGGC suggest that they were emplaced in two phases, i.e. at 2150 Ma and 2000 Ma; thereby the lower age limit of sedimentation is further constrained at 2000 Ma.

The direct age determination obtained during the present study for limestone of Morar Formation i.e. 1914 ± 170 Ma is in agreement with the published results and falls within the range of 1791Ma and 2000 Ma. The original sedimentary textures are excellently preserved in these limestones and are completely unmetamorphosed. Pb-Pb system of limestones are proved to be robust and provide meaningful ages for deposition/diagenesis of sediments which are over printed at temperatures below approximately 300°C (i.e. closure temperature for the system U-Pb in calcite minerals, Bolhar et al., 2002). Therefore 1914 ± 170 Ma is considered to be the pristine age of deposition/diagenesis of limestone of Gwalior Group.

The bulk Pb and PbSL data of BIFs from Sonsa area as discussed in previous section (SNS-1, 2 & 3) define three different ages, i.e. 1797 ± 36 Ma (when all the fractions of entire three samples are considered), 1809 ± 75 Ma (when all the fractions of sample SNS-2 are considered) and 1834 ± 16 Ma (when only three acid leach fractions, minus residue of sample SNS-2 are considered). All the ages agree within their error limit, oldest among these i.e. 1834 ± 16 Ma is considered to be the best representative of deposition of BIFs for several reasons. Firstly, leach fractions represent most homogeneous phase of the sample (Frei et al., 1999). Secondly, this is in excellent agreement with the age derived from the BIFs of Mangora area (1835 ± 260 Ma). Thirdly, the sample SNS-2 represent the most pure chemical precipitate from sea water with least contaminants as it is characterized by very high Y/Ho ratio (41.50), and strong positive Y anomaly (1.86) (Bolhar et al., 2004) in shale normalized REE+Y spidergram (Fig. 6.3). Finally, it is well known that in the case of chemical sediments the Pb-Pb technique dates the redistribution of U and Pb during diagenesis (not deposition). In this case the older age is clearly more likely to approach the depositional age. In order to be in agreement with the age of coeval limestones (i.e. 1914 ± 170 Ma) as discussed in previous section and age of intrusion of mafic dykes (i.e. 1791 ± 200 Ma, the lower age limit of Gwalior sedimentation), it is inferred that the most realistic age of BIF deposition/diagenesis is shifted towards the upper age limit, i.e. 1850 Ma.

The age considered for BIF deposition i.e. 1834 ± 16 Ma is grossly identical with age of mafic dyke intrusion (1791 ± 200 Ma, Crawford and Compston, 1970). It may be speculated that the Pb-Pb system of BIFs dates the remobilization of U and Pb during the thermal episode exerted by mafic intrusion. Still the age i.e. 1850 Ma is considered to be the original age of deposition for several reasons. Firstly, The BIFs show excellent preservation of sedimentary texture and are completely unmetamorphosed. The closure temperature of U-Pb system in magnetite is ~500°C (first order approximate, Sharp, 1991; Frei, 1999) and can be reset only during high grade metamorphism. Secondly, residual silicate fractions of these BIFs are equilibrated with leach (hematite) fractions and conform to the linear array in both the uranogenic and thorogenic diagram and define isochron age, albeit the quality of the isochron line is degraded. This implies that different mineralogical bands viz. hematites and cherts are isotopically homogenous. This is in contrast with the result obtained by Frei et al., (1999) for metamorphosed BIFs of Isua greenstone belt,

Greenland, where residual fractions plot away from the isochron line. As hematite and silica precipitate from seawater, they inherit the isotope systematics of seawater and both hematite and chert bands are expected to show similar isotopic composition. Metamorphic overprint may disturb the isotope systematics of different mineralogical bands in different way and isotope systematics of different mineralogical fractions can be decoupled, as observed by Frei et al., (1999). The field relationship of Gwalior BIFs (away from mafic intrusives), their complete unmetamorphosed nature and isotopic equilibrium between different mineralogical bands indicate that the age i.e. 1834 ± 16 Ma, more precisely 1850 Ma (as discussed in preceding paragraph) represent the depositional/diagenesis age of the BIFs. This is in agreement with the age of limestones, which underlie these BIFs. The result implies that these BIFs represent the late stage of main phase of early Proterozoic BIF metallogeny that believed to be ended at ~1850 Ma (Beukes and Klein, 1992) and are coeval to Gunflint BIFs (Fralick et al., 2002). The age gap between limestones (1914Ma) and BIFs (1850 Ma) implies slow sedimentation and are consistent with their Nd isotopic compositions as discussed in the later section.

7.4.2 Provenance:

The elements like Nd and Pb, with short residence time in seawater (300 years and 50 years respectively, Faure 1986), can be used to trace the provenance of chemogenic sediments. In this regard the Nd has very high crustal residence time and provide best indicator for provenance modelling. Due to short residence time, dissolved Sm and Nd are removed from seawater on relatively rapid time scale. As a consequence, sea water $^{143}Nd/^{144}Nd$ ratios preserved in authigenic mineral records and display differences in isotopic compositions in different time spaces within a basin. These features are controlled by variety of factors including source of REE, weathering rates, continental tectonics and proximity of the source, oceanic hydrothermal activity, paleo-ocean configuration and indirectly by the Sm-Nd evolution of the bulk earth (Pipegras and Wasserburg, 1980; Palmer and Elderfield, 1985; Spivack and Wasserburg, 1988). Although the Sr isotope data can be altered by fluid activity it can be used with caution.

The Pb isotope data of both limestone and BIF indicate a model μ_1 value of ~8.5 which is significantly higher than the μ_1 value of 7.5-8.0 of the contemporary

mantle (Moorbath and Taylor 1981). The high μ_1 value of Gwalior chemical sediments envelop crustal signature and indicates crustal sources of Pb isotopes.

The Sr isotope data are compatible with Pb isotope data for both limestones and BIFs, showing highly evolved radiogenic Sr_i ratios. The limestone indicates Sr_i of ~0.707 at 1.9 Ga which is significantly higher than contemporary seawater (Shields and Viezer 2002). The BIFs also show very high Sr_i (0.71-0.72) and comparable to Isua BIFs (Stecher et al 1986, Frei et al 1999). As the carbonates are diagenetically not altered and contain calcite microsper, the Sr isotope signals may be source representative. The higher Sr_i ratios in the Gwalior carbonates indicate that the basin received significant fluvial input of evolved crustal Sr, from the weathering of basement granitic rock. This is also in agreement with near-shore depositional environment of these carbonates and presence of detrital phases within them.

Seawater Nd compositions are controlled by two potential end-members viz. run-off from continental crust and depleted mantle input from hydrothermal sources along oceanic ridges. The present day and phanerozoic sea water's Nd isotopic composition is dominated by riverine input, charged with weathering flux of continental silicates. While during Precambrian time, hydrothermal inputs seem to be the major player as evidenced from the positive depleted mantle like εNd (T) in the BIFs (Goldstein and Jacobsen, 1987, 1988a b c; Sholkovitz, 1988; Derry and Jacobsen, 1990). The Nd isotope systematics of Gwalior BIFs is already discussed in the previous chapter and indicate a very old crustal LREE enriched source. The εNd value at 1.9 Ga varies from –6.29 to –13.68. The Sm-Nd data of the basement 2.5 Ga granite yields εNd value of –8.75 at 1.9 Ga (Unpublished AMD data) and the basement 3.3 Ga old TTG yields εNd value of the order –13 at 1.9 Ga (Gopalan et al., 1990). The εNd values of the BIFs envelop these signatures and indicate mixing of these two basement components. The high variability of εNd in these BIFs suggests that the BIFs are not completely homogenized with respect to Nd isotopic composition. This is not very unusual for BIFs, similar situations were observed for Isua BIFs (Miller and Onion, 1995, Shimizu et al., 1990, Frei et al., 1997, 1999) where Nd isotopic inhomogenity was found even in different mineralogical bands. Interestingly, a mantle derived component of Fe is required to satisfy the mass balance calculation of Fe in Gwalior BIFs as Fe poor granitic basement rock can not supply the Fe required for huge pile of BIF generation (Jaocobsen and Pimental-Klosel1988 a, b; Alibert and McCulloch 1993, Miller and Onion, 1995). The upper

limit of εNd in these BIF samples is –6.29 which is almost three epsilon unit higher than basement granite (εNd = -8.75). Therefore, it is possible that part of Nd came from mantle/hydrothermal source, but the signature is masked due to elevated Nd content of crustal derived material as discussed in the previous chapter.

The Nd isotope systematics of Gwalior limestones yield εNd values at 1.9 Ga ranging from –2.37 to +1.37 (Table 2.5, Fig. 6.5) and the Sm-Nd model ages (T_{DM}) vary from 2090 Ma to 2562 Ma. The upper limit of model ages corresponds to the average age of continental crust that was available for the weathering and erosion and provided inputs for the carbonate rocks. The part of the model ages is much younger than the provenance rocks (~ 2.5 Ga, Mondal et al., 2002) and also the positive and small negative εNd values indicate inputs from juvenile mantle derived source. The three epsilon unit variations of Nd isotopes in the carbonate rocks indicate large scale inhomogenity with respect to Nd isotopic composition. Positive εNd is not common for carbonate rocks irrespective of age, but are characteristics of BIFs (Bau et al., 1997). Since the limestone unit is only 8-10m thick and interbedded with BIFs, such positive εNd values are not unusual. The enigma is that the BIF units themselves shows high negative continent like εNd values. Since the REEs have small residence time in seawater even little temporal variation in Nd isotopic composition can be preserved. In this connection, as discussed in the previous section, the Pb-Pb ages indicates that the limestone (1914 Ma) unit is slightly older than the analyzed BIFs (1850 Ma) which is also corroborated from their field setting. It is possible that positive εNd with juvenile signature are local in nature and represent only small time frame when these limestones were deposited. Nevertheless, the data indicate intrabasinal mantle derived mafic activity during the time of sedimentation. This also partly satisfies the Fe budget which is required for the generation of the BIFs. It is suggested that Fe was stored in reduced deep bottom waters and received variable Fe influx through hydrothermal exhalations, presumably via volcanic fissures that probably were developed because of rift activation. Rapid delivery of Fe rich waters to the shallower oxygenated parts resulted in precipitation of BIFs. However, such a volcanic episode is not recorded in field till date, the only mafic activities are found in terms of post Gwalior mafic dyke swarms. As the BIF samples come from large part of the basin, they are expected to represent better provenance signals, in contrary to the limestones that come from single out crop.

CHAPTER-VIII
SUMMARY AND CONCLUSION

The north Indian shield, occurring to the north of Son-Narmada lineament/ Central Indian tectonic zone, is comprising of two Archean crustal blocks namely Aravalli block (AB) and Bundelkhand block (BB). Both of these blocks are characterized by presence of Archean basement complexes i.e. Banded Gneissic Complex (BGC) in AB and Bundelkhand Granite-Gneiss Complex (BGGC) in BB. These Archean complexes have served as basement to numerous Proterozoic cover sequences. Most of the cover sequences of Aravalli block are highly folded, deformed and metamorphosed due to their involvement in Aravalli-Delhi Orogeny. However, the cover sequences of Bundelkhand block are flat lying and unmetamorphosed as they have not been affected by Proterozoic orogenic movements. These characteristics make the Bundelkhand cratonic block a good study area the geological processes of early earth's history.

In Gwalior sector of Bundelkhand craton a continuous sedimentary rock record is preserved from Mesoarchean to Mesoproterozoic period. This sector is least deformed as it is away from major orogenic axes i.e. Aravalli-Delhi Fold Belt (ADFB) in north-western India and Satpura orogenic belt in central India and itself composed of low dipping unmetamorphosed Proterozoic sedimentary sequences. This part of Indian shield provides an opportunity to trace the temporal geochemical evolution of upper continental crust and evolutionary changes such as crust building processes across Archean-Proterozoic boundary through geochemical examination of sedimentary rocks. The Paleoproterozoic succession of the area is represented by Gwalior Group sediments comprising a basal clastic sequence (Par Formation) and upper chemical sequence (Morar Formation). The Paleoproterozoic Gwalior Group is unconformably overlained by Mesoproterozoic sandstone-shale sequence of Kaimur Group (Vindhyan Supergroup). The basement of Gwalior Group is predominantly consisting of high K granite (2.5 Ga) with some well preserved xenolithic Archean metasedimentary enclaves of quartzite-phyllite association.

An integrated sedimentological and geochemical study of Gwalior Group was carried out to understand evolutionary history of north Indian shield. The sedimentological facies analysis clearly demonstrates that the Gwalior Group sediments

were deposited in a stable clastic shelf; influenced by tidal, wave and storm activity. A range of sedimentary facies from high-energy shore zone to low-energy outer shelf is preserved, indicating craton interior platformal setting of deposition. Sedimentation was laid down under transgressive system tract in an accommodation dominated shelf. Presence of rare basal alluvial facies suggests that the basin probably started life as an alluvial basin, gradual opening up of the basin resulted in the landward encroachment of the sea. With rapid sea level rise clastic sedimentation ceased and chemical environment prevailed. The deposition of BIF took place in a raised sea level which overlapped all the earlier formed clastic facies.

The extreme quartz richness of sandstones indicates low upliftment and high insitu weathering of basement terrain. The geochemical data of Gwalior group clastic sediments also supports this view. Strong depletion of Ca, Na, Sr and high plagioclase index of alteration (PIA) values (~85) indicate severe weathering of upper crust which is in conformity with global warm and moist climate during the Paleoproterozoic. The sediment suffered post depositional potash metasomatism as indicated by A-CN-K systematics and K enrichment of near zero to as high as 38% is inferred. The positive correlation between TiO_2 and $FeO^{(T)}$ suggests an oxygenated atmosphere where FeO was conserved. The immobile trace elements systematics, compatible to incompatible element ratios and REE pattern of Gwalior Group clastics suggest that upper crust of Bundelkhand craton during the Paleoproterozoic period was consisting of 40% TTG, 40% intracrustal High-K granites and 20% mafic rock. The data convincingly demonstrate the importance of LILE enriched subduction related granites in the Paleoproterozoic upper crust. In contrary, the geochemical data of basement Archean quartzites reveal that the Mesoarchean (~2.9 Ga) upper crust was predominantly consisting of TTG with a possible Low-K Archean granite component, as they are characterized by highly fractionated REE patterns (La/Yb_N ~ 26) and very low K_2O/Na_2O and Rb/Sr ratios. A sole intracrustal granite provenance during the Mesoproterozoic is indicated by the geochemical data of Kaimur Group sandstones. The data demonstrate that Archean upper crust was constituted of TTG. The generation of TTG magmas require a higher thermal regime. Partial melting of thickened mafic root of plume generated submarine plateux where garnet and amphibole were left in residue has been advocated for generation of TTG magma (Martin, 1987, 1993). Systematic unroofing of granite pluton through erosion of TTG cover is indicated during the Paleoproterozoic as revealed by geochemical data of Gwalior Group clastics.

It seems that the TTG cover was almost completely eroded during the Paleoproterozoic thus no significant record of TTG is available in the Mesoproterozoic Kaimur sediments. The changes across the Archean-Proterozoic Boundary (APB) are governed by 'TTG effect' and 'subduction effect' (Condie, 1993, 1997). The REE patterns of sediments were flattened with time as the Archean sediment show steep REE pattern ($La/Yb_N \sim 26.58$) while the Paleoproterozoic Gwalior Group sediment show moderate fractionation ($La/Yb_N \sim 12.57$) and Mesoproterozoic Kaimur Group sediment show still lower fractionation ($La/Yb_N \sim 8.29$) of REE. This is exactly opposite to that of proposed by Taylor and McLennan (1985) and emphasizes the importance of 'TTG effect' over 'komatiite effect' (Condie, 1993, 1997). The excessive enrichment of LILEs and higher K_2O/Na_2O and Rb/Sr ratios in Proterozoic sediments compared to Archean sediments is governed by 'subduction effect'. During the Proterozoic, subduction related intracrustal granite became important where excess LILEs were introduced in mantle wedge through devolatilisation of descending oceanic plate. The data convincingly suggest that Archean crust building processes were different from that of post Archean period. During the Archean heat flow was higher and TTG magma was produced by partial meting of thicken mafic root of submarine plateux. In contrary, during the Proterozoic, Phanerozoic type plate tectonics started operating and arc related high-K granitic magmas were emplaced in the pre-existing continental block. The systematic upliftment of crustal block led to the erosion of upper TTG cover that exposed the granitic batholiths, signatures of which is recorded in Proterozoic sedimentary rocks of studied area..

The Geochemical data of Gwalior Group BIF overwhelmingly suggests that these are near pure chemical precipitates and are compositionally similar to modern day seawater. The modern sea water like components such as negative Ce anomaly, positive La, Gd, Y anomalies and HREE enrichment over MREE and LREE in shale normalized REE+Y spidergram are preserved. The weak negative Ce anomalies suggest beginning of global oxidative process which was considerably less efficient than modern sea water. The HREE enrichment and La spiking indicate importance of carbonate complexation of REEs and signify alkaline pH of sea water like that of modern ocean. The REE data suggest continental derivation of REEs as dissolved and as particulate load. The REE patterns of some samples are identical to those of present day sea water while rest of the samples resemble with the patterns of coeval clastic rocks. The Nd isotope systematics indicate very old crustal source of Nd and support the view of early

crustal component of Bundelkhand craton as proposed by some earlier workers (Sharma, 1998, Mondal et al., 2002). The εNd(T) of BIF varies from –6.29 to –13.67 and can be explained by the mixing of basement components such as 2.5 Ga old granites [εNd(T) ~ -8.75] and 3.3 Ga old Gneisses [εNd(T) ~ -13]. This is in agreement with the results of coeval clastic rocks. Similar features are also attested by Pb and Sr isotope systematics of BIFs and limestones. However the upper limit of εNd(T) =-6.29 is at least three epsilon unit higher than that of the basement granites (εNd(T) ~ -8.75), indicating a depleted mantle input to the sea water. A similar hydrothermal component is also indicated by presence of weak positive Eu anomaly and $(Eu/Sm)_{SN}$ ratio greater than one. The interbedded limestone also attests similar signatures as they are characterized by positive to small negative εNd(T) values (-2.37 to +1.37) and younger Sm-Nd model ages (2090Ma-2562Ma) compared to the basement complex. Mass balance calculations of BIF also require a hydrothermal source of iron, as Fe poor felsic rocks can not yield enough Fe as required for huge pile of BIFs precipitation. The data suggest that the surface water was some what oxic and was buffered with continent, while the anoxic bottom water received hydrothermal inputs from mantle. It is suggested that the mixing of Fe rich anoxic bottom water and oxic surface water through the chemocline gave rise to the precipitation of BIFs. Since the REE content of continent derived surface water was many times higher than hydrothermal solutions. The REE patterns along with Nd isotope systematics prevalently show continent like signatures and juvenile mantle like signatures are masked. The REE patterns and Nd isotope systematics are in conformity with sedimentological data that BIF deposition took place in an open shelf, surface water of which was completely buffered with continent. This is in contrast with the mantle buffered Archean sea as the Archean BIF shows positive depleted mantle like εNd(T) values (for e.g. ; Jaocobsen and Pimental-Klose1988 a, b; Shimizu et al., 1990; Alibert and McCulloch 1993; Khan et al., 1996; Bau et al., 1997; Frei et al., 1999). This also reaffirms the inference based on geochemistry of clastic sediments that the Archean crust building processes were completely different to that of Proterozoic one.

The Pb-Pb systematics of limestone yield an age of 1914 ± 170 Ma and overlying BIFs yield an age of 1850 Ma. Since these lithounits represent the upper sequence of Gwalior Group, an older age of the basal clastic sequence is obvious. As BIFs represent the youngest litho-unit, the age of Gwalior Group seems to be bracketed

between 2000 Ma and 1850 Ma. The BIFs represent the last phase of BIF metallogeny at the end of the Paleoproterozoic and are coeval to Gunflint Formation BIF of Canada. The data reveal that Gwalior Group sediments are equivalent to the upper part of the Aravalli Supergroup of Rajasthan, which is bracketed between the age of 2200 and 1900Ma (Chaudhary et al., 1984; Deb et al., 1989, Deb, 1999; Sreenivas et al., 2001, Deb and Thorpe, 2004) and are older to Cuddapah Supergroup of South India and Semri Group of Vindhyan Supergroup, Central India. The deposition of Vampalle limestone of basal Cuddapah Sequence is constrained at 1756 ± 29 Ma (Zachariah et al., 1999) and the deposition of Semri Group is constrained at ~1600 Ma (Rasmussen et al., 2002; Ray et al., 2002, 2003; Sarangi et al., 2004). The new geochronological data of Gwalior Group thus refutes the normal belief arose from it's undeformed and unmetamorphosed nature (for e.g. Naqvi and Rogers, 1987) that the Gwalior Group is equivalent to Cuddapah Supergroup and younger to Aravalli Supergroup.

The salient conclusions derived from this work are enumerated below:

1. The sedimentary rocks of Paleoproterozoic Gwalior basin was deposited in a craton interior stable platformal setting.
2. Silicilastic sedimentation of Gwalior group was deposited primarily in a shallow marine setting influenced by Tidal, wave and storm activity. The shallow marine setting is inferred on the basis of tabular sheet like bed geometry, textural and mineralogical maturity of sandstones and evidence of reversing currents.
3. The tidal influence is indicated by the presence of herring bone cross bedding, tidal bundles, modified ripples (flat crested, ladder back) that were formed in an intertidal environment in back barrier lagoonal region which was protected from open sea.
4. Wave influences were most dominative in shoreface-foreshore facies which is characterized by different wave produced structures. This represents most preserved facies. The current direction of cross beds show complex set of orientation, indicating complex reworking of sediments in a basinal system.
5. Storm related beds are preserved only in shelf facies as different bouma type beds.
6. The Gwalior clastics provide a unique example of preservation of a complete shore line profile from inshore to offshore facies. Sedimentation

prevalently laid down under transgressive system tract in an accommodation dominated shelf.

7. With rapid sea level rise, clastic sedimentation ceased, chemical environment prevailed, leading to the deposition of huge pile of BIFs.
8. The upper crust suffered severe weathering as indicated by depletion of Ca, Na, Sr and high PIA index of Gwalior sediments. Post depositional K-metasomatism is indicated by position of Gwalior clastics at A-CN-K space. Degree of K enrichment ranges from near 0 to 38% with an average value of 30%.
9. Based on REE patterns and immobile element ratios, the source areas of Gwalior sediments were consisted of 40% granite, 40% TTG and 20% mafic rock.
10. The Mesoarchean upper crust was predominantly composed of TTG with a component of low K-Archean granite as evidenced by the geochemistry of Archean quartzites occurring as enclaves within the BGGC.
11. The Kaimur sediments were derived chiefly from granite. The source area of Kaimur group underwent severe weathering and post-depositional K-metasomatism took place.
12. The upper continental crust evolved from TTG composition at Archean to granitic composition in Proterozoic. The changes across APB are explained in terms of "TTG effect" and "subduction effect" as stated by Condie, 1997. The data indicate systematic unroofing of granite plutons by upliftment and erosion of upper TTG cover by the end of Paleoproterozoic.
13. The REEs of Gwalior BIFs had a continental source as evidenced from REE patterns and Nd isotope systematics.
14. Nd isotope systematics of BIFs indicate that Nd was derived from a 2.5 Ga granite and an older 3.3 Ga Gneissic source components, which is consistent with coeval clastic rock geochemical data.
15. Fe by analogy to the REE should also have been derived from continent, but mass balance consideration of Fe suggests a different source of Fe other than continental source. Part of the Fe was probably derived from hydrothermal exhalations, which is speculative but required to explain the geochemical data and field geological setting. The weak positive europium anomalies, $(Eu/Sm)_{SN}$ ratio grater than one and 3 epsilon unit lesser negative

εNd than basement terrain in some BIF samples also indicate such a component.

16. The late Paleoproterozoic ocean water (Gwalior Sea) was oxidizing, buffered with continent with probable alkaline pH. This is in contrast to Achaean ocean, which was reducing and was buffered with mantle.

17. The depositional age of limestone is 1914 ± 170 Ma and depositional age of BIF is 1834 ± 16 Ma, more precisely 1850 Ma. These ages agree with the existing ages of basement and mafic intrusives. The BIFs represent the last phase of main BIF metallogeny of Paleoproterozoic and are coeval to Gunflint BIFs of Canada. The considerable time lag between limestone and BIF indicate slow sedimentation rate and possible time lag is confirmed by the different Nd isotopic composition in these. The mafic dyke swarms were intruded (1791 Ma) immediately after deposition of these BIFs.

18. Sequential stepwise leaching of BIFs using HBr may help to produce a spread in Pb-isotope ratios from individual samples and thus aid in obtaining useful geochronological data. In this study, the step leaching enabled to suppress the uncertainty of isochron calculation to the limit of ±16 Ma.

19. The Nd isotopic data are capable to resolve isotopic differences even within limited temporal periods as shown in the present study. In this study, the 1914 Ma limestones and 1850 Ma BIFs of otherwise same geological formation yield contrasting εNd signals and can be attributed to the little differences in their age.

20. The Pb, Sr, Nd isotope systematics of BIFs and limestones are consistent with continental source of these elements. However Nd isotope systematics of limestones records local juvenile input from mantle. The overall isotope data is consistent with geochemical data of clastic rocks, which indicate Bundelkhand massif with ~2.5 Ga granite and 3.2 Ga TTG are the dominant source of Gwalior sediments.

REFERENCES

Abott, D.H. (1996) Plumes and hotspots as sources of greenstone belts. Lithos. 37, pp. 113-127.

Adil S.H. (1999) studies of textural parameters for clastic sediments of Gwalior group of rocks, Proc.XVI-convention, Indian Association of Sedimentologists, p-4.

Alibert C. and McCulloch, M. (1993) Rare earth element and neodymium isotopic composition of the banded iron formations and associated shales from Hammersly, western Australia. Geochimica et Cosmochimica Acta, 57, pp. 187-204.

Alibert C. and McCulloch, M. (1993) Rare earth element and neodymium isotopic composition of the banded iron formations and associated shales from Hammersly, western Australia. Geochimica et Cosmochimica Acta, 57, pp. 187-204.

Alibo, D.S. and Nozaki, Y. (1998) Rare earth elements in sea water: particle association, shale normalization and Ce oxidation. Geochimica et Cosmochimica Acta, 63, pp. 363-372.

Allen J. R. L. (1968) Current Ripples. North Holland, Amsterdam, 433 pp.

Arora, M., Naqvi, S.M. 1993. Geochemistry of Archaean arenites formed by anoxic exogenic processes - an example from Bababudan schist belt, India. J. Geol. Soc. India, 42, pp.247-268.

Aspler, L.B., Catuneanu, O., Chiarenzelli, J.R. (1998) Precambrian clastic sedimentation systems. Sediment. Geol.,120, pp.5–53.

Babinski, M., Van Schmus, W.R., Chemale Jr., F. (1999) Pb–Pb dating and Pb isotope geochemistry of Neoproterozoic carbonate rocks from the San Francisco basin, Brazil. Chem.Geol. 160, pp.175–199.

Bajpai, M. P. (1935) The Gwalior traps from Gwalior, India, Jour. Geol. 43, pp 61-75.

Balaram, V., Gnaneswara Tao, T., Anjaiah, K.V. (1999) International proficiency tests for analytical geochemistry laboratories: An assessment of accuracy and precision in routine geochemical analysis. J.Geol.Soc.Ind., 53, pp. 417-423.

Balaram, V., Ramesh, S.L. and Anjaiah, K.V. (1996) New trace element and REE data in thirteen GSF reference samples by ICP-MS. Geostandards Newsletter, 20. pp. 71-78.

Banerjee, D.M., and Bhattacharya, P. (1993) Petrology and geochemistry of greywackes from the Aravalli Supergroup, Rajasthan, India and the tectonic evolution of a Proterozoic sedimentary basin. Precamb.Res. 69, pp.11-35.

Banner, J. L. and Hanson, G. N. (1990) Calculation of simultaneous isotopic and trace element variation during water-rock interaction with applications to carbonate diagenesis. Geochim. Cosmochim. Acta 54, pp.3123-3137.

Basu, A.K (1986) Geology in parts of Bundelkhand granite massif, Central India, Record Geol.Surv.Ind, 117, part-2, pp.61-124.

Bau, M. and Möller P. (1993) Rare earth element systematics of the chemically precipitated component in early Precambrian iron formations and the evolution of the terresteial atmosphere-hydrosphere-lithosphere system. Geochim. Cosmochim. Acta 57, pp.2239-2249.

Bau, M., Dulski, P. (1996) Distribution of Y and rare-earth elements in the Penge and Kuruman Iron Formations, Traansvaal Supergroup, South Africa, Precambrian Research. 79, pp.37– 55.

Bau, M., Höhndorf, A., Dulski P, Beukes N.J (1997) Sources of Rare_Earth Elements and Iron in Paleoproterozoic Iron-Formations from the Transval Supergroup, South Africa: Evidence from Neodymium isotopes. J.Geology. 105, pp.121-129.

Bau, M., Höhndorf, A., Dulski P, Beukes N.J (1997) Sources of Rare_Earth Elements and Iron in Paleoproterozoic Iron-Formations from the Transval Supergroup, South Africa: Evidence from Neodymium isotopes. J.Geology. 105, pp.121-129.

Beukes, N.J., Klein, N.J. (1992) In: Schopf, J.W., Klein, C. (Eds.), The Proterozoic Biosphere. Cambridge University Press, Cambridge, pp. pp.147–152.

Bhat, M.I. and Ghosh, S.K. (2001) Geochemistry of 2.51 Ga old Rampur group pelites, western Himalayas: implications for their provenance and weathering. Precamb.Res. 108, pp.1-16.

Bhatia, M.R. (1983) Plate tectonics and geochemical composition of sandstones. J. Geol., 91, pp.611–627.

Bhatia, M.R., Crook, K.A.W. 1986. Trace element characteristics of graywackes and tectonic setting discrimination of sedimentary basins. Contrib. Mineral. Petrol. 92, pp.181-193.

Bhushan, S.K. (1998) Geochemistry of Archaean and Proterozoic clastic and carbonate rocks of Rajasthan, India. Gondwana Res., 1, pp. 257-265.

Biswas, S.K (1987) Regional tectonic framework, structure and evolution of western marginal basin of India. Tectonophysics, 135, pp. 307-327.

Blatt H., Middleton G. and Murray R. (1980) Origin of Sedimentary Rocks, 2nd edn. Prentice-Hall, Englewood Cliffs, 782 pp.

Boersma J. R. (1969) Internal structure of some tidal megaripples on a shoal in Westerschelde estuary, The Netherlands: Report of a preliminary investigation. Geol. Mijnb, 48, pp.409-414.

Bolhar R., Kambera B.S., Moorbath S., Fedo C.M.,Whitehoused M.J. (2004) Characterisation of early Archaean chemical sediments by trace element signatures. Earth Planet. Sci. Lett. 222, pp.43– 60

Bolhar R., Kambera B.S., Moorbath S., Fedo C.M.,Whitehoused M.J. (2004) Characterisation of early Archaean chemical sediments by trace element signatures. Earth Planet. Sci. Lett. 222, pp.43– 60

Bolhar, R., Hofmann, A., Woodhead, J., Hergt, J., Dirks, P. (2002). Pb- and Nd-isotope systematics of stromatolitic limestones from the 2.7 Ga Ngezi Group of the Beleingwe Greenstone Belt. Precambrin Res. 114, pp.277–294.

Bose, M.K. (1994) Geochemical changes in basalt across Archaean Proterozoic boundary – An evaluation of Dalma basalts from eastern Indian shield. J.Geol.Soc.Ind., 43, pp. 1-18.

Bouma, A. H. (1962) Sedimentology of some Flysch Deposits, a Graphic Approach to Facies Interpretation. Elsevier, Amsterdam, 168 pp.

Bourgeois, J. and Leithold, E. L. (1984) Wave-worked conglomerate—Depositional processes and criteria for recognition. In: Sedimentology of Gravels and Conglomerates (Ed. By E. H. Koster & R. J. Steel). Mem. Can. Soc. Petrol. Geol., 10, 331-343.

Byrne R. H.,Kump L. R.,and Cantrell K. J. (1988) The influence of temperature and pH on trace metal speciation in seawater. Mar. Chem. 25, pp.163-181.

Campbell, I.H., Griffiths, R.W. (1992) The changing nature of mantle hotspotsthrough time: Implications for the chemical evolution of mantle. J.Geol., 92, pp. 497-523.

Cantrell K. J. and Byrne R. H. (1987) Rare earth element complexation by carbonate and oxalate ions. Geochim. Cosmochim.Acta 51, pp. 597-605.

Casshyap S. M., Bhardwaj B. D., Raza M., Singh A., and Khan A. (2001) Barrier Inlet and Associated Facies of Shore Zone: An Example from Khardeola Formation of Lower Vindhyan Sequence in Chittaurgarh, Rajasthan. J. Geol. Soc. Ind., 58, pp. 97-111.

Chaudhary, A.K., Gopalan, K., Sastry, C.A. (1984) Present status of geochronology of the Precambrian rocks of Rajasthan. Tectonophysics, 105, pp. 131-140.

Cheel, R. J. and Leckie, D. A. (1990) A tidal-inlet complex in the Cretaceous epeiric sea of North America: Virgelle Member, Milk River Formation, southern Alberta, Canada. Sedimentology, 37, pp.67-81.

Clifton, H. E. (1973) Pebble segregation and bed lenticularity in wave-worked versus alluvial gravel. Sedimentology, 20, pp.173-187.

Clifton H. E., Hunter R. E. and Phillips R. L. (1971) Depositional structures and processes in the non-barred, high-energy nearshore., J. sedim. Petrol., 41, pp.651-670.

Condie, K.C and Wronkiewiez D.J (1990) The Cr/Th ratio in Precambrian pelites from the Kaapvaal craton as an index of craton evolution. Earth and Planetary Science Letters 97, pp.256-267.

Condie, K.C., 1993. Chemical composition and evolution of the upper continental crust: Contrasting results from surface samples and shales. Chem. Geol. 104, pp.1–37.

Condie, K.C., 1997. Plate Tectonics and Crustal Evolution (4th ed.). Butterworth Heinemann, Oxford.

Condie, K.C., Lee, D., Farmer, G.L. (2001) Tectonic setting and provenance of Neoproterozoic Uinta Mountain and Big Cottonwood groups, northern Utah: constraints from geochemistry, Nd isotopes, and detrital modes. Sed.Geol. 141-142, pp.443-464.

Crawford, A.R., Compston, W. (1970). The age of the Vindhyan system of peninsular India. J. Geol. Soc. London 125, pp.351–371.

Cullers,R.L. (2000) The geochemistry of shales, siltstones, and sandstones of Pennsylvanian-Permian age Colorado, U.S.A.: Implications for provenance and metamorphic studies. Lithos 51, pp.181-203.

Cullers,R.L. and Podkovyrov, V.N. (2000) Geochemistry of Mesoproterozoic Lakhanda shales in southeastern Yakutia, Russia: implications for mineralogical and provenance control, and recycling. Precamb.Res. 104, pp.77-93.

Danielson A., Moller P., and Dulski P. (1992) The europium anomalies in banded iron formations and the thermal history of the oceanic crust. Chem. Geol. 97, pp.89-100.

De Baar H.J.W., Bacon M.P., Brewer P.G. (1985a) Rare earth elements in the Pacific and Atlantic Oceans, Geochimica et Cosmochimica Acta. 49, pp.1943– 1959.

De Baar, H.J.W., Brewer, P.G., Bacon, M.P. (1985b) Anomalies in rare earth distributions in seawater: Gd and Tb, Geochimica et Cosmochimica Acta 49, pp.1961– 1969.

De Raaf, J. F. M. and Boersma, J. R. (1971) Tidal deposits and their sedimentary structures. Geol. Mijnbouw, v. 50, pp. 479-504.

De Raaf, J. F. M., Boersma, J. R. and Van Gelder, A. (1977) Wave-generated structures and sequences from a shallowmarine succession. Lower Carboniferous, County Cork, Ireland. Sedimentology, 24, pp451-483.

Deb, M. (1999) Metallic mineral deposit of Rajasthan. In Proceeding of the seminar on Geology of Rajasthan – status and perspective (ed) P Kataria (Geology Dept. M L Sukhadia univ. Udaipur, India) pp. 213-237.

Deb, M., Thorpe , R.I., Cumming , G.L., Wagner, P.A. (1989) Age, source and stratigraphic implications of Pb isotope data for the conformable, sediment hosted, in the Proterozoic Aravalli-Delhi orogenic belt, North-western India. Precamb.Res. 43, pp. 1-22.

Deb, M., Thorpe , R.I., (2004) Geochronological constraints in the Precambrian geology of Rajasthan and their metallogenic implication. In: Sediment hosted lead-zinc deposit (Edit. Deb, M. and Goodfellow, W.D.), pp. 246-263.

Derry L.A. and Jacobsen S.B. (1990) The chemical evolution of Precambrian seawater: evidence from REEs in banded iron formation, Geochim. Cosmochim. Acta 54. pp. 2965-2977.

Dubey, V. S. (1930) Helium ratio of basic rocks, Gwalior, India, Nature. Vol-126.

Elderfield H., Upstill-Goddard R., and Sholkovitz E. R. (1990) The rare earth elements in rivers, estuaries, and coastal seas and their significance to the composition of ocean waters. Geochim. Cosmochim.Acta 54, pp.971-991.

Erel Y., Harlavan Y., Stein M., and Blum J. D. (1997) U-Pb dating of Fe-rich phases using a sequential method. *Geochim.Cosmochim.Acta* 61, pp.1697–1703.

Eriksson, P.G., Condie. K.C., Tisgaard, H., Mueller, W.U., Alteramann, W., Miall, A.D., Aspler, L.B., Catuneanu, O., Chiarenzelli, J.R. (1998) Precambrian clastic sedimentation systems. Sed.Geol. 120, pp.5-53.

Eriksson, P.G., Martins-Neto, M.A., Nelson,D.R., Aspler, L.B., Chiarenzelli, J.R., Catuneanu, O., Sarkar, S., Altermann, W., Rautenbach, C.J.W., (2001) An introduction to the Precambrian basins: their characteristics and genesis. Sediment. Geol., 141-142, pp.5–53.

Faure G. (1986) Principles of Isotope Geology. Wile, 589pp.

Fedo, C.M., Eriksson, K.A., Krogstad., E.J. 1996. Geochemistry of shales from the Archaean (~3.0) Bhuwa Greenstone belt, Zimbabwe: Implications for provenance and source - area weathering. Geochim. Cosmochim. Acta 60, pp.1751-1763.

Fedo, C.M., Nesbitt, H.W., Young, G.M. 1995. Unraveling the effects of potassium metasomatism in sedimentary rocks and paleosols, with implications for paleoweathering conditions and provenance. Geology 23, pp. 921-924.

Fedo, C.M., Young, G.M., Nesbitt, H.W., Hanchar, J.M. 1997. Potassic and sodic metasomatism in the Southern Province of the Canadian Shield : Evidence from the Paleoproterozoic Serpent Formation, Huronian Supergroup, Canada. Precamb. Res. 84, pp.17-36.

Fee J. A.,Gaudette H. E.,Lyons W. B., and Long D. T. (1992) Rare-earth element distribution in Lake Tyrrell groundwaters,Victoria, Australia. Chem. Geol. 96, pp.67-93.

Fralick, P.W., Davis, D.W., Kissin, S.A., 2002. The age of the Gunflint Formation, Ontario, Canada: single zircon U–Pb age determinations from reworked volcanic ash. Can. J. Earth Sci. 39, pp.1085–1091.

Frei R., Villa I. M., Na¨gler Th. F., Kramers J. D., Przybylowicz W. J., Prozesky V. M., Hofmann B. A., and Kamber B. S. (1997) Single mineral dating by the Pb-Pb step-leaching method; assessing the mechanisms. *Geochim. Cosmochim. Acta* 61, pp.393–414.

Frei, R., Bridgwater, D., Rosing, M., Stecher,O. (1999) Controversial Pb-Pb and Sm-Nd isotope results in the early Archean Isua (West Greenland) oxide iron formation: Preservation of primary signatures versus secondary disturbances. Geochim.Cosmochim.Act., Vol. 63, pp.473–488.

Fryer B. J. (1983) Rare earth elements in iron formation. In Iron Formations: Facts and Problems. (ed. A. Trendall and R. C. Morris), pp. 345-358.Elsevier.

Galloway, W.E., Hobday, D.K., 1983. Terrigenous Clastic Depositional Systems. Springer-Verlag, New York, 423p.

Gao, S and Wedepohl, K.H. 1995. The negative Eu anomaly in Archaean sedimentary rocks : Implications for decomposition, age and importance of their granitic sources. Earth Planet. Sci. Lett. 133, pp.81-94.

Garrels R. M. (1987) A model for the deposition of the microbanded Precambrian iron formations. Am. J. Sci. 287, pp.81-106.

Garrels, R.M. and Mackenzie, F.T. (1971) The evolution of sedimentary rocks. W.W.Norton, New York.

German C.R., Elderfield H. (1989) Rare earth elements in Saanich Inlet, British Columbia, a seasonally anoxic basin, Geochimica et Cosmochimica Acta. 53, pp.2561– 2571.

German C.R., Holliday B.P., Elderfield H. (1991) Redox cycling of rare earth elements in the suboxic zone of the Black Sea, Geochimica et Cosmochimica Acta. 55, pp.3535–3558.

German C.R., Masuzawa T., Greaves M.J., Elderfield H., Edmond J.M. (1995) Dissolved rare earth elements in the Southern Ocean: cerium oxidation and the influence of hydrography, Geochimica et Cosmochimica Acta. 59, pp.1551–1558.

Gibbs A.K, Montgomery C.W.P, Day P.A, Ersley E.A (1986) The Archean-Proterzoic transition: evidence from the geochemistry of metasedimentary rocks of Guyana and Montana. Geochim.Cosmochim.Acta, 50, pp.2125-2141.

Gnaneshwar Rao, T., Naqvi, S.M. (1995)Geochemistry, depositional environment and tectonic setting of the BIF's of the late Archaean Chitradurga schist belt, India. Chem. Geol. 121, pp.217– 243.

Goldstein, S. J. and Jacobsen, S. B. (1987) The Nd Sr isotope systematics of river-water dissolved material: Implications for the sources of Nd and Sr in sea water. Chem. Geol. (Isot. Geosci. Sect.) 66, pp.245-272.

Goldstein S. J. and Jacobsen S. B. (1988a) Nd and Sr isotopic systematics of river water suspended material: Implications for crustal evolution. Earth Planet. Sci. Lett. 87, pp.249-265.

Goldstein S. J. and Jacobsen S. B. (1988b) Rare earth elements in river waters. Earth Planet. Sci. Lett. 89, pp.35-47.

Goldstein S. J. and Jacobsen S. B. (1988c) Rare earth elements in the Great Whale estuary, NW Quebec. Earth Planet. Sci. Lett. 88, pp.241-252.

Gopalan K., Macdougall J.D., Roy A.B., Murali A.V. (1990) Sm-Nd evidence for 3.3 Ga old rocks in Rajasthan, northwestern India. PrecambrianRes. 48, pp.287-297.

Gromet, L.P., Dymek, R.F., Haskin, L.A., Korotev, R.L. (1984) The "North American Shale Composite": its compilation , major and trace-element characteristics. Geochim.Cosmochim.Acta, 48, pp.2469-2482.

Hacket, C. A. (1870) Geology of Gwalior & Vicinity, Rec. Geol. Surv. Ind. Vol-3(2), pp 33-42.

Hamade, T., Konhauser, K.O., Raiswell, R., Goldsmith, S., Morris,R.C. (2003) Using Ge/Si ratios to decouple iron and silica fluxes in Precambrian banded iron formations. Geology 31, pp.35–38.

Harms, J. C., Southard, J. B. and Walker, R. G. (1982) Structures and sequences in clastic rocks. Soc. Econ. Paleont. Miner., Short Course, 9, 251 pp.

Harnois, L.(1988) The CIW index: a news index of weathering. Sediment.Geol. 55, pp.319-322.

Harris, C.W., Eriksson, K.A., 1990. Allogenic controls on the evolution of storm to tidal shelf sequences in the Early Proterozoic Uncompahgre Group, southwest Colorado, U.S.A. Sedimentology 37, pp.189–213.

Hayes M. O. (1967) Hurricanes as geologic agents, south Texas coast. Bull. Am. Ass. Petrol. Geol., 51, pp.937-942.

Hayes M. O. and Boothroyd J. C. (1969) Storms as modifying agents in the coastal environment. Soc. of Econ. Paleont. and Mineral., Eastern Section, Guide Book, pp. 245-265.

Heron, A. M. (1922) The Gwalior and Vindhyan system in SE Rajputana: Mem. Geol. Surv. Ind. Vol-45(2), pp 135-145.

Holland H. D. (1984) The chemical evolution of the atmosphere and the oceans. Princeton University Press, Princeton, N. J.

Holland, H.D., Feekes, C.R., Żbinden, E.A. (1989) The Flin Flon paleosol and the composition of the atmosphere 1.8 BYBP. Am. J. Sci. 289, pp.362–389.

Holland, H.D., Beukes, N.J. (1990) A paleoweathering profile from Griqualand West, South Africa: evidence for a dramatic rise in atmospheric oxygen between 2.2 and 1.9 BYBP. Am. J. Sci. 290A, pp.1–34.

Hoyt J. H. and Henry V. J. (1967) Influence of inlet migration on barrier island sedimentation. Geol. Soc. Amer. Bull., 78, pp. 77-86.

Hubbard D. K. (1977) Variations in tidal inlet processes and morphology in the Georgia Embayment. University of South Carolina, Technical Report No. 14-CRD, 79 pp.

Isley, A.E., 1995. Hydrothermal plumes and the delivery of iron tobanded iron formation. J. Geol. 103, pp.169– 185.

Isley, A.E., Abbott, D.H., 1999. Plume-related mafic volcanism and the deposition of banded iron-formation. J. Geophys. Res. 104, pp.15461– 15477.

Jackson, M.J., Simpson, E.L., Eriksson, K.A., 1990. Facies and sequence stratigraphic analysis in an intracratonic, thermal-relaxation basin: the Early Proterozoic, Lower Quilalar Formation and Ballara Quartzite, Mount Isa Inlier, Australia. Sedimentology 37, pp.1053–1078.

Jacobsen S. B. and Pimentel-Klose M. R. (1988a) A Nd isotopic study of the Hamersley and Michipicoten banded iron formations: the source of REE and Fe in Archean oceans. *Earth Planet. Sci. Lett.* 87, pp.29–44.

Jacobsen S. B. and Pimentel-Klose M. R. (1988b) Neodymium isotopic variations in Precambrian banded iron-formations. Geophys. Res. Lett. 15/4, pp.393-396.

Jahn, B.M., Cuvellier, H., (1994). Pb–Pb and U–Pb geochronology of carbonate rocks: an assessment. Chem. Geol. 115, pp.125–151.

Jain S.C., Gaur V.P., Srivastava S.K., Nambiar K.V., Saxena H.P. (2001) Recent find of a cauldron structure in Bundelkhand vraton. Geol.Surv.Ind.Spl.Pub.No. 64, pp.289-297.

James, H.L. (1983) Distribution of banded iron-formation in space and time. In: A.F.Trendal and R.C.Morris (Ed.) Iron-formation facts and problems. Elsevier Amsterdam. pp.471-490.

Johnson, H.D., Baldwin, C.T., 1986. Shallow siliciclastic seas. In: Reading, H.G. (Ed.), Sedimentary Environments and Facies. Blackwell, Oxford, pp. 229–282.

Khan, R.M.K., Das Sharma, S., Patil, D.J. and Naqvi, S.M. (1996) Trace, rare-earth element, and Oxygen isotopic systematics for the genesis of banded Iron-formations: Evidence from Kushtagi schist belt, Archaean Dharwar Craton, India; Geochimica et Cosmochimica Acta, 60, pp.3285-3294.

Kim K.H., Byrne R.H., Lee J.H. (1991) Gadolinium behaviour in seawater: a molecular basis for gadolinium anomalies, Marine Chemistry. 36, pp.107–120.

Klein, C and Beukes, N.J. (1992a) Time distribution, stratigraphy and sedimentologic setting and geochemistry of Precmbrian iron-formations. In: J.W.Schopf and C.Klein (Ed.) , The Proterozoic Biosphere, a multidisciplinary study. Cambridge University Press. New York. N.Y., pp.140-146.

Klein, C and Beukes, N.J. (1992b) Proterozoic iron-formations. In: K.C.Condie (Ed.) Proterozoic crustal evolution, Elsevier Amsterdam. pp.383-418.

Klein, C., Beukes, N.J. (1989) Geochemistry and sedimentology of facies transition from limestone to iron –formation deposition in the early Proterozoic Transvaal Supergroup, South Africa. Econ.Geol. 84, pp.1733-1742.

Klein, G., De V. (1970) Depositional and dispersal dynamics of intertidal sand bars. Jour. Sediment. Petrol. V. 40, pp. 1095-1127.

Klein, G. De V. (1977a) Clastic tidal facies. CEPCO,Champaign,Illinois, 149 pp.

Klinkhammer G. P., Elderfield H., Edmond J. M., and Mitra A. (1994) Geochemical implications of rare earth element patterns in hydrothermal fluids from mid-ocean ridges. Geochim. Cosmochim. Acta 58, pp.5105-5113.

Klinkhammer G., Elderfield H., and Hudson A. (1983) Rare earth elements in seawater near hydrothermal vents. Nature 305, pp.185-188.

Kumar, N., Sanders, J.E., 1974. Inlet sequence: a vertical succession of sedimentary structures and textures created by the lateral migration of tidal inlets. Sedimentology 21, pp.491–532.

Kumar N., Sanders J.E. (1975) Inlet sequence formed by the migration of Fire Island Inlet, Long Island, New York. In: R. N. Ginsburg (Ed.), Tidal Deposits, Springer-Verlag, New York, pp. 75-83.

Kumar, B., Srivastava, R.K., Jha, D.K., Pant, N.C., Bandaru, B.K. (1990) A revised stratigraphy of the rocks of type area of the Bijawar Group in Central India. Indian minerals, 44, pp. 303-314.

Lahtinen, R. (2000) Archaean-Proterozoic transition: geochemistry, provenance and tectonic setting of metasedimentary rocks in central Fennoscandian Shield, Finland. Precamb.Res. 104, pp.147-174.

Leckie, D. A., Walker, R. G. (1982) Storm- and tide-dominated shorelines in Cretaceous Moosebar-Lower Gates interval-outcrop equivalents of deep basin gas trap in Western Canada. Bull. Am. Ass. Petrol. Geol., 66, pp.138-157.

Levell B. K. (1980a) Evidence for currents associated with waves in Late Precambrian shelf deposits from Finnmark, North Norway. Sedimentology., 27, pp.153-166.

Levell, B.K., (1980b). A late Precambrian tidal shelf deposit, the Lower Sandfjord Formation, Finnmark, North Norway. Sedimentology 27, pp.539–557.

Ludwig, K.R. (1999) Using isoplot/ Ex, version 2.1: a geochronological tool for Microsoft Excell, vol. 1A. Berkley Geochron.Cen. sp. Pub., p 47.

Macfarlane, W.A., Danielson, A., and Holland, H.D. (1994) Geology, major and trace element chemistry of of Late Archean weathering profiles in the Fortescue Group, Western Australia: Implications for atmospheric PO_2; Precamb.Res. 65, pp.297-317.

Mallikharjuna Rao, J., Poornachandra Rao, G.V.S., Widdowson, M. and Kelly, S.P. (2005) Evolution of Proterozoic mafic dyke swarns of the Bundelkhand Granite Massif, Central India. Curr.Sc. 88, pp. 502-506.

Manikyamba, C., Naqvi, S.M., Moeen, S., Gnaneshwar Rao, T., Balaram, V., Ramesh, S.L., Reddy, G.L.N. 1997. Geochemical heterogeneties of metagraywackes from the Sandur schsit belt: implications for active plate margin processes. Precamb. Res. 84, pp.117-138.

Martin J.M., Hogdahl O., Philippot J.C. (1976) Rare earth element supply to the oceans, J. Geophys.Res. 81, pp.3119-3124.

Martin, H. (1987) Petrogenesis of Archean trondhjemite tonalities, and granodiorites from eastern Finland: Major and trace element geochemistry. J.Petrol. 28, pp.921-953.

Martin, H. (1993) The mechanisms of petrogenesis of the Archean continental crust composition with modern processes. Lithos 30, pp.373-388.

Mathur S.M (1982) Precambrian sedimentary sequences of India: Their geochronology and correlation, Precamb.Res., 18: pp. 139-144.

McLennan, S.M. (1982) On the geochemical evolution of sedimentary rocks. Chem.Geol. 37, pp.335-350.

McLennan, S.M., Hemming, S., Taylor, S.R., Erikson, K.A. (1995) Early Proterozoic crustal evolution: Geochemical and Nd-Pb isotopic evidence from metasedimentary rocks southwestern North America. Geochim.Cosmochim.acta. 59, pp.1153-1173.

McLennan, S.M., Taylor, S.R. 1991. Sedimentary rocks and crustal evolution: tectonic setting and secular trends. J. Geol. 99, pp.1-21.

McLennan, S.M., Taylor, S.R., McCulloch, M.T. and Maynard, J.B. (1990) Geochemical and Nd-Sr isotopic composition of deep-sea turbidites: Crustal evolution and plate tectonic associations. Geochim. Cosmochim. Acta, 54, pp.2015–2050.

Medlicott, H. B. (1875) Sketch of the geology of Scindia's territories: Rec. Geol. Surv. Ind. Vol-(8)(2), pp 58-59.

Miall, A. D. (1977) A review of the braided-river depositional environment. Earth-Sci. Rev., 13, pp.1-62.

Miall, A. D. (1985) Architectural-element analysis: A new method of facies analysis applied to fluvial deposits. Earth-Sci. Rev., 22, pp.261-308.

Michard A., Albare'de F. (1986) The REE content of some hydrothermal fluids, Chemical Geology. 55 (1 – 2), pp.51–60.

Michard A.,Albarede F., Michard G., Minster J. F., Charlou J. I. (1983) Rare earth elements and uranium in high temperature solutions from the Fast Pacific Rise hydrothermal vent fields (18°). Nature 303, pp.795-797.

Miller R. G. and O'Nions R. K. (1985) Source of Precambrian chemical and clastic sediments. *Nature* 314, pp.325–329.

Mondal M.E.A & Ahmad T (2001) Bundelkhand mafic dykes, central indian shield: Implications for role of sediment subduction in Proterozoic crustal evolution. Island Arc, 10, pp.51-67.

Mondal, M.E.A & Zainuddin, S.M (1996) Evolution of Archean-Palaeoproterozoic Bundelkhand massif, central india- evidence from granitoid geochemistry. Terra nova, 8, pp.532-539.

Mondal, M.E.A. and Zainuddin, S.M. (1997) Geochemical characteristics of Bundelkhand massif, central India. J.Geol.Soc.India. 50, pp.69-74.

Mondal M.E.A., Deomurari, M.P., Goswami, J.N., Rahman, A., Sharma, K.K. (1997) $^{207}Pb/^{206}Pb$ zircon ages of samples from the Bundelkhand massif, Central India, (abstract) International conference on isotopes in Solar systems, Ahmedabad. India.

Mondal M.E.A., Sharma, K.K., Rahman, A., Goswami, J.N. (1998) Ion microprobe $^{207}Pb/^{206}Pb$ zircon ages for gneiss-granitoid rocks from Bundelkhand massif: Evidence for Archean components. Current Science, 74, pp.70-75.

Mondal M.E.A.(2002) Geochemistry and petrogenesis of the Archean-Proterozoic gneisses and granitoids from central Indian shield. J.appl.Geoch., 4, pp.170-182.

Mondal M.E.A., Goswami, J.N., Deomurari, M.P. Sharma, K.K., (2002) Ion microprobe $^{207}Pb/^{206}Pb$ ages of zircon from the Bundelkhand massif, northern India: implications for crustal evolution of the Bundelkhand-Aravalli protocontinent. Precamb.Res. 117, pp.85-100.

Moorbath S., O'Nions R. K., and Pankhurst R. J. (1973) Early Archean age for the Isua iron formation, West Greenland. *Nature* 245, pp.138–139.

Moorbath, S., Taylor, P.N. (1981) Isotopic evidence for continental growth in the Precambrian. In: Kröner, A. (ed.), Precambrian Plate Tectonics. Elsevier, Amsterdam, pp. 491-525.

Moorbath, S., Taylor, P.N., Orpen, J.L., Treloar, P., Wilson, J.F. (1987) First direct radiometric dating of Archean stromatolitic limestone. Nature 326, pp.865–867.

Nägler Th. F., Pettke T., and Marshall D. (1995a) Initial isotopic heterogeneity and secondary disturbance of the Sm-Nd system in fluorites and fluid inclusions: A study on mesothermal veins from the central and western Swiss Alps. *Chem. Geol.* 125, pp.241–248.

Nägler Th. F., Holzer L., and Frei R. (1995b) Nd and Pb in monazite inclusions within polymetamorphic garnets: Hell or heaven? *Eos.Trans. Amer. Geophys. Union* 76, F707.

Nägler Th. F., Holzer L., and Frei R. (1996) What dominates the Nd and Pb characteristics of garnet? *Journal of Conference Abstracts,Sixth V.M. Goldschmidt conference, 31 March–4 April, Heidelberg,Germany,* 1, 424.

Naqvi, S.M., Hussain, S.M. (1972) Petrochemistry of early Precambrian metasediments from the central part of the Chitradurga schist belt, Mysore, India. Chem. Geol. 10, pp.109-135.

Naqvi, S.M and Rogers, J.J.W (1987) Precambrian Geology of India. Oxford Monographs on Geology and Geophysics. No.6, Oxford University Press.

Naqvi, S.M., Sawkar, R.H., Subba Rao, D.V., Govil, P.K., Gnaneshwar Rao, T. (1988) Geology and geochemistry and tectonic setting of Archaean graywackes from Karnataka Nucleus, India. Precamb. Res. 39, pp.193-216.

Naqvi, S.M., Uday Raj, B., Subba Rao, D.V., Manikyamba C., Nirmal Charan, S., Balaram, V., Sarma, D.S. (2002) Geology and geochemistry of arenite-quartzwacke from the Late Archean Sandur schist belt-implications for provenance and accretion processes. Precamb.Res. 114, pp.177-197.

Nelson C. H. (1982) Modern shallow-water graded sand layers from storm surges, Bering Shelf: a mimic of Bouma sequences and turbidite systems. J. sedim. Petrol., 52, pp.537-545.

Nelson, D.R. (1998) Granite-greenstone crust formation on the Archean Earth – a consequence of two superimposed processes. Earth Planet.Sc.Lett. 158, pp.109-119.

Nemec, W., Muszynski, A. (1982) Volcani clastic alluvian aprons in the Tertiary of Sofia District (Bulgaria). Ann. Soc. Geol. Pol., 52, pp.239-303.

Nemec, W., Postma, G. (1993) Quarternary alluvial fans in south western Crete: Sedimentation processes and geomorphic evolution. In: Alluvial Sedimentation (Ed. by M. Marzo and C. Puigdefabregas), Spec. Pnbl. Int. Ass. Sediment., 17, pp. 235-276.

Nemec, W., Steel, R. J. (1984) Alluvial and coastal conglomerates: Their significant features and some comments on gravelly mass-flow deposits. In: Sedimentology of Gravels and Conglomerate (Ed. by E. H. Koster & R. J. Steel). Mem. Can. Soc. Petrol. Geol., 10, pp.1-31.

Nesbitt, H.W., Marcovics, G., Price, R.C. (1980) Chemical processes affecting alkalis and alkaline earth during continental weathering. Geochim.Cosmochim.Acta, 44, pp.1649-1666.

Nesbitt, H.W., Young, G.M. 1982. Early Proterozoic climates and plate motion inferred from major element chemsitry of lutites. Nature 299, pp.715-717.

Nesbitt H.W and Young G.M (1984) Prediction of some weathering trend of plutonic and volcanic rocks based on thermodynamic and kinetic consideration. Geochim.Cosmochim.Acta, 48, pp.1523-1534.

Nesbitt, H.W., Fedo, C.M.,Young, G.M. (1997) Quartz and feldspar stability, steady and non-steady state weathering and petrogenesis of siliciclastic sands and muds. Jour.Geology. 105, pp.173-191.

Nesbitt, H.W., Young, G.M., McLennan, S.M. and Keays, R.R. (1996) Effects of chemical weathering and sorting on the petrogenesis of siliciclastic sediments, with implications for provenance studies. J. Geol., 104, pp.525–542.

Nottvedt, A., Kreisa, R. D. (1987) Model for the combined-flow origin of Hummocky cross-stratification. Geology, 15, pp.357-361.

Oomkens, E. (1974) Lithofacies relations in the Late Quaternary Niger delta complex. Sedimentology, 21, pp. 701-710.

Palmer, M.R., Elderfield,H. (1985) Variations in the Nd isotopic composition of foraminifera from Atlantic Ocean sediments. Earth Planet. Sci. Lett. 73, pp.299–305.

Pandey, B.K., Gupta J.N., Sarma, K.J., Sastry, C.A. (1987) Sm-Nd, Pb-Pb, Rb-Sr geochronology and petrogenesis of the mafic dyke swarm of Mahbubnagar, South India: implications for the Paleoproterozoic crustal evolution of the Eastern Dharwar Craton. Precamb.Res., 84, pp. 181-196.

Pandey, B.K., Chabria, T., Gupta J.N. (1995) Geochronological characterization of the Proterozoic terrains of Peninsular India: relevance to the first order target selection for uranium exploration. Expl. and Res. Atomic Minerals, 8, pp.187-213.

Paola, C., Wiele, S. M., Reinhart, M. A. (1989) Upper regime parallel lamination as the result of turbulent sediment transport and low-amplitude bed forms. Sedimentology, 36, pp.47-59.

Piepgras D.J. and Jacobsen S.B. (1978) Rare earth elements and Nd isotopes in the N.Pacific (Abstr.). Eos 68, pp.470.

Piepgras D. J. and Wasserburg G. J. (1980) Neodymium isotopic variations in seawater. Earth Planet. Sci. Lett. 50, pp.128-138.

Polat, A., Kerrich, R., Wyman, D.A. (1998) The late Archean Schreiber-Hemlo and White River-Dayohessarah greenstone belts, Superior province: Collages of oceanic plateus, oceanic arcs, and subduction-accretion complexes. Tectonophysics., v. 289, pp. 295-326.

Potter, P.E. and Pettijohn, F.J. (1963) Paleocurrents and basin analysis. Springer-Verlag. pp. 296.

Puchtel, I.S., Hofmann, A,W., Mezger, K., Jochum, K.P., Schhipansky, A.A., Samsonov., A.V. (1998) Oceanic plateu model for continental crustal growth in the Archean: a case study from the Kostomukhsha greenstone belt, NW Baltic Shield. Earth Planet.Sc.Lett. 155, pp.57-74.

Qing H. and Mountjoy E. W. (1994) Rare earth element geochemistry of dolomites in the middle Devonian Presqu'ile barrier, western Canada sedimentary basin: implications for fluid-rock ratios during dolomitization. Sedimentology 41, pp.787-804.

Qureshy, M.N. and Iqbaluddin (1992) A review of the geophysical constraints in modelling the Gondwana Crust in India. Tectonophysics, 212, pp.141-151.

Radhakrishna, B.P. (1983) Archean granite-greenstone terrain of the South Indian Shield. In: Preccambrian of South India, Naqvi, S.M., Rogers, J.J.W. (Eds.), Mem.Geol.Soc.India, pp. 1-46.

Radhakrishna, B.P., Ramkrishnan, M. (1988) Archaean-Proterozoic boundary in India. J.geol.Soc.Ind., v. 32, pp. 263-278.

Radhakrishna, B.P.,Naqvi, S.M. (1986) Precambrian continental crust of India and it's evolution. J.Geol. , v. 94, pp. 145-166.

Rasmussen, B., Bose, P.K., Sarkar, S., Banerjee, S., Fletcher, I.R., McNaughton, N.J., 2002. 1.6 Ga U–Pb zircon age for the Chorhat Sandstone, lower Vindhyan, India. Geology 30, pp.103–106.

Ray, J.S., Martin, M.W., Veizer, J., Bowring, S.A., 2002. U–Pb zircon dating and Sr isotope systematics of the Vindhyan Supergroup, India. Geology 30, pp.131–134.

Ray, J.S., Veizer, J., Davis, W.J. (2003) C, O, Sr and Pb isotope systematics of carbonate sequences of the Vindhyan Supergroup, India: age, diagenesis, correlations and implications for global events. Precambrian Res. 121, pp.103–140.

Raza, M, Cashyap, S.M., Khan, A. (2002) Geochemistry of Mesoproterozoic Lower Vindhyan shales from Chittaurgarh, Southeastern Rajasthan and its bearing on Source Rock Composition, Paleoweathering conditions and Tectono-sedimentary environments. J.Geol.Soc.Ind., 60, pp.505-578.

Reading H. G. and Collinson J. D. (1996) Clastic coasts. In: H. G. Reading (Ed.), Sedimentary Environments: Processes, Facies and Stratigraphy. Blackwell Science Ltd. Oxford, pp. 154-231.

Reimer, T.O. (1985) Volcanic rocks and and weathering in the Plaleoproterozoic Witwatersand Supergroup, South Africa. Geol.Surv.Finland Bull.331, pp.33-49.

Reinson G. E. (1984) Barrier island and associated strand-plain systems. In: R. G. Walker (Ed.), Facies Models (Second Edition), Geoscience Canada, Reprint Series 1, pp. 119-140.

Roser, B.P. and Korsch, R.J. (1986) Determination of tectonic setting of sandstone-mudstone suites using SiO2 and K2O/Na2O ratio. J. Geol., 94, pp.635–650.

Roser, B.P. and Korsch, R.J. (1988) Provenance signatures of sandstone-mudstone suites determined using discrimination function analysis of major-element data. Chem. Geol., 67, pp.119–139.

Roy A.K., Saxena D.N. (2000) Annual report of field season programme1999-2000. Atomic Minerals Directorate for Exploration and Research, Northern Region. (unpublished)

Roy, A.B., Kroner, A; Laul, V (2001) Detrital zircons constraining basement age in a late Archaean green stone belt of south-eastern Rajasthan, India, Current Science, 81, pp. 407-410.

Rye, R. and Holland, H.D. (1998) Paleosols and the evolution of atmospheric oxygen:critical review. Am.J.Sci. 298, pp.621-672.

Saha A, Basu A.R., Garzione C.N., Bandyopadhyay P.K., Chakrabarti A. (2004) Geochemical and petrological evidence for subduction-accretion processes in the Archean Eastern Indian Craton. Earth and Planetary Science Letters., 220, pp.91-106.

Sambasiva Rao V.V.S, Sreenivas B, Balaram V, Govil P.K, Srinivasan R (1999) The nature of Archean upper crust as revealed by the geochemistry of the Proterozoic shales of the Kaladgi basin, Karnataka, southern India. . Precamb.Research 98, pp. 53-65.

Sarangi, S., Gopalan, K., Kumar. S. (2004) Pb–Pb age of earliest megascopic, eukaryotic alga bearing Rohtas Formation, Vindhyan Supergroup, India: implications for Precambrian atmospheric oxygen evolution. Precamb. Research. 132, pp.107–121.

Sarkar, A, Ghosh, S., Sighai, R.K., Gupta, S.N. (1997) Rb- Sr geochronology of the Dargawan sill: constrain on the age of the type Bijawar sequence of Central India. International conference on isotopes in the solar system, Nov. 11-14, 1997. (Abst.vol.) pp. 100-101.

Sarkar, A., Paul, D.K., Potts, P.J. (1996) Geochronology and geochemistry of Mid-archean trondhjemitic gneisses from the Bundelkhand craton, Central India. Rec.Res.Geol.Geophy.Precambrians. 16 pp. 76-92.

Sarkar, A., Trivedi, J.R., Gopalan, K., Singh, P.N., Das, A.K., Paul, D.K. (1984) Rb-Sr geochronology of Bundelkhand granite complex in the Jhansi-Babina-Talbehat sector, U.P., India. Indian J.Earth Sci. CESIM seminar vol., pp. 64-72.

Sarkar, S.N., Miller, J.A. (1996) Potassium-argon age from Bundelkhand granite and associated rocks and their comparison with the rubidium-strontium isochron ages. Indian J.Earth Sci. 23, pp. 71-78.

Schau, M. and Henderson, J.B. (1983) Archean chemical weathering at three localities on the Canadian Shield. Precamb.Res.20, pp.189-224.

Sengupta S., Paul D.K., deLaeter J.R., McNaughten N.J., Bandopadhyay P.K., deSmeth J.B. (1991) Mid-Archean evolution of the eastern Indian craton: Geochemical and isotopic evidence from Bonai pluton, Precamb. Res. 49, pp.23-37.

Sharma, M., Basu A.R., Ray S.L. (1994) Sm-Nd isotopic and geochemical study of the Archean tonalite-amphibolite association from the eastern Indian Craton, Cont. Min. Pet., 117, pp.45-55.

Sharma, K.K & Rahman, A (1995) Occurrence and petrogenesis of Loda Pahar trondhjemitic gneiss from bundelkhand craton, central India: Remnant of early crust. Curr.Sc. 69, pp.613-616.

Sharma, K.K. (1998) Geological evolution and crustal growth of the Bundelkhand craton and its relicts in the sorrounding regions, N. Indian Shield. In: Paliwal, B.S. (Ed.), The Indian Precambrian. Scientific Publishers, India, pp. 33-43.

Sharma, K.K. and Rahman, A (2000) The early Archaean-Paleoproterozoic crustal growth of Bundelkhand Craton, Northern Indian Shield. In: (Ed. M.Deb) Crustal evolution and metallogeny in the Northwestern Indian Shield, Narosa Pub.House, New delhi, pp.51-72.

Sharp Z. D. (1991) Determination of oxygen diffusion rates in magnetite from natural isotopic variations. *Geology* 19, pp.653–656.

Shields G., Veizer J. (2002) Precambrian marine carbonate isotope database: version 1.1. Geochem.Geophys.Geosys. 3, U1-U12.

Shimizu H., Umemoto N., Masuda A., and Appel P. W. U. (1990) Sources of iron-formations in the Archean Isua and Malene supracrustals, West Greenland: Evidence from La-Ce and Sm-Nd isotopic data and REE abundances. *Geochim. Cosmochim. Acta* 54, pp.1147–1154.

Shimizu H., Umemoto N., Masuda A., and Appel P. W. U. (1990) Sources of iron-formations in the Archean Isua and Malene supracrustals, West Greenland: Evidence from La-Ce and Sm-Nd isotopic data and REE abundances. *Geochim. Cosmochim. Acta* 54, pp.1147–1154.

Sholkovitz E.R. (1988) Rare earth elements in the sediments of the North Atlantic Ocean, Amazon delta and East China sea: Reinterpretation of terrigenous input patterns to the ocean. Amer. J. Sci. 288, pp.236-281.

Sholkovitz E.R., Landing W.M., Lewis B.L. (1994) Ocean particle chemistry: the fractionation of rare earth elements between suspended particles and seawater, Geochimica et Cosmochimica Acta. 58. pp.1567– 1579.

Spivack, A.J., Wasserburg, G.J., 1988. Neodymium isotopic composition of the Mediterranean outflow and the eastern North Atlantic. Geochim. Cosmochim. Acta 52, pp.2767–2773.

Sreenivas, B. and Srinivasan, R. (1994) Identification of paleosol in the precambrian metapelite assemblage of Peninsular India- A major element geochemical approach. Curr.Csi. 67, pp.89-94.

Sreenivas, B., Das Sharma, S., Kumar, B., Patil, D.J, Srinivasan, R. (2001) Positive d13C excursion in carbonate and organic fractions from the Paleoproterozoic Aravalli Supergroup, Northwestern India. Precamb. Res., v.106, pp. 277-290.

Sreenivas, B; Sreenivasan, S; Roy, A.B. (1999) Geochemical changes across the Archean-Proterozoic boundary – A case study from the Udaipur area of Aravalli Mountain Belt, Rajasthan, India; In Proceeding of the seminar on Geology of Rajasthan – status and perspective (ed) P Kataria (Geology Dept. M L Sukhadia univ. Udaipur, India) pp. 57-86.

Srinivasan, R. and Naqvi, S.M. (1990) Some distinctive trends in the evolution of Early Precambrian (Archaean) Dharwar Craton, South India. In: Precambrian continental crust and its economic resources (ed.) S M Naqvi (Amsterdam: elsevier), pp.245-266.

Stecher O., Carlson R. W., Shirey S. B., and Nielson T. (1986) Nd isotope evidence for the evolution of metavolcanic rocks from the Archaean block of Greenland and Labrador. *Terra Cognita* 6, pp.236.

Swift D. J. P. (1968) Coastal erosion and transgressive stratigraphy. J. Geol., 76, pp.444-456.

Swift D. J. P., Hudelson P. M., Brenner R. L. and Thompson P. (1987) Shelf construction in a foreland basin: storm beds, shelf sandbodies, and shelf-slope depositional sequences in the Upper Cretaceous Mesaverde Group, Book Cliffs, Utah. Sedimentology, 34, pp.423-457.

Taira A. and Scholle P. (1979) Origin of bimodal sands in some modern environments. Jour. Sed. Pet., v. 49(3), pp. 777-786.

Tankard, A. J. & Hobday, D. K. (1977) Tide-dominated back-barrier sedimentation, early Ordovician Cape Basin, Cape Peninsula, South Africa. Sediment.Geol., 18, pp.135-159.

Taylor, S.R., McLennan S.M. (1985) The Continental Crust: its Composition and its Evolution, Blackwell, Oxford, 312 pp.

Taylor, S.R. and McLennan, S.M. (1988) The significance of rare earths in geochemistry and cosmochemistry. in Gschneider, K.A.Jr., and Eyring,L., eds., Hand book on the Physics and Chemistry of Rare Earths, vol.11: Amsterdam. Elsevier, pp. 485-578.

Taylor, S.R. and McLennan, S.M. (1995) The geochemical evolution of the continental crust. Rev.Geophysics. 33/2, pp.241-265.

Trendall, A.F. and Morris, R.C Eds. (1983) Iron-formation facts and problems. Elsevier. 558pp.

Uhlir, D. M., Akers A. and Vondra, C. F. (1988) Tidal inlet sequence, Sundance Formation (Upper Jurassic), north-central Wyoming. Sedimentology ., 35, pp.739-752.

Varadarajan,S & Verma, V. K. (1971) On the nature of contact between Gwalior sill and Kaimur sandstones around Gwalior. Madhya Pradesh. Curr.Sci. 40, pp. 404-406.

Varadarajan,S & Verma, V. K. (1973) Mineralogy & Petrochemistry of differentiated sills around Gwalior city M. P. Jour. Geol. Soc. Ind. 14, pp. 384-393.

Veizer J. and Compston W. (1976) $^{87}Sr/^{86}Sr$ in Precambrain carbonates as an index of crustal evolution. Geochim. Cosmochim. Acta 40, pp. 905-914.

Veizer J., Compston W., Hoefs J., and Nielsen H. (1982) Mantle buffering of the early oceans. Naturwissenschaftem 69, pp.173-180.

Veizer J., Clayton R. N., Hinton R. W., Von Brunn V., Mason T. R., Buck S. G., and Hoefs J. (1990) Geochemistry of Precambrian carbonates: III. Shelf seas and non-marine environments of the Archean. Geochim. Cosmochim. Acta 54, pp. 2717-2729.

Veizer J., Hoefs J., Ridler R. H., Jensen L. S., and Lowe D. R. (1989a) Geochemistry of Precambrian carbonates: I. Archean hydrothermal systems. Geochim. Cosmochim. Acta 53, 845-857.

Veizer J., Hoefs J., Lowe D. R., and Thurston P. C. (1989b) Geochemistry of Precambrian carbonates: II. Archean greenstone belts and Archean sea water. Geochim. Cosmochim. Acta 53, pp.859-871.

Verma R.K & Banerjee P (1992) Nature of continental crust along the Narmada-Son lineament inferred from gravity and deep seismic sounding data, Tectonophysics,202, pp.357-397.

Visser, M.J. (1980) Neap-spring cycles reflected in Holocene subtidal large-scale bedform deposits: a preliminary note. Geology, 8, pp.543–546.

Wendt, I., Carl, C., (1991) The statistical distribution of the mean squared weighted deviation. Chem.Geo. (Isotope Geoscience Section) v.86, pp. 275-285.

Windley, B.F. (1995) The evolving continents. Wiley, Chichester.

Wronkiewicz, D.J., Condie, K.C. 1987. Geochemistry of Archean shales from the Witwatersrand Supergroup, South Africa: Source-area weathering and provenance. Geochim. Cosmochim. Acta 51, pp.2401-2416.

Wronkiewicz., D.J., Condie, K.C. 1989. Geochemistry and provenance of sediments from the Pongola supergroup, South Africa: evidence for a 3.0 Ga. old continental craton. Geochim. Cosmochim. Acta 53, pp.1534-1549.

Wronkiewiez D.J and Condie K.C (1990) Geochemistry and mineralogy of sediments from the Ventersdrop and Transval Supergroups, South Africa: Cratonic evolution during early Proterozoic. Geochim.Cosmochim.Acta, 54, pp.343-354.

Wunderlich, F. (1970) Genesis and environment of the 'Nellenköpfchenschichten' (lower Emsian, Rheinian Devon) at locus typicus in comparison with modern coastal environment of the German Bay. J. sedim. Petrol., 40, pp.102-130.

Young, G.M. and Nesbitt, H.W. 1998. Process controlling the distribution of Ti and Al in weathering profiles, siliciclastic sediments and sedimentary rocks. Jour. Sed. Res. 68, pp.448-455.

Zachariah J. K., Bhaskar Rao Y. J., Srinivasan R., and Gopalan K. (1999) Pb, Sr and Nd isotope systematics of uranium mineralized stromatolitic dolomites from the Proterozoic Cuddapah Supergroup, south India: constraints on age and provenance. Chem. Geol. 162, pp.49-64.